UNIVERSIDADE DE LISBOA
Faculdade de Medicina de Lisboa

MURID HERPESVIRUS-4 MODULATION OF B-T HELPER CELL INTERACTION

by
Diana Marisa Pinto Freire Fontinha

Thesis supervised by Professor Doutor J. Pedro Simas, Faculdade de Medicina da Universidade de Lisboa

Tese especialmente elaborada para obtenção do grau de Doutor em Ciências Biomédicas, especialização em Microbiologia e Parasitologia

2016

UNIVERSIDADE DE LISBOA

Faculdade de Medicina de Lisboa

MURID HERPESVIRUS-4 MODULATION OF B-T HELPER CELL INTERACTION

Diana Marisa Pinto Freire Fontinha

Thesis supervised by Professor Doutor J. Pedro Simas, Faculdade de Medicina da Universidade de Lisboa

Tese especialmente elaborada para obtenção do grau de Doutor em Ciências Biomédicas, especialização em Microbiologia e Parasitologia

Júri

Presidente: Doutor José Augusto Gamito Melo Cristino, Professor Catedrático e Presidente do Conselho Científico da Faculdade de Medicina da Universidade de Lisboa

Vogais:

- Doutor Alexandre Valentim Xavier Mourão do Carmo, Investigador Principal do Instituto de Biologia Molecular e Celular da Universidade do Porto
- Doutora Margarida Sofia da Silva Santos Saraiva, Investigadora Principal do Instituto de Biologia Molecular e Celular da Universidade do Porto
- Doutor José Henrique Veiga Fernandes, Investigador no Instituto de Medicina Molecular, da unidade de investigação associada à Faculdade de Medicina da Universidade de Lisboa
- Doutor Luís Ricardo Simões da Silva Graça, Professor Associado com Agregação da Faculdade de Medicina da Universidade de Lisboa
- Doutor Mário Nuno Ramos d'Almeida Ramirez, Professor Associado com Agregação da Faculdade de Medicina da Universidade de Lisboa
- Doutor João Pedro Monteiro e Louro Machado de Simas, Professor Associado da Faculdade de Medicina da Universidade de Lisboa

Scholarship - SFRH/BD/80048/2011 from Fundação para a Ciência e a Tecnologia

2016

As opiniões expressas nesta publicação são da exclusiva responsabilidade do seu autor.

A impressão desta dissertação foi aprovada pelo Conselho Científico da Faculdade de Medicina de Lisboa em reunião de 22 de Março de 2016.

PREFACE

The current thesis presents data obtained during my PhD research project, developed at Instituto de Medicina Molecular in the period of February 2012 to November 2015, under the supervision of Professor Doutor João Pedro Simas (Faculdade de Medicina, Universidade de Lisboa).

This thesis is organized in 8 chapters, which are preceded by a summary written in Portuguese and an abstract. Before the description of the results, an introductory review of the subject is provided in chapter 1, followed by the aims of the work. In chapters 2, 3, 4, and 5 the original data obtained during this research project are presented. Final considerations, which integrate the results presented in previous chapters as well as future directions are presented in chapter 6. Finally, chapter 7 concerns the description of the materials and methodologies employed to carry out the presented work. The publications that resulted from the research carried out throughout the duration of this project are included in appendixes 1 to 3.

Data presented in this dissertation were purely the result of work carried out by me and it is clearly acknowledged in the text whenever data or reagents produced by other were utilized. This work has not been submitted for any degree at this or any university.

Diana Fontinha

PUBLICATIONS

Appendix 1

Fontinha, D.*, Lopes, F.B.*, Marques, S., Alenquer, M., Simas, J.P. (2015). **Murid Gammaherpesvirus Latency-Associated Protein M2 Promotes the Formation of Conjugates between Transformed B Lymphoma Cells and T Helper Cells.** PLoS ONE 10(11): e0142540. doi:10.1371/journal.pone.0142540. *shared first authorship.

Data presented in this publication were obtained by me, with the exception of figure 2, panels A and B of figure 3, panels A-C of figure 5. Data in figure 4 were obtained in collaboration. This publication resulted from my PhD research project.

Appendix 2

Decalf, J.*, Godinho-Silva, C.*, Fontinha, D., Marques, S., Simas, J.P. (2014). **Establishment of Murine Gammaherpesvirus Latency in B Cells Is Not a Stochastic Event.** PLOS Pathogens. 2014;10(7):e1004269. doi: 10.1371/journal.ppat.1004269. *shared first authorship.

Data presented in figure 4 was obtained by me. Immunization at day 7 and data regarding immunization and infection at day 0 were obtained in collaboration. This publication resulted from research carried out throughout the duration of my PhD.

Appendix 3

Godinho-Silva, C.*, Marques, S.*, Fontinha, D., Veiga-Fernandes, H., Stevenson, P. G., Simas, J.P. (2014). **Defining Immune Engagement Thresholds for *In Vivo* Control of Virus-Driven Lymphoproliferation.** PLOS Pathogens. 10(6): e1004220. doi: 10.1371/journal.ppat.1004220. *shared first authorship.

I provided technical assistance in organ collection, sample preparation for adoptive transfers and iv injections. This publication resulted from research carried out throughout the duration of my PhD.

ACKNOWLEDGEMENTS

Em primeiro lugar gostaria de agradecer ao meu supervisor Pedro Simas pela oportunidade de realizar o doutoramento no seu laboratório. A sua orientação e os ensinamentos transmitidos ao longo destes quatro anos foram fundamentais para o meu crescimento profissional.

Gostaria também de agradecer aos restantes membros do PSimas Lab por toda a ajuda, disponibilidade e pelo ambiente de amizade. À Sofia Marques, minha tutora, com quem aprendi tanto, por todo o seu apoio, orientação e discussões científicas. À Filipa Lopes e à Marta Alenquer pela sua contribuição para este projeto. À Marta Miranda, pelos momentos divertidos e pelas discussões científicas. À Sofia, minha colega de doutoramento desde o primeiro dia, pelas horas de conversa e por todo o seu apoio. À Cristina, parceira das longas horas de ivs, pelo apoio e amizade. À Inês, à Lénia, ao Jérémie e à Teresa.

Agradeço ao Instituto de Medicina Molecular, por proporcionar todas as condições necessárias à realização deste projeto e por tornar este um local tão estimulante onde fazer ciência. Estendo este agradecimento às facilities e aos seus funcionários, pela sua ajuda e disponibilidade. Igualmente agradeço à unidade de citometria de fluxo do Instituto Gulbenkian de Ciência. Dirijo um agradecimento especial ao Doutor Henrique Veiga Fernandes e ao Diogo Pereira por toda a ajuda e ensinamentos transmitidos, que me permitiram realizar as experiências com quimeras.

Agradeço aos membros do meu Comité de Tese, Doutor Bruno Silva-Santos e Doutor João Barata, pelo apoio e críticas construtivas.

Finalmente, deixo um agradecimento à minha família, com especial carinho para os meus pais, que sempre me apoiaram nos bons e maus momentos. Agradeço também à minha segunda família, os amigos, por me ajudarem a recarregar baterias para uma nova semana de trabalho. Em especial à Raquel, pelo apoio, amizade e cumplicidade de sempre e ao André, pelo seu apoio incondicional e infinita paciência.

RESUMO

A principal característica dos herpesvírus é a sua capacidade de estabelecer infeções persistentes, que permanecem por toda a vida do hospedeiro. Particularmente, os gama-herpesvírus humanos infetam o tecido linfoide e estão consequentemente associados a doenças linfoproliferativas. Para atingir a persistência, os gama-herpesvírus estabelecem latência na população de células B de memória, que são de longa duração. O acesso a este compartimento depende da proliferação e diferenciação de células B latentemente infetadas em reações de centro germinativo, um processo que é dependente da ajuda das células T *helper* (T_H) $CD4^+$. Atualmente é desconhecido se o vírus tem a capacidade de manipular a interação entre células B e células T_H. A proteína M2 associada à fase de latência do gama-herpesvírus de murídeo do tipo 4 (MuHV-4) coordena a formação de complexos multiproteicos com proteínas celulares envolvidas na sinalização da célula B. Logo, M2 interfere com as vias de sinalização que se desenrolam a jusante do recetor da célula B (BCR). Esta habilidade depende de dois resíduos de tirosina que formam um motivo de ativação do imunoreceptor baseado em tirosina (ITAM) não convencional. O presente estudo teve como principal objetivo investigar se a proteína M2 do MuHV-4 desempenha um papel na modulação da interação entre células B e células T_H. Para tal, a interação celular foi investigada com recurso a um sistema restrito para MHC do tipo classe II e específico para o péptido de OVA. A expressão de M2 levou ao aumento de moléculas de superfície em células B transduzidas, nomeadamente moléculas co-estimulatórias e de adesão celular. Consistente com estas descobertas, M2 foi capaz de promover a formação de conjugados B-T_H. Num sistema de competição *in vitro*, esta habilidade traduziu-se numa vantagem competitiva, tal como pôde ser observado pela preferência das células T_H para conjugar com células B que expressavam M2. Contudo, a expressão de M2 em células B não foi suficiente para levar à ativação das células T_H, uma vez que apenas ocorreu na presença de péptido específico. Para avaliar a importância biológica desta capacidade de M2 de promover a formação de conjugados B-T_H, desenhou-se um sistema de competição *in vivo* que assenta na purificação de células B primárias que expressam M2 a partir de ratinhos quimera. A capacidade de M2 de coordenar a formação de complexos multiproteicos com proteínas de sinalização revelou-se deletéria para o desenvolvimento e/ou proliferação de células B nos ratinhos quimera. Como tal, não foi possível obter qualquer conclusão quanto ao papel de M2 na modulação da interação B-T_H *in vivo*. *In vivo*, a mutação dos resíduos de tirosina que compõem o ITAM não convencional de M2 (vírus recombinante M2Y) resulta num atraso no estabelecimento de latência do vírus. Com o intuito de identificar a origem deste

atraso, a infeção com vírus do tipo selvagem (WT) e do tipo mutante (M2Y) foi seguida *in vivo* por métodos quantitativos e qualitativos. Os resultados foram inconclusivos, mas não excluíram a possibilidade de um fenótipo em células B. Coletivamente, estes resultados suportam um modelo em que a proteína M2 promove a formação de conjugados entre células B e T_H. Num contexto fisiológico, esta habilidade pode conferir uma vantagem competitiva à célula B infetada na aquisição de ajuda por parte da célula T_H, deste modo contribuindo para a iniciação de reações de centro germinativo e, consequentemente, para a colonização do hospedeiro.

Palavras-chave: gama-herpesvírus; interação célula B-célula T; célula B; proteína M2.

ABSTRACT

The main feature of herpesviruses is their ability to establish persistent infections. Human gammaherpesviruses, in particular, infect the lymphoid tissue and are associated with lymphoproliferative disorders. To attain persistence, gammaherpesviruses establish latency in the long-lived memory B cell population. Access to this B cell compartment depends on the initiation of germinal center reactions and the subsequent proliferation and differentiation of latently infected germinal center B cells, for which T cell help is essential. Whether the virus is capable of modulating B-T helper cell interaction for its own benefit is still unknown. Latency associated M2 protein, of the experimental mouse model of infection murid herpesvirus-4 (MuHV-4), assembles multiprotein complexes with B cell signaling proteins, therefore interfering with cell signaling pathways downstream of the B cell receptor (BCR). This ability depends on two phosphosites that constitute an unconventional immunoreceptor tyrosine-based activation motif (ITAM). The aim of this thesis was to investigate if the M2 protein played a role in the modulation of B-T helper cell interaction. To that end, cell interaction was addressed in an MHC-II restricted OVA peptide-specific system. M2 led to the upregulation of adhesion and co-stimulatory molecules in transduced B cell lines. Consistent with these findings, M2 promoted the formation of B-T helper cell conjugates. In an *in vitro* competition assay, this translated into a competitive advantage, as T cells preferentially conjugated with M2-expressing B cells. However, expression of M2 alone in B cells was not sufficient to lead to T cell activation, as it only occurred in the presence of specific peptide. To address the role of M2 in B-T helper cell interaction *in vivo*, a competition system was designed, that relied on the purification of M2-expressing primary B cells from chimeric mice. The ability of M2 to assemble multiprotein complexes with cell signaling proteins had a negative effect in the development and/or proliferation of this population in the mouse chimeras. Therefore, conclusions could not be drawn. Mutation of the unconventional ITAM *in vivo* results in a delay in latency establishment. To further understand the origin of this delay, YFP-expressing mutant and wild type viruses were tracked *in vivo* by quantitative and qualitative methods. Data was inconclusive but did not exclude a B cell phenotype. Taken together, these findings support that M2 promotes the formation of B-T helper cell conjugates. In an *in vivo* context this may confer a competitive advantage to the infected B cell in acquisition of T cell help and initiation of a germinal center reaction, hence host colonization.

Keywords: Gammaherpesvirus; B-T cell interaction; B cell; M2 protein.

ABBREVIATIONS

Ag	Antigen
AIDS	Acquired immunodeficiency syndrome
APC	Antigen Presenting Cell
BAC	Bacterial Artificial Chromosome
BCR	B cell receptor
BHK	Baby hamster kidney
BL	Burkitt's lymphoma
BSA	Bovine Serum Albumin
Btk	Bruton's tyrosine kinase
CMAC	7-amino-4-chloromethylcoumarin
CMFDA	5-chloromethylfluorescein diacetate
CMTMR	5-(and-6)-(((4-chloromethyl)benzoyl)amino) tetramethylrhodamine
CMV	Citomegalovirus
cpe	Cytopathic effect
cSMAC	Central Supramolecular Activation Cluster
CSR	Class-switch recombination
CTL	Cytotoxic T lymphocyte
DAPI	4',6-diamidino-2-phenylindole
DMEM	Dulbeco's modified eagle's medium
DMSO	Dimethyl sulfoxide
DNA	Deoxyribonucleic acid
dNTP	Deoxynucleotide triphosphates
dpi	Days post infection
dSMAC	Distal Supramolecular Activation Cluster
EBER	EBV-encoded RNA
EBNA	EBV nuclear antigen
EBV	Epstein Barr Virus
EDTA	Etilenediaminetetraacetic acid
EF1α	Elongation factor 1α
EGFP	Enhanced green fluorescent protein
FACS	Flow activated cell sorting
FDC	Follicular dendritic cell
FLIP	Fas-associated death domain-like interleukin-1β-converting enzyme-inhibitory protein

Fo	Follicular
FSC	Forward Scatter
GC	Germinal Centre
GFP	Green fluorescent protein
h	hour
HAART	Highly active antiretroviral therapy
HCMV	Human cytomegalovirus
HIV	Human immunodeficiency virus
HL	Hodgkin's lymphoma
HSC	Hematopoietic stem cell
HVS	Herpesvirus saimiri
ICA	Infectious center assay
ICAM-1	Intercelular adhesion molecule 1
IE	Immediate early
Ig	Immunoglobulin
IL	Interleukin
IFN	Interferon
i.n.	intranasal
i.p.	intraperitoneal
IRES	Internal ribosomal entry site
IS	Immunological Synapse
ITAM	Immunoreceptor tyrosine-based activation motif
KS	Kaposi's sarcoma
KSHV	Kaposi's Sarcoma-associated Herpesvirus
LANA	Latency-associated nuclear antigen
LB	Luria Bertani
LFA-1	Lymphocyte function-associated antigen 1
LMP	Latent membrane protein
LN	Lymph nodes
MCD	Multicentric Castleman's disease
MHC	Major histocompatibility complex
mIg	Membrane immunoglobulin
min	minutes
MSCV	Murine stem cell virus
MTOC	Microtubule organizing center
MuHV-4	Murid gammaherpesvirus 4
MZ	Marginal Zone

NFAT	Nuclear factor of activated T cells
NK	Natural killer
NPC	Nasopharyngeal carcinoma
NP-CGG	4-Hydroxy-3-nitrophenylacetyl hapten conjugated to Chicken Gamma Globulin
OCT	Optimal cutting temperature compound
ORF	Open reading frame
OVAp	Ovalbumine peptide
PA	Plaque assay
PALS	Periarteriolar lymphoid sheats
PBS	Phosphate-buffered saline
PCR	Polymerase Chain Reaction
PE	Phycoerythrin
PEL	Primary effusion lymphoma
PFA	Paraformaldehyde
pSMAC	Peripheral Supramolecular Activation Cluster
PTDL	Post-transplant lymphoproliferative disease
RT	Room temperature
sec	Seconds
SH2	Src homology domain 2
SH3	Src homology domain 3
SHM	Somatic hypermutation
SSC	Side Scatter
TCR	T cell receptor
T_H	$CD4^+$ T helper cell
Tip	Tyrosine kinase-interacting protein
VLA-4	Very Late Antigen-4
WP	White pulp
WT	Wild type
XLP	X-linked lymphoproliferative syndrome
YFP	Yellow fluorescent protein
ZAP	Tyrosine kinase zeta-associated protein of 70 kDa

TABLE OF CONTENTS

INDEX OF FIGURES

INDEX OF TABLES

CHAPTER 1

INTRODUCTION

1 INTRODUCTION

Gammaherpesviruses, such as Epstein-Barr virus and Kaposi's sarcoma-associated herpesvirus, are widely disseminated in nature. Co-evolution with their hosts has led to a fine balance that allows gammaherpesviruses to persist for the lifetime of the host without causing disease. Disruption of this balance results in lymphoproliferative disorders, especially in immunocompromised patients. The study of gammaherpesvirus infection is therefore of major clinical importance.

Persistent infection depends on the ability of the virus to establish latency in the long-lived memory B cell population. To accomplish that, gammaherpesviruses have developed several strategies that allow them to exploit different aspects of the host B cell, such as the modulation of host cell signaling pathways. Specifically, both the Epstein-Barr virus and the mouse model Murid Herpesvirus-4 take advantage of the germinal center reaction, the process whereby B cells undergo affinity maturation and differentiation into plasma cells or memory B cells. In T cell dependent responses, GC initiation depends on the help provided by specific $CD4^+$ T helper cells. B-T helper cell interaction is therefore a crucial step in GC responses, which makes it a rational target of gammaherpesviruses. Understanding whether B-T helper cell interaction is modulated by the virus for its own benefit will provide useful insight on viral pathogenesis.

1.1 Introduction to Gammaherpesviruses

Herpesviruses are widely disseminated in nature and are thought to originate at the very early stages of the evolution of parasitism. In fact, herpesviruses are thought to have a long co-evolutionary history with their hosts. Supposedly, this is on the basis of their good adaptation to the host. As a result, fatal infections in immunocompetent hosts are extremely rare. Historically, herpesviruses have been placed under the same category due to their common virion architecture. Typically, a virion is composed of a core containing a linear double-stranded DNA, surrounded by an icosahedral capsid composed of 162 capsomeres and a lipid envelope that contains viral glycoproteins at its surface. In some cases, a proteinaceous matrix named tegument can be found surrounding the capsid (Roizman and Pellett 2007). The acquisition of exogenous DNA sequences, DNA rearrangements and nucleotide substitutions are on the basis of herpesvirus diversity. As a result, herpesviruses present both conserved and divergent genome regions (Lacoste, Lavergne et al. 2010). Usually, the conserved part of the genome consists of structural

genes and/or genes involved in lytic replication. Between these conserved regions, specific genes that confer the particular characteristics of a given herpesvirus can be found. The gene products of herpesviruses frequently have multiple disparate functions (Roizman and Pellett 2007).

So far eight human herpesviruses have been isolated and associated to disease. However, herpesviruses are highly divergent and their host range highly variable. Based on the host range, the *Herpesvirales* order is divided into three families: *Herpesviridae* (mammal, bird and reptile herpesviruses), *Alloherpesviridae* (fish and amphibian herpesviruses) and *Malacoherpesviridae* (bivalve herpesviruses) (Davison, Eberle et al. 2009). Members of the *Herpesviridae* family have one defining characteristic in common: the ability to establish latency in their natural hosts. Besides latency establishment, host colonization includes two other stages: primary or lytic infection and reactivation from latency. Upon entry into a naïve host, the virus establishes an acute lytic infection that results in the production of infectious progeny, leading to the destruction of the infected cell. This allows virus spread, both to other hosts and within the host. This stage is then followed by the establishment of latency in a specific set of cells. During latency, the viral genomes are maintained as circular molecules and gene expression is very restricted. Although there is production of infectious progeny, viruses can reactivate from latency and begin a new stage of lytic infection. Such infection kinetics have allowed herpesvirus to establish persistent infections, that last for the lifetime of the host. Besides the ability to latently infect the host, members of the *Herpesviridae* family also share other characteristics. They code for enzymes involved in nucleic acid metabolism, DNA synthesis and processing of proteins. The localization of component steps in virion production is the same, namely viral DNA synthesis and capsid assembly take place in the nucleus, while the final processing of the virion takes place in the cytoplasm. On the other hand, the members of the *Herpesviridae* family differ in biological properties which led to their further division into three sub-families: *Alphaherpesvirinae*, *Betaherpesvirinae* and *Gammaherpesvirinae*. Of the nine gammaherpesviruses that infect humans, herpes simplex virus 1 (HSV-1), herpes simplex virus 2 (HSV-2) and varicella-zoster virus (VZV) belong to the *Alphaherpesvirinae* sub-family; human cytomegalovirus (HCMV), human herpesvirus 6A (HHV-6A), human herpesvirus 6B (HHV-6B) and human herpesvirus 7 (HHV-7) belong to the *Betaherpesvirinae* sub-family; and Epstein-Barr virus (EBV) and Kaposi's sarcoma-associated herpesvirus (KSHV) belong to the *Gammaherpesvirinae* sub-family (Roizman and Pellett 2007). For the purpose of this thesis, only gammaherpesviruses will be described in more detail.

Gammaherpesviruses are usually specific for B or T lymphocytes. Concomitantly, latent virus is frequently detected in the lymphoid tissue. Moreover, some of these viruses are known to cause lytic infections in some types of epithelioid and fibroblastic cells (Roizman and Pellett 2007). On the basis of genome organization and DNA sequence homology this sub-family is further divided into four genera: *Lymphocryptovirus* (also known as gamma1-herpesviruses), *Rhadinovirus* (gamma2-herpesviruses), *Macavirus* and *Percavirus*. The *Lymphocrytovirus* genus has only been found in primates and includes the human gammaherpesvirus EBV. The *Rhadinovirus* genus has been found in both primate and non-primate species, namely rodents, leporids and bovines. This genus includes the human gammaherpesvirus KSHV as well as the rodent virus, widely used as a laboratory model of gammaherpesvirus pathogenesis, Murid Herpesvirus-4 (MuHV-4). The *Macavirus* genus includes bovine, caprine, ovine and swine herpesviruses. The *Percavirus* genus includes equine, carnivore and non-mammalian herpesviruses (Davison, Eberle et al. 2009).

1.1.1 Gammaherpesvirus and disease

EBV and KSHV, the human viruses that belong to the *Gammaherpesvirinae* sub-family, usually coexist with their host without causing disease (Cesarman 2011). However, they have the ability to induce neoplasia in their natural hosts (Damania 2004). In fact, EBV was the first human virus to be related to oncogenesis. All members of this sub-family are capable of driving the proliferation of infected lymphocytes during the establishment and maintenance of latency. This lymphoproliferation is the cause of the majority of the diseases associated to gammaherpesvirus in immunocompromised hosts (Simas and Efstathiou 1998).

More than 90% of the human adult population is infected with EBV. Primary infection usually occurs early in childhood and is most often asymptomatic. In the developed world, another classical presentation of primary infection with EBV is infectious mononucleosis, also known as glandular fever, in adolescents. Clinically, this is characterized by a sore throat, cervical lymphadenopathy, fever, splenomegaly, malaise, headache, sweating and gastro-intestinal discomfort (Ogilvie 2007). However, infectious mononucleosis in patients with X-linked lymphoproliferative syndrome (XLP), which are deficient for an important lymphocyte signaling protein, SAP, can be fatal (Rickinson and Kieff 2007). EBV is also associated with malignant disorders. In immunocompromised hosts, the inability of the immune system to control the EBV-driven B cell proliferation, results in post-transplant

lymphoproliferative diseases and immunoblastic lymphomas. The first occurs in patients that undergo transplantation and are, therefore, iatrogenically immunosuppressed. The latter occurs in patients with acquired immunodeficiency syndrome (AIDS) that are, therefore, immunocompromised due to human immunodeficiency virus (HIV) infection. In immunocompetent hosts, EBV is not considered the causative agent but, instead, it is a component in a complex process of malignant transformation. Other cofactors may be host somatic mutations or infection with other pathogens. EBV has different latency programs, characterized by different latent gene expression, as will be described in more detail in section 1.2.2. These patterns are associated with specific lymphoma subtypes (Mesri, Feitelson et al. 2014). Expression of lytic cycle genes has also been implied in oncogenicity (Thompson and Kurzrock 2004). Furthermore, EBV-encoded miRNAs target host genes that regulate cell growth and apoptosis pathways and are associated with some malignancies (Vereide, Seto et al. 2014). Examples of such malignancies are Burkitt's lymphoma (BL), Hodgkin's lymphoma (HL), nasopharyngeal carcinoma (NPC) and also a small subset of natural killer (NK) and T cell lymphomas, gastric carcinomas, follicular dendritic tumours and other epithelial carcinomas (Mesri, Feitelson et al. 2014). It was in cultured lymphoblasts from BL that EBV was first identified (Epstein, Achong et al. 1964). BL is a germinal center (GC)-derived aggressive B cell lymphoma, that is divided into three different clinical variants on the basis of geographical and HIV status information. Endemic BL, for instance, is the most common cancer of childhood in equatorial Africa, where it overlaps with the geographical distribution of malaria infection. HL is seen worldwide and it has a first peak of incidence in persons aged 15-35 years, and a second one in elderly patients (Ok, Li et al. 2015).

There is no unified therapeutic strategy for EBV-associated lymphoproliferative disorders. Antiviral agents used in the clinic, such as acyclovir, ganciclovir, and valaciclovir are broad-spectrum antivirals and, therefore, their efficiency against EBV is variable. Furthermore, they are only effective during the lytic phase of infection and, in most EBV-associated lymphoproliferative disorders, EBV infection is latent. Recently, induction of EBV lytic phase followed by administration of antiviral drugs has been suggested as a way to overcome this problem (Geng and Wang 2015). In the case of transplant recipient patients, reducing immunosuppression is sometimes an option (Ogilvie 2007). Adoptive immunotherapy with EBV-specific donor-derived or HLA-matched cytotoxic T cells (CTLs), recovered from donors, expanded *in vitro* and infused into the patient is also an option. These CTLs are able to recognize and eliminate EBV-infected tumor cells that express more latent proteins. However, this strategy has several disadvantages, namely it is time-consuming, costly, labor-intensive and carries many potential risks for the patient

(Rooney, Smith et al. 1998, Geng and Wang 2015). Once a tumor is developed, another therapeutic strategy is the use of specific monoclonal antibodies. Rituximab, a monoclonal antibody against CD20, may reduce the size of CD20-expressing B cell lymphomas (Choquet, Leblond et al. 2006). An antibody-drug conjugate, Brentuximab Vedotin, is under clinical trials (Ogura, Tobinai et al. 2014). Another approach is the targeting of oncogenic pathways, since aberrant oncogenic signaling is a characteristic of EBV-associated lymphoproliferative disorders. The proteasome inhibitor Bortezomib, inhibits the NF-κB pathway and induces apoptosis of EBV lymphoblastoid cell lines (Zou, Kawada et al. 2007).

KSHV is not as prevalent in the human population as EBV. Its incidence varies with geographic and demographic factors. Since its discovery, KSHV has been associated with three human malignancies: Kaposi's sarcoma (KS), primary effusion lymphoma (PEL) and multicentric Castleman's disease (MCD). Furthermore, KSHV is associated with several acute inflammatory syndromes (Giffin and Damania 2014). It was in KS lesions that KSHV was first identified (Chang, Cesarman et al. 1994). These lesions usually occur cutaneously or in mucosal surfaces, but can also be found on lymph nodes and visceral organs, such as lung and spleen. KS is divided into four subtypes: classic KS, found in elderly men of Mediterranean and eastern European descent; endemic KS, which occurs in eastern and central African countries; epidemic or AIDS-associated KS, the most common and aggressive form of the disease and the most frequent cancer in many Sub-Saharan countries; and post-transplant or iatrogenic KS, associated with the use of immune suppressive therapy (Giffin and Damania 2014). Tumor cells in KS are of endothelial origin and most of them are latently infected. However, unlike classical tumors, KS lesions are composed of many cell types (Ganem 2007). PEL is an aggressive lymphoma characterized by the lack of a solid tumor mass. Instead, it is composed of a monoclonal population of malignant KSHV-infected B cells that expand within the pericardial, pleural, and peritoneal body cavities (Nador, Cesarman et al. 1996, Giffin and Damania 2014). Nonetheless, cases of solid PEL have been reported (Carbone, Gloghini et al. 2005). It occurs primarily, but not exclusively, in HIV-positive patients. Tumor cells are of B cell origin, most likely post-GC origin, given the expression of plasma cell markers and the evidence of immunoglobulin gene rearrangements and somatic hypermutation of the immunoglobulin genes (Cesarman 2011, Cesarman 2014). The vast majority of the KSHV-infected tumor cells are also infected with EBV (Nador, Cesarman et al. 1996, Cesarman and Knowles 1999). Upon diagnosis, the average survival time is about 6 months (Boulanger, Gerard et al. 2005). PEL-derived cell lines have a consistent growth in culture and have, therefore, been essential for *in vitro* studies regarding the

molecular pathogenesis of KSHV (Renne, Zhong et al. 1996). MCD is an uncommon lymphoproliferative disorder, characterized by an abnormal proliferation of plasmablasts within the mantle zone of B cell follicles. It usually affects several lymph nodes (multicentric) but it can also be localized (Cesarman 2011, Cesarman 2014). Gene expression observed in MCD suggests that, unlike KS and PEL, KSHV infection is mainly lytic (Chadburn, Hyjek et al. 2008, Polizzotto, Uldrick et al. 2012). It is thought that disease symptoms are a consequence of the production of excess cytokines, such as IL-6 (Cannon, Nicholas et al. 1999). In HIV-positive patients MCD is most likely associated to KSHV infection, but that may not be the case in HIV-negative patients. MCF is also frequently observed in transplantation recipients (Kaplan 2013).

Introduction of combination antiretroviral therapy (cART) has decreased the incidence of AIDS-associated KS, and is used to treat systemic disease. Localized KS lesions can be treated locally with liquid nitrogen. In the case of larger lesions, localized radiotherapy is an option. In patients where disease is more advanced, systemic chemotherapy is used. In clinical trials, KS responded to two drugs: imatinib and lenalidomide. There is no standard care for PEL (Kaplan 2013). The most commonly used treatment is chemotherapy, with a poor prognosis (Coen, Duraffour et al. 2014). Response to antiretroviral therapy or rituximab has only been reported in individual cases (Lim, Rubin et al. 2005). In MCD, given that infection is mainly lytic, antiviral therapy has been reported successful (Casper, Nichols et al. 2004). Considering the excess production of IL-6 in MCD, the use of an anti-human IL-6 receptor antibody as well as a novel chimeric monoclonal antibody against IL-6 are promising treatments (Coen, Duraffour et al. 2014).

Summarizing, there is no unified, highly effective, treatment for gammaherpesviruses. Their ability to establish latency and to interfere with host signaling pathways are two of the major problems to overcome. This denotes the importance of understanding gammaherpesvirus pathogenesis and, in particular, latency establishment in order to develop a targeted therapy. Given the specificity of host infection, EBV and KSHV are unable to infect experimentally useful small animal hosts. To fill that gap, MuHV-4, a gammaherpesvirus of the *Rhadinovirus* genus that infects laboratory mice, has been widely used as an animal model of gammaherpesvirus pathogenesis.

1.2 Gammaherpesvirus infection

Gammaherpesviruses establish life-long persistent infections and are highly prevalent in the human population. Furthermore, as described in section 1.1.1, they may be associated with lymphoproliferative disorders, which makes their treatment a major clinical goal. Understanding the different stages of infection, as well as the mechanisms and proteins/RNAs behind it, is essential for the development of a targeted therapy.

Latent infection of circulating memory B cells is crucial to persistence and hence disease ontogeny. To access the memory B cell compartment gammaherpesviruses, such as EBV and murid herpesvirus-4 (MuHV-4), take advantage of germinal center (GC) reactions (Simas and Efstathiou 1998, Flano, Kim et al. 2002, Kim, Flano et al. 2003, Willer and Speck 2003, Roughan and Thorley-Lawson 2009, Barton, Mandal et al. 2011, Thorley-Lawson, Hawkins et al. 2013). Infection with EBV, KSHV, and their mouse virus counterpart MuHV-4 will now be described in detail.

1.2.1 Germinal Center reaction

B cells are an important component of adaptive immunity, that is specialized in the recognition of antigens. Mature naïve B cells are short-lived cells that circulate through the bloodstream and migrate to secondary lymphoid organs, such as the spleen and lymph nodes, where they can encounter a specific antigen (Yuseff, Pierobon et al. 2013). Binding of antigen to the B cell receptor (BCR) provides survival signals to the B cell and promotes its initial activation. The BCR-antigen complexes are then internalized and the antigen is broken down to several peptides. These, in turn, bind to major histocompatibility complex class II (MHC-II) molecules that will present the antigen at the B cell surface. In T cell-dependent humoral immune responses, the specific interaction of these cells with $CD4^+$ T helper (T_H) cells is an essential step that will allow further B cell activation and initiation of a GC reaction (Pierce 2002). For that purpose, antigen-engaged B cells, present in the follicles of secondary lymphoid organs, migrate towards the T cell-rich periarteriolar lymphoid sheaths (PALS) in response to a ligand gradient (Okada, Miller et al. 2005). T_H cells have also been exposed to antigen that is presented to them by dendritic cells (DCs) and macrophages and can, therefore, recognize the same specific antigen being presented by the B cell. Therefore, in the border area between follicles and T cell zones, T_H cells scan for the highest affinity for an appropriate antigen by quickly interacting with antigen-presenting B cells, forming conjugates. Upon cognate interaction,

an immunological synapse is formed, as will be described in more detail in section 1.3.1. Through this interaction the B cells receive cytokine signals from the T_H cells, that promote survival, proliferation and differentiation (Mills and Cambier 2003, De Silva and Klein 2015).

Interaction of antigen-engaged B cells with T_H cells may have three different outcomes. B cells may move to the medullary chords where they differentiate into short-lived plasmablasts that secrete low affinity antibodies. B cells may also differentiate into unswitched memory B cells (Taylor, Pape et al. 2012). Finally, B cells may enter the GC pathway (Figure 1.1) (De Silva and Klein 2015). In this pathway, activated GC precursor B cells move to the center of the follicle to form an early GC. A rapid B cell proliferation takes place and at seven to ten days after antigen exposure a GC is formed. This transient structure supports affinity maturation, a process that generates and selects B cells expressing high affinity BCR. In the classical model the GC is divided into two microenvironments known as the dark zone and the light zone, which harbor different B cell types (Allen, Okada et al. 2007). The dark zone is densely populated by proliferating B cells, named centroblasts, and reticular cells that are morphologically similar to follicular dendritic cells (FDCs) (Bannard, Horton et al. 2013). In this region, B cells not only proliferate but also undergo somatic hypermutation (SHM) of the immunoglobulin variable region genes. The outcome is a diversity of affinities for the immunizing antigen. Centroblasts then move to the light zone for selection. This is more sparsely populated by B cells, named centrocytes, and also contains follicular helper T cells (T_{FH}) and FDCs. Centrocytes with an unfavorable membrane immunoglobulin undergo apoptosis. Immunoglobulins with improved affinity for the immunizing antigen are positively selected. Positive selection depends on interaction with both FDCs and T_{FH} cells. Access to the antigen deposited at the surface of FDCs is limited and only B cell clones that express a high affinity BCR are able to acquire antigen. Recently, it has been proposed that antibodies produced by GC-derived plasma cells help to limit access to antigen in a competitive manner (Zhang, Meyer-Hermann et al. 2013). Next, only the B cells that acquired antigen are able to present it to T_{FH} cells, a crucial step in affinity maturation. Higher BCR affinity leads to greater antigen capture and, consequently, to higher density of peptide presented to the T_{FH} cells. In turn, this results in largest longest contacts with the T_{FH} cells and subsequent selection (Nutt and Tarlinton 2011, De Silva and Klein 2015). At this stage, centrocytes may undergo immunoglobulin class-switch recombination (CSR) which allows daughter B cells to produce antibodies with different isotypes but with the same specificity for the immunizing antigen (Guzman-Rojas, Sims-Mourtada et al. 2002, Klein and Dalla-Favera 2008). A subset of selected cells recirculates to the dark zone, for

further SHM of the immunoglobulin genes, whereas other cells directly differentiate into plasma cells or memory B cells. Cells that could not acquire survival signals from FDCs or selection signals from T_{FH} cells undergo apoptosis (Victora and Mesin 2014, De Silva and Klein 2015). Plasma cells will produce and secrete high affinity antibodies, while memory B cells will survive for a long period of time and, upon secondary exposure to the same antigen, will differentiate into plasma cells (Calame 2001).

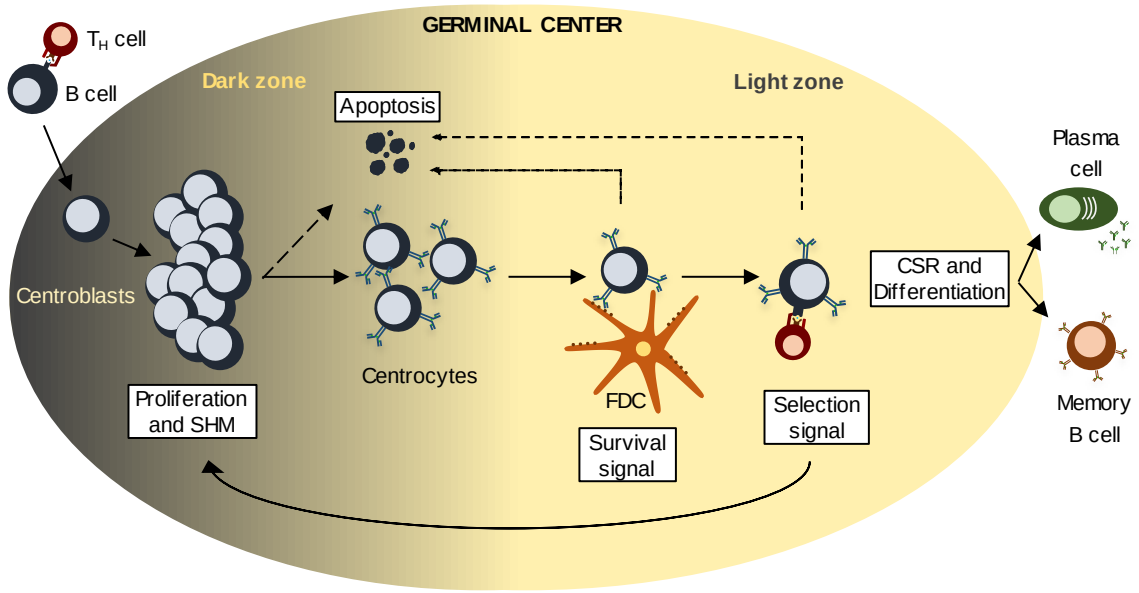

Figure 1.1. Classical model of germinal center reaction. Upon interaction with $CD4^+$ T helper (T_H) cells, antigen-engaged B cells may enter the germinal center (GC) pathway. This transient structure supports a process that generates and selects B cells expressing high affinity BCR, named affinity maturation. In the dark zone of the GC, B cells, now named centroblasts, undergo proliferation and somatic hypermutation (SHM) of the immunoglobulin variable region genes. This process creates a diversity of B cell receptors (BCR) with different affinity for the immunizing antigen. These B cells then move to the light zone of the GC, where they are named centrocytes, to be selected. B cells with high affinity for the antigen interact with follicular dendritic cells (FDC) and T_H cells and are positively selected. Selected centrocytes may recirculate to the dark zone for further SHM or they may undergo class switch recombination (CSR) and differentiation, leaving the GC as either plasma cells or memory B cells. Cells that are not positively selected undergo apoptosis.

1.2.2 Model of EBV infection

The human gammaherpesvirus EBV persists as a life-long infection in the circulating, resting, memory B cell population of healthy hosts. This is true for over 90% of the human population and may be associated with disease. As previously mentioned, EBV has four latency programs, that differ in latent gene expression, each of them associated with specific lymphoma subtypes (Table 1.1). Two main models of infection have been thus far

proposed to explain persistence: the GC model (Thorley-Lawson 2001, Thorley-Lawson 2005, Thorley-Lawson, Duca et al. 2008, Thorley-Lawson, Hawkins et al. 2013) and the direct infection model (Kurth, Spieker et al. 2000, Kurth, Hansmann et al. 2003). The latter, which assumes direct infection of memory B cells, was proposed over 10 years ago but, to date, no strong experimental evidence has been able to support it and explain the mechanism behind it. Furthermore, predictions made according to this model are incorrect. An alternative perspective speculates that latently infected memory B cells derive directly from infected naïve B cells, without the need for a GC reaction (Heath, Begue-Pastor et al. 2012). Similarly, this model does not fit some of the *in vivo* evidences known so far. The GC model of infection, therefore, remains as the only model that can explain persistence in the memory B cell population, as well as account for the different latency programs and their characteristic association with different lymphoma subtypes (Table 1.1). For example, BL is believed to result from latently infected GC B cells that failed to differentiate into resting memory B cells (Thorley-Lawson and Gross 2004). This model considers that EBV exploits the normal biology of the host B cell, driving it to participate in the GC reaction, therefore acquiring access to the long-lived memory compartment, where the virus persists quiescently (Figure 1.2).

Table 1.1. Patterns of EBV latent gene expression in different B cell subsets of healthy individuals and in malignancies. The corresponding expression profiles in malignant lymphomas have been designated latencies I, II and III (adapted from Thorley-Lawson, 2005).

Transcription program	Genes expressed[a]	Infected normal B cell type	Function	Lymphoma type
Growth (Latency III)	EBNA1, 2, 3A, 3B, 3C, LP, LMP1, LMP2A and LMP2B	Naïve	B cell activation	Immunoblastic lymphoma, PTLD
Default (Latency II)	EBNA1, LMP1 and LMP2A	GC	Differentiation of activated B cell into memory	Hodgkin's disease, NK-T cell lymphoma
EBNA1 (Latency I)	EBNA1	Dividing memory	Cellular division of latently infected memory B cells	BL, PEL
Latency (Latency 0)	None	Resting memory	Allow lifetime persistence	
Lytic	All lytic genes	Plasma cell	Viral replication in plasma cell	

[a] Does not include the non-coding EBER and BART RNAs.
PTDL – post-transplant lymphoproliferative disease

Although virus entry is open to other interpretations (Gillet, Frederico et al. 2015), EBV is believed to reach a new host by oral transmission. A productive lytic infection is then established in the oropharynx, which contributes to the high levels of virus shed in saliva (Niederman, Miller et al. 1976). At this stage, viral replication takes place in both squamous epithelial cells and locally infiltrating B cells. This change in cellular tropism is

achieved by changing the composition of the glycoproteins present at the surface of the virion (Shannon-Lowe and Rowe 2014). Latently infected B cells then pass through a series of stages that lead to their activation and proliferation. These are associated with four distinct latency programs, which have been observed both *in vitro* and *in vivo*: growth program or latency III, default program or latency II, EBNA1 program or latency I, and latency program or latency 0 (Table 1.1) (Kempkes and Robertson 2015). The growth program starts upon infection of naïve B cells and is characterized by the expression of all nine known latent proteins, consisting of six EBV nuclear antigens (EBNAs) and three latent membrane proteins (LMPs). As a result, the infected B cells become activated, without the need for any external signals. B cells then migrate to secondary lymphoid organs where they participate in a GC reaction (Figure 1.2) (Babcock, Hochberg et al. 2000, Roughan and Thorley-Lawson 2009). After a few cycles of proliferation, EBV switches to the more restricted default program, where only EBNA1, LMP1 and LMP2A are expressed (Table 1.1). EBNA1 is required to replicate the viral DNA. LMP1 and LMP2A provide the signals that are usually obtained through the BCR and through T cell help, as will be explained in more detail in section 1.4.2. This program, therefore, drives the differentiation of the latently infected B cells, that eventually leave the GC reaction as memory B cells and enter the peripheral circulation (Yates, Warren et al. 1985, Babcock, Hochberg et al. 2000, He, Raab-Traub et al. 2003, Casola, Otipoby et al. 2004). At this stage, EBV expresses only the viral genome tethering protein EBNA1 (EBNA1 program) or, alternatively, it does not express any viral proteins (latency program) (Babcock, Hochberg et al. 2000). The EBNA1 program takes place in dividing memory B cells and ensures the tethering to host chromosomes and segregation of EBV DNA and therefore, maintains the episomal DNA (Thorley-Lawson 2005). The latency or latency 0 program is considered the true latency. By shutting down protein expression the virus is quiescent and invisible to the immune response, allowing long-term persistence (Hawkins, Delgado-Eckert et al. 2013).

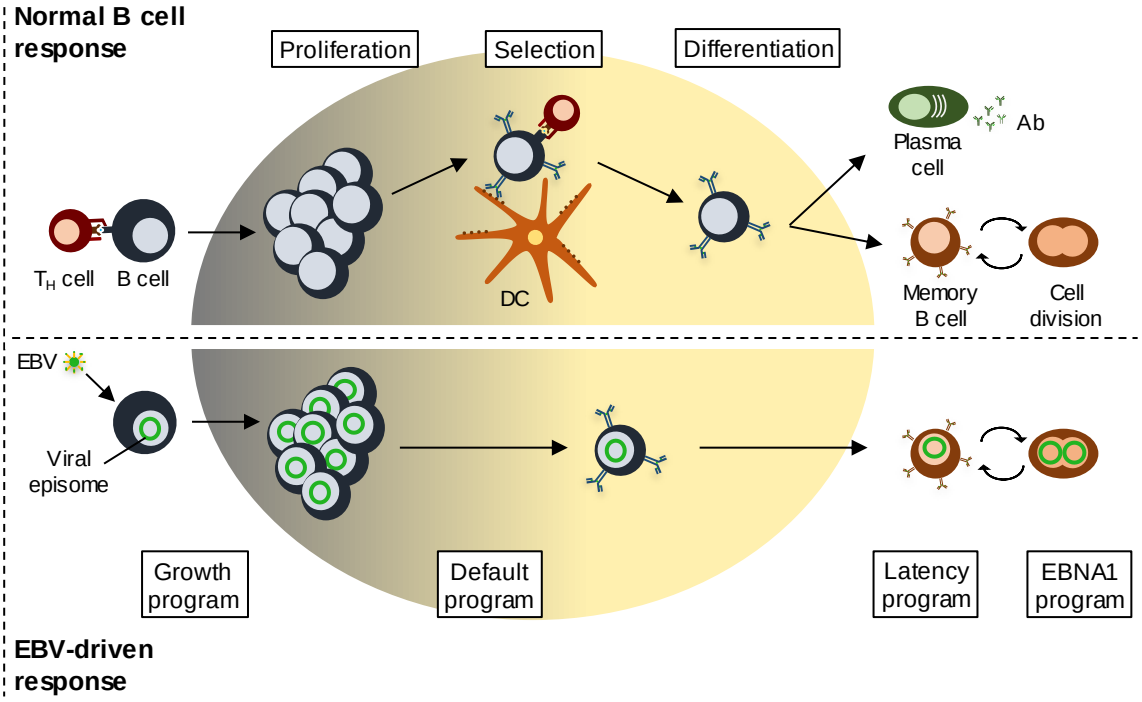

Figure 1.2. Parallel between normal B cell response and EBV-driven response. In the normal B cell response, B cells that have encountered antigen migrate to the border between the B cell zone and the T cell zone, where they can present a specific peptide to $CD4^+$ T helper (T_H) cells. Upon cognate interaction, B cells receive activation signals from T_H cells and establish a germinal center (GC) reaction. In the dark zone B cells undergo several rounds of proliferation, associated with somatic hypermutation. Selection of high affinity clones then takes place in the light zone through interaction with dendritic cells (DC) and T_H cells. Selected cells may then undergo class switch recombination and differentiate into plasma cells or memory B cells, that leave the GC. Memory B cells can occasionally divide to maintain its pool. In the EBV-driven response, EBV infects a naïve B cell where it expresses the growth transcription program. EBV-infected B cells become activated and it is believed that they then establish a GC reaction, without the need for any external signals. Viral transcription then changes to the default program. This replaces the signals provided by T_H cells and DCs and drives the differentiation of the infected B cells into memory B cells, where the latency program is expressed. Upon infected memory B cell division, there is a switch from the latency program to the EBNA1 program. Expression of EBNA1 then ensures episome maintenance during cell division, therefore maintaining the pool of latently infected memory B cells. Adapted from ThorleyLawson, 2001, Thorley-Lawson, 2005 and Klein & Dall-Favera, 2008.

In response to normal physiological signals, latently infected memory B cells may differentiate into plasma cells, resulting in virus reactivation from latency. This lytic reactivation is divided into three phases: immediate early, early and late. During the immediate early phase, there is expression of transcription factors that initiate viral replication. Next, in the early phase, there is production of proteins that are involved in viral DNA replication. Finally, both viral DNA and structural proteins are assembled into virions that are released and can either infect new cells or be shed in saliva (Kieff and

Rickinson 2007, Hawkins, Delgado-Eckert et al. 2013). Infection of new cells, as well as division of resting memory B cells, may be important to ensure the maintenance of a latent pool of virus. Furthermore, infection of epithelial cells may amplify the levels of infectious virus before shedding (Hadinoto, Shapiro et al. 2009). Shedding in saliva then completes the EBV cycle by allowing the infection of new hosts, therefore ensuring the high prevalence of this gammaherpesvirus.

The EBNA proteins localize to the nucleus of the infected cell and are important for gene transcription and viral replication. EBNA1 is expressed in three of the four latency programs, namely growth, default and EBNA1 programs. It binds both to the viral episome and to the host chromosomes ensuring episome maintenance during cell replication. Furthermore, EBNA1 promotes LMP1 transcription and inhibits MHC-I-mediated peptide presentation. The remaining EBNA proteins are only expressed during the growth program. EBNA2 works as a transcriptional activator of the remaining EBNA and LMP proteins, as well as some cellular genes required for latency establishment. EBNA-LP works as a co-activator of EBNA2, enhancing transcriptional activation (Young and Murray 2003, Speck and Ganem 2010). The EBNA3 family is important for the modulation of B cell lymphomagenesis. EBNA3A and EBNA3C target tumor suppressor pathways to promote B cell proliferation and are, therefore, considered oncoproteins. Interestingly, EBNA3B seems to restrain the oncogenic capacity of EBV and is, therefore, considered a tumor suppressor (Allday, Bazot et al. 2015).

The mechanism and function of LMP1 and LMP2A will be described in more detail in section 1.4.2. As mentioned above, these proteins are produced during the growth and default latency programs but their role during the GC reaction is still unclear. On the one hand, *in vitro* studies demonstrate that LMPs have the ability to drive GC B cell survival and differentiation, independently of external signals (Gires, Zimber-Strobl et al. 1997, Caldwell, Wilson et al. 1998, Casola, Otipoby et al. 2004). On the other hand, latently infected B cells bear somatic mutations in their immunoglobulin genes and are isotype switched, suggesting a transition through the normal process of antigen selection and a passive role for the LMPs (Souza, Stollar et al. 2005, Souza, Stollar et al. 2007, Tracy, Kakalacheva et al. 2012). Therefore, the role of these proteins may be only to promote the survival of the infected cells. It is also possible that the LMPs ensure the differentiation of latently infected GC B cells into memory B cells, instead of plasma cells (Thorley-Lawson, Hawkins et al. 2013). Recent studies in mice that conditionally express LMP2A in GC B cells showed that expression of LMP2A reduces the stringency of GC B cell selection, as

observed by the preferential selection of low-afinity antibody-producing B cells (Minamitani, Yasui et al. 2015).

In addition to the above mentioned latent proteins, EBV expresses EBV-encoded RNA (EBER) 1 and 2, which are small non-coding RNAs (Swaminathan 2008). EBV also encodes two clusters of miRNAs. Just like with latent gene expression, different patterns of miRNA expression have been detected and associated with the four latency programs. Furthermore, these miRNAs are expressed in tumor cells, which lack the growth program, where they are associated with viral driven lymphoproliferation (Qiu, Cosmopoulos et al. 2011). Collectively, they confer an increased resistance to apoptosis (Seto, Moosmann et al. 2010). Therefore, they are an important component of EBV infection that contributes to survival and growth of both infected tumor cell and normal infected cell.

Concluding, by exploiting the normal biology of the B cell, EBV is able to persist in a quiescent state, invisible to the immune response, for the lifetime of the host. To do so, the virus alternates amongst four different latency programs, characterized by distinct patterns of latent gene expression. During the growth and default latency programs, virus-specific neutralizing antibodies and cytotoxic T lymphocytes counterweight the B cell proliferation promoted by the virus (Hislop, Taylor et al. 2007). Hence, an equilibrium is established between host and virus that, when disturbed, results in disease. By alternating between latent and lytic infection the virus is also able to increase its numbers and be transmitted to a new host. Although, to date, the GC model of infection is widely accepted as the only model that is able to explain EBV biology and the pathogenesis of EBV-associated lymphomas, the development of a mathematical model of persistence has brought new insights into this field (Delgado-Eckert and Shapiro 2011). According to it, the basis of persistence is the cycle of infection itself, rather than the specific stage of quiescence in the memory compartment. Distinguishing these two possibilities is now crucial, as it will impact on the targets chosen in the future for anti-viral treatments.

1.2.3 Model of KSHV infection

KSHV prevalence in the human population is not as high as it is for EBV. Nonetheless, it is the most frequent cause of malignancy among AIDS patients. Because this is the most recently identified human herpesvirus, the mechanisms behind establishment and maintenance of latency are not as well studied as for EBV. Similar to EBV, the main target for latent infection in immunocompetent hosts is the B cell population (Ambroziak,

Blackbourn et al. 1995). However, KSHV has also been detected in epithelial cells, monocytes and endothelial cells. The latter seems to be limited to KS lesions (Dittmer and Damania 2013).

Primary infection with KSHV may occur during childhood and adulthood and transmission may be through a sexual or non-sexual route (Minhas and Wood 2014). In KSHV-endemic regions, where seroprevalence is high, transmission is most commonly mediated by saliva and occurs among children. In non-endemic regions, where KSHV seroprevalence is low, sexual transmission may be the predominant route (Bagni and Whitby 2009). Although rare, transmission through blood transfusion or among intravenous drug users has been reported (Hladik, Dollard et al. 2006). The fact that KSHV can be found in cervico-vaginal secretions and the fact that KS develops in children under one year of age suggests vertical transmission, from mother to child (Minhas and Wood 2014). Similar to EBV, KSHV alternates between latent and lytic infection, relying on the first to persist in an immunological silent mode and on the latter to be shed and transmitted to new hosts (Coscoy 2007).

During latency, as with EBV, few viral genes and miRNAs are expressed. These ensure genome maintenance, interfere with signaling pathways and manipulate the immune system in a strategy believed to be similar to the one developed by EBV. Studies performed in PEL cell lines allowed the characterization of a major latency locus that includes four major open reading frames (ORFs) which, in turn, encode the latency-associated nuclear antigen (kLANA), the viral cyclin D homolog (v-Cyc), the Fas-associated death domain-like interleukin-1β-converting enzyme-inhibitory protein (vFLIP) and the kaposin family of proteins (Kaposin A, B and C) (Kedes, Lagunoff et al. 1997, Sadler, Wu et al. 1999). Similar to EBNA1, kLANA ensures the maintenance and segregation of the viral genome during host cell division, by binding to the terminal repeat sequences of the viral episome and, simultaneously, to the host chromosome. Although central to KSHV latency, episome maintenance is not the only task carried out by this viral protein. kLANA also interacts with several cellular proteins, namely tumor suppressors, transcription factors, chromatin-binding proteins and signal transducers. Furthermore, it has been proposed to bind to viral promoters, repressing lytic gene transcription and promoting latency (Uppal, Banerjee et al. 2014). v-Cyc, like its cellular homologue cyclin D, is involved in modulation of cell cycle and sustains cell proliferation (Van Dross, Yao et al. 2005). vFLIP activates the NF-κB pathway, thereby promoting cell survival and proliferation. This protein has also been linked to suppression of lytic reactivation, hence contributing to latency maintenance and persistence (Ye, Zhou et al. 2008, Uppal,

Banerjee et al. 2014). The kaposin family of proteins is still poorly understood. Kaposin A is considered an oncogenic protein, while kaposin B acts as an adaptor protein and activates the p38/MAPK signaling pathway (Uppal, Banerjee et al. 2014). The kaposin locus also encodes twelve pre-miRNAs that produce eighteen mature, highly conserved, miRNAs. A function that appears to be common to most viral miRNAs is regulation of latent gene expression (Feldman, Kara et al. 2014). miR-K12-1 and miR-K12-3 repress lytic reactivation by modulating NF-κB, while miR-K12-5 maintains latency by reducing RTA expression. Few miRNAs have also been implicated in induction of viral reactivation. Summarizing, KSHV miRNAs are linked to modulation of host immune response, inhibition of apoptosis, and control of maintenance of latency and lytic reactivation. Besides the major latency locus described above, there are other genes whose expression has been detected during latency. Viral interferon regulatory factor 3 (vIRF-3) interacts with certain cellular IRFs and inhibits the expression of type I interferon. Furthermore, it inhibits NF-κB activation and decreases MHC-II expression. Viral interleukin 6 (vIL-6) promotes B cell proliferation and is an important contributor to the pathogenesis of PEL and MCD (Uppal, Banerjee et al. 2014, Schulz and Cesarman 2015). The terminal membrane proteins K1 and K15, also expressed during latency, are involved in modulation of B cell signaling and will be described in more detail in section 1.4.3. All of the above mentioned proteins are the core of KSHV latency and their expression was confirmed *in vivo* in cells derived from KSHV malignancies (Table 1.2).

Table 1.2. KSHV latent gene expression in different malignancies (adapted from Damania, B., 2004 and Wen, K.W. & Damania, B., 2010).

Malignancy	Proteins expressed in most tumor biopsies	Proteins expressed in few tumor biopsies
KS	LANA, v-Cyc, vFLIP, kaposin	vIL-6, K1
PEL	LANA, v-Cyc, vFLIP, kaposin, vIRF-3, vIL-6	K1
MCD	LANA, v-Cyc, vFLIP, vIRF-3, vIL-6	K1

Certain environmental and physiological factors may lead to virus reactivation from latency, namely: viral co-infection, hypoxia, oxidative stress, inflammatory cytokines and histone deacetylase inhibitors. As with EBV, lytic reactivation of KSHV is divided into three phases: immediate early, early and late. Immediate early genes are responsible for the latent-to-lytic switch. Although several genes are associated with this phase, there is one central protein that is sufficient to disrupt latency and promote a complete lytic cascade, RTA or ORF50. Early genes encode proteins that are required for viral DNA replication and gene expression. Finally, late genes encode viral structural proteins that are required for virion assembly. New infectious progeny is then produced, ultimately resulting in host

cell death. This phase of KSHV infection is crucial for viral propagation and KSHV-induced tumorigenesis (Uppal, Banerjee et al. 2014, Purushothaman, Uppal et al. 2015).

As in EBV infection, it is possible that the germinal center reaction plays a role in KSHV infection. PEL, for instance, is a B cell lymphoma of post germinal center origin. MCD cells, however, do not show signs of previous participation in the germinal center reaction (Dittmer and Damania 2013). Further studies are required to address this issue. Nonetheless, like EBV, KSHV seems to exploit the normal B cell biology and its pathways in order to promote cell proliferation and establish latency. Persistence is the result of an equilibrium between host and viral factors that, when perturbed, may result in disease.

1.2.4 Model of MuHV-4 infection

Understanding gammaherpesvirus pathogenesis is critical for the development of targeted therapies. Although much has been learned from *in vitro* studies with EBV and KSHV infected cells, *in vivo* studies remain the better way to understand host-pathogen interactions. Due to their narrow species tropism, the study of EBV and KSHV infection *in vivo* has been a difficult task. Although EBV is known to infect some primate species, this system does not properly reproduce a natural infection. Even infection of humanized mice does not reproduce a realistic infection. Isolation of a murine gammaherpesvirus from two species of free living small rodents, *Apodemus flavicollis* (yellow-necked mouse) and *Clethrionomys glareolus* (bank vole), in Slovakia in 1980 was the solution to this problem (Blaskovic, Stancekova et al. 1980). This virus, MuHV-4, was later on isolated in the United Kingdom from what is believed to be its natural host species, the *Apodemus sylvaticus* (wood mice) (Blasdell, McCracken et al. 2003).

MuHV-4 lytically infects a variety of epithelial and fibroblast cells, and latently infects murine B cell lines such as NS0 (Svobodova, Blaskovic et al. 1982, Sunil-Chandra, Efstathiou et al. 1993). A B cell line has also been established from tumors of mice persistently infected with MuHV-4 (Usherwood, Stewart et al. 1996). Together, these cells allow the *in vitro* study of murid gammaherpesvirus infection. More importantly, MuHV-4 is able to infect laboratory mice, initiate a primary lytic infection and establish and maintain latency in B cells, as described for human gammaherpesviruses. It is classified as a rhadinovirus and is more closely related to KSHV than to EBV. In fact, 80% of MuHV-4 genes are homologous to KSHV genes (Virgin, Latreille et al. 1997). Nonetheless, MuHV-4 also genetically resembles EBV and shares its epithelial and B cell tropism, virus-driven

B cell proliferation, and an acute infectious mononucleosis syndrome (Simas and Efstathiou 1998, Doherty, Christensen et al. 2001, Nash, Dutia et al. 2001, Blackman and Flano 2002, Stevenson and Efstathiou 2005). Therefore, infection of laboratory mice with MuHV-4 provides a small tractable animal model for the study of gammaherpesvirus pathogenesis. The existence of a variety of transgenic mice, susceptible to MuHV-4 infection, that are deficient for specific host proteins has also helped in understanding host-pathogen interaction. Furthermore, the development of a system of easy production of recombinant viruses allows the study of the function of specific viral proteins in an *in vivo* context (Adler, Messerle et al. 2000). Potentially, this is also a system where the effectiveness of therapeutic strategies against gammaherpesvirus infection may be assessed (Stevenson and Efstathiou 2005). In the immunology field, because it drives GC reactions, MuHV-4 can be used as a stimulus of immune response.

MuHV-4 genome corresponds to 118kb of DNA flanked by terminal repeats, which contains approximately 80 ORFs. Although 80% of these genes are homologous to KSHV genes, MuHV-4 also encodes unique genes. ORFs M1-4, located at the left end of the genome, share no sequence relationship with any known viral or cellular genes. They may, however, have conserved functions. The M2 protein, for instance, is a presumed functional homologue of LMP1 and LMP2A from EBV and K1 and K15 from KSHV (Damania 2004, Pires de Miranda, Lopes et al. 2013). Because it is the focus of this thesis, the M2 protein will be described in detail in section 1.5. M1 is reminiscent of a viral superantigen and induces activation and proliferation of $CD8^+$ $V\beta4^+$ T cells (Evans, Moser et al. 2008). In turn, these produce IFN-γ that is required for virus reactivation from latency in macrophages. The secreted M3 protein binds several chemokines, therefore blocking normal $CD8^+$ T cell function (Parry, Simas et al. 2000, Bridgeman, Stevenson et al. 2001). M4 codes for another secreted glycoprotein and is thought to act as an immunomodulatory and/or immunostimulator. *In vivo*, absence of M4 expression attenuates latency establishment (Geere, Ligertwood et al. 2006).

Both the route of virus administration and the infection dose administered have an impact in MuHV-4 infection, and should be taken into account when comparing literature results. In pathogenesis studies, MuHV-4 has been administered intranasaly, intraperitonealy, orally and even subcutaneously into the footpad (Milho, Smith et al. 2009, Frederico, Chao et al. 2015). In adult mice oral MuHV-4 is non-infectious, unless it reaches the respiratory tract. Intranasal (i.n.) inoculation is believed to reproduce the physiological route. Nonetheless, intraperitoneal (i.p.) inoculation is also commonly used. Although they differ in the patterns of lytic infection following inoculation, both i.n. and i.p. routes allow

the virus to reach the lymphoid tissue (Milho, Smith et al. 2009). Furthermore, the steps of spleen colonization followed by MuHV-4 after i.n. or i.p. inoculation are the same (Frederico, Chao et al. 2014). The use of anesthesia in intranasal inoculation also alters the pattern of MuHV-4 infection. In the anaesthetized mice, MuHV-4 infects lung epithelial cells before spreading, while in the absence of anesthesia, MuHV-4 infects only the nose before spreading to the lymphoid tissue (Milho, Smith et al. 2009). Another possible route of virus shed is sexual transmission from female to male laboratory mice. MuHV-4 was identified in a vaginal excretion but this was not linked to vertical transmission nor horizontal transmission to other female mice (Francois, Vidick et al. 2013).

Following i.n. inoculation of laboratory mice, MuHV-4 targets the olfactory neuroepithelium (Milho, Frederico et al. 2012). Free viruses then infect $CD11c^+$ myeloid cells, which provide a conduit to lymph nodes (LN) (Figure 1.3) (Gaspar, May et al. 2011, Frederico, Milho et al. 2012). Simultaneously, the virus establishes a productive lytic infection in epithelial cells of the lungs, that peaks at 5 to 7 days post infection (dpi). At this stage, lung cells can be collected and co-cultured with permissive cells to measure the lytic viral load. $CD8^+$ T cells, also known as cytotoxic T lymphocytes (CTL), with specificity for lytic viral antigens play an important role in immune response, and lung infection is resolved within 10 to 12 days. $CD4^+$ T cells are also important for an efficient long-term response of CTLs (Cardin, Brooks et al. 1996). Besides the lungs, low titers of infectious virus can also be detected in the heart, kidney, major lymphoid organs, adrenal glands and whole blood (Sunil-Chandra, Efstathiou et al. 1992, Cardin, Brooks et al. 1996). Lytic infection is not a pre-requisite for latency establishment, as it has been observed by the ability of recombinant viruses, that cannot undergo lytic replication, to establish latency. However, lytic replication is a pre-requisite for virus trafficking and spleen colonization (Flano, Jia et al. 2005, Moser, Farrell et al. 2006).

Once in the LN, subcapsular sinus macrophages limit acute virus dissemination by absorbing virions from the afferent lymph in a non-productive manner (Frederico, Chao et al. 2015). It is believed that MuHV-4 then infects B cells that differentiate into plasma cells, releasing virus into the afferent lymph. By accessing the bloodstream, MuHV-4 reaches the spleen (Figure 1.3). There, the virus explores normal splenic communication routes to get access to GC reactions (Frederico, Chao et al. 2014). Latently infected B cells proliferate, increasing the pool of latent virus. Expansion attains maximum levels at 14dpi, which then decrease to a steady state characterized by low numbers of infected cells that persist throughout the life of the host without causing disease. The peak of latent infection is also accompanied by a large increase in $CD4^+$ and $CD8^+$ T cell numbers. Together, the

increased numbers of latently infected B cells, $CD4^+$ T cells and $CD8^+$ T cells result in a transient splenomegaly and lymphadenopathy (Sunil-Chandra, Efstathiou et al. 1992). It is also at this stage that the unique secreted viral protein M1 activates and promotes a selective expansion of $CD8^+$ $V\beta4^+$ T cells, in a manner reminiscent of a viral superantigen (CS Evans et al., 2008). In addition, there are high levels of non-virus-specific antibodies in the peripheral blood, therefore resembling the infectious mononucleosis caused by EBV (Tripp, Hamilton-Easton et al. 1997, Blackman, Flano et al. 2000, Hardy, Silins et al. 2000).

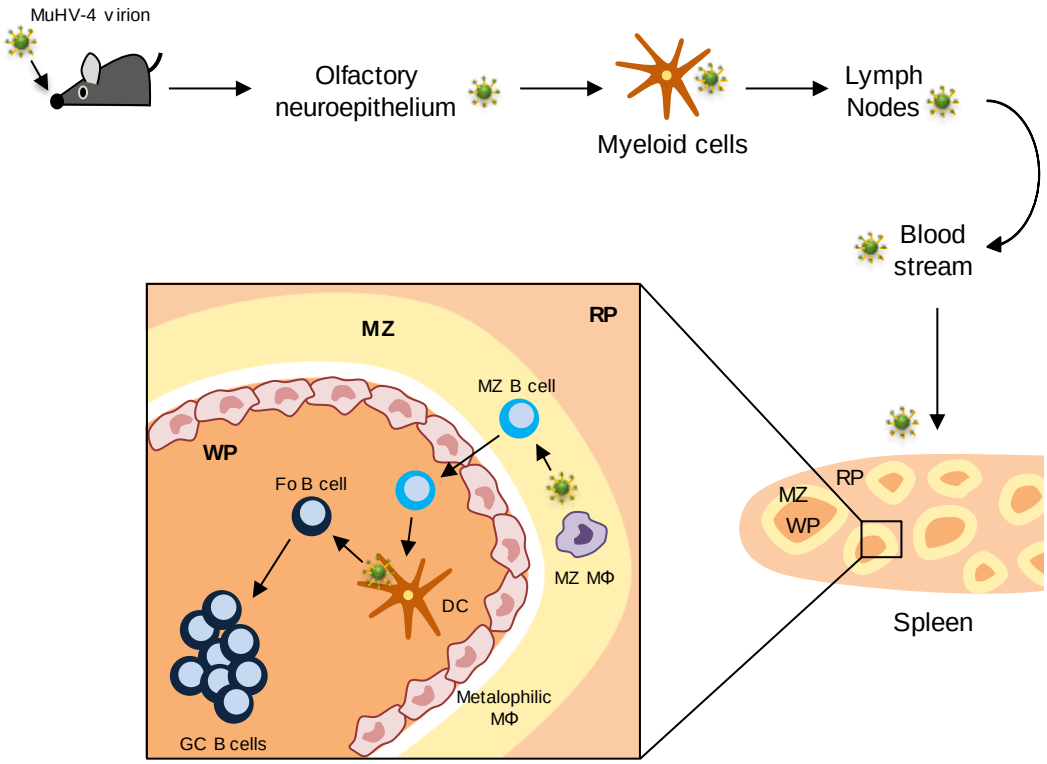

Figure 1.3. Schematic representation of MuHV-4 infection of a murine host. Upon intranasal infection with MuHV-4, mice develop a lytic infection in the olfactory neuroepithelium. Through myeloid cells the virus reaches the lymph nodes. Next, by entering the blood stream, MuHV-4 spreads to the spleen. Once in the spleen, the virus starts by infecting marginal zone (MZ) and metalophilic macrophages (MΦ). Then, it spreads to MZ B cells, which relocate to the white pulp (WP). Dendritic cells (DCs) then make the bridge between these cells and follicular (Fo) B cells. These, in turn, are able to participate in germinal center (GC) reactions. RP, red pulp. Adapted from Frederico, Chao et al. 2014 and Gillet, Frederico et al. 2015.

Although memory B cells are the long-term target population of MuHV-4, other B cell subsets and other cell types are also infected during latency establishment (Flano, Kim et al. 2002, Marques, Efstathiou et al. 2003, Willer and Speck 2003, Collins, Boss et al. 2009). In fact, it was demonstrated that, following i.p. infection, MuHV-4 is able to latently

infect mice that are deficient for mature B cells (Weck, Barkon et al. 1996). Initial analysis showed the presence of latent viral genomes in macrophages and dendritic cells, besides the already known B cell population (Flano, Husain et al. 2000). More recent studies have revealed the splenic populations exploited by the virus, as well as the order in which they are infected (Figure 1.3). MuHV-4 begins spleen colonization by infecting marginal zone macrophages. At this stage, infection is considered to be lytic and can also be detected in other macrophage populations, such as marginal metalophilic macrophages. Macrophages provide access to marginal zone B cells which, in turn, relocate to the white pulp. Follicular dendritic cells then transfer the virus to follicular B cells in a way that is reminiscent of their presentation of immune complexes to GC B cells (Frederico, Chao et al. 2014). Infected follicular B cells may then participate in a GC reaction. This is a critical step for persistence, as participation in a GC reaction provides access to the long-lived memory B cell population. In fact, at the latency peak, 70-80% of the infected B cells have a germinal center phenotype. Decrease of infection levels to a steady state corresponds to regression of GCs (Flano, Kim et al. 2002, Willer and Speck 2003). Therefore, MuHV-4 infection resembles EBV infection in that it exploits the GC reaction to increase the pool of latently infected B cells and promote their differentiation into memory B cells, a population that supports long-term infection.

Like EBV, MuHV-4 gene expression during latency is restricted. Furthermore, it is dependent on the type of cell infected. Gene transcription during this stage was analyzed by different groups but, due to the differences in study design, results were not consensual (Simas, Swann et al. 1999, Virgin, Presti et al. 1999, Rochford, Lutzke et al. 2001, Marques, Efstathiou et al. 2003, Martinez-Guzman, Rickabaugh et al. 2003). A study performed by our group has looked into gene expression in macrophages, dendritic cells and different B cell subsets at the peak of latent infection (Marques, Efstathiou et al. 2003). The unique genes M1 to M4, described above, were detected in all subsets of latently infected B cells, namely newly formed, marginal zone, follicular and GC B cells. Other ORFs that were transcribed during latency establishment were M8, M9, M11, K3, ORF72, ORF73 (mLANA) and ORF74. M8 and M9 function is still not clearly determined. Given its homology with KSHV and EBV proteins, M8 is predicted to encode a post-transcriptional regulator (Mackett, Stewart et al. 1997). Similarly, M9 is predicted to encode a capsid protein (Nash, Dutia et al. 2001). M11, only detected in newly formed and marginal zone B cells, encodes a viral homologue of bcl-2 and is a potent inhibitor of apoptosis (Wang, Garvey et al. 1999). Furthermore, it contributes to viral latency amplification in the lymphoid tissue (de Lima, May et al. 2005). K3 downregulates the surface expression of MHC-I, therefore contributing to immune evasion from CTLs

(Boname and Stevenson 2001). ORF72 encodes a viral cyclin D homologue. ORF73 or mLANA, like EBNA1 from EBV and kLANA from KSHV, ensures viral episome maintenance. Also like its human counterparts, mLANA acts as an immune evasion protein, limiting epitope presentation to $CD8^+$ T cells (Bennett, May et al. 2005). Furthermore, mLANA inhibits NF-κB transcriptional activity by promoting its ubiquitination and subsequent proteasome degradation of the sub-unit p65/RelA. Mutation of the SOCS box responsible for this function results prevents the expansion of latently infected GC B cells, therefore impairing persistence (Rodrigues, Filipe et al. 2009). Through its E3 ubiquitin ligase activity, mLANA also promotes a heterotypic poly-ubiquitination of c-myc increasing its stability, which results in an increased progression through the cell cycle (Rodrigues, Popov et al. 2013). Recent resolution of the crystal structure of the C-terminal domain of mLANA allowed the identification and targeted mutation of a DNA binding region and a set of lysine residues that are predicted to mediate interaction with host cellular proteins. Their mutation has an impact in virus-driven GC B cell proliferation (Correia, Cerqueira et al. 2013). Therefore, mLANA promotes the expansion of MuHV-4 in GC B cells. ORF74, only detected in newly formed and marginal zone B cells, encodes a G-protein coupled receptor that is required for increased viral replication in response to chemokines (Wakeling, Roy et al. 2001, Lee, Koszinowski et al. 2003).

Like its human virus counterparts EBV and KSHV, MuHV-4 encodes several miRNAs at the left end of its genome. *In vitro*, these are expressed in both lytic and latent infection (Pfeffer, Sewer et al. 2005, Zhu, Strehle et al. 2010). *In vivo*, they are highly expressed in GC B cells and hence are used as a marker of latent infection (Bowden, Simas et al. 1997, Simas, Swann et al. 1999). However, their function is still unknown.

MuHV-4 reactivation from latency is still poorly studied but, like with EBV and KSHV, it has been linked to plasma cell differentiation. The unique latency-associated M2 protein can drive plasma cell differentiation *in vitro* and it is required for an efficient differentiation of infected B cells to plasma cells *in vivo*. Therefore, this protein has been linked to virus reactivation from B cells (Liang, Collins et al. 2009). Manipulation of ORF50 expression, a gene that is responsible for the switch from latency to lytic virus replication, has been used to address this issue. A single study has demonstrated that exposure of infected cells to hypoxia conditions results in the up-regulation of ORF50 (Polcicova, Hrabovska et al. 2008). Another study has placed the ORF50 gene under a doxycycline-inducible promoter to create an *in vitro* system where the latent to lytic switch can be controlled (May, Bennett et al. 2010).

Recent work from our laboratory assessed the role of BCR specificity in B cell susceptibility to latent infection. By taking advantage of the switch hen egg lysozyme (SW_{HEL}) mice, where approximately 10% of the B cell population is specific for hen egg lysozyme (HEL), it was possible to observe that latency was restricted to HEL^- B cells. This demonstrates that latency establishment is not a stochastic event in what concerns BCR specificity (Decalf, Godinho-Silva et al. 2014). Another study from our group has determined critical MHC-I and $CD8^+$ T cell engagement thresholds for *in vivo* CTL control of virus-driven B cell proliferation, a step that is fundamental for the development of immunotherapies and vaccines (Godinho-Silva, Marques et al. 2014).

Concluding, MuHV-4 is a critical tool in the study of gammaherpesvirus pathogenesis, that provides an understanding of host-pathogen interactions and allows the dissection of viral protein function in an *in vivo* context. Like EBV, MuHV-4 exploits the normal biology of the B cell. In particular, it takes advantage of the GC reaction to amplify the pool of latent genomes and get access to the long-lived memory B cell population, attaining persistence without causing disease.

1.3 Gammaherpesviruses and B-T helper cell interaction

$CD4^+$ T cells are an important component of the immune response. For gammaherpesviruses they may have a dual role. On the one hand, they are important for immune surveillance against the virus. On the other hand, in cases where the virus takes advantage of the GC reaction, they are putatively important for B cell activation and GC initiation.

1.3.1 B-T helper cell interaction

As described in section 1.2.1, T cell help is critical for the initiation of a GC reaction in T cell-dependent immune responses. Antigen-presenting cells (APCs), such as B cells, process pathogen-derived peptides and present them in MHC-II molecules at the cellular surface. In response to a ligand gradient, B cells migrate within the follicles and towards the T cell zone. In that border area, T_H cells may then scan for the highest affinity with particular B cells. The initial contact is peptide-independent and mediated by adhesion molecules, resulting in the formation of B-T_H cell conjugates. This interaction is transient, unless the T_H cell TCR recognizes the peptide for which it is specific at the surface of the B cell. In that case, the transient interaction is replaced by a stronger cognate interaction,

where an organized signaling structure, the immunological synapse (IS), is formed (Grakoui, Bromley et al. 1999). The final outcome is the activation of the interacting B cell, its subsequent proliferation and establishment of a GC (Allen, Okada et al. 2007). B-T_H cell interaction is also important at a later step of the GC pathway, when B cells submitted to SHM are selected through interaction with DCs and T_{FH} cells.

B-T cell interaction is a highly dynamic process, as T cells can interact with several APCs simultaneously, selectively polarizing towards the strongest stimulus (Depoil, Zaru et al. 2005). Typically, an IS is composed of spatially separated supramolecular activation clusters (SMACs), arranged in a bull's eye shape (Figure 1.4) (Monks, Freiberg et al. 1998, Grakoui, Bromley et al. 1999, Huppa and Davis 2003). The center of the contact zone is named central SMAC (cSMAC), which bears cell activation molecules, as well as TCR-CD3/MHC-II partners. The latter control the specificity of the immune response. Similar to the B cell receptor, the TCR complex contains ITAMs that, when phosphorylated, can recruit the tyrosine kinase zeta-associated protein of 70 kDa (ZAP-70) and initiate signal transduction (Irving and Weiss 1991). CD80 and CD86 co-stimulatory molecules can bind CD28 present at the surface of the interacting T_H cell. In turn, this molecule contains a cytoplasmic tail with motifs that recruit Lck and, indirectly, PKC-Ɵ, which are involved in signaling (Kong, Yokosuka et al. 2011). T cell activation is followed by the upregulation of another co-stimulatory molecule, the inducible T-cell costimulator (ICOS). This binds ligand of ICOS (LICOS) on the B cell and is important in GC reactions (Dustin 2014). Cell adhesion molecules, such as CD48 and ICAM1, locate to the periphery of the cSMAC, forming the peripheral SMAC (pSMAC). By promoting B-T_H cell interaction, these molecules are essential for sensitive antigen recognition. Surrounding these two regions is the distal SMAC (dSMAC) where larger molecules can be found (Huppa and Davis 2003, Krummel and Cahalan 2010). Advances in IS study have led to a revision of the canonical view of this signaling structure. It is now known that TCR-MHC-II partners are concentrated in microclusters that are formed in the dSMAC and then migrate through the pSMAC towards the cSMAC (Varma, Campi et al. 2006). TCR microcluster formation depends on the actin cytoskeleton, while their migration relies on both the actin cytoskeleton and microtubules (Alarcon, Mestre et al. 2011). This reinforces the vision of the IS as a highly dynamic structure. CD28 also co-localizes with the TCR micro-clusters but is segregated upon convergence in the cSMAC (Yokosuka, Kobayashi et al. 2008). The latter is now sub-divided into the endo-cSMAC, where CD28-enhanced signaling continues, and the exo-cSMAC, composed of TCR-enriched extracellular vesicles that are collected by the B cell and moved away from the contact zone (Figure 1.4) (Dustin 2014).

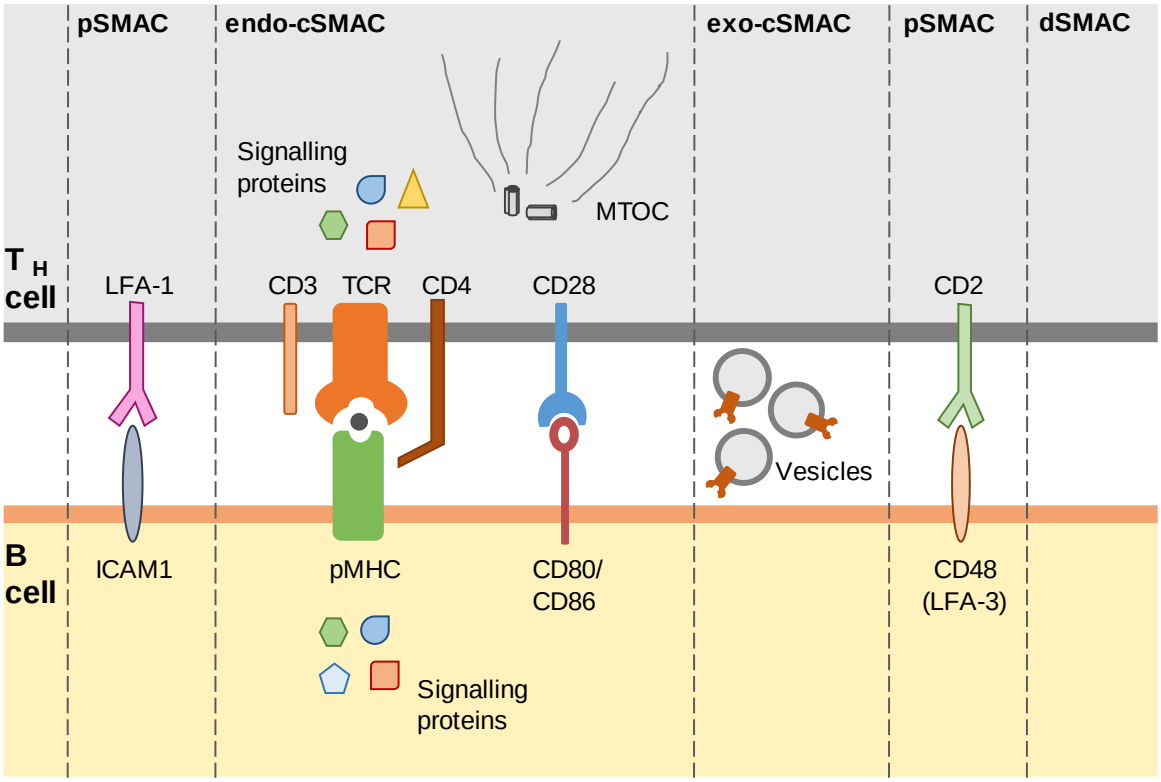

Figure 1.4. Organization of representative receptor classes in B-T_H immunological synapse. Immunological synapse formed between a B cell and a T_H cell, with representative receptor classes organized in supramolecular activation clusters (SMACs). The central SMAC (cSMAC) is divided into two regions: exo-cSMAC and endo-cSMAC. The first is the site for budding of TCR-enriched vesicles and, therefore, does not support signaling. The latter contains TCR-MHC-II partners and co-stimulatory molecules. Signaling proteins are recruited to this region to allow signal transduction. This is also the place to where the microtubule organizing center (MTOC) polarizes to allow the polarized secretion of cytokines. The cSMAC is surrounded by the peripheral SMAC (pSMAC), which contains adhesion molecules. In turn, the pSMAC is surrounded by the distal SMAC (dSMAC). Adapted from Huppa and Davis, 2003, Friedl, 2005 and Dustin, 2014.

Besides the reorganization at the cellular surface level, T cells also undergo morphological and cytoskeletal changes. Filamentous actin (F-actin) forms a ring that surrounds the previously mentioned structures (Le Floc'h and Huse 2015). Furthermore, there is polarization to the contact zone of the microtubule organizing center (MTOC) (Figure 1.4) (Monks, Freiberg et al. 1998, Huppa and Davis 2003, Depoil, Zaru et al. 2005), an event that aligns the secretory organelles with the IS and enables the polarized secretion of cytokines like IL-2, IL-4, IL-5 and IFN-γ to the extracellular opening that exists between the interacting cells, named synaptic cleft (Friedl, den Boer et al. 2005, Huse 2012). Cellular organelles and signaling machinery also polarize to the contact zone (Allen, Okada et al. 2007, Dustin 2014). Such polarization is reciprocal, as B cells also have the ability to polarize their MTOC and endocytic/exocytic compartments to the interface, although the functional role of such polarization has not been determined

(Duchez, Rodrigues et al. 2011). The IS therefore constitutes a local platform for signaling. As a result, the interacting B and T_H cells are mutually activated.

1.3.2 Modulation of B-T helper cell interaction by gammaherpesviruses

Immune evasion is crucial for pathogen survival in the host. Gammaherpesviruses have developed several strategies, many of them revolving around downregulation of surface MHC-I expression and consequent dodging of CTL recognition. K3 and K5 from KSHV encode two endoplasmic reticulum proteins that downregulate surface MHC-I molecules by promoting their endocytosis (Coscoy and Ganem 2000, Ishido, Wang et al. 2000, Stevenson, Efstathiou et al. 2000). Further studies have shown that K5, which is part of the lytic replicative cycle of KSHV, also has an impact in B-T cell interaction and immunological synapse formation (Coscoy and Ganem 2001). Expression of K5 in the BJAB B cell line reduces ICAM-1 and CD86 surface expression by promoting their endocytosis and degradation. As a result, K5-expressing B cells lose the ability to activate T cells in the presence of superantigen, as assayed by the measurement of T cell transcription factors known to be stimulated upon B-T cell interaction. This suggests that K5 renders the infected B cells less visible to T_H cells, thereby reducing antiviral cytokine responses and impairing the upregulation of stimulatory signals for CTL generation.

Another gammaherpesvirus encoded protein implicated in the modulation of B-T cell interaction is the tyrosine kinase-interacting protein (Tip) of Herpesvirus Saimiri (HVS). Like K5 from KSHV, Tip inhibits T cell activation as a mechanism to disarm host immune surveillance. Unlike KSHV, HVS is a T-lymphotropic virus and, therefore, the mechanism behind such inhibition is different. Tip interacts with cellular tyrosine kinase Lck and the endosomal protein p80. By sequestering Lck, Tip inhibits ZAP70 tyrosine kinase activation and, consequently, inhibits TCR-mediated intracellular signal transduction. Tip also inhibits the movement of TCR and Lck to the site of B-T cell interaction and suppresses the formation of the immunological synapse (Cho, Feng et al. 2004). Furthermore, interaction of Tip with Lck recruits TCR complex to lipid rafts and, subsequently, the interaction of Tip with p80 induces their internalization. The concerted action of the two interactions results in downregulation of TCR complexes (Park, Cho et al. 2003).

Despite the importance of $CD4^+$ T cells in MuHV-4 infection, there are no known mechanisms of modulation of B-T helper cell interaction. Like for its human counterparts, $CD4^+$ T cells play an important role in immune surveillance against the virus because they

are required for maturation of the antibody response and for antiviral cytokine activity, in particular IFN-γ (Christensen, Cardin et al. 1999, Stevenson and Doherty 1999, Sangster, Topham et al. 2000). Therefore, inhibition of B-T helper cell interaction in this context could be beneficial for the virus. Notably, $CD4^+$ T cells play another major role in MuHV-4 infection which is their requirement for GC initiation. In fact, in CD4-depleted mice, it is not possible to observe the normal increased B cell activation and increased levels of total serum IgG that is associated to MuHV-4 infection (Stevenson and Doherty 1998, Stevenson and Doherty 1999). Furthermore, absence of T_H cells results in impaired proliferation in GC reactions, reduced latency amplification and no splenomegaly (Ehtisham, Sunil-Chandra et al. 1993, Usherwood, Ross et al. 1996, Kim, Flano et al. 2003). During the GC response, insufficient help from T follicular helper cells also results in an inefficient establishment of latency in B cells. Fewer cells have a GC phenotype and, the ones that have, fail to proliferate. This is in contrast with what is believed to happen during EBV infection, which presumably bypasses the T cell help requirement (Collins and Speck 2014). For example, EBV expresses a protein that mimics CD40 signaling and, therefore, replaces T cell help. Infection of $CD40^+CD40^-$ chimeric mice with MuHV-4 revealed that latency is progressively lost in $CD40^-$ B cells, which fail to proliferate and differentiate into memory B cells through the GC reaction. On the other hand, $CD40^+$ cells, which are able to receive signals from T_H cells, selectively enter GC reactions and differentiate into memory B cells (Kim, Flano et al. 2003). Therefore, unlike EBV, MuHV-4 depends on normal $CD4^+$ T cell help for B cell activation, proliferation and differentiation. In this specific context, promotion of B-T helper cell interaction may be important to drive the infected B cells through a GC reaction contributing to host colonization. Although this putative role may be irrelevant for EBV infection, which encodes proteins believed to replace T cell help, that may not be the case for KSHV.

1.4 Gammaherpesvirus terminal membrane proteins involved in modulation of cell signaling

For a successful colonization of the host, gammaherpesviruses code for proteins that directly or indirectly promote immune evasion, cell survival, cell proliferation, cell differentiation and, in some cases, cell transformation and tumorigenesis. A set of those proteins is responsible for the modulation of the host B cell signaling. In human herpesviruses, these proteins correspond to LMP1 and LMP2A from EBV, and K1 and K15 from KSHV. Although different in sequence, these proteins share a functional homology as well as a positional homology, as their sequence can be found at the ends of

the coding region of the viral genomes. Furthermore, some of these proteins have a transforming potential, which has been linked to their ability to activate specific signaling pathways (Brinkmann and Schulz 2006).

1.4.1 B cell signaling

B cells are a component of adaptive immunity, specialized in the recognition of antigens (Yuseff, Pierobon et al. 2013). To carry out their function, B cells express a B cell receptor (BCR) at the cell surface. This is composed of an antigen-recognition subunit, the membrane immunoglobulin (Ig), and an Igα/Igβ heterodimer. The latter contains an immunoreceptor tyrosine-based activation motif (ITAM) at the cytoplasmic tail of each Ig, which is responsible for signal transduction (Reth 1989, Dal Porto, Gauld et al. 2004). Binding of antigen to the BCR drives its aggregation in lipid rafts (Pierce 2002). These domains are rich in Src family kinases, which phosphorylate the tyrosine residues of the ITAMs creating docking sites that allow the recruitment and activation of the Syk kinase. In turn, this recruits several cellular signaling proteins such as: Vav, phosphoinositide 3-kinase (PI3K) and phospholipase C-γ2 (PLCγ2). These proteins contain SH2 and/or SH3 domains that allow them to interact with other proteins and with each other. The outcome is the formation of a signalosome that will impact several signaling pathways. The cytosolic tail of CD19, a member of the B cell co-receptor, also contains tyrosine residues that are phosphorylated and interact with cellular signaling proteins, further enhancing BCR signaling (Dal Porto, Gauld et al. 2004, Harwood and Batista 2008).

The PI3K pathway leads to the production of PIP3 and recruitment and activation of the serine/threonine kinase Akt, which interacts with proteins and transcription factors that control apoptosis, promoting B cell survival (Andjelkovic, Alessi et al. 1997). Moreover, Akt interacts with nuclear transcription factor NF-κB, which upregulates genes involved in B cell development and proliferation (Okkenhaug and Vanhaesebroeck 2003). Activation of PLCγ2 results in the cleavage of phosphoinositide PIP2 into the second messengers IP3 and DAG, which promote the mobilization of calcium and the activation of mitogen-activated protein kinases (MAPK), respectively. These events promote the activation of the transcription factors NFAT and NF-κB, ultimately contributing to B cell proliferation and differentiation (Niiro and Clark 2002). Vav proteins promote GDP/GTP exchange on Rho/Rac proteins which, when activated, promote changes in intracellular pathways related to cytoskeletal change, mitogenesis and cell survival (Etienne-Manneville and Hall 2002). Vav proteins also play in role in the activation of the before mentioned signaling

pathways, PLCγ2 and PI3K pathways, and it modulates the activity of the NFAT and NF-κB transcription factors (Bustelo 2000, Turner and Billadeau 2002).

1.4.2 EBV LMP1 and LMP2A proteins

LMP1 is a transmembrane protein, encoded by the first ORF of the EBV genome, that localizes to lipid rafts. It has a short amino terminus, six transmembrane-spanning domains and a 199-amino acid long cytoplasmic tail (Damania 2004, Brinkmann and Schulz 2006). Functionally, this viral protein mimics the CD40 receptor, which promotes B cell survival and proliferation, GC and memory B cell differentiation, isotype switching and affinity maturation (Bishop and Hostager 2003). In contrast to CD40, which requires binding to the ligand CD154 present in T_H cells to be activated, LMP1 is a constitutively active receptor molecule that does not require the presence of specific extracellular signals (Gires, Zimber-Strobl et al. 1997, Kilger, Kieser et al. 1998). This ability was shown to be dependent on the transmembrane domains of the protein (Yasui, Luftig et al. 2004), which allow ligand-independent oligomerization, trafficking to membrane lipid rafts and constitutive C-terminal tail signaling. The cytoplasmic tail of LMP1 is divided into two C-terminal activation regions, CTAR1 and CTAR2, also termed transformation effector sites, TES1 and TES2. These regions are involved in the interaction with tumor-necrosis factor (TNF)-receptor-associated factors (TRAFs) and TNF-receptor-associated death domains (TRADDS), resulting in the activation of NF-κB. This, in turn, is responsible for the ability of LMP1 to induce immortalization of human primary B lymphocytes (Devergne, Hatzivassiliou et al. 1996). LMP1 was also described to activate the PI3K pathway (Dawson, Tramountanis et al. 2003), associated with suppression of apoptosis and cell survival, the mitogen-activated protein kinase (MAPK) pathway and the interferon-regulatory factor 7 (IRF7) pathway. The latter is known to up-regulate LMP1 expression, constituting a positive feedback circuit (Ning, Hahn et al. 2003). Furthermore, LMP1 activates the JNK pathway (Eliopoulos and Young 1998), which can lead to the expression of proteins involved in cell proliferation and transformation, linking the ability of the viral protein to modulate cell signaling with its ability to promote cell transformation. Concomitantly, LMP1 is expressed in latently-infected B cells in transplant lymphoma, nasopharyngeal carcinoma and Hodgkin's disease and its expression *in vivo* is associated with an increased frequency of B cell lymphomas (Uchida, Yasui et al. 1999). Furthermore, LMP1 can transform rodent fibroblasts, which can generate multiple tumors upon injection into nude mice (Wang, Liebowitz et al. 1985), and its expression is essential for the immortalization of primary human B lymphocytes (Dawson, Rickinson et

al. 1990, Kaye, Izumi et al. 1993). Its expression has also been detected during the lytic cycle of infection, in epithelial and B cells (Boos, Berger et al. 1987, Contreras-Salazar, Ehlin-Henriksson et al. 1990). Collectively, the functions of LMP1 described above indirectly promote the activation, survival, proliferation and transformation of EBV-infected cells (Damania 2004, Brinkmann and Schulz 2006). Furthermore, the ability to mimic the CD40 receptor suggests that LMP1 renders the infected B cell independent of T cell help.

The LMP2 gene of EBV, located at the 3' end of the genome, is transcribed into two mRNAs that share exons 2-9 and give rise to the two isoforms LMP2A and LMP2B. LMP2A is a transmembrane protein that localizes to lipid rafts and consists of a short C-terminal domain, 12 transmembrane-spanning domains and a 119 amino acid-long N-terminal domain. The latter contains eight tyrosine residues, two of which form an ITAM, and multiple PXXP motifs, which are responsible for the molecular functions of the protein. The LMP2B isoform lacks the N-terminal domain found in LMP2A (Damania 2004, Brinkmann and Schulz 2006, Kempkes and Robertson 2015). Through the tyrosines present in the N-terminal domain, LMP2A is able to bind to the tyrosine kinase Lyn, a member of the Src family. This, in turn, phosphorylates the tyrosine residues within the ITAM resulting in the recruitment of another tyrosine kinase, Syk. By binding to these kinases and by preventing the BCR from entering lipid rafts, LMP2A inhibits BCR signaling (Thorley-Lawson 2001, Brinkmann and Schulz 2006, Rovedo and Longnecker 2008). Moreover, through the PXXP motifs present in the N-terminal domain, LMP2A interacts with WW domains of several members of the Nedd4-like ubiquitin protein ligase family, resulting in the ubiquitination and degradation of LMP2A and LMP2A-associated proteins, contributing to BCR inhibition (Ikeda, Ikeda et al. 2000). Since binding of specific antigen to the BCR has been associated to virus reactivation from latency, LMP2A inhibition of BCR signaling is an important mechanism for the maintenance of the latency pool. Signal transduction following binding of specific antigen to the BCR results in the activation of growth-promoting signaling cascades. Blocking this mechanism would therefore negatively impact B cell survival. However, expression of LMP2A was found to be capable of replacing the survival signal usually provided by the BCR. This was observed *in vivo* when expression of LMP2A was able to rescue B cells from death, driving those cells out of the bone marrow to the periphery in BCR-deficient transgenic mice (Caldwell, Wilson et al. 1998). This function of LMP2A is most likely due to the activation of the PI3K pathway, which results in AKT activation (Fukuda and Longnecker 2004). Among other outcomes, AKT results in inhibition of apoptosis, therefore promoting B cell survival. Collectively, results indicate that LMP2A may both mimic and inhibit active BCR signaling.

The C-terminal domain of LMP2A mediates the homodimerization and heterodimerization of LMP2 protein isoforms (Cen and Longnecker 2015). Binding of LMP2B to that region of LMP2A prevents its phosphorylation and restores normal BCR signaling (Rovedo and Longnecker 2007). As an outcome, EBV latently-infected cells are more prone to switch to lytic infection (Rechsteiner, Berger et al. 2008). Like LMP1, LMP2A expression is detected in latently-infected B cells in transplant lymphoma, nasopharyngeal carcinoma and Hodgkin's disease. Although initially thought to not be an oncogenic protein (Kim and Yates 1993), more recent studies have shown that expression of LMP2A results in cell transformation (Scholle, Bendt et al. 2000, Fukuda and Longnecker 2007, Fukuda and Kawaguchi 2014). Summarizing, LMP2A ensures latency maintenance by inhibiting B cell activation through BCR signaling and, at the same time, promoting B cell survival.

1.4.3 KSHV K1 and K15 proteins

Similar to EBV LMP1, K1 is a transmembrane protein encoded by the first ORF of the KSHV genome. It contains an N-terminal extracellular domain, a single transmembrane region and a short C-terminal cytoplasmic tail (Lagunoff and Ganem 1997, Damania 2004, Brinkmann and Schulz 2006). The extracellular domain has a high degree of amino acid sequence variability and is implicated in K1 oligomerization (Lee, Veazey et al. 1998, Lagunoff, Majeti et al. 1999). Structurally, K1 resembles the Igα/Igβ heterodimer. In agreement, the cytoplasmic tail contains a functional ITAM that allows signal transduction in a constitutive manner (Lee, Guo et al. 1998, Lee, Veazey et al. 1998, Lagunoff, Majeti et al. 1999). Specifically, two phosphorylated tyrosines of the ITAM allow binding to SH2-containing molecules and, consequently, the assembly of a signalosome that includes Lyn, Syk, p85α subunit of PI3K, PLCγ2, RasGAP120, Vav1/3 and the protein tyrosine phosphatases SHP1/2 (Lee, Lee et al. 2005). Signal transduction then induces calcium mobilization, tyrosine phosphorylation of cellular kinases and activation of the transcription factors NF-κB, NFAT and AP-1, all indicative of lymphocyte activation (Lee, Veazey et al. 1998, Lagunoff, Majeti et al. 1999, Prakash, Tang et al. 2002). Binding of K1 to the p85α subunit of PI3K results in Akt activation. Furthermore, in B cells, K1 was found to inactivate the negative regulator of the PI3K/Akt pathway, PTEN. Accordingly, K1 protects the infected cell from FKHR- and FAS-mediated apoptosis (Lee, Guo et al. 1998). K1 expression is also described to induce the expression of cytokines (Lee, Lee et al. 2005). Further studies have shown that K1 is internalized via clathrin-mediated endocytosis. Blocking this phenomenon prevents K1-mediated activation of the PI3K/Akt pathway demonstrating that, even though K1 is a transmembrane protein, internalization is

required for its signaling function (Tomlinson and Damania 2008, Sousa-Squiavinato, Silvestre et al. 2015). Similar to LMP2A, K1 downregulates BCR expression at the cell surface, inhibiting normal signaling from the BCR. However, the mechanisms used by the two proteins are different. The extracellular domain of K1 induces the retention of BCR subunits in the endoplasmic reticulum by interacting with the μ chains of the BCR complex (Lee, Alvarez et al. 2000). Summarizing, the known functions of K1 suggest that it promotes the proliferation and survival of the infected cells and, at the same time, inhibits normal BCR signaling, as described for LMP2A.

K1 expression is detected in PELs, MCD and KS lesions (Damania 2004). Like LMP1, K1 is an oncogenic protein able to induce transformation *in vitro* and cell proliferation *in vivo*. Transgenic K1 mice, for example, develop spindle-cell sarcomas and malignant plasmablastic lymphomas (Prakash, Tang et al. 2002, Prakash, Swamy et al. 2005). In contrast to the EBV latent membrane proteins LMP1 and LPM2A, K1 appears to be primarily expressed during lytic replication. Despite the functional characterization of K1 described above, the *in vivo* role of the protein is not fully understood. Given the apparent restriction of K1 to lytic infection, its role in disease may be related to paracrine effects of the expression of cellular cytokines induced by the viral protein, upon virus reactivation from latency. However, a role for K1 in latent infection cannot be excluded since there are some reports that show K1 is expressed at low levels during latent infection (Cousins and Nicholas 2014).

Similar to EBV LMP2A, K15 protein localizes to lipid rafts and is coded by a multiply spliced gene located at the 3’ end of the KSHV genome that originates different isoforms. These differ in the number of transmembrane domains, which ranges from four to twelve, and have in common a cytoplasmic tail at the C-terminal end. The latter contains several putative signaling motifs, namely: one SH3-binding motif, two SH2-binding sites and a TRAF binding site (Glenn, Rainbow et al. 1999, Choi, Lee et al. 2000, Brinkmann, Glenn et al. 2003). Although different in sequence, K15 is structurally and functionally similar to LMP1 and LMP2A. Like LPM1, K15 interacts with TRAF proteins, activating MAPKs and ultimately leading to activation of the transcription factors NF-κB and AP-1 (Glenn, Rainbow et al. 1999, Brinkmann, Glenn et al. 2003). Furthermore, through its cytoplasmic tail, K15 interacts with Hax-1, inhibiting Bax-induced apoptosis (Sharp, Wang et al. 2002). K15 is also able to recruit Src family kinases which, in turn, are responsible for a constitutive phosphorylation of the tyrosine residues present at its cytoplasm tail. Like LMP2A, by interacting with Src family kinases, K15 reduces their availability to the Igα/Igβ complex, resulting in BCR downregulation. Moreover, due to its localization, it is possible

that K15 is able to block BCR entry to lipid rafts, contributing to the inhibition of normal signaling downstream of the BCR (Choi, Lee et al. 2000, Brinkmann, Glenn et al. 2003). Like with LMP2A, this strategy may be related to latency maintenance, as KSHV reactivation from latency has also been associated to the activation of the infected cell. K15 expression is also related to cell motility, achieved through the induction of expression of microRNAs miR-21 and miR-31, a function that may contribute to KSHV-mediated tumor metastasis (Tsai, Wu et al. 2009). *In vivo*, K15 function is not yet fully understood. In part, this is due to the difficulty in understanding when K15 is expressed, which has been associated with both lytic (Glenn, Rainbow et al. 1999, Choi, Lee et al. 2000) and latent infection (Sharp, Wang et al. 2002). One of the studies that links K15 expression to lytic infection also shows that the viral protein is capable of inducing the expression of multiple cytokines and chemokines (Brinkmann, Pietrek et al. 2007). Summarizing, K15 promotes the proliferation and survival of the infected cells by activating specific pathways and, at the same time, may inhibit normal BCR signaling and, therefore, virus reactivation from latency.

1.5 MuHV-4 M2 protein

M2 was initially classified as a latency-candidate protein due to the genomic position of its coding gene, homologous to the position of genes that code for latency proteins in other gammaherpesviruses (Virgin, Latreille et al. 1997, Virgin, Presti et al. 1999). This idea was reinforced when M2 transcripts were detected by reverse transcriptase PCR in the latently infected murine B cell lymphoma line S11 and in splenocytes obtained from mice, intranasaly infected with MuHV-4, during the establishment of latency (Husain, Usherwood et al. 1999). Moreover, no M2 transcripts were detected in lyticaly infected fibroblasts (Husain, Usherwood et al. 1999, Virgin, Presti et al. 1999). Initial long-term *in vivo* studies demonstrated that, following intranasal inoculation with MuHV-4, *M2* is expressed in GC B cells and memory B cells (Flano, Kim et al. 2002). Further studies on the establishment of latency in the spleen confirmed that *M2* gene is expressed in GC B cells and demonstrated that it is also expressed in DCs and other B cell subsets, namely: marginal zone B cells and follicular B cells (Flano, Kim et al. 2002, Marques, Efstathiou et al. 2003). In agreement with M2 being a latency-associated protein, expression of *M2* is not detected in macrophages (Marques, Efstathiou et al. 2003), a population shown to be lyticaly infected (Frederico, Chao et al. 2014).

The *M2* gene is composed of two exons that, upon splicing, produce a unique 192 amino acid-long protein, which bears no discernable homology to any other known cellular or pathogen protein (Husain, Usherwood et al. 1999). Although it has no obvious conserved domains or intracellular localization signals, examination of its primary structure revealed the presence of eight proline-rich regions and three tyrosine residues, two of which correspond to phosphorylation sites that are part of a motif recognized by Src family kinases (Rodrigues, Pires de Miranda et al. 2006) (Figure 1.5). M2 also contains an epitope that is recognized by $CD8^+$ T cells from BALB/c ($H2^d$) mice but not from C57BL76J ($H2^b$ mice), and is therefore an $H2K^d$-restricted epitope (Husain, Usherwood et al. 1999).

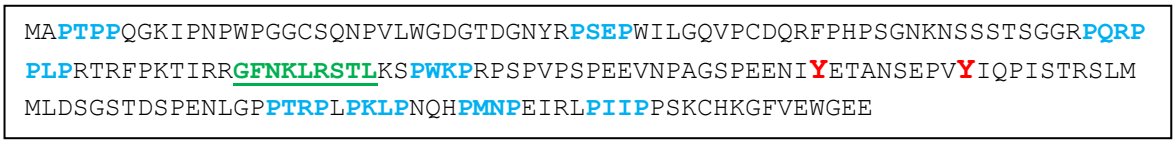

Figure 1.5. Primary sequence of the M2 protein. The proline residues organized in PxxP motifs (P represents a proline residue and x any amino acid) are shown in blue, the H2Kd-restricted epitope is shown in green and underlined and two tyrosine residues with the potential to be phosphorylated by kinases are shown in red.

To specifically address the role of M2 in MuHV-4 pathogenesis different groups constructed M2-deficient recombinant viruses, revealing that M2 plays an important role in both latency establishment and reactivation from latency (Jacoby, Virgin et al. 2002, Macrae, Usherwood et al. 2003, Herskowitz, Jacoby et al. 2005). Concomitant with M2 being a latency-associated protein, all three studies demonstrated that the lack/deficiency of M2 has no impact in the lytic infection that develops in the lungs following intranasal inoculation. *Jacoby el al* observed a decrease in the establishment of latency in the spleen at 16 days post intranasal inoculation of C57BL/6J mice with MuHV-4. Moreover, the authors demonstrated that the mutant virus also has an inefficient reactivation from latency, when compared to the WT virus. Long-term infection was similar for both WT and M2 mutant viruses suggesting that M2 is more important in the initial stages of latency establishment. Strikingly, following intraperitoneal infection, no differences in latency establishment nor reactivation from latency were observed. However, a second study performed by the same group showed that, by decreasing the virus dose administered intraperitoneally, it is possible to reproduce the defects in latency establishment observed via the intranasal route (Herskowitz, Jacoby et al. 2005). This demonstrated that M2 plays a role in latency establishment, independently of the administration route. *Macrae et al* also observed the impairment in latency establishment following intranasal inoculation of

BALB/c mice, confirming the previous results. In contrast with the previous experiments, long-term infection with the M2 mutant virus led to higher frequencies of infection, when compared to WT levels. Furthermore, these authors showed that, in B cells, the M2 protein is predominantly localized in the cytoplasm and plasma membrane (Macrae, Usherwood et al. 2003).

The studies described above were performed in total splenocytes. A more detailed study from our group addressed the role of M2 in the establishment of latency in different B cell subsets (Simas, Marques et al. 2004). Infection of BALB/c mice with a M2 frame-shift mutant virus (M2FS) resulted in a reduced number of infected splenic follicles, as analyzed by *in situ* hybridization on spleen sections. However, the mean number of infected cells per infected follicle was equivalent between M2FS and WT viruses. Together, these observations indicate that M2 is required for an efficient colonization of splenic follicles but is dispensable for the expansion of latently infected cells within infected follicles. Analysis of the frequency of virus genome-positive cells in total, GC and memory B cells revealed lower frequencies of infection in all of the populations analyzed in M2FS-inoculated mice, when compared to WT. At late times post infection, 50 and 70dpi, the absence of M2 resulted in an increased and sustained infection of GC B cells. Concomitantly, the percentage of infected follicles as well as the percentage of infected cells per infected follicle were increased in M2FS-infected mice. The fact that these increased latency levels did not result in an increased infection of memory B cells suggested that M2 is important for an efficient differentiation of infected GC B cells into memory B cells and/or termination of the GC reaction.

As demonstrated by the studies described above, long term latency levels in M2-deficient virus infection are dependent on the host H2 haplotype. While inoculation of C57BL/6J mice ($H2K^b$) results in low levels of infection, equivalent to WT infection (Jacoby, Virgin et al. 2002), inoculation of BALB/c mice ($H2K^d$) is associated with increased long term latent loads (Macrae, Usherwood et al. 2003, Simas, Marques et al. 2004). This is the result of an immunological effect, rather than abrogation of the M2 functions. As mentioned before, M2 protein contains an $H2K^d$-restricted epitope that is recognized by $CD8^+$ T cells of BALB/c mice. In infection of these mice with M2-deficient viruses, infected cells cannot be recognized by $CD8^+$ T cells and their proliferation is not controlled. In agreement, a study performed by our lab, has shown that mutation of the epitope anchor residues, which allow binding of the epitope to MHC-I molecules and consequent presentation to $CD8^+$ T cells, leads to increased viral loads (Marques, Alenquer et al. 2008).

The fact that M2 seemed to be important to drive the differentiation of GC B cells into memory B cells allied to the localization of M2 in the cytoplasm and plasma membrane of B cells, raised the possibility of M2 having a role in signaling. In order to characterize the molecular function of the M2 protein, several biochemical assays were conducted by different groups.

The first *in vitro* study confirmed the previous observation that M2 localizes to the cytoplasm and plasma membrane of lymphocytes. Furthermore, it showed that M2 localization is cell type dependent, as the protein localized to the nucleus in infected epithelial cells and fibroblasts (Liang, Shin et al. 2004). *Liang et al* also showed that M2 is able to interact with the cellular p32 acidic protein promoting its translocation to the nucleus, which contributed to the downregulation of STAT1 and STAT2 proteins, thereby inhibiting the IFN-α/β- and IFN-γ-mediated transcriptional activation. The same authors also found that M2 suppresses DNA damage induced apoptosis (Liang, Pickering et al. 2006). Viral replication is sensed by the host cell as DNA damage stress, which promotes a DNA damage signal transduction that ultimately leads to cell apoptosis. By interacting with the DDB1/COP9/cullin DNA repair system and the ATM DNA damage signal transducer, M2 was able to inhibit that response. Collectively, these two studies suggest that M2 may be protecting the latently infected cells from elimination by affecting two defense mechanisms of host innate immunity, the IFN-mediated antiviral pathway and DNA damage induced apoptosis. However, the relevance of these functions has not been confirmed *in vivo*.

Through yeast two-hybrid screen, the signaling molecule Vav1 was the first to be found to interact with M2 (Madureira, Matos et al. 2005). The same study also demonstrated that M2 similarly binds Vav2 but not Vav3. Further studies performed by our group allowed the identification of other binding partners of M2 (Rodrigues, Pires de Miranda et al. 2006, Pires de Miranda, Alenquer et al. 2008, Pires de Miranda, Lopes et al. 2013). At the core of these interactions are a C-terminal proline-rich SH3 binding region and two closely spaced tyrosine residues of M2 (Y^{120} and Y^{129}) (Figure 1.5). The first is responsible for the interaction of M2 with Src family kinases, which in turn is crucial for the juxtamembranar localization of M2 in B cells and the consequent phosphorylation of the mentioned tyrosine residues. The latter constitute an unconventional ITAM, where each phosphomotif binds directly and selectively to several cellular SH2 containing signaling molecules, namely: Fyn, Lyn, Vav1, NCK1, PLCγ2, the p85α subunit of PI3K and the tyrosine phosphatase SHP2 (Rodrigues, Pires de Miranda et al. 2006, Pires de Miranda, Lopes et al. 2013). Surprisingly, functional analysis of some of the mentioned interactions revealed that they

do not point to the same outcome. On the one hand, M2 interaction with the Fyn/Vav pathway leads to the activation of Vav1. Furthermore, M2 drives tyrosine phosphorylation of PLCγ2. On the other hand, M2 expression leads to inhibition of AKT activation upon BCR stimulation, a kinase that is linked to proliferation, survival and differentiation in B cells. However, it is possible that this inhibitory effect is compensated by the activation of Vav1 and PLCγ2. Summarizing, M2 acts as a modulator protein, mediating the assembly of multiprotein complexes with cell signaling proteins. This ability is lost upon mutation of the tyrosine residues (M2Y mutant protein). *In vivo* work as demonstrated the physiological importance of the unconventional ITAM for the establishment of latency. Intranasal infection with a recombinant virus, designated M2Y, where the tyrosine residues were mutated to phenylalanines, resulted in a delay in latency establishment (Pires de Miranda, Alenquer et al. 2008). This was characterized by a deficit in latent infection levels and splenic follicle colonization at the latency peak (14dpi). Maximal levels of GC infection were only observed at 21dpi. Long term comparison between the levels of infection of WT and M2Y viruses showed no differences, indicating that the unconventional ITAM of the M2 protein is not important for the maintenance of long term latency. Biochemical dissection of the interactions carried out by each tyrosine residue has shown that they are differentially required. More recently, *in vivo* analysis of the phosphomotifs revealed that only Y^{129} is critical for reactivation from latency and plasma cell differentiation (Rangaswamy, O'Flaherty et al. 2014).

M2 was also shown to drive IL-10 dependent B cell proliferation and survival, both *in vitro* and *in vivo* (Madureira, Matos et al. 2005, Siegel, Herskowitz et al. 2008). Further *in vitro* work provided insight on the possible mechanism behind the upregulation of IL-10 (Rangaswamy and Speck 2014). Expression of M2 activated the NFAT pathway in a Src kinase-dependent manner leading to the induction of IRF4. This, in turn, is able to regulate the IL-10 promoter in B cells. Manipulation of IL-10 expression may be a common strategy among gammaherpesviruses, as EBV not only encodes an IL-10 homolog but it also encodes a protein, LMP2A, that upregulates IL-10 production in mitogen-stimulated primary B cells and B cell lymphomas, promoting the survival of these cells (Incrocci, McCormack et al. 2013).

Analysis of cell surface markers in M2-transduced B cells suggested that M2 expression leads to B cell activation and differentiation similar to a functional activated, pre-plasma memory B cell phenotype (Siegel, Herskowitz et al. 2008, Liang, Collins et al. 2009). Plasma cells have been linked to virus reactivation from latently infected cells. In agreement to M2 promoting B cell differentiation into plasma cells, infection of mice with a

M2-null mutant virus results in the absence of virus infected plasma cells at the latency peak. Therefore, M2 may be responsible for virus reactivation from latency, by manipulating plasma cell differentiation (Siegel, Herskowitz et al. 2008, Liang, Collins et al. 2009).

Collectively, studies of M2 have classified it as a B cell signaling modulator protein. M2 is, therefore, a putative functional homologue of the transmembrane proteins LMP1 and LMP2A encoded by EBV, and K1 and K15 encoded by KSHV, which either mimic or interfere with BCR signaling (Damania 2004). Contrarily to these proteins, M2 is a cytosolic protein that is not known to be tumorigenic.

1.6 Aims

Successful colonization of the host by gammaherpesviruses requires proliferation and access to the memory B cell compartment, attained through GC reactions. Interaction with T_H cells provides the B cell with proliferation and survival signals and is required for GC initiation in T cell-dependent responses. T_H cells are required for normal levels of MuHV-4 latent infection. B-T_H cell interaction is, therefore, a possible target of virus manipulation. The M2 protein is able to assemble multiprotein complexes with cell signaling proteins through an unconventional ITAM and is required for a normal establishment of latency. Therefore, the main aim of this thesis was to assess whether the molecular functions of M2 allowed it to beneficially modulate B-T_H cell interaction. This possibility was analyzed *in vitro*, in the context of a peptide-specific system. Another aim of this thesis was to address this possibility *in vivo*, in the context of an immune response to T cell-dependent stimulus.

Abrogation of the ability of M2 to assemble multiprotein complexes with cell signaling proteins (M2Y virus) results in a delay in latency establishment and spleen colonization. The stages of splenic infection with MuHV-4 are now well characterized. Using that knowledge, the final aim of this thesis was to identify the step of spleen colonization where M2Y virus is delayed.

CHAPTER 2

M2 PROMOTES THE FORMATION OF B-T HELPER CELL CONJUGATES

2 M2 PROMOTES THE FORMATION OF B-T HELPER CELL CONJUGATES

2.1 Introduction

Gammaherpesvirus latent infection of circulating memory B cells is crucial to persistence and hence disease ontogeny. To access the memory B cell compartment gammaherpesviruses take advantage of germinal center (GC) reactions (Simas and Efstathiou 1998, Flano, Kim et al. 2002, Kim, Flano et al. 2003, Willer and Speck 2003, Roughan and Thorley-Lawson 2009, Barton, Mandal et al. 2011, Thorley-Lawson, Hawkins et al. 2013). In the case of MuHV-4, at the latency peak (14dpi), it has been estimated that 70% of the infected B cells have a GC phenotype (Collins, Boss et al. 2009), which suggests some modulation of this route by the virus.

T cell help is critical for the initiation of a GC reaction in T cell-dependent immune responses. Before engaging in a cognate interaction with a B cell that will lead to its activation, proliferation and establishment of a GC (Allen, Okada et al. 2007), T helper (T_H) cells scan for the highest affinity with particular antigen-presenting cells (APC). Such transient interactions occur in the border area between follicles and T cell zones and are mediated by adhesion molecules, resulting in the formation of B-T_H cell conjugates. Upon peptide recognition, the formation of an organized signaling structure, the immunological synapse (IS), takes place (Grakoui, Bromley et al. 1999). This process has been shown to be highly dynamic as T cells can interact with several APCs simultaneously, selectively polarizing towards the strongest stimulus (Depoil, Zaru et al. 2005). Typically, an IS is composed of spatially separated supramolecular activation clusters (SMACs), which contain TCR-CD3/MHC II partners, co-stimulatory molecules and cell adhesion molecules (Monks, Freiberg et al. 1998, Grakoui, Bromley et al. 1999, Huppa and Davis 2003). Besides this reorganization at the cellular surface level, T cells also undergo morphological and cytoskeletal changes. Filamentous actin (F-actin) forms a ring that surrounds the previously mentioned structures (Le Floc'h and Huse 2015).

MuHV-4 is known to exploit normal splenic immune communication routes, eventually reaching follicular B cells (Frederico, Chao et al. 2014). At this pre-GC stage, the ability of the infected follicular B cells to attract T cell help would be a major advantage for these viruses. In fact, importance of T cell help is reflected in studies that show defects in *in vivo* B cell activation (Stevenson and Doherty 1999) or demonstrate lower latency levels in the

absence of $CD4^+$ T cells (Ehtisham, Sunil-Chandra et al. 1993, Usherwood, Ross et al. 1996) or T follicular helper cells (T_{FH}) (Collins and Speck 2014).

To investigate if MuHV-4 had the ability to modulate B-T_H cell interactions, the latency-associated M2 protein was chosen as a potential candidate. Although no sequence homology is known for this protein, M2 is a putative functional homologue of the transmembrane proteins LMP1 and LMP2A encoded by EBV, and K1 and K15 encoded by KSHV, which either mimic or interfere with BCR signaling (Madureira, Matos et al. 2005, Rodrigues, Pires de Miranda et al. 2006, Pires de Miranda, Alenquer et al. 2008). Contrarily to these proteins, M2 is a soluble cytoplasmic protein expressed in B cells (Marques, Efstathiou et al. 2003), where it localizes to juxtamembranar areas of the cell (Macrae, Usherwood et al. 2003, Liang, Shin et al. 2004, Pires de Miranda, Lopes et al. 2013). It contains two phosphosites (tyrosine residues Y^{120} and Y^{129}), that are constitutively phosphorylated by Src family kinases (Rodrigues, Pires de Miranda et al. 2006, Pires de Miranda, Alenquer et al. 2008), that form an unconventional ITAM. This ITAM is implicated in M2 ability to work as a modulator protein, coordinating the assembly of multiprotein complexes with cell signaling proteins, namely NCK1, Vav1, PLCγ2, the tyrosine phosphatase SHP2 and the p85α subunit of PI3K (Pires de Miranda, Lopes et al. 2013). Therefore, just like its putative functional homologues, M2 mediates the assembly of specific signalosomes. Mutation of the phosphosites *in vitro* results in the loss of such ability. *In vivo*, M2 is important for latency establishment and efficient proliferation of infected GC B cells (Jacoby, Virgin et al. 2002, Macrae, Usherwood et al. 2003, Simas, Marques et al. 2004). Infection of mice with a virus encoding the M2Y mutant (designated vM2Y, with Y^{120} and Y^{129} residues mutated to phenylalanine) results in a delay in latency establishment (Pires de Miranda, Alenquer et al. 2008).

Preliminary data, obtained by Dr. Filipa Lopes in the framework of this project, revealed that in the context of an MHC class II-restricted OVAp-specific system, where M2-expressing B cells presenting OVAp are placed in contact with OVAp-specific $CD4^+$ T cells, M2 polarizes to the B-T_H cell contact zone and promotes an incomplete polarization of the B cell MTOC to that interface. Given all of the above, the ability of the latency-associated M2 protein to modulate B-T_H cell interaction was investigated. To control the requirement of the assembly of a signalosome in such modulation, the M2Y mutant protein was included as a control. M2 was first analyzed for its ability to upregulate cell surface molecules involved in B-T_H cell interaction. Subsequently, expression of M2 was tested for the ability to promote the formation of B-T_H cell conjugates, in the context of an MHC class II-restricted OVAp-specific system.

2.2 Results

2.2.1 The A20 B cell-TCR Tg DO11.10 CD4⁺ T cell system

T_H cells interact with B cells while scanning for the highest affinity, forming conjugates. Upon cognate interaction, the formation of an organized signaling structure, the IS, takes place. To address B-T_H cell interaction, a MHC class II-restricted OVAp-specific in vitro cellular system was chosen. This system comprises A20 B cells and primary transgenic CD4⁺ T cells, that have a TCR with specificity for the ovalbumin peptide (OVAp, ISQAVHAAHAEINEAGR, aa 323-339). These primary cells were purified by negative selection (MACS, Miltenyi Biotech) from the spleen of Balb/c DO11.10 mice, as described in detail in section 7.2.3.2. Flow cytometric analysis of the initial splenocyte suspension, in parallel with the purified population, confirmed the enrichment in CD4⁺ T cells (Figure 2.1). CD4⁺ T cell purity was consistently above 90%.

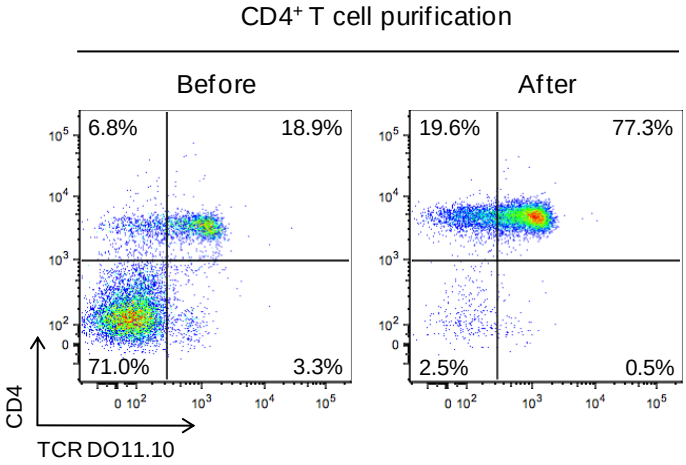

Figure 2.1. Flow cytometric analysis of DO11.10 CD4⁺ T cell purity. Briefly, CD4⁺ T cells were purified from the spleen of DO11.10 mice, using a negative selection kit (MACS, Miltenyi Biotec), according to manufacturer's instructions. A fraction of the splenocyte suspension (before) and a fraction of the purified population (after) were stained with anti-CD4 and anti-TCR DO11.10 antibodies and analyzed on a LSR Fortessa flow cytometer (BD Biosciences). The percentage of cells in each quadrant is shown. CD4⁺ T cell purity was consistently above 90%.

Following purification, CD4⁺ T cells were stimulated by incubation with Dynabeads® Mouse T-activator CD3/CD28 (Invitrogen) and 60U/mL of mrIL-2. To ensure that B-T_H cell interaction observations resulted from the specific interaction with B cells and not from the activated state of the T_H cells, Dynabeads® were removed from T cell culture for a resting period, prior to cell use in B-T_H cell interaction analysis. To decide on the duration of this

resting period, T cell death and TCR down-regulation were monitored by flow cytometry (Figure 2.2 and Table 2.1). As expected, T cell size and complexity, as assessed by FSC and SSC parameters, decreased with time resulting in a well-defined cellular population (Figure 2.2A). This was accompanied by a downregulation of the transgenic TCR, visible from day 5 onwards as a decrease in the percentage of double positive events (Figure 2.2B). Such downregulation was also observed as a decrease in TCR mean fluorescence intensity (MFI) (Figure 2.2C).

The use of propidium iodide, a cell viability dye, showed an increase in cellular death with time (Figure 2.2A). To investigate if adding a higher amount of mrIL-2 to the culture, during the resting period, could improve T cell survival, the use of 90 and 120U/mL of mrIL-2 was tested in parallel with the initial 60U/mL, in cells purified from two spleens (Table 2.1). Results showed that an increased IL-2 concentration did not significantly impact cell survival. For that reason, primary $CD4^+$ T cells were cultured with 60U/mL of mrIL-2 throughout this study. Furthermore, the use of T cell populations purified from the spleens of two independent mice showed that variability among individuals is to be expected.

Collectively, results showed that the choice of the duration of the resting period was a balance between $CD4^+$ T cell resting and T cell death. For flow cytometric analysis, cells were rested for seven to eight days, since dead or dying cells could be easily excluded from analysis. For confocal microscopy analysis, T cells were rested for five days. This timepoint was chosen because the cells had already decreased in size and complexity, there was a visible downregulation of the TCR, and it was still possible to recover 25-40% of live cells. Live resting $CD4^+$ T cells were then sorted prior to their use (Figure 2.3). Purity of the sorted T cell population was assessed by flow cytometry and was consistently above 96% (Figure 2.3, *post-sort*).

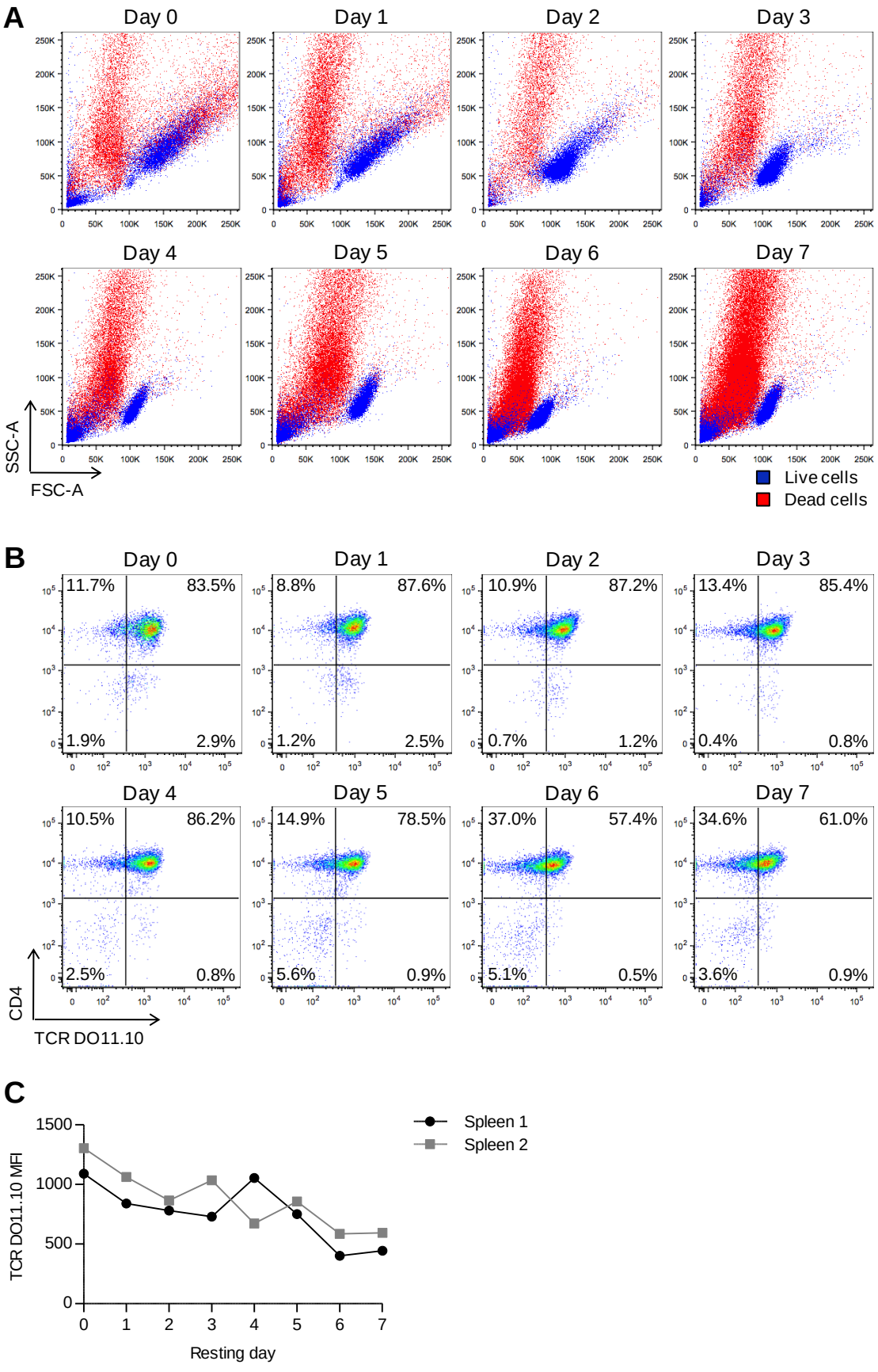

Figure 2.2. Analysis of a CD4⁺ T cell population during the resting period. Please see figure legend on the next page.

Figure 2.2. Analysis of a CD4⁺ T cell population during the resting period. CD4⁺ T cells were purified from two spleens of DO11.10 mice (spleen 1 and 2), using a negative selection kit (MACS, Miltenyi Biotec). Cells were stimulated by incubation with Dynabeads® Mouse T-activator CD3/CD28 (Invitrogen), according to manufacturer's instructions. After three days of stimulation, Dynabeads® were removed to initiate the resting period (day 0) and cells were cultured in 24-well plates ($1x10^6$ cells/well) in the presence of 60U/mL of mrIL-2. On each resting day, cells were collected from a different well for analysis. Representative FACS plots shown correspond to spleen 1. (A) Cells were stained on each resting day with propridium iodide to allow the discrimination between live (blue) and dead (red) cells. (B) and (C) Cells were stained on each resting day with anti-CD4 and anti-TCR DO11.10 antibodies, to assess TCR downregulation. (B) The percentage of cells in each quadrant is shown. (C) TCR DO11.10 mean fluorescence intensity (MFI) for both spleens on each resting day. This experiment was performed by me in collaboration with Dr. Sofia Marques.

Table 2.1. Percentage of live CD4⁺ T cells during the resting period. Percentage of live cells identified in Figure 2.2A. was analyzed using FlowJo (Tree Star, Inc.).

		Resting day							
Spleen[a]	**IL-2 (U/mL)[b]**	**0**	**1**	**2**	**3**	**4**	**5**	**6**	**7**
1	**60**	64.6	57.0	65.2	55.8	50.6	41.9	28.2	17.5
	90	64.6	54.7	67.7	57.9	53.1	45.6	29.9	17.3
	120	64.6	-	-	58.0	-	43.5	30.8	18.3
2	**60**	66.0	50.3	67.2	39.7	30.5	27.8	17.7	9.3
	90	66.0	51.1	69.8	40.7	31.5	25.7	15.4	8.9
	120	66.0	-	-	-	-	25.0	17.6	15.2

[a] Two independent spleens were analyzed.
[b] Three IL-2 concentrations were tested.
- Analysis not performed.

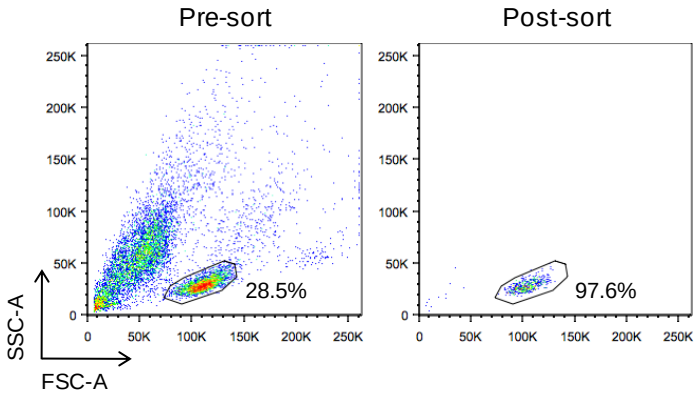

Figure 2.3. Sorting live resting CD4⁺ T cells. CD4⁺ T cells were purified from the spleen of DO11.10 mice, using a negative selection kit (MACS, Miltenyi Biotec). Cells were stimulated by incubation with Dynabeads® Mouse T-activator CD3/CD28 (Invitrogen). After three days of stimulation, Dynabeads® were removed to initiate the resting period. For confocal microscopy analysis, live resting CD4⁺ T cells were flow cytometrically sorted, based on their FSC-A SSC-A profile (pre-sort). Purity of the isolated T cell population was assessed (post-sort) and was consistently above 96%.

A20 B cell lines stably expressing M2 or M2Y proteins had been previously generated by Dr. Marta Alenquer, and will be referred to as A20 B cell lines. To exclude the possibility of the observations made throughout the study being a cell line effect, independent cell lines were generated by transduction of A20 B cells with the appropriate viral particles, as described in section 7.2.3.6. In these cell lines, M2 and M2Y proteins were N-terminally fused to EGFP. These will be referred to as independent A20 B cell lines. Since the M2Y mutant only controls the requirement of the assembly of a signalosome, an EGFP expressing cell line was generated as a second negative control. The most efficiently transduced cells were sorted by gating on the 10-20% brightest EGFP$^+$ events, for EGFP-M2 and EGFP-M2Y samples (Figure 2.4). The same gate was then applied to the EGFP sample, which was more efficiently transduced. Constitutive expression of M2, M2Y or EGFP/EGFP-tagged proteins was confirmed on both A20 B cell lines and independent B cell lines by Western Blot analysis (Figure 2.5).

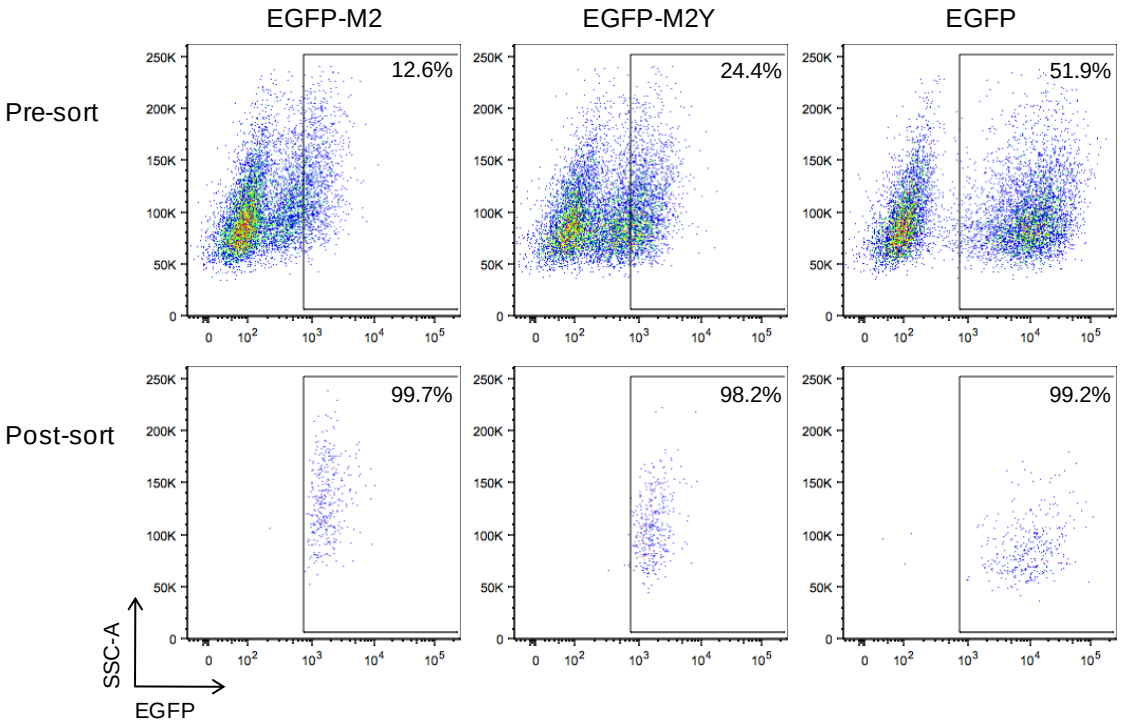

Figure 2.4. Sorting EGFP$^+$ A20 B cells for the generation of EGFP/EGFP-M2/EGFP-M2Y-expressing cell lines. For the generation of independent B cell lines, A20 B cells were transduced with retroviruses that allow the expression of EGFP-M2, EGFP-M2Y or EGFP. The most efficiently transduced cells were sorted by gating on the 10-20% brightest EGFP$^+$ events, for M2 and M2Y samples (pre-sort). The same gate was applied to the EGFP sample. Purity of the isolated B cell populations was assessed (post-sort) and was consistently above 98%.

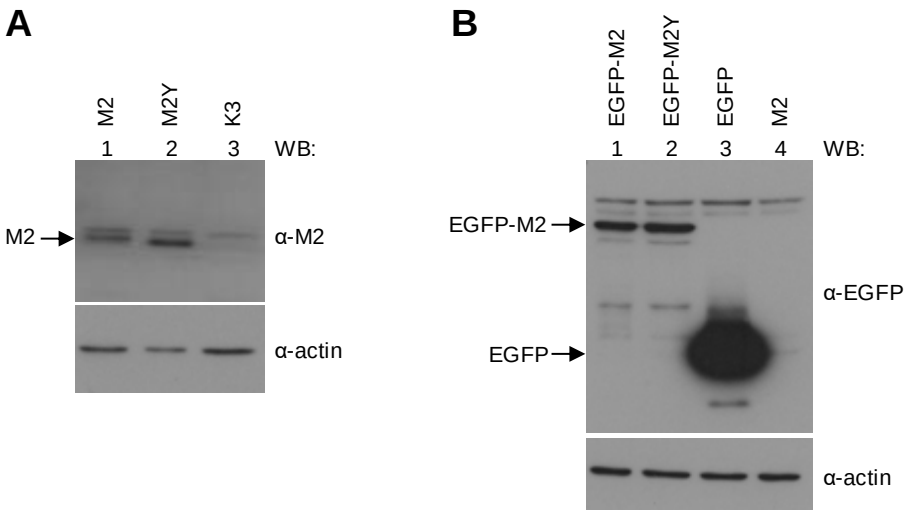

Figure 2.5. A20 B cell lines express M2/M2Y. (A) M2/M2Y expression on total cellular lysates of the A20 B cell lines. M2/M2Y proteins were detected on Western Blot with an anti-M2 antibody. An A20 B cell line expressing the viral protein K3 (lane 3) was used as a negative control. (B) M2/M2Y expression on total cellular lysates of the independent A20 B cell lines. EGFP or EGFP-M2/M2Y fusion proteins were detected on Western Blot with an anti-EGFP antibody. An A20 B cell line expressing non-tagged M2 (lane 4) was used as a negative control. (A) and (B) An anti-actin antibody was used to demonstrate that similar amounts of cellular lysates were used.

A20 B cell lines and independent A20 B cell lines interact with the OVAp-specific TCR-transgenic $CD4^+$ T cells, forming B-T_H cell conjugates. In the presence of high concentrations of OVAp (above 1μM), such interaction results in the formation of a highly organized signaling structure at the interface between both cells, the IS. Previous work from Dr. Filipa Lopes, carried out in the context of this project, has shown that the M2 protein polarizes to the B-T_H contact zone in this *in vitro* system. This polarization is dependent on the integrity of the unconventional ITAM, as the M2Y mutant protein remains localized in juxtamembrane areas of the cell. Dr. Filipa Lopes has also observed that M2 promotes B cell polarization, as its expression increases the B cell MTOC proximity to the contact zone. Collectivelly, these observations validate the use of this system and are concomitant with an involvement of M2 in the modulation of B-T_H cell interaction, that is dependent on the protein ability to assemble specific signalosomes (Fontinha, Lopes et al. 2015).

2.2.2 Expression of the latency-associated M2 protein leads to the upregulation of adhesion and co-stimulatory molecules in B cells

In order to investigate if M2 plays a role in B-T_H cell interaction, the influence of the viral protein on the levels of selected B cell surface molecules, some of which are involved in IS, was evaluated. The M2Y mutant protein was used in parallel to assess the requirement of the unconventional ITAM motif. A20 B cell lines stably expressing M2 or M2Y were stained for the indicated markers and analyzed by flow cytometry (Figure 2.6). Untransduced A20 B cells were used as a negative control. Mean fluorescence intensity (MFI) fold change of M2 or M2Y relative to that of the control was then quantified (Figure 2.6A). Levels of CD80, a co-stimulatory molecule found in the cSMAC of IS (Monks, Freiberg et al. 1998, Grakoui, Bromley et al. 1999, Huppa and Davis 2003), was 2-fold higher in M2-expressing B cells (open bars) than in the control (black bars). The cell adhesion molecules ICAM1 and CD48, found in the pSMAC of IS (Monks, Freiberg et al. 1998, Grakoui, Bromley et al. 1999, Huppa and Davis 2003), were 1.5- and 1.2-fold upregulated, respectively. These differences can be observed as a shift in fluorescence intensity in the representative FACS histograms (Figure 2.6B). This upregulation was specific as M2 expression did not significantly alter the levels of CD86, CD40, MHCII, CD19, CD21, CD23, CD69, and CD95. M2Y-expressing B cells (grey bars) did not show increased levels of any of these molecules, denoting the requirement of the ITAM for such upregulation. Moreover, this observation corroborates the use of M2Y as a negative control.

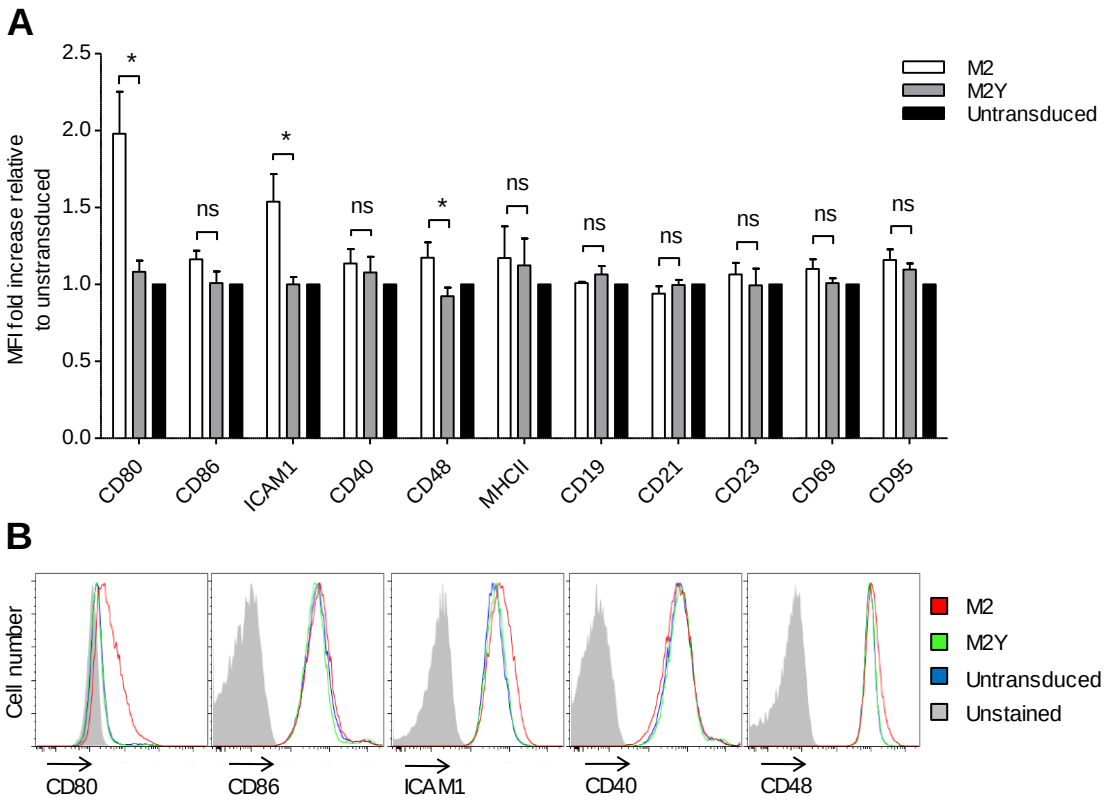

Figure 2.6. M2 expression leads to the upregulation of adhesion and co-stimulatory molecules in B cells. (A) Fold increase of the mean fluorescence intensities (MFI) of several surface molecules, relative to untransduced A20 B cells. A20 B cells (black bars) and A20 B cells stably expressing M2 or M2Y were stained with fluorescently labeled antibodies and the surface expression of the indicated molecules was analyzed on a LSR Fortessa flow cytometer. Bars represent the mean of three independent experiments. Error bars represent standard error of the mean. Statistical significance was evaluated using a one-tailed Students t-test. (B) Representative FACS histogram plots for the indicated surface molecules.

To exclude the possibility of a cell line effect, the influence of M2 on the levels of CD80, CD86 and ICAM-1 was evaluated on the independent A20 B cells lines (Figure 2.7). EGFP-expressing B cells were used as a negative control. CD80 and ICAM-1 were up-regulated in EGFP-M2-expressing B cells, 2.5- and 2.3-fold, respectively (Figure 2.7A). This upregulation can be observed as a shift in fluorescence intensity in the representative FACS histograms (Figure 2.7B). CD86 up-regulation, which was slight and non-significant in the A20 B cell lines, was visible as a 1.4-fold significant increase. This difference observed between both B cell lines may be a consequence of choosing the 10-20% brightest $EGFP^+$ events and, therefore, the cells with higher expression of M2 or M2Y, when generating the EGFP-M2- and EGFP-M2Y-expressing B cells.

The levels of the surface molecules analyzed in the EGFP-M2Y-expressing B cells were comparable to those of the EGFP-expressing B cells. This demonstrates that the upregulation observed upon expression of M2 is entirely dependent on the unconventional ITAM and further corroborates the use of M2Y as a negative control.

These results show that expression of M2 leads to the upregulation of B cell co-stimulatory and adhesion molecules that participate in the formation of an IS. This function is dependent on tyrosine phosphorylation at the ITAM, hence related to the ability of M2 to assemble multiprotein complexes with B cell signaling proteins.

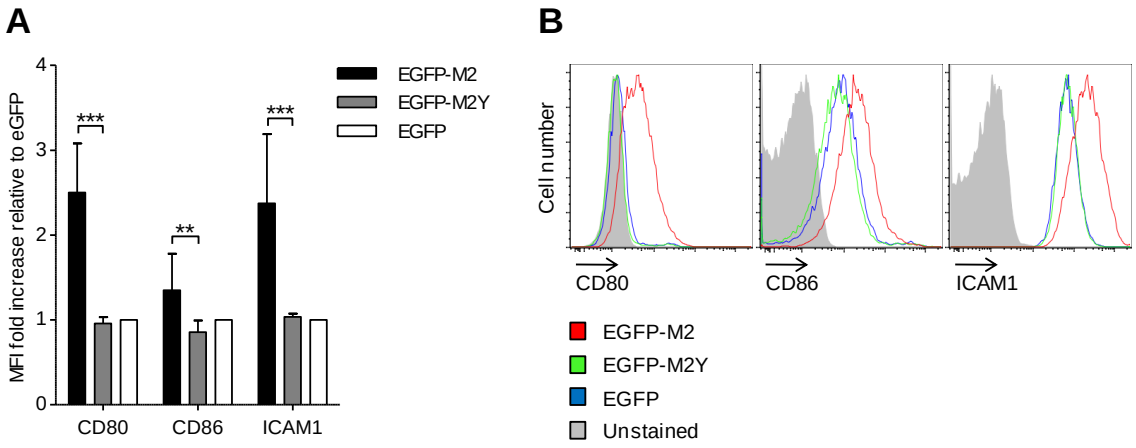

Figure 2.7. M2-expressing independent B cell line shows upregulation of adhesion and co-stimulatory molecules. (A) Fold increase of the mean fluorescence intensities (MFI) of several surface molecules in the independent B cell lines, relative to the EGFP-expressing A20 B cell line. A20 B cells stably expressing EGFP, EGFP-M2 or EGFP-M2Y were stained with fluorescently labeled antibodies and the surface expression of the indicated molecules was analyzed on a LSR Fortessa flow cytometer. Bars represent the mean of eight independent experiments. Error bars represent standard error of the mean. Statistical significance was assessed with a one-tailed Students t-test. (B) Representative FACS histogram plots for the indicated surface molecules.

2.2.3 M2 competitively promotes the formation of B-T_H cell conjugates

B and T_H cells interact with each other forming conjugates, a process that is mediated by adhesion molecules. Given that M2-expressing B cells showed increased levels of such molecules, the impact of M2 in B-T_H cell conjugate formation was investigated in the MHC class II-restricted OVAp-specific system described above.

Mouse A20 B cells, stably expressing M2 or M2Y, were loaded with CMFDA live dye and pulsed with increasing concentrations of OVAp. $CD4^+$ T cells were loaded with DDAO live

dye. M2- or M2Y-expressing B cells and T cells were then incubated in a 2:1 ratio, for 30 minutes. Conjugate formation was next assessed by flow cytometry, based on the percentage of $CMFDA^+DDAO^+$ events in the total $DDAO^+$ population (Figure 2.8A and B).

The percentage of T cells conjugating with M2- (black circles) or M2Y-expressing B cells (grey squares), pulsed or not with increasing concentrations of OVAp, was then quantified (Figure 2.8C). Conjugate formation occurred in a peptide dose-dependent manner. In the absence of peptide, there was a basal level of conjugate formation, where less than 10% of the T_H cells conjugated with M2Y-expressing B cells. Conjugate formation in the M2Y condition only exceeded basal levels when the B cells were loaded with 0.01µM of OVAp. In contrast, the integrity of the phosphosites resulted in a three-fold increase in conjugate formation with M2-expressing B cells, even in the absence of specific peptide. Expression of M2 was therefore able to promote conjugate formation up to 0.1µM of OVAp. Above 0.1µM of OVAp, conjugate formation reached a *plateau* for both M2 and M2Y conditions.

To exclude a cell line effect, the impact of M2 in B-T_H cell conjugate formation was investigated with the independent A20 B cell lines. Conjugate formation was assessed by flow cytometry, based on the percentage of $EGFP^+DDAO^+$ events in the total $DDAO^+$ population (Figure 2.8A). The percentage of T cells conjugating with EGFP-M2- (black circles), EGFP-M2Y- (grey squares) or EGFP-expressing B cells (grey triangles), loaded or not with increasing concentrations of OVAp, was then quantified (Figure 2.8D). Results reproduced the observations made with the A20 B cell lines. Conjugate formation in the EGFP-M2Y and EGFP conditions was the same, demonstrating that the increased conjugate formation promoted by the M2 protein was entirely dependent on the unconventional ITAM.

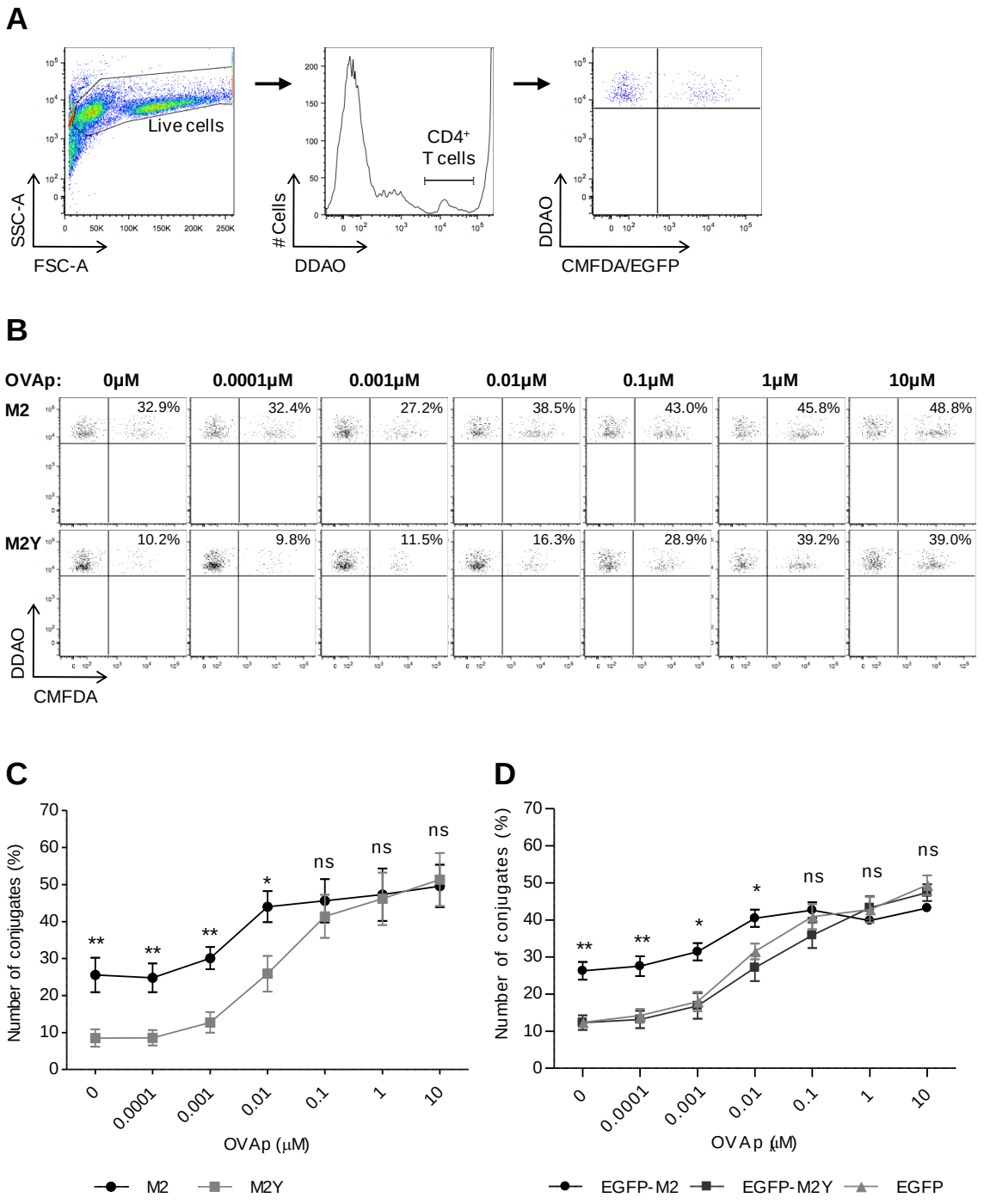

Figure 2.8. M2 promotes the formation of B-T_H cell conjugates, as assessed by flow cytometric analysis. A20 B cells stably expressing the indicated proteins were pulsed overnight, or not, with different concentrations of OVA peptide (OVAp) and incubated with OVAp-specific $CD4^+$ T cells at a 2:1 ratio for 30min. Prior to incubation B and T cell populations were incubated with the live dyes CMFDA and DDAO, respectively, to allow their discrimination. In the case of EGFP-expressing B cell lines, the use of CMFDA was not necessary. (A) Gating strategy used to assess B-T_H cell conjugate formation. (B) Representative FACS plots for the percentage of conjugates upon variation of the OVAp concentration. Conjugate formation was evaluated as the percentage of $CMFDA^+DDAO^+$ events in the total $DDAO^+$ population. (C) Quantification of the percentage of conjugates upon variation of the OVAp concentration, after 30min of incubation. Symbols represent the mean of four independent experiments. This experiment was performed by

Dr. Sofia Marques. (D) Quantification of the percentage of conjugates after 30min of incubation upon variation of the OVAp concentration, after 30min of incubation, for independent EGFP-expressing A20 B cell lines. Conjugate formation was evaluated as the percentage of $EGFP^+DDAO^+$ events in the total $DDAO^+$ population. Symbols represent the mean of three independent experiments. (C) and (D) Error bars represent standard error of the mean. Statistical significance between groups was evaluated by a one-tailed unpaired Student's t test.

To further address conjugate formation, B-T_H cell interaction was assessed by confocal microscopy, including a marker for phosphorylated tyrosines (pTyr). Using the MHC class II-restricted OVAp-specific system, M2- or M2Y-expressing B cells, pulsed or not with different concentrations of OVAp, were incubated with $CD4^+$ T cells in a 2:1 ratio, for 30 minutes. Prior to incubation, B cells were loaded with CMFDA live dye. Cells were also stained for F-actin, to allow the visualization of B-T_H cell interaction. Conjugate count was blind and based on B-T_H cell contact and pTyr (purple) accumulation at the contact zone (Figure 2.9A).

The percentage of T cells conjugating with either M2- (black circles) or M2Y-expressing (grey circles) B cells was then quantified (Figure 2.9B). Corroborating the previous results, confocal microscopy revealed that M2 expression in B cells promoted conjugate formation with T_H cells, as indicated by the increased percentage of conjugates relative to the control. Notably, in the absence of peptide, there was a basal level of conjugates with pTyr accumulation at the contact zone in the M2Y condition, which was significantly higher under M2 expression. This is indicative of signaling and peptide-independent formation of a functional immunological synapse. However, in this particular case, it can also be associated with the constitutive phosphorylation of the tyrosine residues of M2, and the consequent phosphorylation of Vav1 and PLCγ2 (Rodrigues, Pires de Miranda et al. 2006, Pires de Miranda, Alenquer et al. 2008, Pires de Miranda, Lopes et al. 2013).

To exclude a cell line effect, the impact of M2 in B-T_H cell conjugate formation was investigated by confocal microscopy with the independent A20 B cell lines, in a single experiment. Overall, the percentage of conjugates was higher than the one obtained with the A20 B cell lines. Nonetheless, expression of EGFP-M2 promoted the formation of conjugates with $CD4^+$ T cells, when compared to the EGFP-M2Y and EGFP conditions.

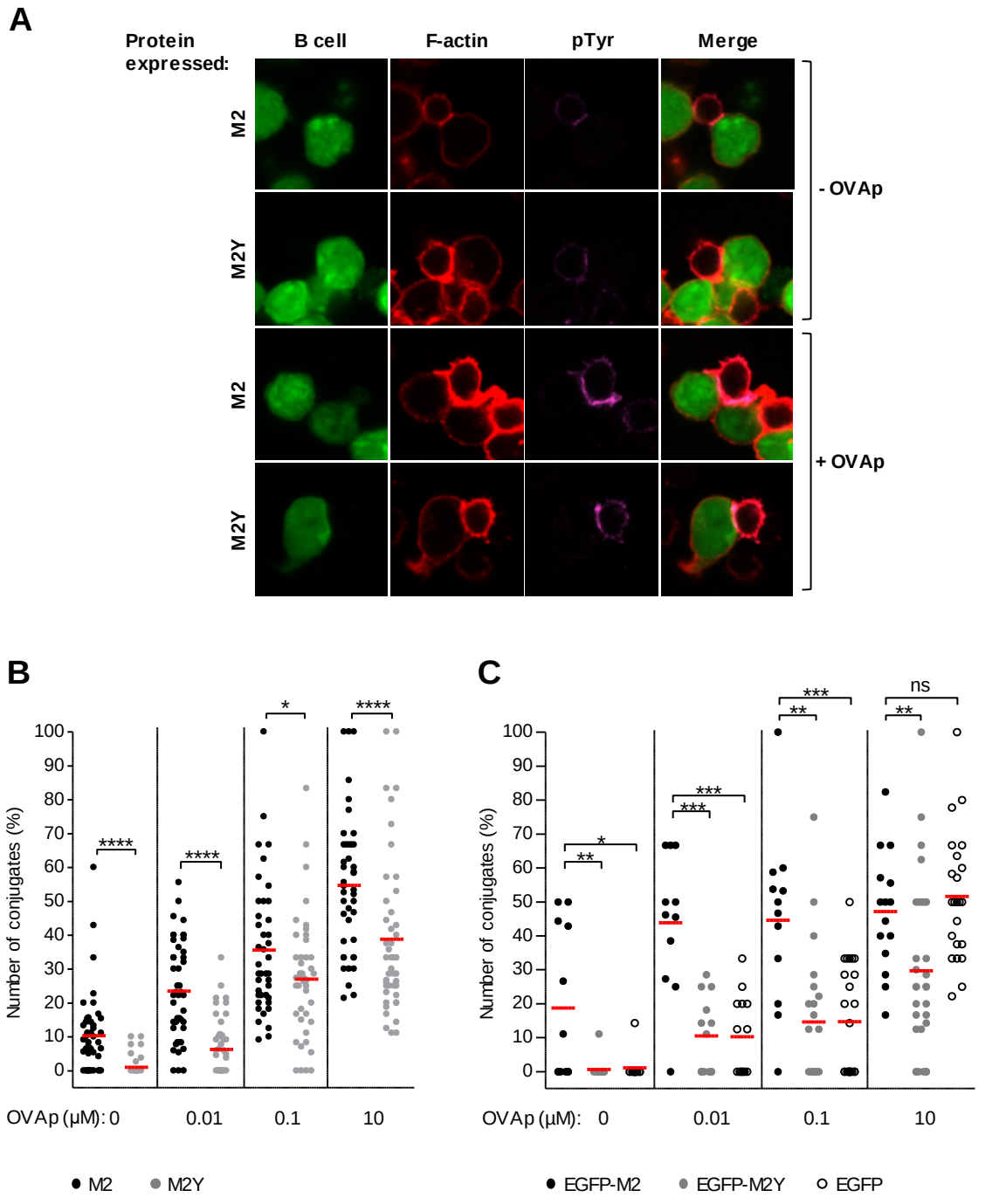

Figure 2.9. M2 promotes the formation of B-T_H cell conjugates, as assessed by confocal microscopy. A20 B cells stably expressing the indicated proteins were pulsed overnight, or not, with different concentrations of OVA peptide (OVAp) and incubated with OVAp-specific $CD4^+$ T cells at a 2:1 ratio. Prior to incubation B cell populations were incubated with the live dye CMFDA, to allow their discrimination. (A) Representative images of pTyr polarization to the contact zone. After 30min of incubation, cells were fixed and stained for F-actin with TRITC-phalloidin (red), and for pTyr (purple). Images are from one representative experiment out of three. (B) Percentage of conjugates per field after 30min of incubation, as determined by confocal microscopy, upon variation of the OVAp concentration. A total of 45 images were taken per sample from three independent experiments. Only images with a minimum of three T cells were considered for analysis. (C) Percentage of conjugates per field after 30min of incubation, for the independent EGFP-expressing A20 B cell lines. 15 to 35 images were taken per sample in a single experiment.

(B) and (C) Conjugate count was blind and based on B-T_H cell contact and pTyr polarization to the contact zone. Statistical significance of the difference between groups was evaluated by a Mann-Whitney U test.

To understand whether the increase in conjugate formation described above translated into a competitive advantage, M2- and M2Y-expressing B cells were placed in direct competition for conjugation with $CD4^+$ T cells, in an *in vitro* competition assay. Briefly, $CD4^+$ T cells were simultaneously incubated with equal numbers of M2- and M2Y-expressing B cells, pulsed with the same concentration of OVAp, in a 1:1:1 ratio. Prior to incubation, M2-expressing B cells, M2Y-expressing B cells and $CD4^+$ T cells were loaded with CMFDA, CMTMR and DDAO live dyes, respectively, to allow their discrimination (Figure 2.10A).

Conjugate formation with M2-expressing B cells was evaluated as the percentage of $CMFDA^+CMTMR^-$ events, while conjugate formation with M2Y-expressing B cells was evaluated as the percentage of $CMFDA^-CMTMR^+$ events in the total $DDAO^+$ population (Figure 2.10A, *B cell lines*, and 2.10B). The fold difference of the percentage of T cells conjugating with M2-expressing B cells relative to the M2Y condition was then quantified (Figure 2.10C). Up to 0.01µM of OVAp, on average, there were 2.5-fold more M2 conjugates. Above 0.1µM of OVAp this difference was smaller, although it was still visible. This shows that T_H cells preferentially conjugated with B cells expressing the wild-type viral protein.

To exclude the possibility of a cell line effect, the in vitro competition assay was performed with the independent A20 B cell lines. Prior to incubation, M2Y-expressing B cells and $CD4^+$ T cells were loaded with CMTMR and DDAO live dyes, respectively, to allow their discrimination (Figure 2.10A). Identification of M2-expressing B cells relied solely on the expression of EGFP. Conjugate formation with M2-expressing B cells was evaluated as the percentage of $EGFP^+CMTMR^-$ events, while conjugate formation with M2Y-expressing B cells was evaluated as the percentage of $EGFP^+CMTMR^+$ events in the total $DDAO^+$ population (Figure 2.10A, *Independent B cell lines*, and 2.10D). The fold difference of the percentage of T cells conjugating with EGFP-M2-expressing B cells relative to the EGFP-M2Y condition reproduced the preferentiality of T_H cells to conjugate with M2-expressing B cells (Figure 2.10E).

Taken together, these results show that expression of M2 favors the formation of conjugates with T_H cells, in a competitive manner. Such ability is dependent on the

integrity of the unconventional ITAM and, therefore, dependent on the ability of M2 to assemble multiprotein complexes with B cell signaling proteins.

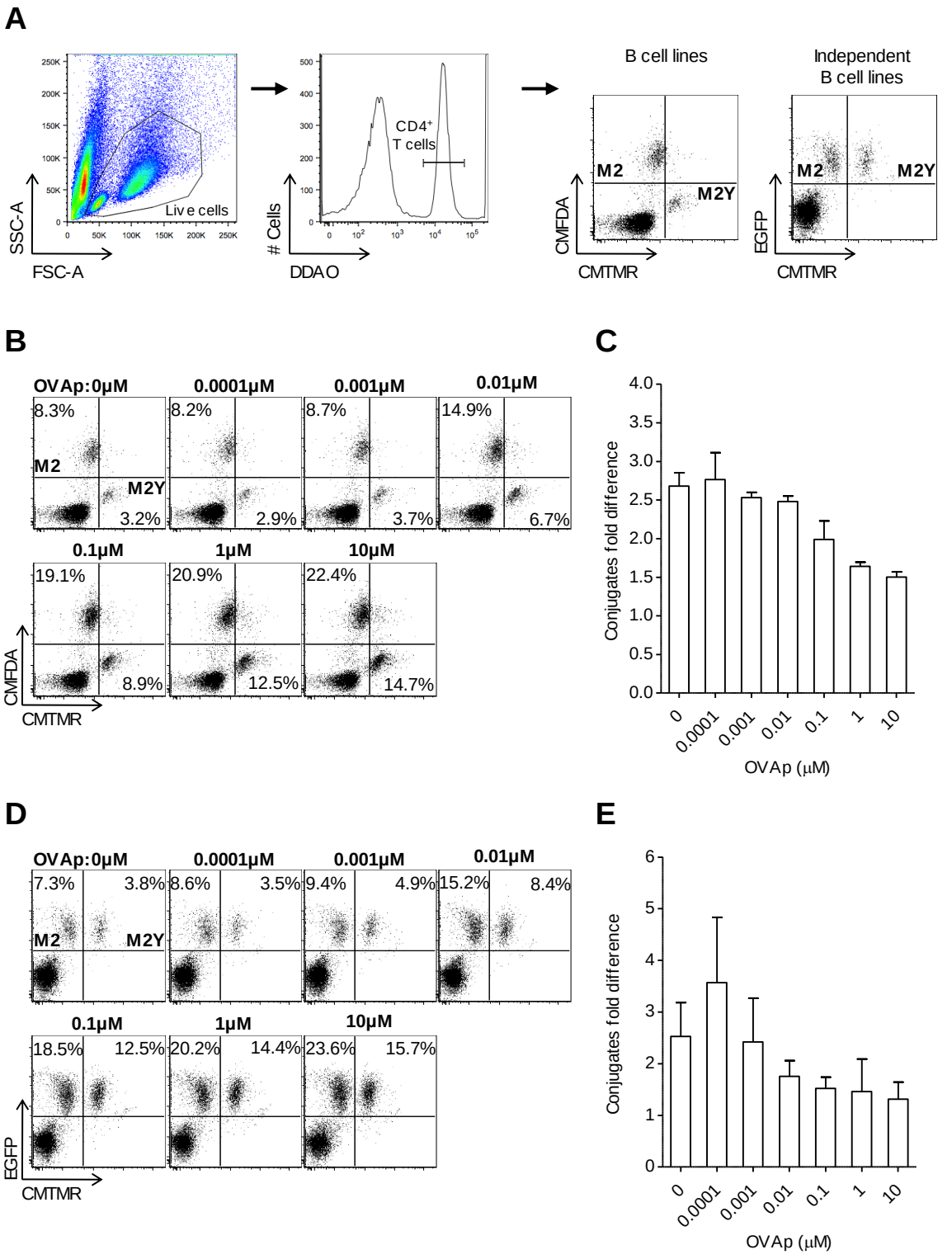

Figure 2.10. M2 promotes the formation of B-T_H cell conjugates in a competitive manner. A20 B cells stably expressing the indicated proteins were pulsed overnight, or not, with different concentrations of OVA peptide (OVAp). M2-expressing B cells, M2Y-expressing B cells and T cells

were mixed on the same tube at a 1:1:1 ratio and incubated for 30min. Prior to incubation M2-expressing B cells and M2Y-expressing B cells were incubated with the live dyes CMFDA and CMTMR, respectively, to allow their discrimination. In the case of the independent A20 B cell lines, only EGFP-M2Y-expressing B cells were incubated with the live dye CMTMR. T cells were incubated with the live dye DDAO. (A) Gating strategy used to assess B-T_H cell conjugate formation. (B) Representative FACS plots for the percentage of conjugates upon variation of the OVAp concentration. Conjugate formation with M2-expressing B cells was evaluated as the percentage of $CMFDA^+CMTMR^-$ events in the total $DDAO^+$ population. Conjugate formation with M2Y-expressing B cells was evaluated as the percentage of $CMFDA^-CMTMR^+$ events in the total $DDAO^+$ population. (C) Fold difference of the number of conjugates formed with M2-expressing B cells relative to the M2Ycondition. (D) Representative FACS plots for the percentage of conjugates upon variation of the OVAp concentration. Conjugate formation with EGFP-M2-expressing B cells was evaluated as the percentage of $EGFP^+CMTMR^-$ events in the total $DDAO^+$ population. Conjugate formation with EGFP-M2Y-expressing B cells was evaluated as the percentage of $EGFP^+CMTMR^+$ events in the total $DDAO^+$ population. (E) Fold difference of the number of conjugates formed with EGFP-M2-expressing B cells relative to the EGFP-M2Y condition. (B) and (D) The percentage of T cells conjugating with M2- or M2Y-expressing B cells is indicated in the respective quadrant. (C) and (E) Bars represent the mean of three independent experiments. Error bars represent standard error of the mean.

2.3 Discussion

Although *in vivo* studies show that the M2 protein is required for the initial colonization of the lymphoid follicles, the mechanism behind this process is still unknown. The data described in this chapter supports a model where expression of MuHV-4 M2 protein competitively promotes interaction with T_H cells *in vitro*, in the context of a MHC class II-restricted OVAp-specific cellular system. This process was independent of presentation of specific antigen, as indicated by the increased number of M2-expressing B-T_H cell conjugates observed in the absence of peptide, and may be the outcome of the upregulation of adhesion molecules observed in M2-expressing B cells. Preliminary work performed by Dr. Sofia Marques in our laboratory has shown that upregulation of the costimulatory molecules CD80 and CD86 also occurs *in vivo* in infected GC B cells, upon intranasal infection of C57BL/6J mice with 10^4 PFU of MuHV-4. This observation supports that there may be a physiological significance for the *in vitro* results obtained in this chapter.

The previously observed B cell polarization (Fontinha, Lopes et al. 2015) and the upregulation of co-stimulatory molecules observed under expression of M2 suggest a role for the viral protein in IS modulation. Furthermore, measurement of B-T_H cell conjugates by confocal microscopy revealed a pTyr accumulation in the contact zone in the absence of peptide, that may be indicative of signaling and peptide-independent formation of a functional IS, raising the possibility of M2 replacing the need for cognate T cell help.

Modulation of T-APC interaction, and more specifically IS, by a viral protein has been previously described. Protein Nef from Human Immunodeficiency Virus type 1 (HIV-1) has been shown to impair IS formation, as a means of optimizing the environment for HIV infection (Haller, Rauch et al. 2006, Thoulouze, Sol-Foulon et al. 2006, Haller, Rauch et al. 2007, Saxena, Shrivastava et al. 2012). In the *Gammaherpesvirinae* sub-family there are also two examples of impairment of B-T_H cell interactions and IS formation, namely K5 from Kaposi Sarcoma-associated Herpesvirus (KSHV) (Coscoy and Ganem 2001), and tyrosine kinase-interacting protein (Tip) from the T lymphotropic Herpesvirus Saimiri (HVS) (Cho, Feng et al. 2004). In contrast, the results obtained with the M2 protein support a model where a viral protein promotes B-T_H cell interaction, instead of impairing it. This is concomitant with the high prevalence of infection in GC B cells. Such positive effect does not exclude the possibility that, at some point during infection, MuHV-4 impairs IS formation as a mechanism of immune evasion.

Collectively, results support a model where the latency-associated M2 protein competitively promotes B-T_H cell interaction, a process that is dependent on the modulation of B cell signaling. *In vivo*, this ability to attract T cell help in a competitive manner during the T cell scanning process, carried out in secondary lymphoid organs, may account for the selection of infected B cells for GC initiation, a crucial step in latency establishment, hence host colonization.

CHAPTER 3

M2-EXPRESSING B CELLS DO NOT PROMOTE T CELL ACTIVATION INDEPENDENTLY OF SPECIFIC PEPTIDE

3 M2-EXPRESSING B CELLS DO NOT PROMOTE T CELL ACTIVATION INDEPENDENTLY OF SPECIFIC PEPTIDE

3.1 Introduction

Formation of an IS upon cognate B-T_H cell interaction triggers signaling cascades that lead to T cell activation. One of the outcomes of such interaction is the increase of intracellular calcium concentration (Gray, Gnarra et al. 1988, Friedl, den Boer et al. 2005). This step is critical as it induces the nuclear localization of nuclear factor of activated T cells (NFAT), resulting in changes in gene expression (Feske, Giltnane et al. 2001). The IS is also a place for the polarized secretion of cytokines, namely: IL-2, IL-4, IL-5 and IFN-γ (Kupfer, Mosmann et al. 1991, Kupfer, Monks et al. 1994, Trautmann and Valitutti 2003). Typically, an IS is composed of spatially separated supramolecular activation clusters (SMACs), arranged in a bull's eye shape, forming a synaptic cleft between the interacting cells (Grakoui, Bromley et al. 1999, Huppa and Davis 2003, Krummel and Cahalan 2010). The pSMAC, where there is an accumulation of adhesion molecules, helps stabilize the cell-cell interaction. It is possible that this outer adhesive ring also prevents leakage of cytokines from the synaptic cleft and, therefore, promotes a focal delivery of the released factors (Friedl, den Boer et al. 2005).

In the context of an adaptive immune response, this cognate interaction between a T_H cell and a B cell presenting the appropriate antigen is required for germinal center (GC) initiation. There, B cells undergo affinity maturation and class-switch recombination, giving rise to plasma cells and to the long-term target population of gammaherpesviruses, memory B cells (Allen, Okada et al. 2007, De Silva and Klein 2015),.

The results presented in chapter 2 revealed that expression of M2 in B cells promoted their interaction with T_H cells. This was true even in the absence of specific peptide and was accompanied by pTyr accumulation at the interface between B and $CD4^+$ T cells (section 2.2.3), suggesting peptide-independent signaling and IS formation. To address that possibility, T cell activation was assessed by measurement of intracellular calcium and analysis of IFN-γ polarization in $CD4^+$ T cells, in the context of the MHC class II-restricted OVAp-specific system.

3.2 Results

3.2.1 M2 expression in B cells increases the number of CD4$^+$ T cells mobilizing calcium, but not the magnitude of individual responses

To investigate if conjugation with M2-expressing B cells resulted in T cell activation, intracellular calcium was measured on CD4$^+$ T cells.

To measure the intracellular calcium, TCR-transgenic CD4$^+$ T cells were loaded with the calcium indicator Indo-1, which changes its emission spectrum by chelating free calcium ions. As a result, the intensity of the emission at 405nm increases and, simultaneously, the intensity of the emission at 530nm decreases. Therefore, the 405/530 ratio provides a measure of intracellular calcium increase. To assure that the events would be within the scale of the FACS plot after calcium increase, the 405nm laser was set at a low voltage, while the 530nm laser was set at a high voltage, as can be observed in the middle column plots of Figure 3.1. A baseline of 405/530 MFI through time was then established by acquiring unstimulated T_H cells alone, for approximately two minutes (Figure 3.1, *baseline condition, third plot*), as has been described (Valitutti and Dessing 2000). To assess whether the primary CD4$^+$ T cells were able to respond by mobilizing calcium, these were stimulated with ionomycin (Figure 3.1, *ionomycin condition*). This stimulation was followed by a strong response, as observed by the increase in the 405/530 ratio of nearly all analyzed T cells. To confirm that calcium mobilization would occur in the MHC class II-restricted OVAp-specific system, Indo-1 loaded CD4$^+$ T cells were incubated with M2-expressing B cells pulsed with a saturating concentration of OVAp (10μM). Calcium mobilization, although lower than the one observed after the ionomycin stimulus, was clearly visible as an increase in the 405/530 ratio (Figure 3.1, *M2 + 10μM OVAp condition*).

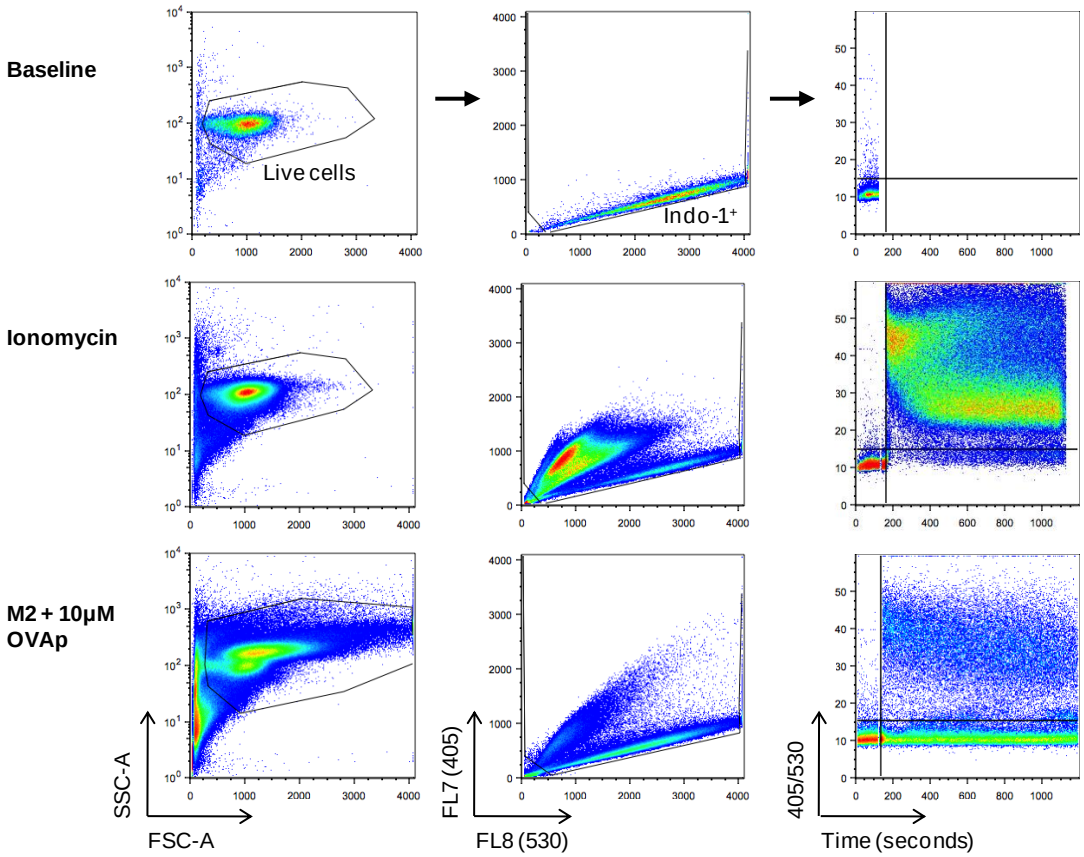

Figure 3.1. Intracellular calcium quantification by flow cytometry. For all three conditions, live resting OVAp-specific CD4⁺ T cells were sorted as described in section 2.2.1 and loaded with the calcium indicator Indo-1. FACS plots depict the gating strategy used for calcium mobilization analysis. After gating on live cells, analysis was restricted to CD4⁺ T cells by gating in Indo-1⁺ events (405⁺530⁺). The 405nm laser was set at a low voltage, while the 530nm laser was set at a high voltage to account for the change in Indo-1 emission spectrum upon calcium increase. Next, the 405/530 ratio was measured against time. In the first condition a baseline was established by acquiring unstimulated T cells for two minutes. In the second condition, ionomycin was used to stimulate the T cells as a positive control. In the third condition, Indo-1 loaded CD4⁺ T cells were incubated with M2-expressing B cells, previously pulsed with 10µM of OVAp.

Two minute baselines were established for every sample by acquisition of unstimulated CD4⁺ T cells. Next, the effect of incubation with M2- or M2Y-expressing B cells on T_H cell intracellular calcium increase was assessed (indicated by an arrow in Figure 3.2A). The percentage of activated T_H cells, determined as the percentage of 405/530 positive events above baseline (Figure 3.2A), was quantified (Figure 3.2B). The positive control, ionomycin, led to the activation of more than 97% of the T cell population. The percentage of activated T_H cells increased with the OVAp concentration (Figure 3.2B). Between 0.005µM and 0.1µM of OVAp, M2-expressing B cells (filled bars) led to an increase in the number of T_H cells mobilizing calcium, compared to M2Y-expressing B cells (open bars). This correlated with the increased number of B-T_H cell conjugates observed in section

2.2.3. However, this difference was only statistically significant for the 0.01µM of OVAp condition. To assess if M2-expressing B cells were also able to promote stronger individual responses, the 405/530 ratio MFI of responding T_H cells was quantified (Figure 3.2C). M2 and M2Y conditions showed no statistically significant differences in MFI demonstrating that, even though there were more T_H cells mobilizing calcium, there was no difference in the magnitude of individual responses. In the absence of peptide, M2-expressing B cells did not promote intracellular calcium increase in T_H cells. This indicates that expression of M2 in the context of B-T_H cell interaction is not enough to drive T cell activation.

To exclude the possibility of a cell line effect, T_H cell calcium increase was measured after incubation with the independent A20 B cell lines, in a single experiment (Figure 3.2D). The increase in the number of $CD4^+$ T cells mobilizing calcium after incubation with EGFP-M2-expressing B cells (filled bars) pulsed with 0.005µM or 0.01µM of OVAp, corroborated the previous results. 405/530 MFI for the EGFP-M2 condition was the same or lower than that of the controls, which was in agreement with the inability of M2 to promote a stronger individual T cell response, observed with the A20 B cell lines.

Measurement of intracellular calcium in T_H cells showed that incubation with M2-expressing B cells did not promote T cell activation in the absence of peptide. In the presence of specific peptide, M2 expression in B cells increased the number of activated T_H cells, but not the magnitude of individual responses.

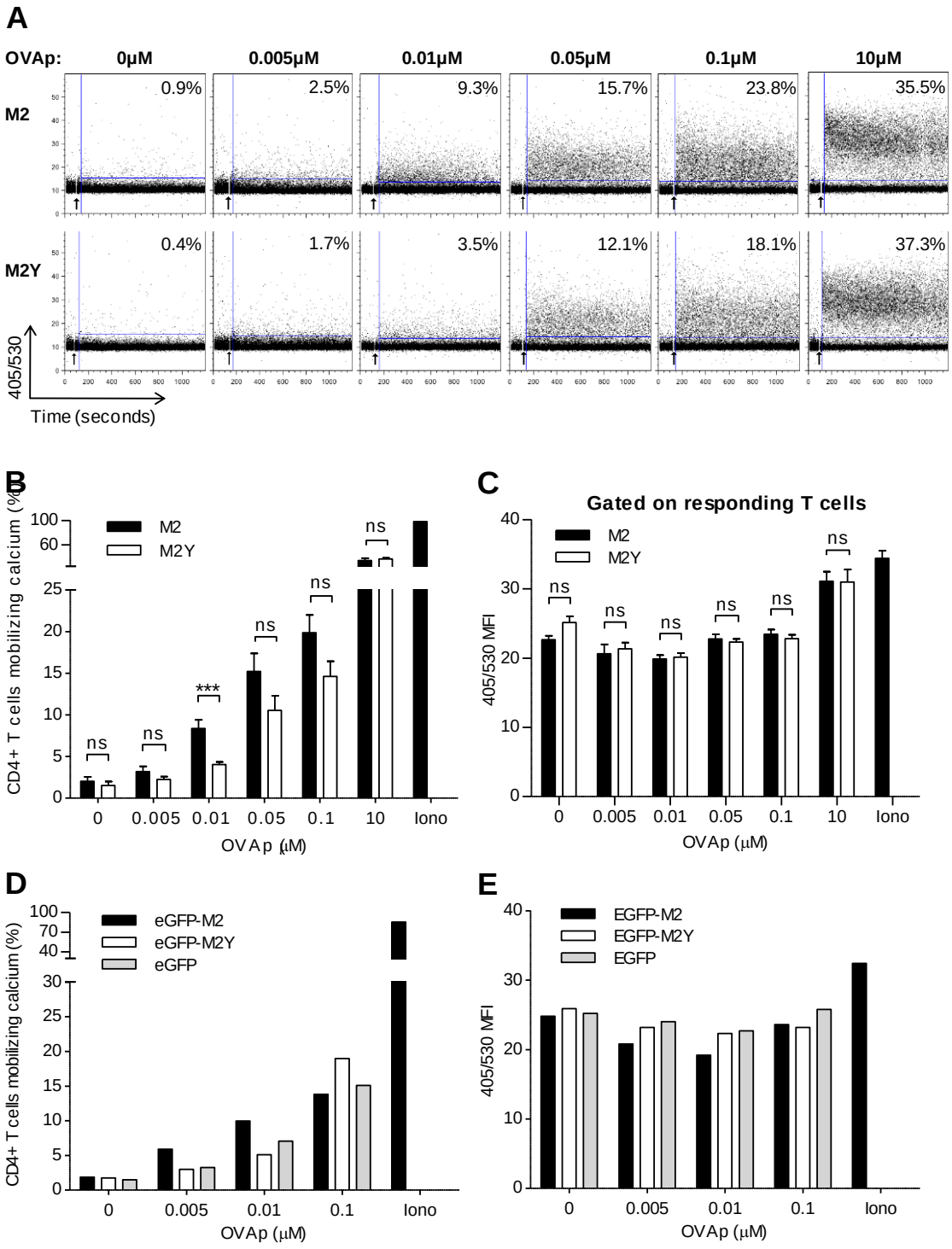

Figure 3.2. Calcium mobilization in M2-expressing B-T_H cell conjugates requires specific peptide presentation. A20 B cells stably expressing the indicated proteins were pulsed overnight, or not, with different concentrations of OVAp and incubated with OVAp-specific $CD4^+$ T cells for 5 min. Live resting $CD4^+$ T cells were sorted as described in section 2.2.1. Prior to conjugation T cells were loaded with the calcium indicator Indo-I. Ionomycin (Iono) was used as a positive control. (A) Representative FACS plots of calcium measurements. A baseline was established by acquiring unstimulated T_H cells alone, for approximately two minutes. Calcium fluxes were then measured on a MoFlow cytometer for 18 minutes (when indicated by the arrow) and were based on the 405/530 emission ratio over time. 405/530 mean fluorescence intensity (MFI) is shown. (B) Average of the

percentage of $CD4^+$ T cells mobilizing calcium when conjugated with M2- (filled bars) or M2Y-expressing (open bars) B cells. (C) 405/530 MFI average within responding T cells. (B) and (C) Bars represent the results from three to seven experiments. Error bars represent standard error of the mean. Statistical significance of the difference between groups was evaluated by a one-tailed unpaired Student's T test. This experiment was performed in collaboration with Dr. Sofia Marques. (D) Average of the percentage of $CD4^+$ T cells mobilizing calcium when conjugated with EGFP-M2- (filled bars), EGFP-M2Y- (open bars) or EGFP-expressing B cells (grey bars). (E) 405/530 MFI average within responding T cells conjugating with the independent A20 B cell lines. (D) and (E) Bars represent the results from a single experiment.

3.2.2 M2-expressing B cells do not promote IFN-γ polarization in $CD4^+$ T cells in the absence of specific peptide

To further investigate if conjugation with M2-expressing B cells resulted in T cell activation, IFN-γ polarization to the contact zone was assessed by confocal microscopy.

Using the MHC class II-restricted OVAp-specific system, M2- or M2Y-expressing B cells, pulsed or not with different concentrations of OVAp, were incubated with $CD4^+$ T cells in a 2:1 ratio, for 2.5 hours. Prior to incubation, B and $CD4^+$ T cells were loaded with CMFDA (green) and CMAC (blue) live dyes, respectively. Cells were then stained for IFN-γ and for the previously used pTyr marker. Conjugate count was blind and based on B-T_H cell contact and IFN-γ (red) accumulation at the contact zone (Figure 3.3A). The percentage of T cells conjugating with either M2- (black circles) or M2Y-expressing (grey circles) B cells, that polarized IFN-γ to the contact zone, was then quantified (Figure 3.3B). IFN-γ polarization was at all times accompanied by pTyr accumulation at the contact zone. Presentation of a specific peptide was an absolute requirement, as demonstrated by the absence of IFN-γ polarization to the contact zone when B cells were not pulsed with OVAp. In the presence of specific peptide, conjugate formation with M2-expressing B cells resulted in more activated T_H cells, compared to the M2Y condition, as was previously observed with intracellular calcium measurements (section 3.2.1).

To exclude the possibility of a cell line effect, the detection of IFN-γ polarization to the contact zone by confocal microscopy was performed after incubation of $CD4^+$ T cells with the independent A20 B cell lines, in a single experiment (Figure 3.3C). Once again, cognate interaction was an absolute requirement, as observed by the absence of conjugating T cells with IFN-γ polarization to the contact zone upon interaction with unpulsed B cells (0μM of OVAp). Presentation of specific peptide in the context of M2 expression resulted in an increased number of T cells conjugating and polarizing IFN-γ to the contact zone, compared to the M2Y condition. This observation was in agreement with the results obtained with the A20 B cell lines (Figure 3.3B).

IFN-γ analysis revealed that expression of M2 in B cells was not sufficient to promote T cell activation. Presentation of specific peptide by the B cell is, therefore, an absolute requirement for T cell activation upon B-T_H cell interaction. In the presence of specific peptide, consistent with the increased number of conjugates, interaction with M2-expressing B cells increased the number of activated T_H cells.

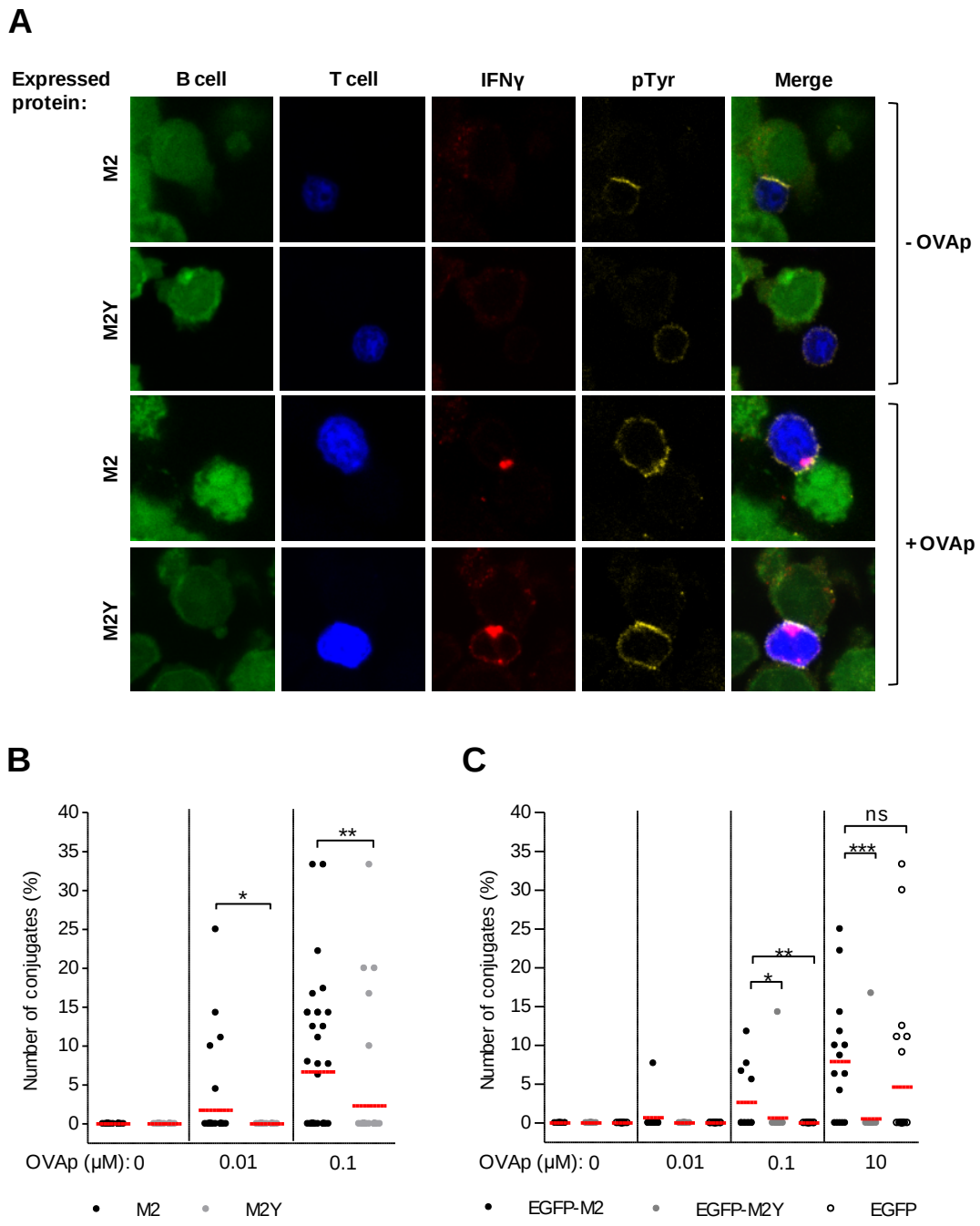

Figure 3.3. IFN-γ production in M2-expressing B-T_H cell conjugates requires specific peptide presentation. A20 B cells stably expressing the indicated proteins were pulsed overnight, or not, with different concentrations of OVA peptide (OVAp) and incubated with OVAp-specific $CD4^+$ T cells. (A) Representative confocal images of IFN-γ polarization to the contact zone. Prior to incubation B and T cells were labelled with CMFDA (green) and CMAC (blue) live dyes, respectively. Cells were incubated for 2.5h, fixed and stained for IFN-γ (red), and for pTyr (yellow). Images are from one representative experiment out of three and were obtained using a Zeiss LSM 510 META microscope. (B) Quantification of conjugates with IFN-γ polarization, upon variation of the OVAp concentration. 45 to 55 images were acquired per sample from three independent experiments. (C) Quantification of conjugates with IFN-γ polarization, for the independent EGFP-expressing A20 B cell lines. 15 to 35 images were acquired per sample from a single experiment.

(B) and (C) Conjugate count was blind and based on B-T_H cell contact and IFN-γ polarization to the contact zone. Only images with a minimum of three T cells were considered for analysis. Statistical significance of the difference between groups was evaluated by a Mann-Whitney U test.

3.3 Discussion

The previous chapter allowed to conclude that expression of M2 protein in B cells promotes their interaction with T_H cells. However, it did not clearly discriminate between productive and non-productive B-T_H cell contact, *i.e.* whether such interaction resulted in T cell activation. The fact that B-T_H cell interaction was increased in the absence of peptide and the fact that pTyr accumulation at the B-T_H contact zone was observed in those conditions raised the possibility of M2 promoting the formation of a functional IS and, therefore, T cell activation, independently of specific peptide.

Measurement of intracellular calcium levels and IFN-γ polarization in T_H cells revealed that conjugate formation with M2-expressing B cells in the absence of peptide does not lead to T cell activation. This dependence on the presence of specific peptide therefore suggested that the pTyr accumulation observed in the previous chapter (section 2.2.3) was not an indication of T cell signaling and activation, but was instead due to the constitutive phosphorylation of the tyrosine residues of M2, and the consequent phosphorylation of Vav1 and PLCγ2 on the B cell side (Rodrigues, Pires de Miranda et al. 2006, Pires de Miranda, Alenquer et al. 2008, Pires de Miranda, Lopes et al. 2013). Nevertheless, concomitant with the increased number of conjugates, the number of activated T_H cells was higher in the presence of M2-expressing B cells.

Just like IFN-γ, the cytokines IL-2, IL-4 and IL-5 are also known to be secreted to the synaptic cleft following T cell activation (Friedl, den Boer et al. 2005). Measurement of the production of these cytokines by ELISA, performed by Dr. Filipa Lopes in our laboratory, revealed no differences between the conjugation of $CD4^+$ T cells with M2- or M2Y-expressing B cells.

These findings support a model where expression of M2 in B cells promotes their interaction with T_H cells but does not drive T cell activation. Instead, T cell activation upon conjugate formation is a product of cognate interaction.

CHAPTER 4

M2 AND M2Y PROTEIN IN VIVO COMPETITION

4 M2 AND M2Y PROTEIN *IN VIVO* COMPETITION

4.1 Introduction

During T cell-dependent responses, naïve B cells present in the follicles of secondary lymphoid organs are activated by exogenous antigen (Batista and Harwood 2009), migrate towards the border area between follicles and T cell zones and interact with antigen-specific T_H cells to become fully activated (Okada, Miller et al. 2005). Consequently, B cells follow one of three destinies: differentiation into short-lived plasmablasts, GC-independent differentiation into unswitched memory B cells (Taylor, Pape et al. 2012), and differentiation into plasmablast and memory B cells through the GC pathway (De Silva and Klein 2015). Access to the latter is a crucial step in gammaherpesvirus pathogenesis. T cell help is limited and selective, which requires that B cells compete with each other for this interaction (Schwickert, Victora et al. 2011).

Hematopoietic stem cells (HSCs) are a self-renewing population capable of differentiating into all blood cell lineages. Furthermore, these cells can be efficiently transduced by retroviruses, allowing the expression of a protein of interest (Ide, Javazon et al. 2008). Due to these characteristics, HSCs are widely used in transplantation as they have the ability to repopulate adult mice and sustain hematopoiesis, the developmental process that ensures the formation of all blood cell types. HSCs can be recovered from the bone marrow of adult mice or from fetal liver, a major hematopoietic organ in the 12.5-15.5 days-old mouse embryo (Morrison, Hemmati et al. 1995, Medvinsky, Rybtsov et al. 2011). Notably, the repopulation potential of fetal liver HSCs has been shown to surpass that of bone marrow HSCs, in that they present a greater proliferative activity (Rebel, Miller et al. 1996). Purification of HSCs has been the focus of many studies and strategies. The tyrosine kinase receptor cKit (CD117), along with Sca-1, is a widely used marker for HSC enrichment. However, this marker is also expressed in many hematopoietic progenitor cells that, like HSCs, do not express lineage markers (Ogawa, Matsuzaki et al. 1991). Therefore, the use of cKit enriches a population for hematopoietic reconstituting activity but it does not convey a pure population of HSCs.

The CD45 congenic marker system is widely used in mouse transplantation experiments. This takes advantage of the easy discrimination of the different CD45 alleles, for which there are commercially available monoclonal antibodies. Cells can be isolated from CD45.1 donor mice and adoptively transferred to CD45.2 recipient mice, or vice-versa,

where exogenous cells are easily distinguished from the endogenous population. Although CD45.1 and CD45.2 are considered to be functionally equivalent, differences in host reconstitution upon adoptive cell transfer have been described (Waterstrat, Liang et al. 2010, Basu, Ray et al. 2013).

MuHV-4 exploits the GC reaction pathway to proliferate and get access to the long-lived memory B cell population. Results from Chapter 2 demonstrated the ability of the M2 viral protein to competitively promote B-T_H cell interaction *in vitro*, when expressed in B cells. To assess whether this ability occurred *in vivo* and translated into a better access to GC reactions, a competition system was designed in collaboration with Dr. Henrique Veiga-Fernandes. This consists of placing primary M2- or M2Y-expressing B cells in direct competition with mock B cells, in the context of a T cell-dependent stimulus. To obtain primary B cells expressing M2-IRES-GFP, M2Y-IRES-GFP and GFP, mouse chimeras were generated by transplantation of transduced, HSC-enriched, fetal liver populations using the CD45 congenic marker system to allow tracking of cells.

4.2 Results

4.2.1 The *in vivo* competition system

B cell cognate interaction with T_H cells, in the context of an immune response to T-cell dependent antigens, results in the initiation of a GC reaction, a critical step in the life cycle of MuHV-4. *In vitro*, expression of M2 in B cells competitively promoted conjugation with T_H cells. To assess whether this advantage had a physiological significance, an *in vivo* competition system was designed (Figure 4.1), in collaboration with Dr. Henrique Veiga-Fernandes.

Briefly, the system consists of placing GFP- (also referred to as mock or empty) and M2-IRES-GFP- (Figure 4.1A) or M2Y-IRES-GFP-expressing (Figure 4.1B) primary B cells in competition for acquisition of T cell help and, consequently, initiation of a GC reaction. These primary B cells are recovered from chimera mice (described in detail in section 4.2.2) and co-transferred in direct competition (1:1 ratio) to sub-lethally irradiated B6 recipient mice. To allow the tracking and discrimination of the adoptively transferred cellular populations the CD45 congenic marker system is used. Therefore, CD45.1/CD45.2 M2-IRES-GFP- and CD45.1 GFP-expressing B cells are co-transferred to CD45.2 B6 mice (Figure 4.1A), while CD45.2 M2Y-IRES-GFP- and CD45.1 GFP-

expressing B cells are co-transferred to CD45.1/CD45.2 B6 mice (Figure 4.1B). Moreover, expression of M2 and M2Y in those populations can be confirmed by detection of GFP. In addition to B cells, $CD4^+$ T cells are also transferred to the recipient mice to compensate for the decrease in the correspondent endogenous population, caused by irradiation. Recipient mice are then administered a T cell-dependent stimulus, 4-Hydroxy-3-nitrophenylacetyl chicken gamma-globulin (NP-CGG) adsorbed to alum (Hikida, Casola et al. 2009), to drive GC formation. 10 days post stimulus, the percentage of M2- or M2Y-expressing B cells within the GC population is assessed by flow cytometry, based on the CD45 marker and GFP expression, and compared to the percentage of the co-transferred mock B cells. The putative competitive advantage provided by the expression of M2 would translate into a predominance of M2-expressing B cells in the GC population.

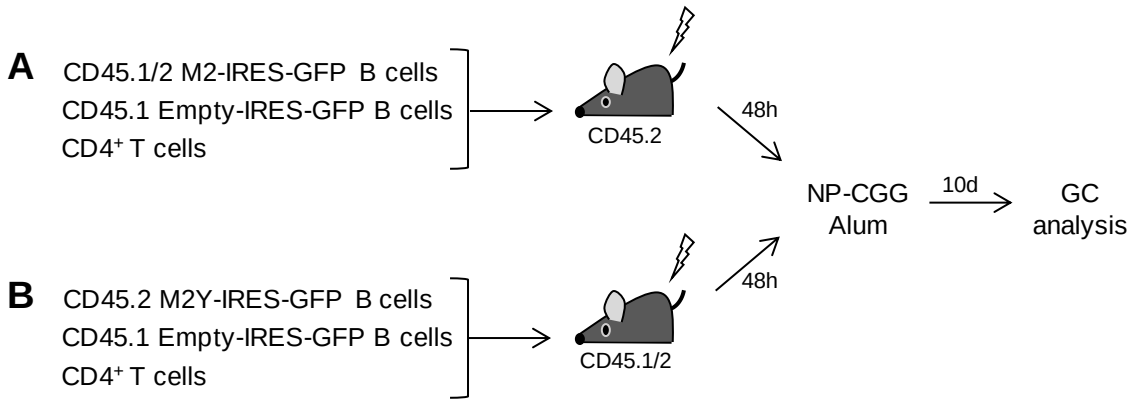

Figure 4.1. Schematic representation of the *in vivo* competition system. The indicated B cell populations are co-transferred, at a 1:1 ratio, along with $CD4^+$ T cells, to irradiated mice. (A) M2-expressing B cells are placed in direct competition with mock B cells (empty). (B) M2Y-expressing B cells are placed in direct competition with mock B cells. The CD45 congenic marker system is used to allow the tracking and discrimination of the different cellular populations. 48h after transfer, mice are administered intraperitoneally a T cell-dependent stimulus, NP-CGG adsorbed to alum. GC is analyzed 10 days post stimulus.

To optimize the conditions for adoptive transfer of primary B cells to recipient mice several irradiation doses and several numbers of adoptively transferred B cells were tested. B cells were recovered by negative selection from the lymph nodes of CD45.1 B6 background mice, as described in detail in section 7.2.3.3. Flow cytometric analysis of the initial cell suspension, in parallel with the purified population, confirmed the enrichment in $B220^+$ cells (Figure 4.2). B cell purity was consistently above 98%. CD45.1 B cells were then intravenously transferred to sex-matched C57BL/6J recipient mice (CD45.2). One to two days post transfer, recipient mice were intraperitoneally injected with a T cell dependent stimulus, NP-CGG adsorbed to alum, to drive GC formation. 10 days post

transfer the spleen was collected for flow cytometric analysis (Figure 4.3). A naïve mouse, that was not adoptively transferred nor injected with the stimulus, was used as a negative control. The presence of adoptively transferred cells ($CD45.1^{+}CD45.2^{-}$) was assessed in the GC population, defined as $B220^{+}CD95^{hi}GL7^{hi}$ (Figure 4.3A).

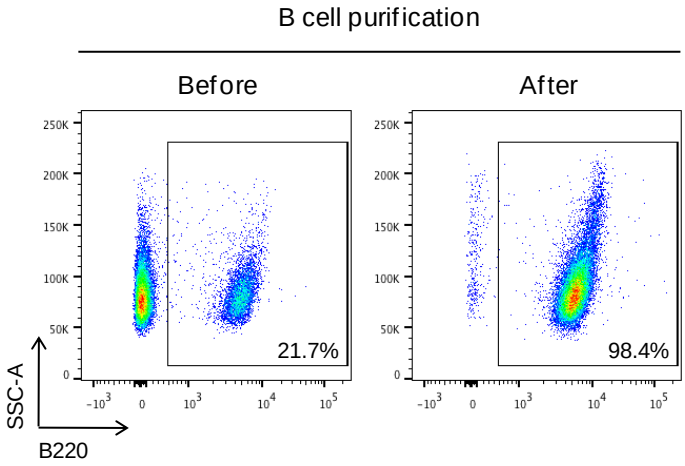

Figure 4.2. Flow cytometric analysis of B cell purity. Briefly, B cells were purified from the lymph nodes of CD45.1 B6 background mice, using a negative selection kit (MACS, Miltenyi Biotec), according to manufacturer's instructions. A fraction of the initial cell suspension (before) and a fraction of the purified population (after) were stained with an anti-B220 antibody and analyzed on a LSR Fortessa flow cytometer (BD Biosciences). The percentage of cells in the B cell gate is shown. B cell purity was consistently above 98%.

Upon adoptive transfer of 10^6 B cells to recipient mice, followed by stimulation, very few CD45.1 B cells were found in the GC (Figure 4.3B). This could be explained by an incorrect homing of these cells to the spleen or by the lack of space for the cells to proliferate. To test the latter hypothesis, recipient mice were irradiated (250rad) prior to adoptive transfer (Figure 4.3C). This led to a higher percentage of transferred cells within the GC population (0.5%). An increase in the irradiation dose, from 250rad to 500rad, further improved that result to an average of 6.5% of CD45.1 B cells (Figure 4.3D). Together, these results show that irradiation of the recipient mice is required for survival of the adoptively transferred population. Transfer of a higher number of adoptively transferred B cells ($3.5x10^6$ cells) to irradiated mice (500rad) resulted in a major increase, with an average of 35% transferred B cells within the GC (Figure 4.3E). Therefore, use of a 500rad irradiation dose and transfer of $1\text{-}3.5x10^6$ B cells were chosen as the optimal conditions for *in vivo* competition analysis.

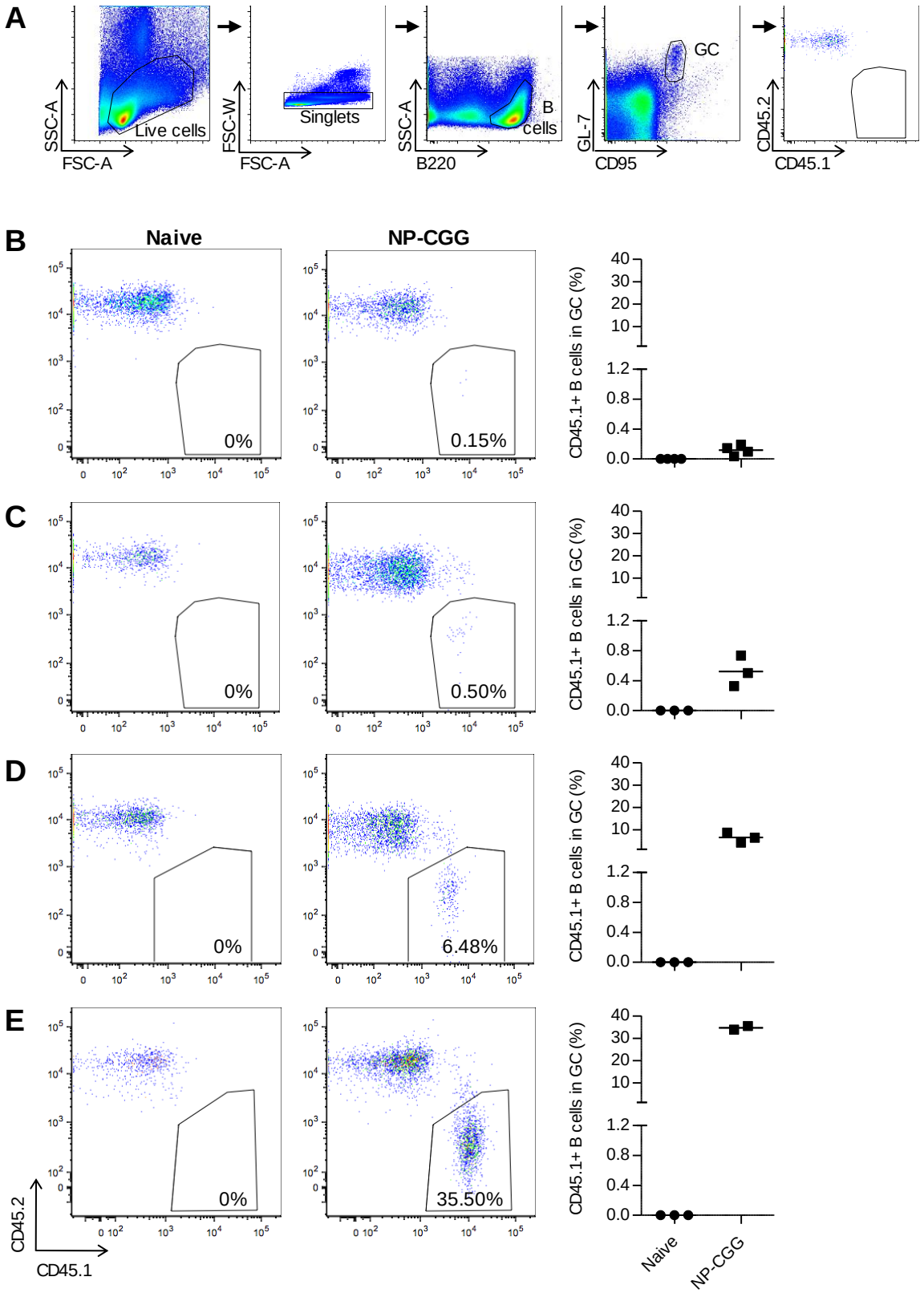

Figure 4.3. Optimization of the conditions for adoptive transfer of B cells to C57BL/6J mice. B cells were purified from the lymph nodes of CD45.1 B6 background mice and adoptively transferred to C57BL/6J mice by intravenous injection. One or two days after transfer, recipient mice were intraperitoneally injected with a T cell dependent stimulus, 4-Hydroxy-3-nitrophenylacetyl hapten conjugated to Chicken Gamma Globulin (NP-CGG) adsorbed to alum.

Germinal center (GC) analysis by flow cytometry was carried out ten days after the stimulus. A naïve mouse, that was not adoptively transferred nor injected with the stimulus, was used as a negative control. (A) Gating strategy used for GC analysis defined in a naïve mouse. GC B cells were identified as $B220^{+}CD95^{hi}GL7^{hi}$. The adoptively transferred population was identified, within the GC population, as $CD45.1^{+}CD45.2^{-}$, in contrast with the $CD45.1^{-}CD45.2^{+}$ endogenous population. (B) 10^6 CD45.1 B cells were adoptively transferred to recipient mice and stimulus was injected one day after transfer. (C) 10^6 CD45.1 B cells were adoptively transferred to irradiated (250rad) recipient mice and stimulus was injected two days after transfer. (D) 10^6 CD45.1 B cells were adoptively transferred to irradiated (500rad) recipient mice and stimulus was injected two days after transfer. (E) $3.5x10^6$ CD45.1 B cells were adoptively transferred to irradiated (500rad) recipient mice and stimulus was injected two days after transfer. (B) to (E) Representative FACS plots are shown on the left and compiled data is shown on the right. Values correspond to the percentage of transferred cells within GC.

4.2.2 Generation of mouse chimeras

To produce the mock, M2- or M2Y-expressing primary B cells, mouse chimeras were generated (Figure 4.4). Fetal liver cellular suspensions were obtained from 15 days-old mouse embryos expressing the allelic forms CD45.1, CD45.2 or CD45.1/CD45.2 heterozygous (section 7.2.7.2). Suspensions were then enriched for hematopoietic stem cells (HSCs) by using an antibody against cKit, as described in detail in section 7.2.3.4. This enrichment was confirmed with a staining for cKit, followed by flow cytometric analysis (Figure 4.5A). As described in detail in section 7.2.3.6, CD45.1, CD45.2 and CD45.1/CD45.2 HSC-enriched populations were then transduced with viral particles that allowed the expression of GFP alone (empty or mock condition), M2Y-IRES-GFP or M2-IRES-GFP, respectively. Transduction efficiency was evaluated on the next day as the percentage of GFP^{+} cells (Figure 4.5B). In the empty condition, approximately 50% of the cells were transduced. Addition of the M2 or M2Y DNA sequence to the expression cassette reduced this efficiency to 36-37%. Sorting of transduced GFP^{+} cells prior to adoptive transfer resulted in cell death and poor reconstitution of the host. Therefore, irradiated Rag*1*$^{-/-}$ CD45.1 hosts were reconstituted with the total cell populations that were subjected to transduction.

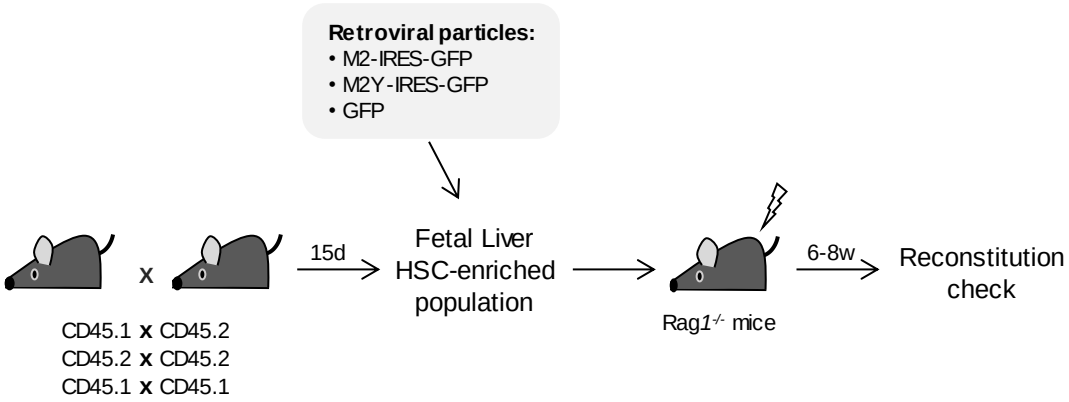

Figure 4.4. Schematic representation of the generation of mouse chimeras. CD45.1 and CD45.2 B6 mice were breed as indicated. 15days post breeding, fetal liver HSC-enriched populations were obtained from B6 CD45 heterozygous, CD45.2 or CD45.1 embryos and transduced with M2-IRES-GFP, M2Y-IRES-GFP or GFP retrovirus, respectively. $2x10^6$ cells of each population were then transferred intravenously to independent irradiated (600rad) Rag*1*$^{-/-}$ mice. 6 to 8 weeks following transplantation, blood was collected for flow cytometric analysis, to confirm reconstitution.

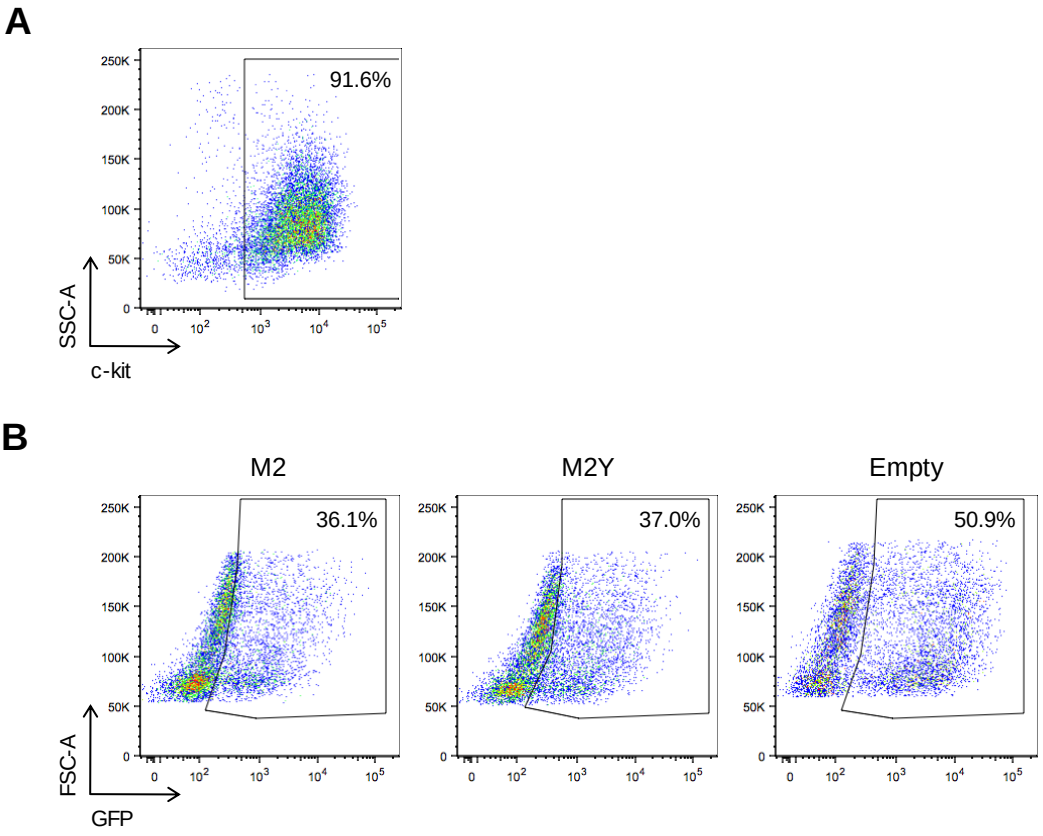

Figure 4.5. Flow cytometric analysis of fetal liver cell enrichment and transduction. CD45.1, CD45.2 and CD45.1/2 fetal liver was obtained from 15 days-old mouse embryos (as described in section 7.2.7.2). Cell suspensions were enriched for hematopoietic stem cells (HSCs) by positive selection of c-kit expressing cells (as described in section 7.2.3.4). Next, cells were transduced with viral particles that allow the expression of M2-IRES-eGFP, M2Y-IRES-eGFP or eGFP alone

(empty), used as a control. (A) Flow cytometric confirmation of HSC enrichment, as determined by expression of c-kit. (B) Flow cytometric analysis of transduction efficiency. Following transduction cells were cultured O/N. Transduction efficiency was then assessed as the percentage of GFP-expressing cells.

Chimera mice were analyzed 6 to 8 weeks after adoptive transfer to confirm reconstitution. To that end, blood was collected from the facial vein of chimera mice and stained for B cells ($B220^+$), myeloid cells ($MAC1^+GR1^+$), $CD4^+$ T cells and $CD8^+$ T cells (Figure 4.6). In mice reconstituted with M2-transduced HSCs, there was a dramatic reduction in the percentage of B cells (15%), which was not observed in mice reconstituted with M2Y- (48%) or Empty-transduced HSCs (50%) (Figure 4.6A). The decrease in the B cell population observed in the M2 condition allowed an increase in the myeloid cell population (Figure 4.6B). No differences were observed in the analyzed T cell populations (Figure 4.6C). Together, results suggest that the ability of M2 to assemble multiprotein complexes with cell signaling proteins had a negative effect in the development and/or proliferation of the M2-transduced B cell population.

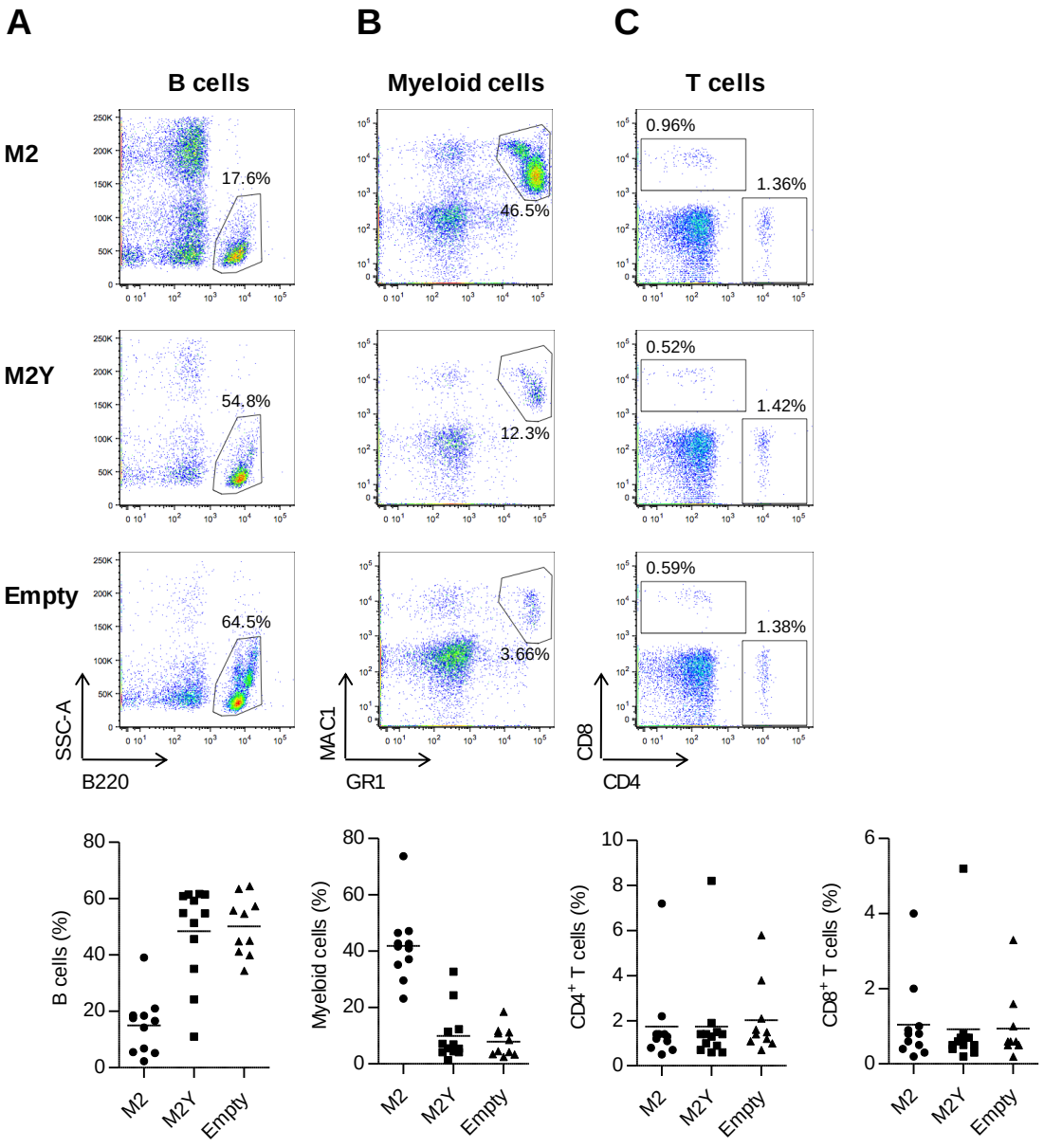

Figure 4.6. Flow cytometric analysis of chimera mice reconstitution. 6-8 weeks following adoptive transfer, blood was collected from the facial vein of chimera mice and stained for (A) B cells ($B220^+$), (B) myeloid cells ($MAC1^+GR1^+$), and (C) $CD4^+$ T cells and $CD8^+$ T cells. Representative FACS plots are shown on top and compiled data obtained from the analysis of 10-12 mice per group is shown below.

The use of a bi-cistronic vector for viral particle production (section 7.2.3.5) allowed the expression of GFP in addition to M2 or M2Y, facilitating the identification of cells that successfully integrated and expressed the retroviral vector. Therefore, the percentage of B cells and myeloid cells expressing M2 or M2Y was assessed by flow cytometry as the percentage of GFP positive events within the indicated populations (Figure 4.7). Mice reconstituted with the empty control had an average of 9% of GFP^+ B cells (Figure 4.7A)

and 4% of GFP$^+$ myeloid cells (Figure 4.7B). Mice reconstituted with M2-transduced HSCs had very small percentages of GFP-expressing B cells (0.2%) (Figure 4.7A) and myeloid cells (0.3%) (Figure 4.7B). The same was true for mice reconstituted with M2Y-transduced HSCs, which had 0.3% of GFP$^+$ B cells (Figure 4.7A) and 1% of GFP$^+$ myeloid cells (Figure 4.7B). Comparing these percentages with the initial percentage of GFP$^+$ HSCs that were used to reconstitute the Rag*1*$^{-/-}$ mice (Figure 4.5) suggests that there was shutdown of the expression cassette to a certain level.

Due to the intrinsic characteristics of the M2 protein, there was a poor B cell reconstitution. Furthermore, in all three conditions, there was shutdown of the expression cassette to a certain level. In the case of the M2 and M2Y conditions, this translated to the impossibility of recovering M2- or M2Y-expressing primary B cells from the chimera mice. Therefore, the *in vivo* competition experiment could not be performed.

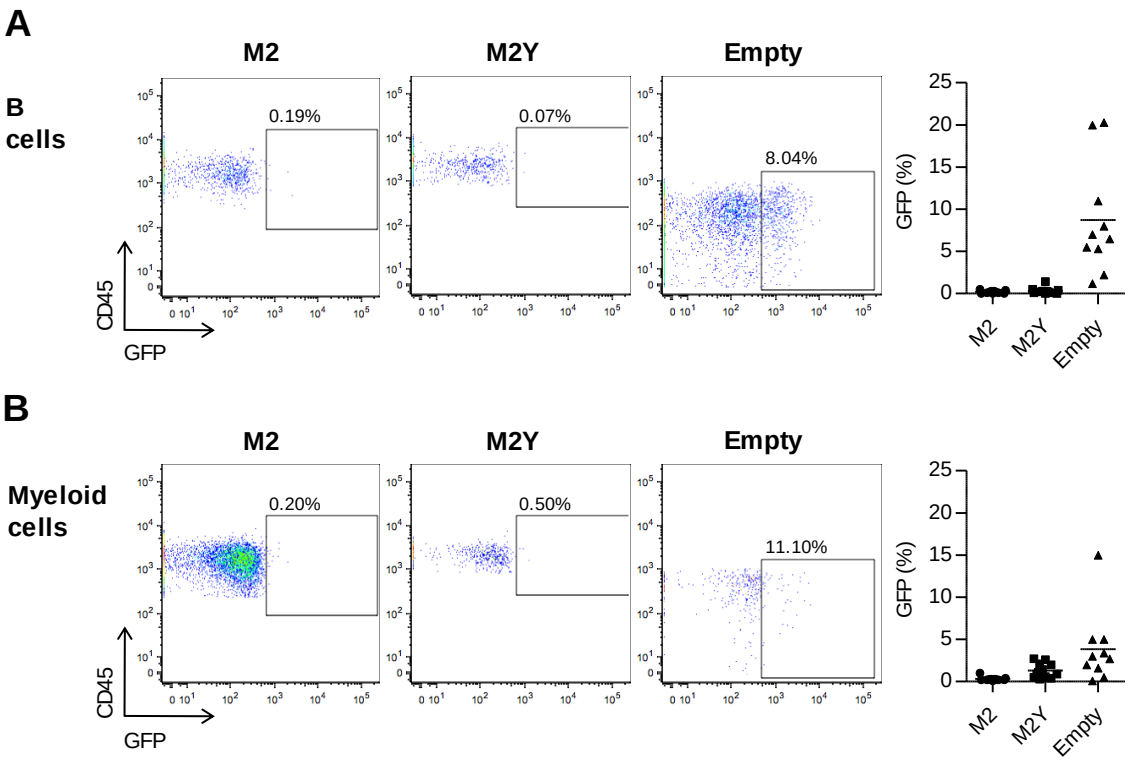

Figure 4.7. Flow cytometric analysis of GFP expression in B and myeloid cell populations of chimera mice. 6-8 weeks following adoptive transfer, blood was collected from the facial vein of chimera mice and stained for several cellular populations. GFP expression was then analyzed in (A) B cells and (B) myeloid cells. Representative FACS plots are shown on the left and compiled data obtained from the analysis of 10-12 mice per group is shown on the right.

4.3 Discussion

To assess whether the *in vitro* ability of M2 to competitively promote B-T_H cell interaction *in vitro* occurred *in vivo*, and translated into a better access to GC reactions, a competition system was designed in collaboration with Dr. Henrique Veiga-Fernandes. Since this system depended on the purification of primary B cells from mouse chimeras, where reconstitution of the B cell compartment in the M2 condition was unsuccessful, the experiment could not be performed.

Irradiated RagKO mice reconstituted with M2-transduced HSC-enriched fetal liver population presented a dramatic deficit in the B cell compartment, which was related to the ability of the viral protein to assemble multiprotein complexes with B cell signaling proteins. The stage of B cell development that was affected by the expression of M2 was not determined.

HSC-enriched fetal liver cells transduced for expression of M2-IRES-GFP, M2Y-IRES-GFP or Empty-GFP were of different allotypes, CD45.1/CD45.2, CD45.2 and CD45.1, respectively. Differences in host reconstitution upon adoptive co-transfer of CD45.1 and CD45.2 cells have been described (Waterstrat, Liang et al. 2010, Basu, Ray et al. 2013). However, these correspond to a differential representation of some B cell subsets, namely the CD45.1 allele is associated with an increased percentage of splenic marginal zone B cells, while the CD45.2 allele is associated with an increased percentage of mature B cells in the lymph nodes and bone marrow. Therefore, these differences in host reconstitution do not explain the dramatic reduction in the circulating B cell population observed in the reconstitution of mice with M2-IRES-GFP-transduced HSC-enriched population.

During hematopoiesis, HSCs give rise to multipotent progenitors that will be on the basis of mature blood cell development. One such progenitor is the common lymphoid progenitor (CLP), included in classical models of hematopoiesis (Metcalf 2007), or the common myelolymphoid progenitor (CMLP), mentioned in more recent models (Lu, Kawamoto et al. 2002). Regardless of the model, these cells are on the basis of pro-B cells which give rise to pre-B cells, and, consequently, immature B cells (LeBien and Tedder 2008). The absence of a key signal at any stage of development, if not corrected, results in apoptosis (Yankee and Clark 2000). The process of B cell development is therefore tightly regulated. One of the checkpoints of this process is the expression of the pre-B cell receptor (pre-BCR) (Martensson, Almqvist et al. 2010). Signaling downstream of this receptor is required for cell proliferation, survival and recombination of the light

chain gene. Changes in this signaling pathway result in defects in early B cell development, as is the case of patients with mutations in Bruton's tyrosine kinase (Btk), a signaling molecule located downstream of the pre-BCR (Martensson, Almqvist et al. 2010). Signaling also includes the PI3K-AKT pathway, where activation of AKT promotes proliferation, survival and differentiation in B cells (Werner, Hobeika et al. 2010). Expression of M2 in B cell lines has been shown to inhibit AKT activation upon BCR stimulation (Pires de Miranda, Lopes et al. 2013), an observation that is dependent on the unconventional ITAM. Therefore, it is possible that expression of M2 during B cell development negatively affected the survival and proliferation of B cell progenitors and, consequently, led to a reduced amount of mature B cells.

An alternative strategy would be the use of an inducible gene expression system, such as the SparQ™ Cumate Switch (by System Biosciences) (Mullick, Xu et al. 2006), that would allow the expression of M2 or M2Y only in the final recipient mice, where competition for GC entry takes place. The SparQ™ Cumate Switch (by System Biosciences), currently being optimized for *in vivo* use, employs lentivectors and consists on the utilization of the CymR repressor that binds the cumate operator sequences. Addition of Cumate, a non-toxic molecule, alleviates this repression and allows gene expression. Transduction of the HSC-enriched fetal liver population is not 100% efficient. Consequently, not all B cells in the chimera mice would carry the expression cassette that includes the coding sequences for M2/M2Y-IRES-GFP. Therefore, an induction step could also be required in the chimera mice to allow the selection of GFP-expressing B cells. Considering that expression of M2 may influence B cell development, induction would have to be performed after those development stages. In the final recipient mouse, further challenges would be to ensure that expression would be induced in the same number of M2- and M2Y-carrying cells, and at the same level, so that results would not be biased. An alternative strategy to the generation of mouse chimeras would be the direct transduction of primary B cells. This approach was initially rejected because most protocols require the prior activation of the B cell, which could mask the putative competitive advantage provided by expression of M2. Nonetheless, efficient *in vitro* transduction of primary murine B cells with lentivirus, without prior activation, has been described (Warncke, Vogt et al. 2004).

CHAPTER 5

CHARACTERIZATION OF THE M2Y RECOMBINANT VIRUS DELAY IN LATENCY ESTABLISHMENT

5 CHARACTERIZATION OF THE M2Y RECOMBINANT VIRUS DELAY IN LATENCY ESTABLISHMENT

5.1 Introduction

Primarily considered to enter the host orally and directly infect B cells, in-depth studies have proven that there is more complexity associated with the infection pathway of MuHV-4 than initially thought. Following intranasal (i.n.) infection of laboratory mice, believed to reproduce the physiological route, MuHV-4 targets the olfactory neuroepithelium (Milho, Frederico et al. 2012). Free viruses then infect $CD11c^{+}$ myeloid cells, which provide a conduit to lymph nodes (LN) (Gaspar, May et al. 2011). It is proposed that, at this stage, MuHV-4 infects B cells, which may differentiate into plasma cells and release virus into the afferent lymph (Gillet, Frederico et al. 2015). Next, by entering the blood stream, MuHV-4 reaches the spleen, where it exploits normal systemic immune communication routes. Particularly, infection reaches GC reactions, where latency is amplified, attaining maximal levels at day 14 post infection. Infected B cells may then emerge from this process as memory B cells, the long term target population for latent gammaherpesvirus infection.

Tracking of MuHV-4 infection in spleen sections, using recombinant viruses that express fluorescent proteins, revealed the specific splenic populations that the virus infects as well as the order in which they are infected (Frederico, Chao et al. 2014). i.n. infection, although thought to be the route that better mimics the physiological one, implies virus replication in epithelial cells and LNs, the outcome being a more asynchronous splenic infection, where it is difficult to distinctly observe the different stages. Therefore, the knowledge on the order of infection of the different splenic populations was only possible to obtain due to the use of the intraperitoneal (i.p.) route of infection. Nonetheless, this study has proven that i.p. and i.n. infections show the same component steps of splenic colonization, thus validating the use of i.p. infection. The first step of spleen colonization, as detected at 4dpi, is infection of marginal zone (MZ) macrophages. The use of a virus that expresses EGFP from a viral M3 promoter, that is active mainly in lytic infection, allowed to conclude that MZ infection is mainly lytic. At 8dpi, MuHV-4 is already detected in B cell subsets, with approximately 75% of the infection being restricted to the WP. Thorough analysis revealed that macrophages provide access to MZ B cells which, in turn, relocate to the white pulp (WP). Follicular dendritic cells (DCs) then make the bridge between MZ and follicular (Fo) B cells, which are able to participate in GC reactions.

M2 was initially classified as a latency-candidate protein due to the genomic position of its coding gene, homologous to the position of genes that code for latency proteins in other gammaherpesviruses (Virgin, Latreille et al. 1997, Virgin, Presti et al. 1999). This was later on confirmed experimentally (Husain, Usherwood et al. 1999, Virgin, Presti et al. 1999). Further studies on the establishment of latency in the spleen demonstrated that *M2* gene is expressed in DCs and in several B cell subsets, namely: MZ B cells, Fo B cells and GC B cells (Flano, Kim et al. 2002, Marques, Efstathiou et al. 2003). In agreement with M2 being a latency-associated protein, expression of *M2* is not detected in macrophages, a population shown to be lyticaly infected (Frederico, Chao et al. 2014).

The tyrosine residues Y120 and Y129 constitute an unconventional ITAM that is involved in the assembly of multiprotein complexes with cell signaling proteins (Pires de Miranda, Lopes et al. 2013). i.n. infection with a recombinant virus, designated M2Y, where these residues were mutated to phenylalanines, resulted in a delay in latency establishment (Pires de Miranda, Alenquer et al. 2008). This was characterized by a deficit in latent infection levels and splenic follicle colonization at the latency peak (14dpi). Maximal levels of GC infection were only observed at 21dpi. Long term comparison between the levels of infection of WT and M2Y viruses showed no differences, indicating that the unconventional ITAM of the M2 protein is not important for the maintenance of long term latency.

Given what is known on the unconventional ITAM of M2, the M2Y delay in latency establishment may be explained by a B cell phenotype. Moreover, it may be due to an inefficient colonization of GCs, resultant from the lack of promotion of B-T_H cell interaction described in Chapter 2. In order to determine the exact step of spleen infection in which the M2Y recombinant virus is delayed, infection with a fluorescent mutant virus was tracked *in vivo*, quantitatively by flow cytometry and representatively by immunofluorescence of spleen sections. In contrast to what was done by *Frederico, Chao et al. 2014*, the fluorescent viruses used in this study expressed YFP through a human cytomegalovirus (HCMV) immediate early (IE) promoter, instead of the viral M3 promoter or the elongation factor 1α (EF1α) promoter. In similarity to what was done by *Frederico, Chao et al. 2014*, i.p. infection was used as the route for virus delivery. The existence of delay in latency establishment following i.p. virus delivery was confirmed by *ex vivo* reactivation assay and flow cytometric analysis of B cell infection at different times post infection.

5.2 Results

5.2.1 Characterization of M2Y recombinant virus in the context of intraperitoneal infection

Following i.n. inoculation with MuHV-4, the virus replicates in epithelial cells and LN, with lytic viruses reaching the spleen at different times post infection. As observed by *Frederico, Chao et al. 2014* these results in an asynchronous splenic infection, making it difficult to distinctly observe the different stages of infection of splenic populations. For this reason, in this study, intraperitoneal (i.p.) infection was chosen as the appropriate route for virus delivery. Since infection with M2Y recombinant virus has only been characterized in the context of i.n. infection, M2Y latent and lytic viral loads were determined at different timepoints following i.p. infection (Figure 5.1).

C57BL/6J mice were i.p. injected with 10^6 PFU of M2Y YFP-expressing recombinant MuHV-4 and spleens were collected at 4, 8, 10, 14, and 21dpi. A second group of mice was infected with WT YFP-expressing recombinant virus, for comparative purposes. The M2Y YFP-expressing MuHV-4 recombinant virus (vM2Y-YFP) was constructed in our lab by Dr. Marta Alenquer through a methodology that utilizes the MuHV-4 genome cloned in a bacterial artificial chromosome (BAC) (Adler, Messerle et al. 2000). Introduction of the M2Y mutation was confirmed by sequencing across the *M2 ORF*. The genomic integrity of the mutant virus was verified by analysis of restriction enzyme digestion profiles of BAC DNA, performed by Dr. Marta Alenquer. The WT YFP-expressing MuHV-4 recombinant virus (vYFP) was a kind gift from Dr. Samuel Speck (Collins, Boss et al. 2009). Latent infection was then quantified, at each timepoint, by infectious center assay (ICA) (Figure 5.1, closed symbols), as described in detail in section 7.2.8.3. This is an *ex vivo* reactivation assay, in which single cell splenocyte suspensions obtained from infected mice are co-cultured with fibroblast cells permissive to infection with MuHV-4. Reactivation of latent viruses then causes cytopathic effects (cpe) in the form of cell lysis plaques. However, if there are pre-formed infectious virus present at the time of spleen collection, these will contribute to the cpe. Therefore, to assess if the viral load determined by ICA is due to latent and/or lytic viral infection, pre-formed infectious viruses are quantified by plaque assay (PA) (Figure 5.1, open symbols), as described in detail in section 7.2.8.4. To that end, single cell splenocyte suspensions are subjected to freeze-thawing, which disrupts the cells resulting in the impossibility of reactivation from latency. Cell suspensions are then co-cultured with permissive cells, later on examined for cpe.

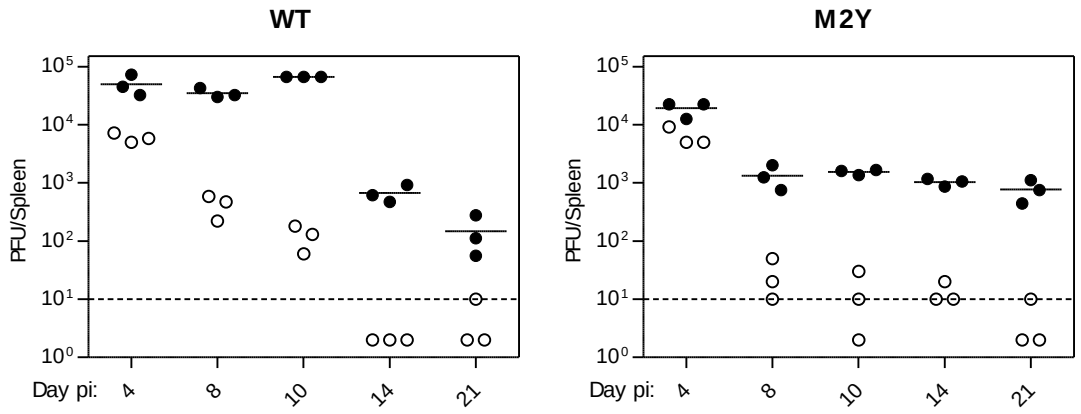

Figure 5.1. Characterization of intraperitoneal infection of C57BL/6J mice with WT and M2Y recombinant viruses. C57BL/6J mice were intraperitoneally inoculated with 10^6 PFU of either WT or M2Y YFP-expressing MuHV-4. At the indicated days post infection (Day pi), spleens were isolated and infection was quantified by *ex vivo* reactivation assay (closed symbols) in each sample. Pre-formed infectious viruses were analyzed by plaque assay (open symbols). Each point represents the titer of an individual mouse. Horizontal bars show arithmetic means. The dashed horizontal line indicates the limit of detection of the assay.

At 4dpi the latent viral load was slightly (2.6-fold) higher for the WT virus, as determined by ICA (Figure 5.1, closed symbols). However, pre-formed infectious virus levels were the same, as determined by PA (Figure 5.1, open symbols). Given that the first step of spleen colonization consists of lytic infection of macrophage populations (Frederico, Chao et al. 2014), results suggested that both viruses equally arrived at the spleen and were able to infect macrophages. However, at 8dpi, the levels of pre-formed M2Y infectious viruses decreased, when compared to the WT virus. The latter presented an increase in latent infection, with a peak at 10dpi, that started to decrease at day 14pi. This was accompanied by a continuous decrease in lytic infection, that was undetectable from day 14pi onward. In contrast, the highest levels of infection with M2Y virus were detected at days 14 and 21pi, never attaining WT levels. This is concomitant with the delay in latency establishment described for i.n. infection with the mutant virus.

MuHV-4 latent infection is associated with the B cell population. To further confirm that the M2Y recombinant virus has a delay in latency establishment following i.p. infection, YFP expression was analyzed in total B cells (Figure 5.2). Briefly, C57BL/6J mice were i.p. infected with 10^6 PFU of WT or M2Y YFP-expressing viruses. Spleens were then collected at 4, 8, 10, 14 and 21dpi and analyzed by flow cytometry. A non-infected mouse was used at each timepoint as a negative control and is represented as a dashed line. WT infection was visible from day 8pi onward, with a peak at day 10 (Figure 5.2, closed symbols).

Subsequently, it decreased from day 14pi onward to nearly undetectable levels at day 21pi. In contrast, B cell infection with M2Y virus only peaked at 14dpi (Figure 5.2, open symbols), never attaining WT levels. This confirmed the latency delay described for this virus.

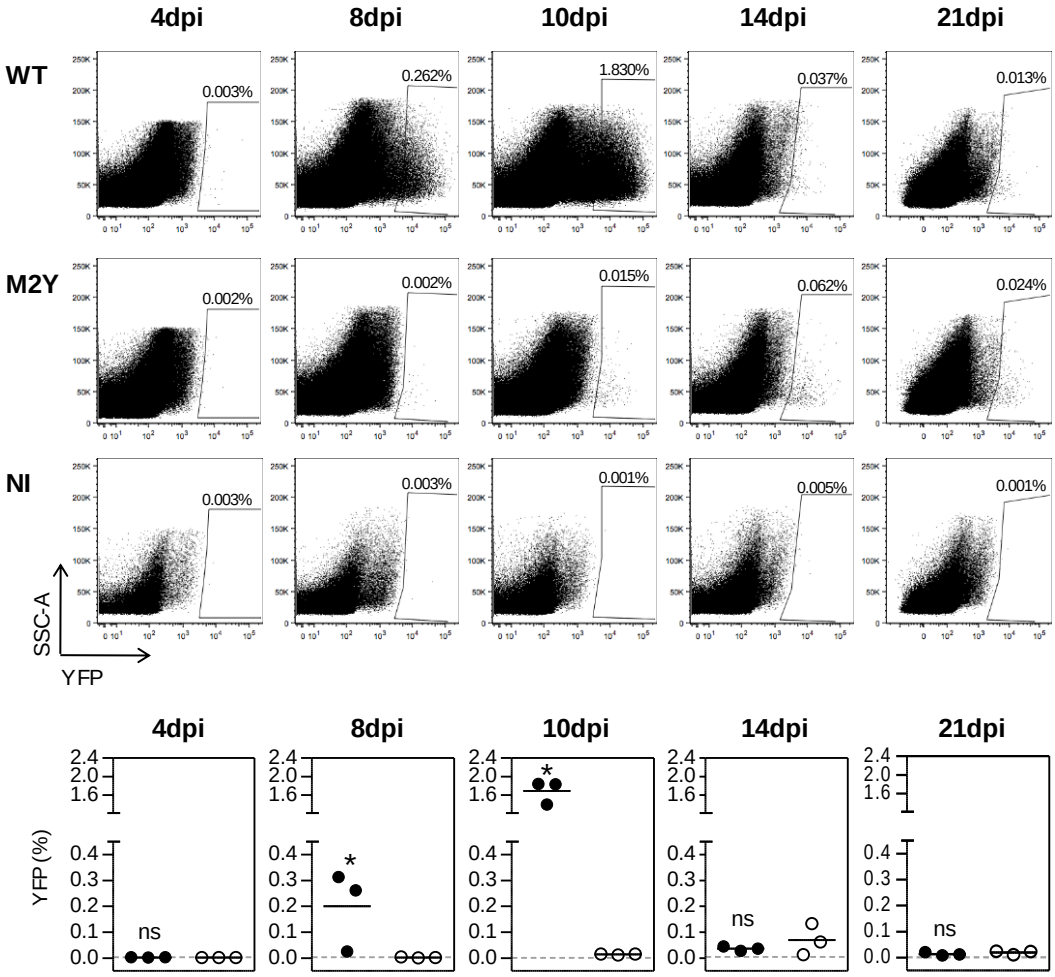

Figure 5.2. Characterization of B cell infection following intraperitoneal inoculation with WT and M2Y YFP-expressing MuHV-4. C57BL/6J mice were intraperitoneally infected with 10^6 PFU of WT (closed symbols) or M2Y (open symbols) YFP-expressing MuHV-4. At the indicated days post infection (dpi), spleens were isolated for flow cytometric analysis of the percentage of YFP^+ cells in total B cells, defined as $CD19^+$ cells. Representative FACS plots are shown on top and compiled data from a single experiment is shown below. Each dot represents a mouse. The dashed line represents the limit of detection, as determined by the percentage of YFP^+ cells obtained with a non-infected (NI) mouse.

5.2.2 Tracking M2Y virus infection of splenic populations

MuHV-4 disseminates to secondary lymphoid organs with the purpose of establishing latency in memory B cells. Once in the spleen, the virus infects macrophages, a step mainly attributed to lytic infection. It then spreads to MZ B cells and follicular B cells, which in turn are able to interact with $CD4^+$ T cells and initiate a GC reaction. In order to determine the step at which the M2Y virus is delayed, infection was tracked in the mentioned cellular populations through flow cytometry (Figure 5.3), namely: Fo B cells ($CD19^+$ $CD21^{int}$ $CD23^+$), MZ B cells ($CD19^+$ $CD23^-$ $CD21^+$), GC B cells ($CD19^+$ $GL7^{hi}$ $CD95^{hi}$), DCs ($B220^-$ $CD11b^{int}$ $CD11c^+$), and macrophages ($B220^-$ $CD11c^-$ $CD11b^+$). The limit of detection of the assay was determined by the YFP^+ events obtained with a non-infected mouse and represented in the graphs as a dashed line.

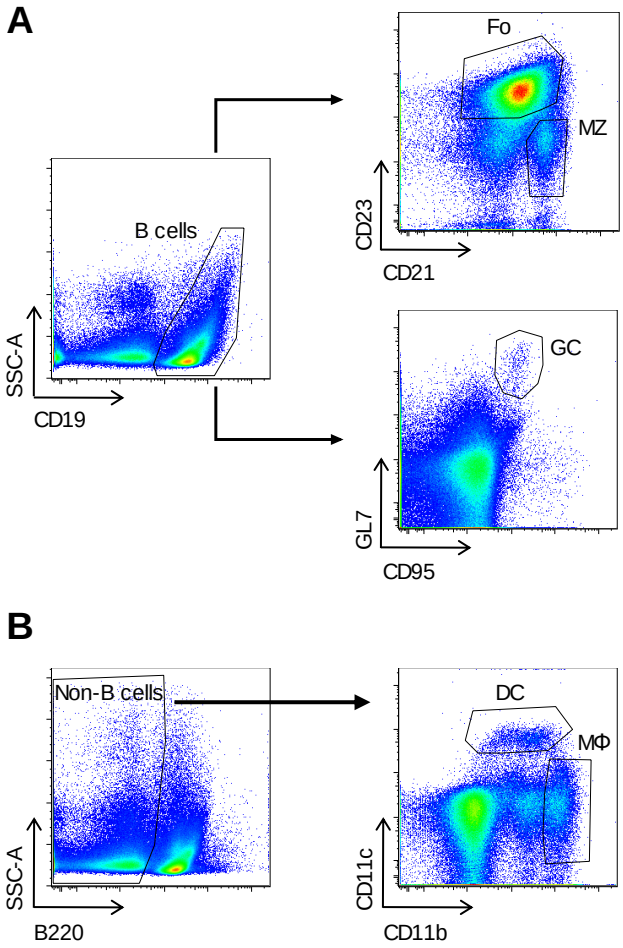

Figure 5.3. Splenic populations analyzed in this study. C57BL/6J mice were intraperitoneally inoculated with 10^6 PFU of WT or M2Y YFP-expressing MuHV-4. At different days post infection, spleens were isolated for flow cytometric analysis. (A) After gating on B cells ($CD19^+$), the following populations were discriminated: follicular (Fo) B cells ($CD19^+$ $CD21^{int}$ $CD23^+$), marginal zone (MZ) B cells ($CD19^+$ $CD21^{hi}$ $CD23^-$), and germinal center (GC) B cells ($CD19^+$ $CD95^{hi}$ $GL7^{hi}$). (B) After

gating on non-B cells ($B220^-$), the following populations were discriminated: dendritic cells (DC) ($B220^-$ $CD11b^{int}$ $CD11c^+$), and macrophages ($B220^-$ $CD11b^{hi}$ $CD11c^-$).

As demonstrated Frederico et al, 2014 infection at 4dpi is mainly lytic. Furthermore, it is mainly restricted to macrophage populations. Therefore, high levels of macrophage infection were expected at this timepoint. However, only 0.011% and 0.003% of macrophages were found to be infected with WT or M2Y viruses, respectively. These percentages were disregarded because they corresponded to very few YFP^+ events (3 to 11). Therefore, neither WT nor M2Y virus infection could be detected by flow cytometry at 4dpi (Figure 5.4). This indicates that either the YFP expression cassette is not expressed during lytic infection or that the expression per cell is too low to be distinguished from the negative population. At 8dpi, when latency is increasing, the WT virus was already detected in several populations, particularly in MZ (3.18% on average), Fo (0.09% on average) and GC B cells (3.32% on average). In contrast, M2Y was still below detection limits for all populations analyzed except MZ B cells (0.014%) (Figure 5.5). This infection was once more disregarded due to the very few positive events (11 on average). Percentages of infection of MZ and Fo B cells are most likely underestimated, as the markers used to discriminate these populations, CD21 and CD23, have been shown to be downregulated as a consequence of MuHV-4 infection (Collins, Boss et al. 2009). Nonetheless, infection was detectable with the WT virus and there was a significant difference between the latter and M2Y infection of MZ B cells, suggesting a B cell phenotype.

To exclude the possibility that at 4dpi the levels of YFP expression per cell were too low to be detected by flow cytometry, and in similarity to what was done by *Frederico, Chao et al. 2014*, infection was analyzed by immunofluorescence of frozen spleen sections, with an antibody against YFP to amplify the signal. Briefly, C57BL/6J mice were i.p. infected with 10^6 PFU of WT or M2Y YFP-expressing viruses. At the appropriate days post infection, spleens were collected, fixed, frozen in OCT and sectioned for immunofluorescence (described in detail in section 7.2.9). At 4dpi, spleen sections were stained for the two macrophage populations known to be infected by MuHV-4 at that timepoint: MZ macrophages (MARCO) and MZ metallophilic macrophages (CD169) (Frederico, Chao et al. 2014). No YFP accumulation was detected in any of the populations analyzed, independently of the virus tested (Figure 5.6), confirming that YFP-expressing viruses do not allow the detection of lytic infection. To validate the absence of YFP signal observed at 4dpi, as a positive control, immunofluorescence of spleen sections was performed at 8dpi, a timepoint when YFP could be detected by flow

cytometry. Given that MuHV-4 is known to me mainly found in the WP at this timepoint (Frederico, Chao et al. 2014), spleen sections were stained for endothelial cells (MAdCAM-1) and follicular B cells (IgD) (Figure 5.7). WT, but not M2Y, infection was promptly detected and was mainly restricted to the WP, as denoted by the position of the infected cells relative to the endothelial and follicular B cell staining. Together, results confirm that lytic infection with YFP-expressing viruses cannot be detected by immunofluorescence of frozen spleen sections. As observed by flow cytometry, latent infection with M2Y could not be detected. In contrast, WT latent infection was in agreement with the observations made by *Frederico, Chao et al. 2014*.

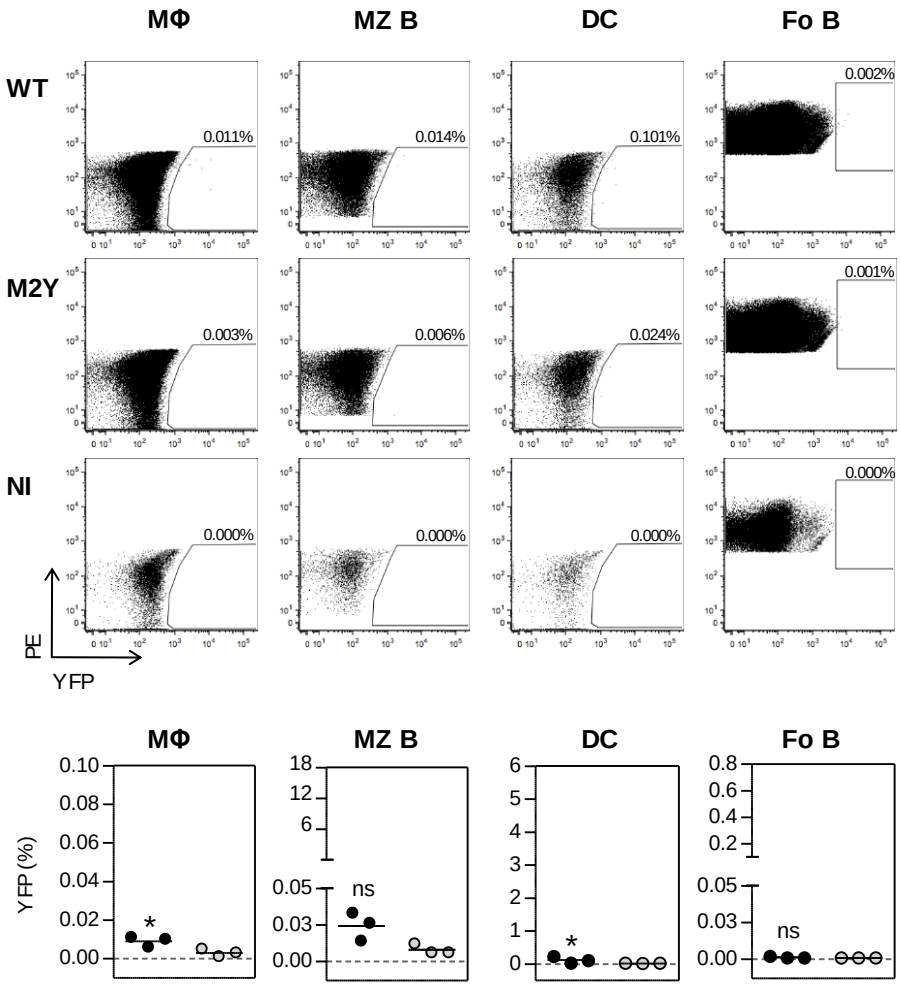

Figure 5.4. Lytic infection following intraperitoneal infection with MuHV-4 is not detectable by flow cytometry. C57BL/6J mice were intraperitoneally infected with 10^6 PFU of WT (closed symbols) or M2Y (open symbols) YFP-expressing MuHV-4. At 4 days post infection (dpi), spleens were isolated for flow cytometric analysis of the percentage of YFP^+ cells in the indicated populations. Representative FACS plots are shown on top and compiled data from a single experiment is shown below. Each dot represents a mouse. The dashed line represents the limit of detection, as determined by the percentage of YFP+ cells obtained with a non-infected (NI) mouse. MΦ, macrophages; MZ B, marginal zone B cells; DC, dendritic cells; Fo B, follicular B cells.

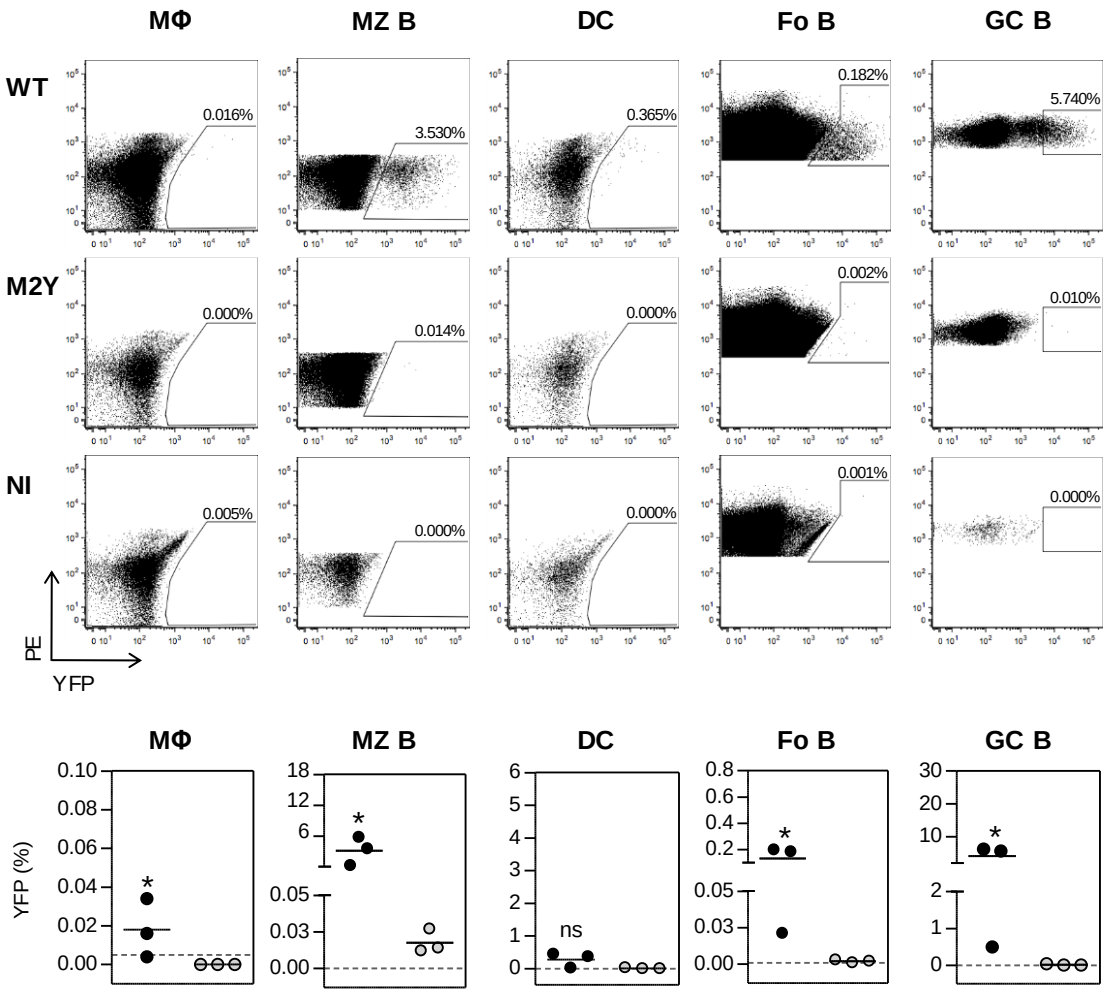

Figure 5.5. WT, but not M2Y, infection has reached GC B cells at 8dpi. C57BL/6J mice were intraperitoneally infected with 10^6 PFU of WT (closed symbols) or M2Y (open symbols) YFP-expressing MuHV-4. At 8 days post infection (dpi), spleens were isolated for flow cytometric analysis of the percentage of YFP^+ cells in the indicated populations. Representative FACS plots are shown on top and compiled data from a single experiment is shown below. Each dot represents a mouse. The dashed line represents the limit of detection, as determined by the percentage of YFP+ cells obtained with a non-infected (NI) mouse. MΦ, macrophages; MZ B, marginal zone B cells; DC, dendritic cells; Fo B, follicular B cells.

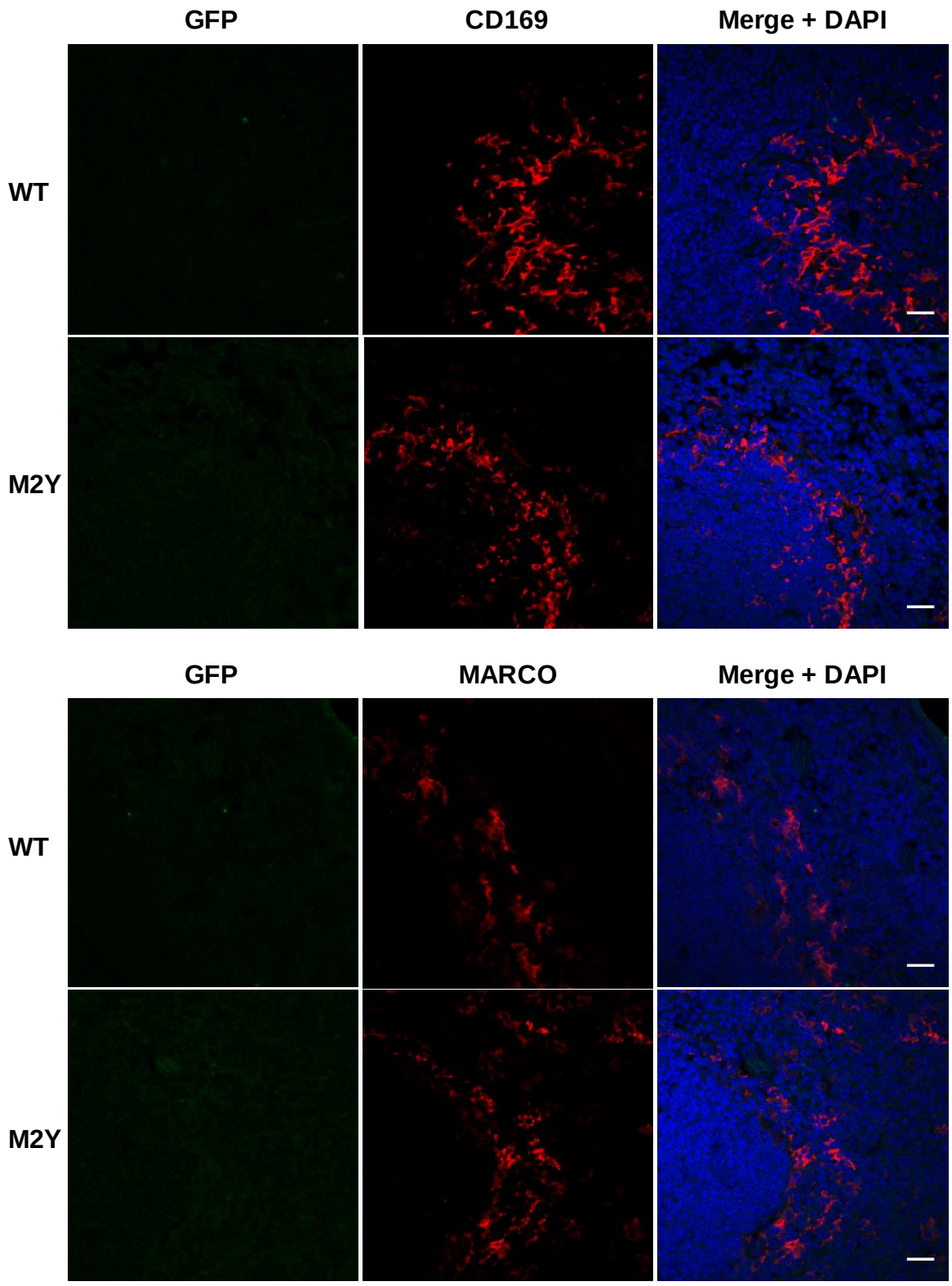

Figure 5.6. Lytic infection following intraperitoneal infection with MuHV-4 is not detectable by immunofluorescence of frozen spleen sections. C57BL/6J mice were intraperitoneally infected with 10^6 PFU of WT or M2Y YFP-expressing MuHV-4. At 4 days post infection (dpi), spleens were isolated, fixed, frozen in OCT and sectioned. Spleen sections were then stained for YFP (green) and either CD169 (MZ metallophilic macrophages) or MARCO (MZ macrophages) (red). Nuclei were stained with DAPI (blue). Scale bars = 20µm. Equivalent results were obtained in three mice.

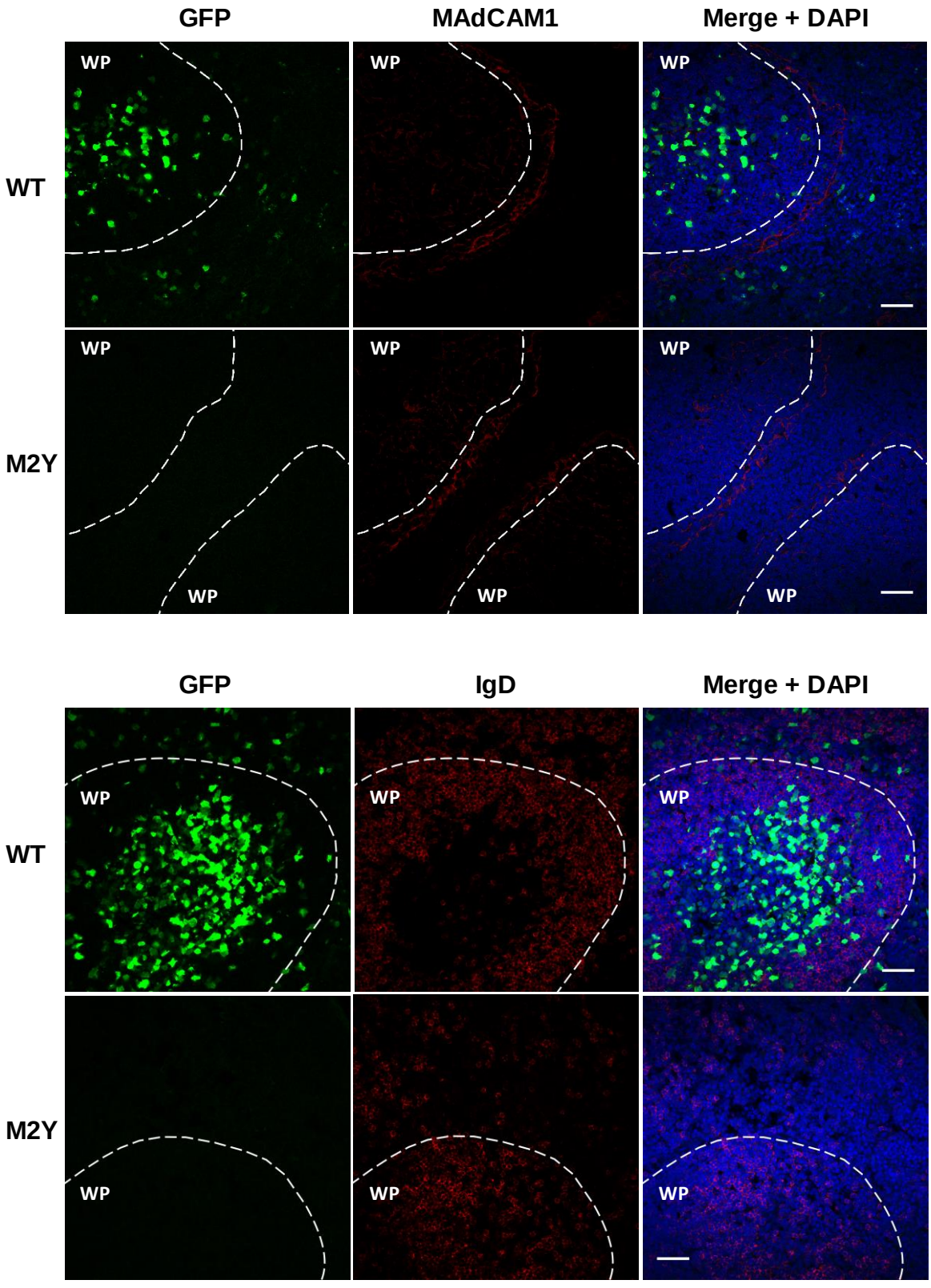

Figure 5.7. WT, but not M2Y, virus has reached the WP at 8dpi. C57BL/6J mice were intraperitoneally infected with 10^6 PFU of WT or M2Y YFP-expressing MuHV-4. At 8 days post infection (dpi) spleens were isolated, fixed, frozen in OCT and sectioned. Spleen sections were then stained for YFP (green) and either MAdCAM-1 (endothelial cells) or IgD (Fo B cells) (red). Nuclei were stained with DAPI (blue). Scale bars = 40μm. Equivalent results were obtained in three mice.

As observed previously by ICA and PA (Figure 5.1), 10dpi was the latency peak for the WT virus, as depicted by the maximal levels of MZ B cell (13.53% on average), DC (3.52% on average), Fo B cell (0.50% on average) and GC B cell infection (20.90% on average) (Figure 5.8). At that timepoint, infection with M2Y virus could be detected at very low levels in Fo (0.006% on average) and GC B cells (0.18% on average). This reached a peak at 14dpi, with an average of 0.02% infected Fo B cells and 0.69% infected GC B cells, once more confirming M2Y delay in latency establishment and revealing that, although the virus is delayed, it is still able to reach germinal centers (Figure 5.9). In contrast, WT levels of infection started to decrease, as observed by the lower percentages of MZ B cell (0.13% on average), DC (0.20% on average), Fo B cell (0.009% on average) and GC B cell (0.74% on average) infection (Figure 5.9). At 21dpi, the levels of infection decreased for both viruses, with WT and M2Y infection being indistinguishable from each other (Figure 5.10).

Since macrophage infection, the first step of spleen colonization, could not be quantified with neither WT nor M2Y virus, it was not possible to conclude with certainty that there were no differences between both viruses at that stage. Consequently, no conclusions can be made as to the population in which the M2Y virus is delayed. Nonetheless, the major difference between WT and M2Y infection was observed in the B cell compartment, as soon as WT infection reached MZ B cells. Therefore, data is not exclusive of a B cell phenotype.

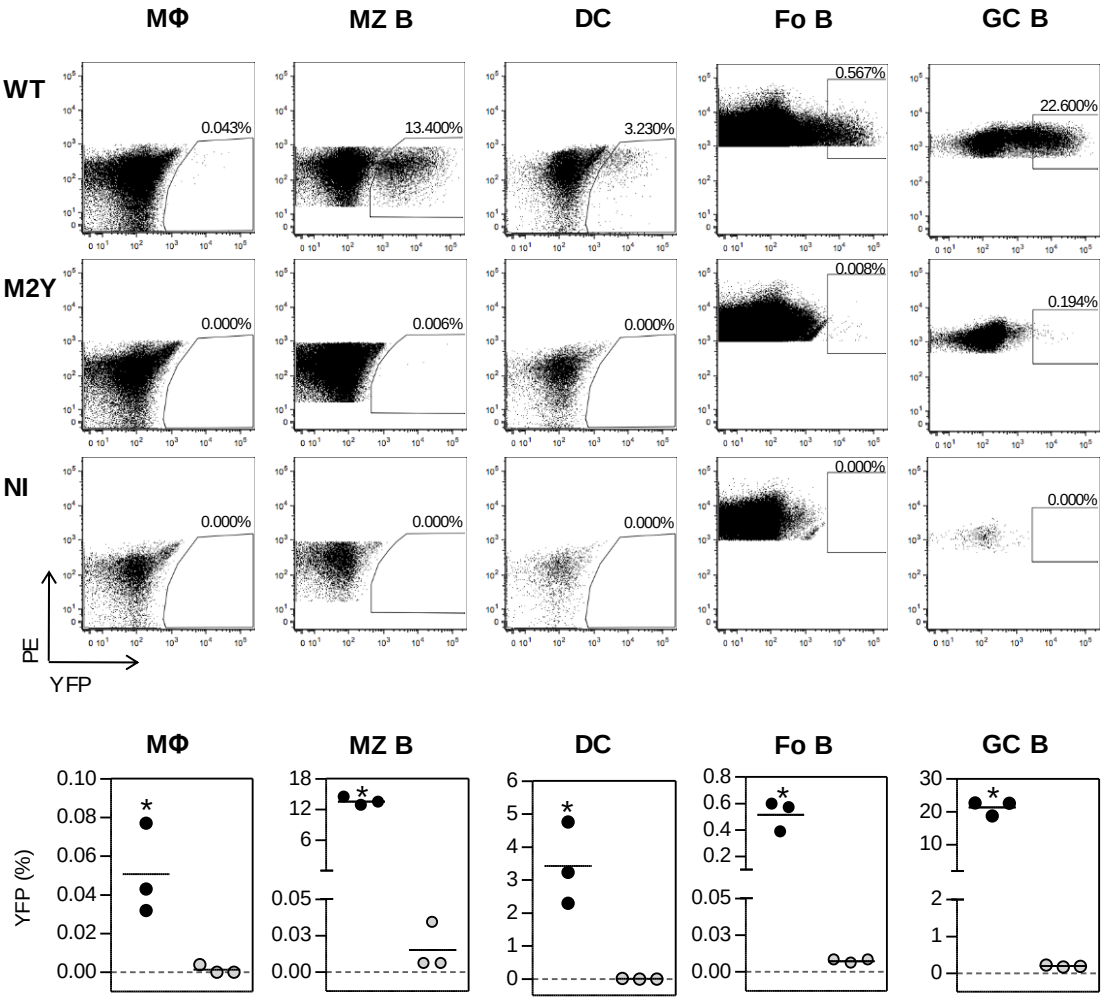

Figure 5.8. Low levels of M2Y infection are detected at 10dpi. C57BL/6J mice were intraperitoneally infected with 10^6 PFU of WT (closed symbols) or M2Y (open symbols) YFP-expressing MuHV-4. At 10 days post infection (dpi), spleens were isolated for flow cytometric analysis of the percentage of YFP^+ cells in the indicated populations. Representative FACS plots are shown on top and compiled data from a single experiment is shown below. Each dot represents a mouse. The dashed line represents the limit of detection, as determined by the percentage of YFP+ cells obtained with a non-infected (NI) mouse. MΦ, macrophages; MZ B, marginal zone B cells; DC, dendritic cells; Fo B, follicular B cells.

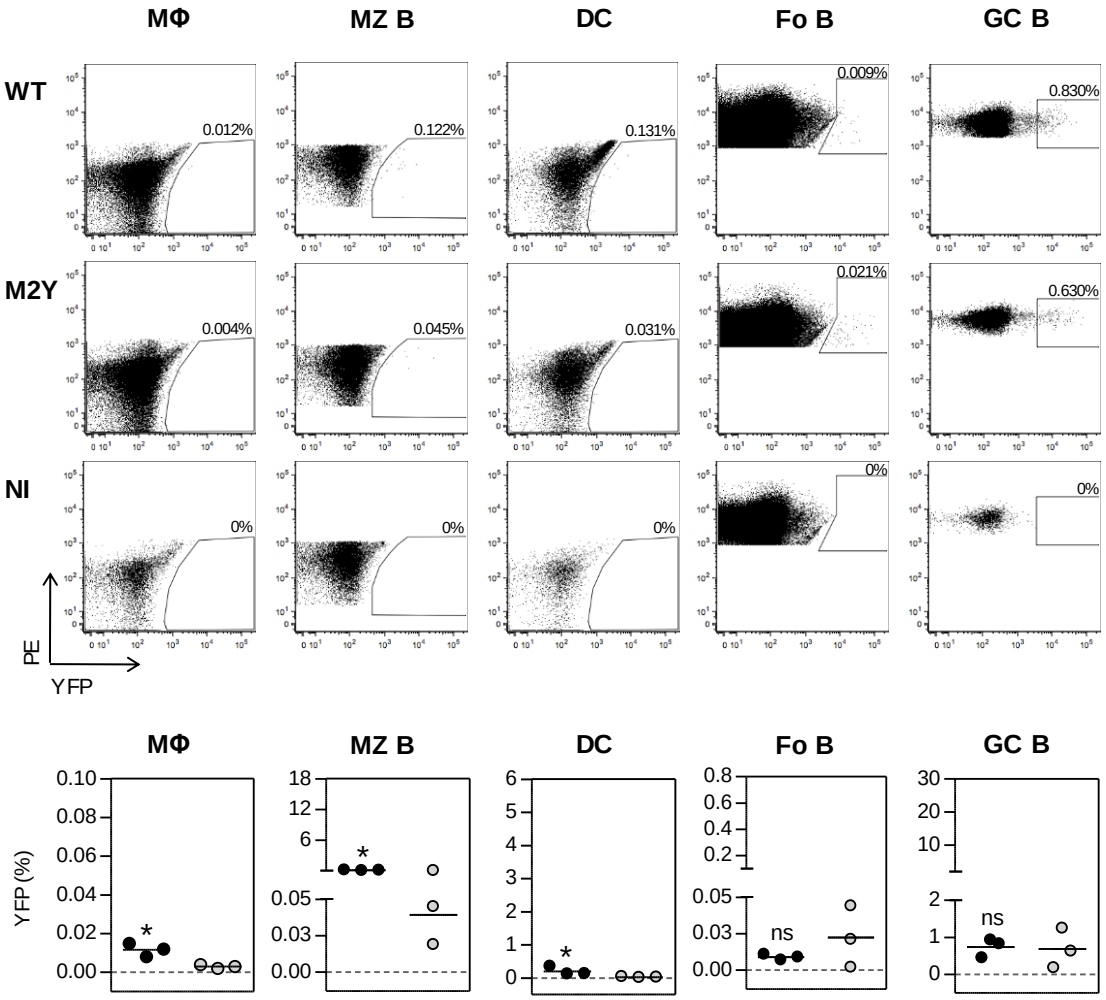

Figure 5.9. M2Y virus reaches a peak of infection at 14dpi. C57BL/6J mice were intraperitoneally infected with 10^6 PFU of WT (closed symbols) or M2Y (open symbols) YFP-expressing MuHV-4. At 14 days post infection (dpi), spleens were isolated for flow cytometric analysis of the percentage of YFP^+ cells in the indicated populations. Representative FACS plots are shown on top and compiled data from a single experiment is shown below. Each dot represents a mouse. The dashed line represents the limit of detection, as determined by the percentage of YFP+ cells obtained with a non-infected (NI) mouse. MΦ, macrophages; MZ B, marginal zone B cells; DC, dendritic cells; Fo B, follicular B cells.

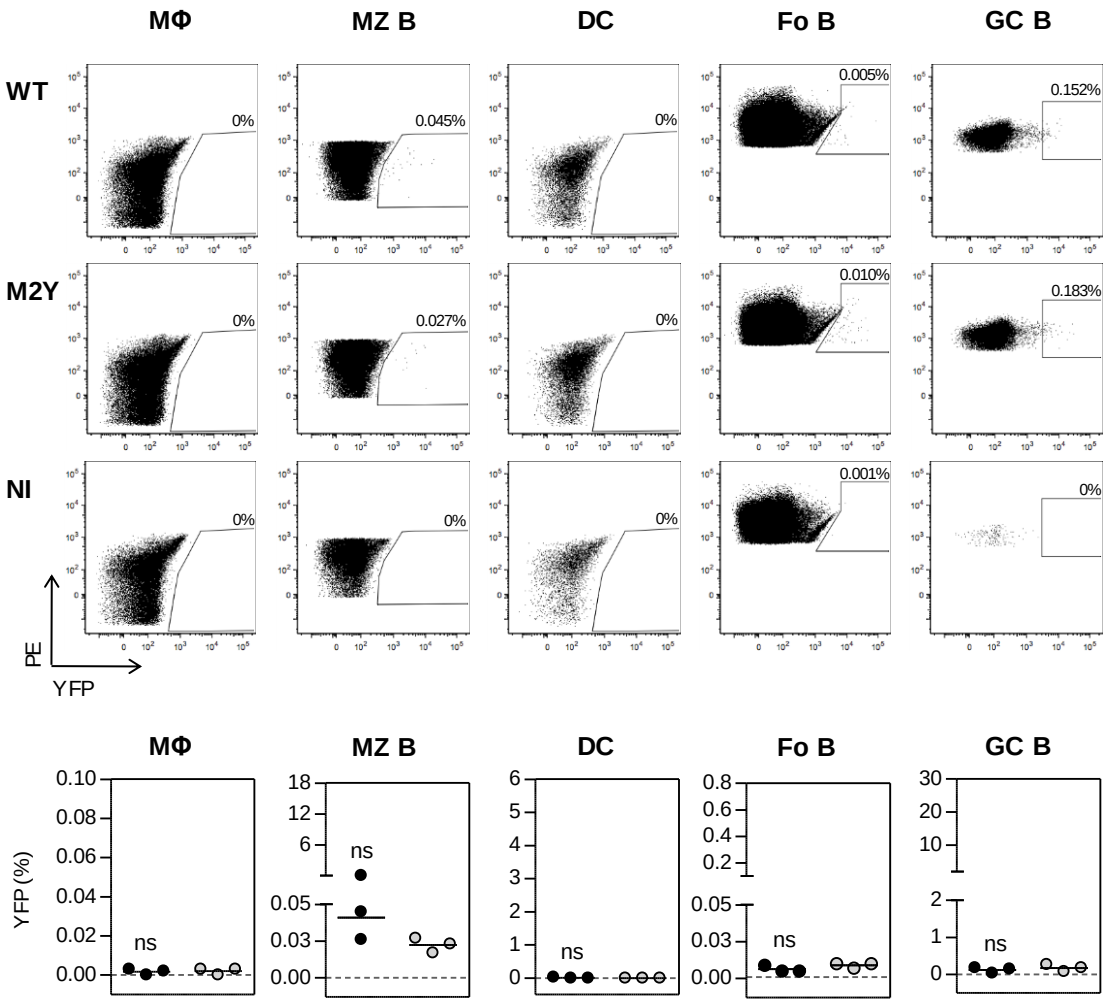

Figure 5.10. Both WT and M2Y infection levels decrease at 21dpi. C57BL/6J mice were intraperitoneally infected with 10^6 PFU of WT (closed symbols) or M2Y (open symbols) YFP-expressing MuHV-4. At 21 days post infection (dpi), spleens were isolated for flow cytometric analysis of the percentage of YFP^+ cells in the indicated populations. Representative FACS plots are shown on top and compiled data from a single experiment is shown below. Each dot represents a mouse. The dashed line represents the limit of detection, as determined by the percentage of YFP+ cells obtained with a non-infected (NI) mouse. MΦ, macrophages; MZ B, marginal zone B cells; DC, dendritic cells; Fo B, follicular B cells.

5.3 Discussion

Characterization of i.p. infection with M2Y YFP-expressing recombinant virus confirmed that, as has been demonstrated for intranasal infection with this mutant (Pires de Miranda, Alenquer et al. 2008), there is a delay in latency establishment.

The first stage of spleen colonization is lytic infection of macrophages, detectable four days after i.p. infection with MuHV-4 (Frederico, Chao et al. 2014). Given that M2 is a

latency-associated protein (Virgin, Latreille et al. 1997, Husain, Usherwood et al. 1999, Virgin, Presti et al. 1999) that is not expressed in infected macrophages (Marques, Efstathiou et al. 2003), no differences should be expected at this stage. In fact, results obtained by PA at this timepoint showed that the total levels of lytic infection with WT and M2Y viruses were the same, which is concomitant with a normal macrophage infection with M2Y recombinant virus. Surprisingly, at 8dpi the load of pre-formed infectious M2Y viruses was lower than the WT. A similar observation has been previously described for a M2-deficient virus (Jacoby, Virgin et al. 2002). One possible explanation is that viruses reactivate from latency and contribute to the lytic viral load. Therefore, the lower load of pre-formed infectious M2Y viruses would reflect the latency deficit that characterizes this virus. Due to the difficulty in detecting YFP expression during lytic infection, it was not possible to confirm by flow cytometric analysis that macrophage infection was the same for both viruses. Concluding, lytic infection with M2Y virus could not be clarified. In the future, efforts could be made to detect lytic infection by RT-PCR in sorted macrophage populations from mice infected with WT or M2Y viruses.

In their study *Frederico, Chao et al. 2014* use recombinant viruses where EGFP is under an EF1α promoter or the lytic M3 promoter, and the expression cassette is located between ORF57 and ORF58 of the virus genome. The fact that the viruses used in this study had YFP expression driven by an HCMV IE promoter, from the ORF27-ORF29b intergenic site may account for the difficulty in detecting YFP expression during lytic infection. In fact, in their characterization of the YFP-expressing MuHV-4, *Collins, Boss et al. 2009* could not detect YFP expression neither following i.p. infection nor in long term analysis. They propose that the HCMV IE promoter/enhancer is directly targeted for silencing by specific host responses, which could explain the absence of YFP expression during lytic infection.

The role of M2 in the modulation of B cell signaling pathways downstream of the BCR (Madureira, Matos et al. 2005, Rodrigues, Pires de Miranda et al. 2006, Pires de Miranda, Alenquer et al. 2008, Pires de Miranda, Lopes et al. 2013), as well as its ability to promote B-T_H cell interaction point out to the possibility of mutation of the Tyr residues leading to a B cell phenotype. In agreement, significant differences were observed in infection of all the B cell subsets analyzed. However, the impossibility of confirming the equal WT and M2Y virus infection of macrophages, the first stage of spleen colonization, does not allow to take definite conclusions on the delay in latency establishment presented by the mutant virus. Nonetheless, results do not exclude a B cell phenotype, which fits the known functions of the unconventional ITAM of M2.

CHAPTER 6

FINAL CONSIDERATIONS

6 FINAL CONSIDERATIONS

Gammaherpesviruses have the ability to persist for the lifetime of the host. Following the initial productive infection, EBV and KSHV reach an equilibrium with their human host where there are no signs of disease. However, this equilibrium may be disturbed giving rise to lymphoproliferative disorders, especially in immunocompromised patients (Damania 2004). Persistence is attained through the exploitation of normal B cell biology, the main target population of these pathogens. Immune evasion, modulation of B cell signaling and latency establishment are some of the strategies used during host colonization. In particular, accessing the long-lived memory B cell population is a crucial step for long-term survival on the host. To achieve that, EBV exploits the GC reaction, driving infected B cells through the process of proliferation and differentiation, presumably without the need for normal T cell help (Thorley-Lawson 2001, Thorley-Lawson 2005, Thorley-Lawson, Duca et al. 2008, Thorley-Lawson, Hawkins et al. 2013). EBV expresses the terminal membrane proteins LMP1 and LMP2A that mimic the function of the B cell receptor and CD40 receptor, respectively, promoting the activation and differentiation of the infected B cell. KSHV, which was more recently discovered, has not yet been clearly linked to this strategy. Nonetheless, it is possible that it similarly exploits the GC. KSHV also possesses two terminal membrane proteins, K1 and K15, that interfere with B cell signaling (Damania 2004).

MuHV-4, the mouse model of gammaherpesvirus infection, belongs to the same genus of KSHV and is also related to EBV. Like the latter, MuHV-4 exploits the GC reaction to have access to the memory B cell compartment. Unlike EBV, this mouse pathogen seems to depend on normal T cell help (Ehtisham, Sunil-Chandra et al. 1993, Usherwood, Ross et al. 1996). The MuHV-4 putative functional homologue of the EBV and KSHV proteins involved in B cell signaling is the M2 protein. This is associated with the latency phase and its expression is detected in several B cell subsets, namely: marginal zone, follicular and GC B cells (Marques, Efstathiou et al. 2003). Furthermore, this protein contains two phosphosites (Y^{120} and Y^{129}), constitutively phosphorylated in B cells, that form an unconventional ITAM. Similar to K1, M2 works as a modulator protein, coordinating the assembly of multiprotein complexes with several cell signaling proteins. M2 therefore assembles a specific signalosome, and it does so independently of BCR stimulation. Such ability is lost upon mutation of the phosphosites (M2Y mutant protein). *In vivo*, the same mutation (M2Y recombinant virus) results in a delay in latency establishment characterized by a reduced number of infected cells and splenic follicles (Madureira,

Matos et al. 2005, Rodrigues, Pires de Miranda et al. 2006, Pires de Miranda, Alenquer et al. 2008). This may be explained by the lack of B cell activation promoted by the M2-associated signalosome. Additionally, this may reflect a delay in accessing the GC reaction, for which T cell help is essential.

Given the delay in latency establishment of M2Y recombinant viruses, the role played by M2 in modulation of B cell signaling and the importance of T cell help for MuHV-4 infection, this thesis set out to investigate the possibility of a role for M2 in the modulation of B-T_H cell interaction. Hypothetically, by manipulating signaling pathways M2 could activate the B cell and induce a pro-synaptic state that would attract T cell help. Given that T cell-dependent responses and, in particular, GC initiation are dependent on cognate interaction (Mills and Cambier 2003, De Silva and Klein 2015), experiments were carried out in a MHC class II-restricted OVAp-specific system, where M2- or M2Y-expressing B cells presenting OVAp were placed in contact with OVAp-specific $CD4^+$ T cells. To address the dependence of M2 function on specific peptide, conjugation experiments were carried out in the absence and in the presence of increasing concentrations of peptide.

In *in vitro* studies, M2 localization is cell type-dependent (Liang, Shin et al. 2004). In B cells, where M2 is known to be expressed *in vivo*, the protein has a juxtamembranar localization. This is dependent on the interaction of a C-terminal proline-rich SH3 binding region of M2 with Src family kinases and is, therefore, not affected in the M2Y mutant. Hence, unlike its putative functional homologues LMP1 and LMP2A from EBV and K1 and K15 from KSHV that are transmembranar proteins, M2 is a cytosolic protein. Nonetheless, the protein can perform its signaling-related functions (Rodrigues, Pires de Miranda et al. 2006, Pires de Miranda, Alenquer et al. 2008, Pires de Miranda, Lopes et al. 2013). Interestingly, K1 was shown to be internalized and act from internal cellular compartments (Tomlinson and Damania 2008), showing that modulation of cell signaling downstream of the BCR by a viral protein is not restricted to a transmembranar localization. In the context of the MHC class II-restricted OVAp-specific system, work from Dr. Filipa Lopes in our laboratory revealed that M2 localizes to the contact zone upon B-T_H cell interaction (Fontinha, Lopes et al. 2015). This was the first evidence pointing to a potential role for M2 in B-T_H cell interaction. Polarization of M2 to the contact zone required the integrity of M2 phosphosites, especially of the tyrosine residue Y^{120}, suggesting that it is dependent on the correct assembly of the signalosome.

The work described in this thesis showed that expression of M2 in B cells *per se* resulted in increased levels of both co-stimulatory and adhesion molecules, which are involved in B-T_H cell interaction. Upregulation of the co-stimulatory molecule CD80 is usually a downstream consequence of antigen binding to the BCR and the resulting B cell activation. Therefore, the upregulation of cell surface molecules observed under the expression of M2 was probably a consequence of the assembly of a specific signalosome, independently of external signals, carried out by the viral protein. Up-regulation of such molecules could hypothetically render the B cell more prone to interact with T_H cells. In agreement, in the context of the MHC class II-restricted OVAp-specific cellular system, expression of M2 competitively promoted B-T_H cell interaction independently of specific antigen presentation. This was most likely due to the increased cell adhesion molecules, which are responsible for initial contacts between B and T_H cells. Mutation of the phosphosites abrogated the ability of M2 to promote B-T_H cell interaction, suggesting that this process is dependent on the capacity of the viral protein to assemble specific signalosomes. Despite the ability of M2 to promote B-T_H cell interaction independently of specific peptide presentation, its expression was not sufficient to lead to T cell activation. Instead, T cell activation upon conjugate formation was a product of cognate interaction.

Cognate interaction between B and T_H cells results in the formation of an IS at the contact zone (Grakoui, Bromley et al. 1999). The fact that expression of M2 increased the levels of co-stimulatory molecules suggests a role for M2 in IS formation. Furthermore, work performed by Dr. Filipa Lopes in our laboratory demonstrated that the B cell MTOC distance to the contact zone was decreased in the presence of both the WT and the mutant viral proteins, when compared to mock B cells (Fontinha, Lopes et al. 2015). MTOC polarization is one of the hallmarks of IS formation in T cells. Although the functional significance of such polarization is yet to be determined, it has also been observed in B cells in the context of IS formation between B and T cells (Duchez, Rodrigues et al. 2011). Thus, the incomplete MTOC polarization promoted by M2 reinforces the possibility of a role for the viral protein in IS. Moreover, NCK is modulated by M2 and it is able to promote actin polymerization (Chaki and Rivera 2013), an important process during immunological synapse formation. In the future, it would be interesting to further dissect the role of M2 in IS. Moreover, the B-T_H cell conjugates formed in the absence of peptide, which do not lead to T cell activation, could be further investigated. In particular, address if they are long-lasting contacts and understand if there are any cell surface rearrangements at the contact zone.

Previous studies in the B-T cell interaction and IS field have demonstrated that T_H cells scan several APCs and choose the one that presents a stronger stimulus (Depoil, Zaru et al. 2005). The *in vitro* competition experiment described in section 2.2.3 showed that T_H cells preferentially conjugated with M2-expressing B cells, to the detriment of M2Y-expressing B cells, even though they were loaded with the same amount of specific peptide. This suggests that the stimulus provided by the first is stronger and is able to attract T cell help. In this experiment, competition was assessed in terms of the number of conjugates formed. It is known that, in individual encounters, T_H cells polarize toward the B cell encountered. However, when T cells simultaneously interact with two B cells with different activation states they polarize toward the activated B cell. Therefore, to complement these observations, another interesting aspect would be to assess T cell polarization upon simultaneous interaction with M2- and M2Y-expressing B cells, loaded with the same amount of peptide. A major challenge to overcome in this experimental setting is the fact that these cell triplets would be rare events. *In vivo*, the ability to attract T cell help would be a major advantage to promote the participation of infected B cells in GC reactions, a crucial step in host colonization. B-T_H cell interaction is also important during the GC reaction, where it contributes to the selection of B cells that have been submitted to SHM (Mills and Cambier 2003, De Silva and Klein 2015). Although M2 is not necessary for the expansion of latently infected GC B cells (Rodrigues, Pires de Miranda et al. 2006, Pires de Miranda, Alenquer et al. 2008, Pires de Miranda, Lopes et al. 2013), the protein is expressed in these cells, which suggests that it plays a role in the GC reaction. Due to the intrinsic characteristics of the M2 protein, that did not allow the generation of mouse chimeras with M2-expressing B cells, these observations could not be confirmed *in vivo*.

Infection of laboratory mice with the M2Y recombinant virus results in a delay in latency establishment in the spleen, which could possibly be explained by the lack of promotion of B-T_H cell interaction observed *in vitro* with M2Y. However, this virus is still able to reach GC reactions, suggesting that there are other players involved in this process (Pires de Miranda, Alenquer et al. 2008). For example, a putative viral superantigen (Evans, Moser et al. 2008) may drive IS formation. Another possibility lies with the choice of B cells for latency establishment. This has been demonstrated not to be a stochastic event, in what concerns BCR specificity, and to be linked to the formation of GCs (Decalf, Godinho-Silva et al. 2014). The delay in latency establishment could also precede the step of GC initiation. Tracking of M2Y virus following intraperitoneal infection did not allow the determination of the exact step of spleen infection in which M2Y recombinant virus was delayed. Nonetheless, the decreased infection of marginal zone B cells, the first B cell

population to be infected in the spleen, suggests that the delay starts before GC initiation. This does not mean that B-T_H cell interaction is not important *in vivo*, as the delay in latency establishment may result from a poor colonization of more than one splenic population. Although evidence points out to a general B cell phenotype, it was not possible to clearly confirm a normal macrophage infection, the first step of spleen colonization. Future studies would benefit from the use of an M2Y recombinant virus that can be tracked during lytic infection, similar to the ones used by Frederico et al (Frederico, Chao et al. 2014). Furthermore, the measurement of viral load by PCR in the macrophage population could be used to address this point.

The two tyrosine residues that constitute the unconventional ITAM of M2 have been described to be differentially required (Rodrigues, Pires de Miranda et al. 2006, Pires de Miranda, Alenquer et al. 2008, Pires de Miranda, Lopes et al. 2013). Work from Rangaswamy et al shows that, although both tyrosines are required *in vitro* for the induction of IL-10 expression, only Y^{129} is required for reactivation from latency and plasma cell differentiation *in vivo* (Rangaswamy, O'Flaherty et al. 2014). In our laboratory, Dr. Marta Alenquer has analyzed individual M2Y mutants, M2Y M2Y120F and M2Y129F, with the first or the second tyrosine residues of the unconventional ITAM mutated to phenylalanines, respectively. Results have shown that at the latency peak, following intranasal inoculation, both individual mutant recombinant viruses have slightly higher levels of latency, when compared to the M2Y recombinant virus. Like what was observed by Rangaswamy et al, Y^{129} was more important for latency establishment, as could be observed by the relatively lower latency levels. Unlike the above mentioned study, Y^{120} was not completely dispensable, as it also showed a delay when compared to a WT virus. This suggests that both phosphosites play a role in the establishment of latency in the spleen. Y^{120} and Y^{129} are known to selectively bind distinct cellular partners and are, therefore, associated with different signaling pathways. In this line of thought it would be interesting to further dissect the contribution of each tyrosine residue for the delay in latency establishment. For that purpose, YFP-expressing individual M2Y mutants have been created by me in our laboratory, in order to track infection in the same splenic populations that were analyzed in Chapter 5. In agreement with the data obtained by Dr. Marta Alenquer, preliminary results have shown that both tyrosines are required, with Y^{129} being more important for latency establishment to some extent. At eight days following intraperitoneal infection this was true for all B cell populations analyzed. Again, Y^{120} was not dispensable. As mentioned above, work from Dr. Filipa Lopes has shown that the polarization of M2 to the contact zone during B-T_H cell interaction was especially

dependent on Y^{120}. Therefore, in the future, the role of each tyrosine residue in B-T_H cell interaction could be further explored.

It is not the first time that the modulation of T-APC interaction, and more specifically IS, by a viral protein has been described. Inclusively, there are two examples of such modulation in the *Gammaherpesvirinae* sub-family (Coscoy and Ganem 2001). In those cases, the viral proteins impair T-APC interaction, instead of promoting it like the MuHV-4 M2 protein does. These results do not have to be mutually exclusive. It is possible that different viral proteins coordinate different aspects of T-APC interaction, at different stages of the virus life cycle. For example, K5, which was shown to impair B-T_H cell interaction and IS formation, is part of the lytic replicative cycle of KSHV, a step where the virus could benefit from this impairment as a mechanism to escape immune surveillance. During the latency phase it is possible that another viral protein promotes B-T_H cell interaction to drive infected B cells through a GC reaction. Similarly, it is reasonable that at earlier timepoints of MuHV-4 infection, there is a viral protein that impairs IS formation as a mechanism of immune evasion.

Although it is not clear yet, like EBV and MuHV-4, KSHV may take advantage of the GC reaction. During this process, EBV is believed to bypass T cell help. Therefore, promotion of B-T_H cell interaction would not be beneficial for the virus. MuHV-4, on the contrary, is dependent on normal T cell help to successfully colonize the host. While EBV is a lymphocryptovirus, both KSHV and MuHV-4 are rhadinoviruses (Davison, Eberle et al. 2009). It is conceivable that these two genera use different strategies to expand B cell latency during the early phase of infection. A practical example of the differences between the two genera can be observed in X-linked lymphoproliferative disease (XLP) patients. In XLP there is a genetic defect in the gene that encodes the slam associated protein (SAP) (Sayos, Wu et al. 1998), whose expression is required in $CD4^+$ T cells for the generation of GC reactions (Qi, Cannons et al. 2008). These patients appear to be more susceptible to EBV infection, which can replace T cell help, than to KSHV. Concluding, other gammaherpesviruses, such as KSHV, may also promote B-T_H cell interaction as a mechanism of host colonization. M2 is a putative functional homologue of LMP1 and LMP2A encoded by EBV, and K1 and K15 encoded by KSHV (Madureira, Matos et al. 2005, Rodrigues, Pires de Miranda et al. 2006, Pires de Miranda, Alenquer et al. 2008). Moreover, KSHV K1 protein has been shown to assemble a signaling complex similar to the one assembled by MuHV-4 M2 protein, which this work suggests is implied in the modulation of B-T_H cell interaction. Therefore, this work sets the base for future studies

with the mentioned proteins of the human gammaherpesviruses, in what regards T-APC interaction.

Summarizing, this work further characterized the role of the latency associated M2 protein, involved in the assembly of multiprotein complexes with cell signaling proteins (Pires de Miranda, Lopes et al. 2013), and linked it to the modulation of B-T_H cell interactions. Results suggest a model where expression of M2 in B cells increases the surface levels of adhesion and co-stimulatory molecules, competitively promoting the formation of B-T_H cell conjugates, independently of specific peptide (Figure 6.1). Upon cell interaction, the adaptor protein increases the B cell MTOC proximity to the contact zone, to where it also polarizes. Presentation of a specific peptide in MHC class II molecules is then required for T cell activation. Collectively, all the functions that have been attributed to M2 in *in vitro* studies set it as a protein that potentially promotes B cell activation, survival and facilitated access to the GC reaction. In agreement, *in vivo*, its expression is required for a normal establishment of latency.

Viruses are clinically important pathogens. Although gammaherpesvirus infection is not always associated with disease, it is linked to the development of lymphoproliferative disorders (Damania 2004, Cesarman 2011). Currently, there is no unified, highly effective, treatment. HIV-1 causes AIDS which affects millions of people globally (Saxena, Shrivastava et al. 2012). Although the use of highly active antiretroviral therapy (HAART) has substantially improved the survival of patients affected by HIV, it does not cure the disease and it is not always effective. Therefore, for both gammaherpesviruses and HIV, new therapeutic approaches are needed. Modulation of T-APC interaction seems to be an important mechanism that contributes to virus survival. Both HIV and KSHV have been described to inhibit T-APC interaction in order to escape immune surveillance and promote virus survival (Coscoy and Ganem 2001, Haller, Rauch et al. 2006, Thoulouze, Sol-Foulon et al. 2006, Haller, Rauch et al. 2007, Saxena, Shrivastava et al. 2012). Furthermore, this work has shown that gammaherpesviruses may possibly promote B-T cell interaction to enhance host colonization. This knowledge highlights potential viral targets whose abolishment may, on the one hand, allow host immunity to take its course of action and, on the other hand, weaken host colonization. Drugs developed against these and other important viral targets may potentially be used in combination therapy as an effective treatment for infected patients.

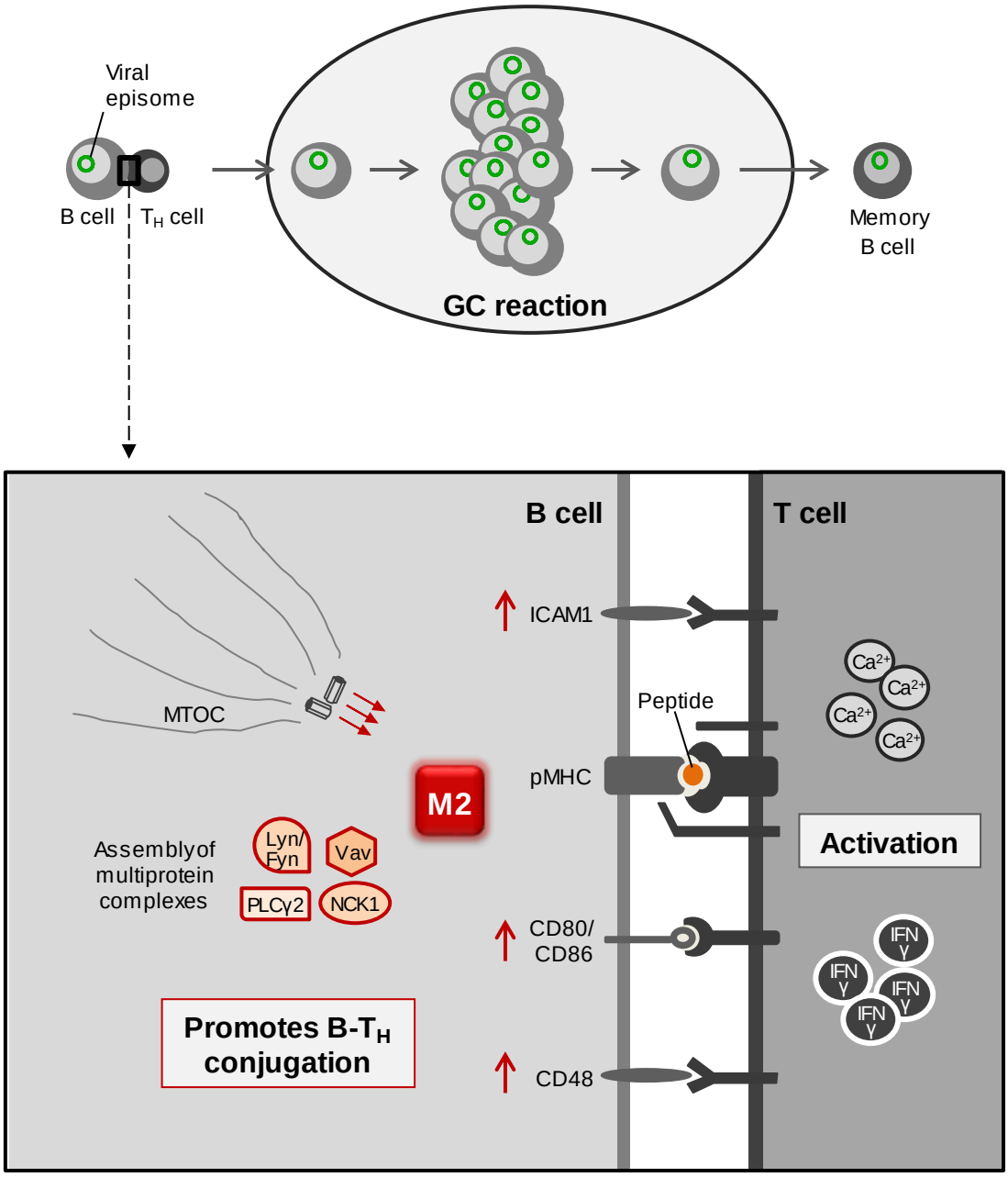

Figure 6.1. Modulation of B-T_H cell interaction by the M2 protein of MuHV-4. B-T_H cell interaction is required for GC initiation, a pathway that is crucial for gammaherpesviruses to access the memory B cell compartment. The latency-associated protein M2 of MuHV-4, represented in red, is an adaptor protein that assembles multiprotein complexes with cell signaling proteins and modulates B-T_H cell interaction. Its effects are also depicted in red. The protein polarizes to the contact zone, upregulates the cell surface levels of adhesion (ICAM1 and CD48) and co-stimulatory (CD80/CD86) molecules, and increases the B cell MTOC polarization to the contact zone. As a result, M2 promotes B-T_H cell conjugation, a step that peptide-independent. Upon the presentation of specific peptide (in orange) in MHC class II molecules, this contact results in increased cytosolic calcium concentration and polarization of IFN-γ to the contact zone, both hallmarks of T cell activation.

CHAPTER 7

MATERIALS AND METHODS

7 MATERIALS AND METHODS

7.1 Materials

7.1.1 General Reagents

Analytical or molecular biology grade chemicals used throughout this work were obtained from Sigma, Bio-Rad, Calbiochem, Fluka, Merck, VWR, Nzytech, Thermo Scientific and Invitrogen. Molecular biology reagents and enzymes were obtained from Roche, Fermentas, New England Biolabs, Promega, and Invitrogen. Tissue culture reagents and supplements were obtained from GIBCO® BRL, Invitrogen and Peprotech. Synthetic oligonucleotides and peptides were synthesized by Thermo Fisher Scientific.

7.1.2 Antibodies and live dyes

7.1.2.1 Primary antibodies

Anti-M2 polyclonal serum (Madureira, Matos et al. 2005) was produced by immunization of New Zealand white rabbits with the fusion protein GST-M2. This antibody was used for Western-blot assays.

The remaining antibodies used in this study are commercially available and are listed in the table below:

Table 7.1. Primary antibodies.

Name	Clone	Use	React.	Host/Isotype	Company
pTyr-AF647	PY99	IF	NA	Mouse IgG2b	Santa Cruz Biotechnology
IFN-γ	AN-18	IF	M	Rat IgG1, κ	BD Pharmingen™
TCR DO11.10-PE	KJ1.26	FC	M	Mouse IgG2a, κ	MBL – medical and biological lab
CD4-AF405	RM4-5	FC	M	Rat IgG2a	Invitrogen
CD80-PB	16-10A1	FC	M, D	Armenian Hamster IgG	BioLegend
CD86-PE-Cy7	PO3	FC	M	Rat IgG2b, κ	BioLegend
CD54/ICAM1-APC	YN1/1.7.4	FC	M	Rat IgG2b, κ	BioLegend
CD40-PE-Cy7	3/23	FC	M	Rat IgG2a, κ	BioLegend
CD48-APC	HM48-1	FC	M	Armenian Hamster	Bio Legend

				IgG	
MHC-II-PB	M5/114.15.2	FC	M	Rat IgG2b, κ	BioLegend
CD19-APC-H7	1D3	FC	M	Rat IgG2a, κ	BD Biosciences
CD21/35-APC	7G6	FC	M	Rat IgG2b, κ	BD Biosciences
CD23-PE	B3B4	FC	M	Rat IgG2a, κ	BD Biosciences
CD69-FITC	H1.2F3	FC	M	Armenian Hamster IgG	BioLegend
CD95-PE	Jo2	FC	M	Armenian Hamster IgG2, λ2	BD Biosciences
GL7-eF660	GL7	FC	M	Rat IgM	eBioscience
CD45.2-v450	104	FC	M	Mouse IgG2a, κ	BD Biosciences
CD45.2-APC	104	FC	M	Mouse (SJL) IgG2a, κ	BD Pharmingen™
CD45.1-APC-Cy7	A20	FC	M	Mouse (A.SW) IgG2a, κ	BioLegend
B220-APC	RA3-6B2	FC	M	Rat IgG2a, κ	BD Biosciences
CD117 (c-kit)-APC	2B8	Pur	M	Rat IgG2b, κ	eBioscience
CD11c-APC	HL3	FC	M	Armenian Hamster IgG1, λ2	BD Pharmingen™
IgM-PerCP-Cy™5.5	R6-60.2	FC	M	Rat (LOU) IgG2a, κ	BD Pharmingen™
IgD-V450	11-26c.2a	FC	M	Rat IgG2a, κ	BD Horizon™
Ly-6G (Gr-1)-PerCP-Cy5.5	RB6-8C5	FC	M	Rat IgG2b, κ	eBioscience
CD21/CD35	7G6	IF	M	Rat (SD) IgG2b, κ	BD Pharmingen™
IgM-biotin	Polyclonal	IF	M	Goat	Southern Biotec
IgD	11-26	IF	M	Rat IgG2a, κ	Southern Biotec
MAdCAM-1	MECA-367	IF	M	Rat IgG2a	AbD Serotec®
F4/80	CI:A3-1	IF	M	Rat IgG2b	AbD Serotec®
MARCO	ED31	IF	M	Rat IgG1	AbD Serotec®
CD169	3D6.112	IF	M	Rat IgG2a	AbD Serotec®
GFP-AF488	Polyclonal	IF	M	Rabbit IgG	Molecular Probes
EGFP	NA	WB	NA	Mouse IgG2a	Clontech
Actin	Polyclonal	WB	V	Rabbit	Sigma-Aldrich

React. – Reactivity; IF – Immunofluorescence; FC – Flow Cytometry; Pur – purification; WB – Western-blot; NA – non-applicable; M – mouse; D – dog; V – vertebrates.

7.1.2.2 Secondary Antibodies

Anti-rabbit (GE Healthcare) and anti-mouse (Jackson Immunoresearch) secondary antibodies, conjugated with horse radish peroxidase (HRP) were used in Western blot assays. A streptavidin-AF633 (Life Technologies) and an anti-rat AF568 (Molecular Probes) secondary antibodies were used in immunofluorescence assays.

7.1.2.3 Live Dyes

In conjugation experiments cells were incubated with live dyes from Molecular Probes®, Invitrogen: CellTracker™ Blue CMAC (7-amino-4-chloromethylcoumarin; #C2110), CellTracker™ Green CMFDA (5-chloromethylfluorescein diacetate; #C7025), CellTracker™ Orange CMTMR ((5-(and-6)-(((4-chloromethyl)benzoyl)amino) tetramethylrhodamine; #C2927), and CellTrace™ Far-Red DDAO-SE (#C34553).

7.1.3 Peptides

OVA peptide (aa 323-339), with the protein sequence ISQAVHAAHAEINEAGR, was acquired from GenWay Biotech, Inc. (#06-271-83379).

7.1.4 Cell lines

BHK-21 cells – baby hamster kidney cells. Used for growth and titration of viral stocks, for *ex vivo* reactivation assay and for plaque assay.

HEK 293T cells – human embryonic kidney cells. Used for production of viral transduction particles.

A20 B cells – BALB/c B cell lymphoma line, derived from a spontaneous reticulum cell neoplasm found in an old BALB/cAnN mouse. Used for conjugate and immunological synapse assays.

7.1.5 Bacterial strains

Plasmids were grown for the general purpose in *Escherichia coli* strain DH5α (Invitrogen) with the following genotype F^- Φ80*lac*ZΔM15 Δ(*lac*ZYA-*arg*F)U169 *rec*A1 *end*A1 *hsd*R17 (r_K^- m_K^+) *pho*A *sup*E44 *thi*-1 *gyr*A96 *rel*A1 λ^-.

7.1.6 Plasmids

pMSCV-K3-IRES-Zeo – this plasmid contains ORF K3 of MuHV-4 cloned in pMSCV-IRES-zeo. It was used to produce viral transduction particles for the generation of

zeocin-resistant stable A20 B cell lines, expressing K3. This plasmid was constructed by P. Madureira (Madureira, Matos et al. 2005).

pMSCV-M2-IRES-Zeo – this plasmid contains ORF M2 of MuHV-4 cloned in pMSCV-IRES-zeo. It was used to produce viral transduction particles for the generation of zeocin-resistant stable A20 B cell lines, expressing M2. ORF M2 was excised from pMSCV-M2-IRES-GFP (Rodrigues, Pires de Miranda et al. 2006) by digestion with *Eco*RI and *Xho*I, and subcloned to pMSCV-K3-IRES-Zeo, using the same restriction sites and replacing K3. This plasmid was constructed in our lab by C. Silva.

pMSCV-M2Y-IRES-Zeo – this plasmid contains ORF M2Y of MuHV-4 cloned in pMSCV-IRES-zeo. It was used to produce viral transduction particles for the generation of zeocin-resistant stable A20 B cell lines. ORF M2Y was excised from pMSCV-M2Y-IRES-GFP (Rodrigues, Pires de Miranda et al. 2006) by digestion with *Eco*RI and *Xho*I, and subcloned to pMSCV-K3-IRES-Zeo, using the same restriction sites and replacing K3. This plasmid was constructed in our lab by C. Silva.

pMSCV-EGFP-M2-IRES-Zeo – this plasmid was used to produce viral transduction particles for the creation of a zeocin-resistant, eGFP-M2-expressing, stable cell line. eGFP was amplified by PCR from pEGFP-N1vector without the STOP signal, and flanked by *Eco*RI and *Bam*HI restriction sites, using the following primers: 5' – AAA GAA TTC CGC CAC CAT GGT GAG (*Eco*RI) and 3' – AAA GGA TCC CTT GTA CAG CTC GTC (*Bam*HI). Insert was cloned in the pSP72 vector. ORF M2 was amplified by PCR from the *Hind*III-E shuttle plasmid using the following primers: 5' – AAA GGA TCC ATG GCC CCA ACA CC (*Bam*HI) and 3' – AAA CTC GAG TTA CTC CTC GCC CCA (*Xho*I). Insert was cloned in the pSP72 vector that contained the EGFP insert. M2, N-terminally fused to EGFP, was then excised by digestion with *Eco*RI and *Xho*I restriction enzymes, and subcloned to pMSCV-K3-IRES-Zeo, replacing K3. This plasmid was constructed in this study.

pMSCV-EGFP-M2Y-IRES-Zeo – this plasmid was used to produce viral transduction particles for the creation of a zeocin-resistant, eGFP-M2Y-expressing, stable cell line. eGFP was amplified by PCR from pEGFP-N1vector without the STOP signal, and flanked by *Eco*RI and *Bam*HI restriction sites, using the following primers: 5' – AAA GAA TTC CGC CAC CAT GGT GAG (*Eco*RI) and 3' – AAA GGA TCC CTT GTA CAG CTC GTC (*Bam*HI). Insert was cloned in the pSP72 vector. ORF M2Y

was amplified by PCR from the M2Y shuttle plasmid using the following primers: 5' – AAA GGA TCC ATG GCC CCA ACA CC (*Bam*HI) and 3' – AAA CTC GAG TTA CTC CTC GCC CCA (*Xho*I). Insert was cloned in the pSP72 vector that contained the EGFP insert. M2Y, N-terminally fused to EGFP, was then excised by digestion with *Eco*RI and *Xho*I restriction enzymes, and subcloned to pMSCV-K3-IRES-Zeo, replacing K3. This plasmid was constructed in this study.

pMSCV-EGFP-IRES-Zeo – this plasmid was used to produce viral transduction particles for the creation of a zeocin-resistant, eGFP-expressing, stable cell line. eGFP was amplified by PCR from pEGFP-N1vector with the STOP signal, and flanked by *Eco*RI and *Xho*I restriction sites, using the following primers: 5' – AAA GAA TTC CGC CAC CAT GGT GAG (*Eco*RI) and 3' – AGC CTC GAG TTA CTT GTA CAG CTC (*Xho*I). Insert was cloned in the pSP72 vector. EGFP was then excised by digestion with *Eco*RI and *Xho*I restriction enzymes, and subcloned to pMSCV-K3-IRES-Zeo, replacing K3. This plasmid was constructed in this study.

pEQPAM3 – this was the packaging plasmid used in the production of viral transduction particles for the creation of zeocin-resistant A20 B cell lines. It encodes the genes *gag*, *pol* and *env* of murine stem cell virus (Persons, Mehaffey et al. 1998).

pMigR1-empty – this was the retroviral expression vector used in the production of viral particles for the transduction of fetal liver cells. It contains IRES-GFP. The plasmid was a kind gift from Dr. H. Veiga-Fernandes (Instituto de Medicina Molecular, Lisbon, Portugal).

pMigR1-M2 – this was the retroviral expression vector used in the production of viral particles for the transduction of fetal liver cells. M2 was excised from pMX-M2 (constructed in our lab by S. Marques) using the restriction enzymes *Bam*HI and *Xho*I. Insert was cloned into pMigR1, using the restriction sites *Bgl*II and *Xho*I. This plasmid was constructed in this study.

pMigR1-M2Y – this was the retroviral expression vector used in the production of viral particles for the transduction of fetal liver cells. M2Y was excised from pMX-M2Y (constructed in our lab by S. Marques) using the restriction enzymes *Bam*HI and *Xho*I. Insert was cloned into pMigR1, using the restriction sites *Bgl*II and *Xho*I. This plasmid was constructed in this study.

pCL-Eco – this was the packaging plasmid used in the production of viral particles for the transduction of fetal liver cells. It encodes the genes *gag*, *pol*, and *env*. pCL-Eco was a gift from Inder Verma (Addgene plasmid # 12371).

pCMV-VSV-G – this plasmid encodes the G protein of vesicular stomatitis virus, which can serve as a surrogate viral envelope protein, and was used in the production of viral particles for the transduction of fetal levar cells. pCMV-VSV-G was a gift from Bob Weinberg (Addgene plasmid # 8454).

7.1.7 Mice

C.Cg-Tg(DO11.10)10Dlo/J (DO11.10) mice carry an MHC class II restricted rearranged T cell receptor transgene that reacts to OVAp. Mice were a kind gift from Prof. Luís Graça (Instituto de Medicina Molecular, Lisbon, Portugal).

B6.SJL-*Ptprc*^{a} *Pep3*^{b}/BoyJ (CD45.1) is a congenic strain which carries the differential B cell antigen originally designated Ly5.1 and CD45.1. The *b* allele of *Ptprc* is normally present in the BALB and C57BL inbred strains.

B6.129S7-*Rag1*^{tm1Mom}/J (Rag1$^{-/-}$) mice are homozygous for the *Rag1*^{tm1Mom} mutation and produce no mature T cells or B cells (lack all mature lymphocytes, i.e. are "non-leaky").

CD45.1/CD45.2 (CD45.1/2) mice were obtained by breeding CD45.1 C57BL/6 with C57BL/6J mice.

C57BL/6J mice were purchased from Charles River Laboratories International Inc. CD45.1 C57BL/6 and Rag1$^{-/-}$ mice were purchased from Jackson Laboratory.

Mice were bred and/or housed under specific pathogen-free conditions at Instituto de Medicina Molecular animal facility, Lisbon, Portugal.

7.1.8 Viruses

Murid herpesvirus-4 (MuHV-4) used in this study belongs to the strain MHV-68 (murine herpesvirus 68) that was originally isolated by Prof. Dr Blaskovic (Blaskovic, Stancekova

et al. 1980). Clone G2.4 was isolated from virus grown in BHK-21 cells by Dr Stacey Efstathiou (Efstathiou, Ho et al. 1990).

YFP-expressing MuHV-4 recombinant virus (vYFP) used in animal experiments was derived from a genomic bacterial artificial chromosome (BAC) and was a kind gift from Dr Samuel Speck. This virus expresses the enhanced yellow fluorescent protein (YFP), driven by the human cytomegalovirus (HCMV) immediate-early (IE) promoter and enhancer, from a neutral locus in the viral genome located between open reading frames 27 and 29b (Collins, Boss et al. 2009). The expression cassette is flanked by a chromatin insulator from the human major histocompatibility complex II locus, an attempt to prolong YFP expression after the onset of latency. This virus allows direct detection of infected cells based on YFP expression and phenotypic analysis of the infected cell populations.

M2Y YFP-expressing MuHV-4 recombinant virus (vM2Y-YFP) used in animal experiments was constructed in our lab by Dr. Marta Alenquer and engineered by mutagenesis of the virus genome in *E.coli* using the YFP MuHV-4 BAC (Collins, Boss et al. 2009). M2Y contains tyrosine residues at positions 120 and 129 replaced by phenylalanines.

7.2 Methods

7.2.1 Isolation and analysis of nucleic acids

7.2.1.1 Plasmid DNA isolation

Plasmid DNA was isolated from plasmid-containing *E.coli* strain DH5α (section 7.1.5) grown in Luria Bertani (LB) (1% tryptone, 0.5% yeast extract, 1% NaCl) broth containing the appropriate antibiotic(s), using an alkaline lysis method modified accordingly to the scale of the preparation and plasmid size. Antibiotics were used at the following concentrations: 100μg/mL ampicilin, 17μg/mL chloramphenicol and 30μg/mL kanamycin.

Small scale plasmid preparation

For small scale plasmid preparations (plasmid minipreps), 2-5mL of LB broth cultures containing the appropriate antibiotic(s) were inoculated with single bacterial colonies and

incubated overnight (12-18h) at 37ºC, with vigorous shaking. Cultures were pelleted by centrifugation at 4000rpm for 10min. Plasmid DNA was obtained using the Wizard Plus SV Minipreps DNA Purification System (Promega), by column purification of DNA prepared by alkaline lysis, according to manufacturer's instructions. DNA was eluted in 50µL of MilliQ water and stored at -20ºC until further use.

Large scale plasmid preparation

For large scale plasmid preparations (plasmid maxipreps), 5mL of LB broth cultures containing the appropriate antibiotic(s) were inoculated with single bacterial colonies and incubated overnight (12-18h) at 37ºC, with vigorous shaking. Bacteria were then sub-cultured 1:500 into 200 mL LB containing the appropriate antibiotic(s) and incubated under the same conditions. Bacterial cultures were pelleted by centrifugation at 6000rpm for 15min at 4ºC and DNA was purified using the LFU / Plasmid Purification MAXI Kit (JETSTAR), according to manufacturer's instructions. DNA was resuspended in 500µL of MilliQ water and stored at -20ºC until further use.

7.2.1.2 Mouse tail or ear DNA extractions

Mouse tail or ear were digested by overnight incubation at 55ºC with 100µL of DirectPCR Lysis Reagent (mouse tail) (Viagen Biotec Inc.) supplemented with 0.2-0.4 mg/ml of Proteinase K. Proteinase K was then inactivated by heating at 85ºC for 1h. 1µL of lysate was used directly in PCR reactions for mice genotyping (section 7.2.1.4).

7.2.1.3 Quantification of nucleic acids

DNA was quantified by UV spectrophotometry using a Nanodrop (ND-1000) spectrophotometer.

7.2.1.4 Polymerase chain reaction (PCR)

Polymerase chain reaction was used in this study for different purposes.

Some of the inserts used in cloning procedures (section 7.2.1.9) were amplified by PCR. Reaction mixes were prepared in a total volume of 50µL (made up in sterile MilliQ water) and consisted of <100ng of template DNA, 300nM of each primer, 200µM of each deoxynucleotide triphosphate (dNTP), 1U of high fidelity *Pfu* DNA polymerase (Promega), and PCR buffer (Promega), according to manufacturer's instructions. Primers used for the

amplification of EGFP for cloning into pSP72 or pMSCV vectors (section 7.2.1.9.1) are described in table 7.2. Primers used for the amplification of M2 or M2Y for cloning into pSP72 vector (section 7.2.1.9.1) are described in table 7.3. DNA was amplified on a MyCycler thermal cycler (BioRad), under the following conditions: an initial melting step of 95ºC for 2min followed by 30 cycles of amplification, composed of denaturation at 95ºC for 30sec, annealing at 55ºC for 30sec and extension at 72ºC for 2min. A final extension step was performed at 72ºC for 10min. 5µL of each PCR product was analyzed by gel electrophoresis (section 7.2.1.6) to assess if products had the expected size.

Table 7.2. Primers used for the amplification of EGFP for cloning into pSP72 or pMSCV vectors.

Construct	Oligonucleotide	Sequence and restriction site	Amplicon (bp)
M2/M2Y constructs (pSP72)	Forward primer	5' – AAA GAA TTC CGC CAC CAT GGT GAG – 3' (*Eco*RI)	742
	Reverse primer	3' – AAA GGA TCC CTT GTA CAG CTC GTC – 5' (*Bam*HI)	
EGFP construct (pMSCV)	Forward primer	5' – AAA GAA TTC CGC CAC CAT GGT GAG – 3' (*Eco*RI)	745
	Reverse primer	3' – AGC CTC GAG TTA CTT GTA CAG CTC – 5' (*Xho*I)	

Table 7.3. Primers for the amplification of M2 or M2Y for cloning into pSP72 vector.

Oligonucleotide	Sequence and restriction site	Amplicon (bp)
Forward primer	5' – AAA GGA TCC ATG GCC CCA ACA CC – 3' (*Bam*HI)	597
Reverse primer	3' – AAA CTC GAG TTA CTC CTC GCC CCA – 3' (*Xho*I)	

PCR was also used for genotyping Rag1$^{-/-}$ mice. Genotyping was performed using the primers described in Table 7.4. PCR reaction and conditions were performed according to the recommendations of Jackson Laboratory. PCR products were analyzed by gel electrophoresis (section 7.2.1.6).

Table 7.4. Primers used for Rag1$^{-/-}$ genotyping.

Allele	Oligonucleotide	Sequence	Amplicon (bp)
Rag1^{tm1Mom}	WT forward primer	5'- GAGGTTCCGCTACGACTCTG-3'	WT: 474
	Mutant forward primer	5'- TGGATGTGGAATGTGTGCGAG-3'	Mutant: 530
	Common reverse primer	5'- CCGGACAAGTTTTTCATCGT-3'	Heterozygote: 474 + 530

7.2.1.5 Restriction digestion

Restriction endonuclease digestion of plasmids or PCR products was used to prepare linear or insert purified DNA, and to confirm the presence of inserts cloned in expression vectors. Digestions were performed using the appropriate restriction endonucleases and correspondent reaction buffers, according to manufacturer's instructions. DNA amount, reaction volume and enzymes used depended on the purpose of the assay.

For digestion of plasmids or PCR products for subsequent ligation and cloning, 1-2µg of DNA, 10U of restriction endonuclease per µg of DNA and an appropriate buffer were incubated for 2h at 37ºC. Digestion volume ranged from 50-80µL. Diagnosis digestion was performed in a 20µL total volume with 1µg of DNA, 10U of restriction endonuclease and the appropriate buffer. Multiple digestions of the same DNA were performed with the same buffer. Restriction profile and completeness of the digestion were assessed by analytical agarose gel electrophoresis (section 7.2.1.6).

7.2.1.6 Analysis and isolation of DNA by gel electrophoresis

Linear DNAs were size fractioned and visualized on agarose gels stained with gel red (Biotium) or red safe (iNtRON Biotechnology), according to manufacturer's instructions. Gels were prepared using 0.8-2% agarose in 1x TAE (40mM Tris-acetate, 1mM EDTA, pH 8.0). Prior to loading on wells, DNA samples were mixed with the appropriate volume of DNA loading buffer (10mM EDTA, 5% glycerol, 0.025% bromophenol blue and 0.025% xylene cyanol). Samples were electrophoresed at 0.5-5.0 V/cm in 1x TAE buffer. DNA was visualized by UV transillumination. Size of DNA bands was estimated by comparison with linear DNA standards of known molecular weight (1 Kb plus DNA ladder, Invitrogen) that was ran along with samples. Following analysis of DNA by agarose gel electrophoresis, DNA fragments of interest were purified by excision of the resolved bands from the gel and recovered with the High Pure PCR Product Purification kit (Roche), according to manufacturer´s instructions. Typically, DNA was eluted in 50µL of MilliQ water and a fraction of the purified samples (usually 1/10 of the total volume of the eluate) was re-run on an agarose gel, in order to check the DNA purification.

7.2.1.7 DNA sequencing

Integrity of the pMSCV-EGFP-IRES-Zeo, pMSCV-EGFP-M2-IRES-Zeo and pMSCV-EGFP-M2Y-IRES-Zeo plasmids, namely the EGFP and M2/M2Y sequences introduced, was confirmed by sequencing. The primers used are described in table 7.5.

Table 7.5. Primers used for DNA sequencing.

Sequence to confirm	Oligonucleotide	Sequence
EGFP	Forward primer	5' CCC TTG AAC CTC CTC GTT CGA CC 3'
M2	Forward primer	5' AAA GGT ACC AAC ACC CCC ACA AGG AAA GA 3'
	Reverse primer	5' AAA AAG CTT CTC CTC GCC CCA CTC CA 3'

DNA was sequenced at STAB VIDA according to the Sanger method and using an automatic DNA sequencer (ABI 3730XL). DNA sequences were analyzed and compared to sequences deposited in the NCBI (National Centre for Biotechnology Information) database using the BioEdit Sequence Alignment Editor software.

7.2.1.8 DNA ligation

Digested inserts and vectors were ligated using T4 DNA ligase (Roche Applied Science). Approximately, 100ng of vector DNA and a similar amount of insert were ligated in 20µL reactions containing ligase buffer (Roche Applied Science) and 1U of T4 DNA ligase (Roche Applied Science) (made up in sterile MilliQ water). Cohesive-end ligations were performed overnight at 14ºC.

7.2.1.9 Cloning procedures

7.2.1.9.1 Cloning of pMSCV plasmids used for viral particle production

This strategy was designed by Dr. Marta Alenquer.

EGFP insert without the STOP signal was obtained by amplification from pEGFP-N1 vector, with introduction of *Eco*RI and *Bam*HI restriction sites (section 7.2.1.4). After purification using the High Pure PCR Product Purification, insert size was confirmed by analysis on agarose gel (section 7.2.1.6). EGFP inserts and pSP72 vector were then digested with *Eco*RI and *Bam*HI restriction enzymes, as described in section 7.2.1.5.

Digested inserts and vector were then isolated by gel electrophoresis and purified from agarose gel using a High Pure PCR Product Purification kit from Roche (section 7.2.1.6). Inserts and vector were ligated as described in section 7.2.1.8. Ligations were transformed into competent bacteria as described in section 7.2.2.2. DNA was isolated from colonies by plasmid miniprep (section 7.2.1.1). To confirm successful cloning, plasmid DNA was digested with *Eco*RI and *Bam*HI restriction endonucleases. Next, M2 insert was obtained by amplification from shuttle p*Hind*III-E, with introduction of *Bam*HI and *Xho*I restriction sites (section 7.2.1.4). M2Y insert was amplified from shuttle M2Y, with introduction of *Bam*HI and *Xho*I restriction sites (section 7.2.1.4). After purification using the High Pure PCR Product Purification, insert size was confirmed by analysis on agarose gel. M2/M2Y inserts and EGFP-pSP72 vector constructed on the previous step were digested with *Bam*HI and *Xho*I restriction endonucleases. Digested inserts were then isolated by gel electrophoresis and purified from agarose gel using a High Pure PCR Product Purification kit from Roche. Inserts and vector were ligated as described in section 7.2.1.8. Ligations were transformed into competent bacteria. DNA was isolated from colonies by plasmid miniprep. To confirm successful cloning, plasmid DNA was digested with *Bam*HI and *Xho*I restriction endonucleases and analyzed on agarose gel.

EGFP-M2 and EGFP-M2Y inserts were obtained by digestion of EGFP-M2-pSP72 and EGFP-M2Y-pSP72 plasmids, respectively, with *Eco*RI and *Xho*I restriction endonucleases (section 7.2.1.5). pMSCV-K3-IRES-Zeo vector was also digested with *Eco*RI and *Xho*I restriction endonucleases. Digested inserts and vector were then isolated by gel electrophoresis and purified from agarose gel using a High Pure PCR Product Purification kit from Roche (section 7.2.1.6). Inserts and vector were ligated as described in section 7.2.1.8. Ligations were transformed into competent bacteria as described in section 7.2.2.2. DNA was isolated from colonies by plasmid miniprep (section 7.2.1.1). To confirm successful cloning, plasmid DNA was digested with *Eco*RI and *Xho*I restriction endonucleases. DNA integrity was confirmed by sequencing as described in section 7.2.1.7. Large scale plasmid preparations were prepared as described in section 7.2.1.1 and their integrity was confirmed by digestion with *Eco*RI and *Xho*I restriction endonucleases and analysis on agarose gel.

For the construction of the pMSCV-EGFP-IRES-Zeo plasmid, EGFP insert with the STOP signal was obtained by amplification from pEGFP-N1 vector, with introduction of *Eco*RI and *Xho*I restriction sites (section 7.2.1.4). After purification using the High Pure PCR Product Purification, insert size was confirmed by analysis on agarose gel (section 7.2.1.6). EGFP insert and pMSCV-K3-IRES-Zeo vector were then digested with *Eco*RI

and *Xho*I restriction enzymes (section 7.2.1.5). Digested inserts and vector were then isolated by gel electrophoresis and purified from agarose gel using a High Pure PCR Product Purification kit from Roche. Inserts and vector were ligated as described in section 7.2.1.8. Ligations were transformed into competent bacteria as described in section 7.2.2.2. DNA was isolated from colonies by plasmid miniprep (section 7.2.1.1). To confirm successful cloning, plasmid DNA was digested with *Eco*RI and *Xho*I restriction endonucleases and analyzed on agarose gel. DNA integrity was confirmed by sequencing as described in section 7.2.1.7. Large scale plasmid preparations were prepared as described in section 7.2.1.1 and their integrity was confirmed by digestion with *Eco*RI and *Xho*I restriction endonucleases and analysis on agarose gel.

7.2.1.9.2 Cloning of pMigR1 plasmids used for viral particle production

M2 and M2Y inserts were obtained by digestion of pMX-M2 and pMX-M2Y plasmids with *Bam*HI and *Xho*I restriction enzymes (section 7.2.1.5). Since *Bam*HI and *Bgl*II produce compatible sticky ends, pMigR1 empty vector was digested with *Bgl*II and *Xho*I restriction enzymes. Digested inserts were then isolated by gel electrophoresis and purified from agarose gel using a High Pure PCR Product Purification kit from Roche (section 7.2.1.6). Inserts and vector were ligated as described in section 7.2.1.8. Ligations were transformed into competent bacteria as described in section 7.2.2.2. DNA was isolated from colonies by plasmid miniprep (section 7.2.1.1). To confirm successful cloning, plasmid DNA was digested with *Xho*I and *Nde*I restriction endonucleases. Large scale plasmid preparations were prepared as described in section 7.2.1.1 and their integrity was confirmed by digestion with *Xho*I and *Nde*I restriction endonucleases and analysis on agarose gel.

7.2.2 Bacterial methods

7.2.2.1 Preparation of competent cells

Competent *E.coli* strain DH5α was prepared by the modified H. Inoue method (Inoue, Nojima et al. 1990). Approximately 5µL of *E.coli* glycerol stock were inoculated into 10mL of LB and incubated overnight (12-18h) with vigorous shaking at 37ºC. 10mL of the resulting culture were inoculated into 400mL of fresh LB and incubated at 37ºC, 225 rpm. When the bacterial culture reached an optical density (OD) at 600nm of 0.6 the cell culture was cooled on ice. Cells were pelleted by centrifugation at 4000 rpm (Beckman Coulter Avanti J-25, rotor JA-14) for 15 min at 4ºC. Cell pellet was gently resuspended in 100mL

of ice cold sterile solution A (0.03M KCH_3COO, 0.05M $MnCl_2$, 0.01M $CaCl_2$, 0.1M KCl and 15% glycerol in sterile MilliQ water). Cells were centrifuged at 4000 rpm for 8 min at 4ºC and resulting pellet was resuspended in 20 mL of ice cold solution B (0.01M NaMOPS pH 7.0, 0.075M $CaCl_2$, 0.01M KCl and 15% glycerol in sterile MilliQ water). 100µL and 300µL aliquots were made. Each aliquot was quickly frozen by transferring the vials to dry ice immersed in ethanol. Competent cells were stored at -80ºC until further use.

7.2.2.2 Transformation of competent cells

Competent *E.coli* strain DH5α cells were transformed by the heat shock method. 100µL of competent cells were incubated on ice for 30min with 100ng of plasmid DNA or 1-10µL of ligation mix. Cells were heat shocked for 45sec at 42ºC and subsequently chilled on ice for 2 min. 400-900 µl of SOC medium (2% tryptone, 0.5% yeast extract, 10mM NaCl, 2.5mM $MgCl_2$, 10mM $MgSO_4$, 20mM glucose) were added to each vial and cells were incubated for 1h at 37ºC. Cells were then spread onto LB agar plates containing the appropriate antibiotic(s) and incubated at 37ºC, overnight or until colonies were visible. Ampicilin was used at 100µg/mL ampicilin, chloramphenicol at 17µg/mL and kanamycin at 30µg/mL.

7.2.3 Cell culture, transfection and transduction

7.2.3.1 Media and culture conditions

HEK 293T cells were cultured in Dulbecco's modified Eagle's medium (DMEM) supplemented with 10% fetal bovine serum (FBS), 2mM glutamine, 100U/mL penicillin and streptomycin. BHK-21 cells were cultured in Glasgow's modified Eagle's medium (GMEM) supplemented as described above with the addition of 10% tryptose phosphate broth. A20 B cells were grown in RPMI 1640 supplemented as described above. In the case of zeocin-resistant stable cell lines, 4µg/mL of zeocin was added to the culture. Conjugates were incubated in RPMI 1640 supplemented with 5% fetal bovine serum, 2mM glutamine, 100u/mL penicillin and streptomycin and 10mM HEPES. Primary mouse $CD4^+$ T cells purified from DO11.10 mice were cultured in RPMI 1640 supplemented as described above in addition to 50µM 2-mercaptoethanol, 100µM sodium pyruvate, 10mM HEPES and 60U/mL rmIL-2. Primary mouse fetal liver cells were cultured in DMEM supplemented with 15% FBS, 2mM glutamine, 100U/mL penicillin and streptomycin, 20ng/mL of IL-3, 50ng/mL of IL-6 and 100ng/mL of SCF. All cell cultures were grown in a humidified tissue culture incubator at 37ºC under 5% CO_2.

7.2.3.2 Isolation, stimulation and resting of T cells

$CD4^+$ T cells were obtained and purified from spleens of 8-week to 4-months old naïve DO11.10 mice (section 7.1.7). Briefly, spleens were collected into 5mL of complete RPMI. Single cell suspensions were obtained by mechanical disruption. Cell debris were removed by filtering through a 100µm cell strainer and red blood cells were lysed by incubation with red blood cell lysis buffer (154mM ammonium chloride, 14mM sodium hydrogen carbonate, 1mM EDTA pH7.3) for 5min on ice. Cell suspensions were washed with medium, centrifuged at 1200rpm for 5min at 4ºC, resuspended in medium and filtered through a 40µm cell strainer. Cells were counted using trypan blue (for cell viability), centrifuged at 1200rpm for 10min at 4ºC and resuspended in ice-cold sterile MACS buffer (0.5% bovine serum albumine and 2mM EDTA in PBS pH 7.2) at an appropriate cell density. $CD4^+$ T cells were then purified by depletion of indirect magnetically labeled non-$CD4^+$ T cells (negative selection) using mouse $CD4^+$ T cell isolation kit (MACS, Miltenyi Biotech), according to manufacturer's instructions. Purity of the enriched $CD4^+$ T cell population was evaluated by flow cytometry (section 7.2.4.1) and was consistently > 90%.

Purified $CD4^+$ T cells were grown in 24-well plates in the presence of Dynabeads® Mouse T-activator CD3/CD28 (Invitrogen), according to manufacturer's instructions. Briefly, $1x10^6$ cells were resuspended in 1mL of T cell culture media (section 7.2.3.1) and Dynabeads®. Beads and cells were cultured at a 1:1 proportion and incubated for three days.

After three days of stimulation, Dynabeads® were removed from culture, according to manufacturer's instructions. Cells were then culture in T cell culture media for a resting period that ranged from 5 to 8 days.

7.2.3.3 Isolation of B cells

B cells were obtained and purified from the lymph nodes of CD45.1 B6 background mice (section 7.1.7). Briefly, lymph nodes were collected into 5mL of complete RPMI. Single cell suspensions were obtained by mechanical disruption. Cell debris were removed by filtering through a 100µm cell strainer and red blood cells were lysed by incubation with red blood cell lysis buffer (154mM ammonium chloride, 14mM sodium hydrogen carbonate, 1mM EDTA pH7.3) for 5min on ice. Cell suspensions were washed with medium, centrifuged at 1200rpm for 5min at 4ºC, resuspended in medium and filtered through a 40µm cell strainer. Cells were counted using trypan blue (for cell viability), centrifuged at 1200rpm for 10min at 4ºC and resuspended in ice-cold sterile MACS buffer

(0.5% bovine serum albumine and 2mM EDTA in PBS pH 7.2) at an appropriate cell density. B cells were then purified by depletion of indirect magnetically labeled non-B cells (negative selection) using mouse B cell isolation kit (MACS, Miltenyi Biotech), according to manufacturer's instructions. Purity of the enriched B cell population was evaluated by flow cytometry (section 7.2.4.1) and was consistently > 98%.

7.2.3.4 Isolation of c-kit$^+$ fetal liver cells

CD45.1, CD45.2 and CD45.1/2 fetal liver cells were obtained from 15 days-old mouse embryos (section 7.2.7.2). Briefly, mouse fetal liver was dissected to 10mL of DMEM supplemented with 15% fetal bovine serum, 2mM glutamine, 100U/mL penicillin and streptomycin. Single cell suspensions were obtained by mechanical disruption. Cell debris were removed by filtering through a 40µm cell strainer. An aliquot of cells was removed for cell count with trypan blue. Cells were centrifuged at 300g for 10min at 4ºC and resuspended in MACS buffer (0.5% bovine serum albumine and 2mM EDTA in PBS pH 7.2) at a density of $5x10^7$ cells/100µL of buffer. Anti-c-kit-APC antibody (table 7.1) was next added to the cells at 1:100 dilution and incubated for 25min at 4ºC. Cells were then washed and incubated with anti-APC Microbeads (Miltenyi Biotech). Positive selection of c-kit expressing cells was carried out according to manufacturer's instructions.

7.2.3.5 Viral particle production

Viral particles for transduction of A20 B cells were produced by calcium phosphate transfection of 293T cells. On the day prior to transfection, 293T cells were seeded in 10cm cell culture dishes, at the density of $3x10^6$ cells per dish in 10mL of complete DMEM (section 7.2.3.1). In a tube labeled A, 20µg of pEQPAM3 packaging vector and 20µg of p-MSCV-IRES-zeo plasmid (carrying EGFP, EGFP-M2, EGFP-M2Y) (section 7.1.6) were added to a 0.2M $CaCl_2$ solution in a total volume of 600µL. 600µL of a 2x concentrated HEPES buffered saline (HBS) solution was added to a tube labeled B. Solution A was added dropwise to solution B, while bubbling air through solution B with a pipette. This mix was incubated for 30min at RT. The DNA precipitate was then added dropwise to the cells. Following a 4h incubation period, culture medium was removed, cells were washed twice with PBS and a 10% Dimethyl sulfoxide (DMSO) solution was added to the monolayer for exactly 2.5min at RT. DMSO solution was then replaced by 10mL of complete DMEM and cells were incubated for 48-72h at 37ºC in a humidified CO_2 incubator. Viral supernatants were recovered at 48h and 72h post transfection, aliquoted and stored at -80ºC.

Viral particles for transduction of fetal liver cells were produced by transfection of 293T cells with X-tremeGENE HP DNA transfection reagent by Roche, according to manufacturer's instructions. On the day prior to transfection, 293T cells were seeded in 10cm cell culture dishes, at the density of $4x10^6$ cells per dish in 8mL of complete DMEM. On transfection day, 3µg of pMigR1-empty/M2/M2Y, 2.5µg of pCL-Eco, 0.5µg of pCMV-VsVg (section 7.1.6) and 3µL of transfection reagent per microgram of DNA were mixed in simple DMEM. After 20min of incubation at RT, this mix was added dropwise to the cells. On the next day, the culture medium was changed. 48h after transfection, supernatant was recovered and cell debris was removed using a 0.45µm filter. Supernatant was then centrifuged at 25000rpm for 3h at 4ºC, with a 10min break-off at 500rpm. The pellet was then resuspended in complete DMEM (800µL per 10cm dish used initially), aliquoted and stored at -80ºC.

7.2.3.6 Transduction

For the generation of A20 stable cells lines expressing EGFP, EGFP-M2 or EGFP-M2Y, A20 B cells were infected with the viral particles produced as described in section 7.2.3.5. Cells were subjected to two rounds of infection on two consecutive days. For that purpose, $2x10^6$ A20 B cells, in exponencial growth phase, were washed and resuspended in 1mL of complete RPMI (section 7.2.3.1) supplemented with 8µg/mL of polybrene. On a 6-well plate, 1mL of the appropriate retrovirus was then added to the cells. Next, cells were centrifuged at 700g for 1h at 37ºC to increase transduction efficiency. On the next day, another 1mL of the same retroviral supernatant was added to the cells, followed by centrifugation as before. 48h after the second infection, the 20% brightest A20 B cells, for the GFP color, were sorted as described in section 7.2.4.2. After sorting cells were cultured in complete RPMI supplemented with gentamycin to avoid contamination, and 400µg/mL of zeocin for selective pressure.

For transduction of fetal liver cells (section 7.2.3.4), $1\text{-}1.5x10^6$ cells in 100µL of complete DMEM, 400µL of complete DMEM, 400µL of the appropriate retrovirus (section 7.2.3.5) and 8µg/mL of polybrene were mixed per well of a 24-well plate and centrifuged at 860g for 45min at 37ºC. A well containing the same density of fetal liver cells was kept untransduced to serve as a negative control in flow cytometric analysis of transduction efficiency (section 7.2.4.3). After the centrifugation, cells were cultured in complete DMEM supplemented with 20ng/mL of IL-3, 50ng/mL of IL-6 and 100ng/mL of SCF.

7.2.4 Flow cytometry

7.2.4.1 Cell staining

Staining for B cell markers

Staining of B cell markers was used for the analysis of the levels of selected cellular surface markers on A20 B cell lines by flow cytometry. This staining was also performed every time a new aliquot of A20 B cell lines was placed in culture or every time new EGFP cell lines were produced. For those purposes, cells were washed twice with FACS buffer (2% FBS in PBS) and $5x10^5$ cells were added, per condition, to the U-shaped wells of a 96-well plate. The plate was centrifuged at 2000rpm for 1min at 4ºC and cells were incubated with the appropriate antibodies (table 7.1) for 15min on ice, in the dark. Cells were then washed twice, resuspended in FACS buffer, and kept on ice, protected from light, until flow cytometric analysis (section 7.2.4.3).

Checking $Rag^{-/-}$ reconstitution

To assess $Rag^{-/-}$ reconstitution, approximately 50µL of blood was collected from the facial vein of each mouse into an eppendorf containing 15µL of heparin leo (Leo), 7-8 weeks after adoptive transfer of transduced fetal liver cells (section 7.2.7.3). Whole blood was then incubated with 10µL of staining mix containing the appropriate antibodies (table 7.1) for 20min on ice, in the dark. Samples were then transferred to FACS tubes and washed with FACS buffer (2% FBS in PBS). Red blood cell lysis was carried out by incubation with BD FACS Lysing Solution (BD Biosciences), according to manufacturer's instructions. Next, cells were washed twice, resuspended in FACS buffer, and kept on ice, protected from light, until flow cytometric analysis (section 7.2.4.3).

Staining for different splenic cell populations

Spleens were dissected from mice into 5mL of FACS buffer (2% FBS in PBS) and kept on ice until mechanical disruption to obtain single splenocyte suspensions. Cell debris was removed by filtering through a 100µm cell strainer. Red blood cells were lysed by incubation with red blood cell lysis buffer for 5 min on ice. Cell suspensions were washed with FACS buffer and blocked by incubation with anti-CD16/32 (2.4G2) (BD Pharmingen) for 15min at 4ºC. Splenocytes were stained by incubation for 25 min, at 4ºC, in the dark, with the appropriated antibodies diluted in FACS buffer (table 7.1). Unbound antibodies were removed by washing twice with FACS buffer. Cells were resuspended in FACS buffer and were kept on ice, protected from light, until flow cytometric analysis (section 7.2.4.3).

Checking cell purity

$CD4^+$ T, B and c-kit^+ cell populations purified using the Miltenyi Biotec technology (sections 7.2.3.2, 7.2.3.3, and 7.2.3.4 respectively) had their purity verified by flow cytometric analysis. For that purpose, a small aliquot of cells was washed with FACS buffer (2% FBS in PBS) and incubated with the appropriate antibodies (table 7.1). Cells were then washed twice, resuspended in FACS buffer, and kept on ice, protected from light, until flow cytometric analysis (section 7.2.4.3).

7.2.4.2 Purification of cell populations

Single cell suspensions of $CD4^+$ T cells (section 7.2.3.2) or EGFP/EGFP-M2/EGFP-M2Y transduced A20 B cells (section 7.2.3.6) were enriched for the wanted populations using a FACSAria flow cytometer (BD Biosciences). $CD4^+$ T cells were sorted at 37ºC and kept on T cell culture media (section 7.2.3.1) at all times. A20 B cells were sorted at 4ºC and kept on ice until further use.

7.2.4.3 Flow cytometric analysis

Total splenocytes, A20 B cell lines, enriched cell populations and mouse blood were analyzed on a LSR Fortessa flow cytometer (BD Biosciences), using FACSDiva software (BD Biosciences) for acquisition and FlowJo (Tree Star, Inc.) for analysis.

7.2.5 Protein methods

7.2.5.1 SDS-Polyacrylamide Gel Electrophoresis

To confirm expression of M2/M2Y on A20 B cell lines, $2x10^6$ cells were washed with PBS, resuspended in 30µL of lysis buffer (10mM Tris-HCl pH 7.5, 150mM NaCl, 1% Triton X-100, 1mM NaF, 100µM Na_3VO_4, and cømplete from Roche, according to manufacturer's instructions), and centrifuged at 14000rpm for 30min at 4ºC. Supernatant was recovered and added to Laemmli's sample buffer (50mM Tris-HCl pH 6.8, 10% glycerol, 2% SDS, 5% β-mercaptoethanol, 0.1% bromophenol blue). Next, protein samples were heated at 100ºC for 10min and separated through SDS-PAGE, in 1.5mm mini-slab gels of the Bio-Rad mini-protean II electrophoresis system. Resolving gel was prepared with 12% polyacrylamide (Acrylamide:bis-acrylamide 37.5:1, Bio-Rad), 375mM Tris-HCl (pH 8.8), 0.1% SDS, 0.1% APS, and 0.04% TEMED. The solution was covered with sterile MilliQ water and allowed to polymerize at RT. Stacking gel was prepared with 5%

polyacrylamide, 125mM Tris-HCl (pH 6.8), 0.1% SDS, 0.1% APS, and 0.1% TEMED. Electrophoresis was performed in running buffer (25mM Tris-base, 192mM glycine and 0.1% SDS), at 120V until maximal resolution of protein bands.

7.2.5.2 Western blot

After separation by SDS-PAGE, proteins were transferred to a nitrocellulose membrane (GE Healthcare) using a Trans-Blot Cell (Bio-Rad), assembled according to manufacturer's instructions, in transfer buffer (25mM Tris-base, 200mM glycine and 10% methanol) for 1h and 15min at the constant current of 250mA. Protein transfer to the nitrocellulose membrane was confirmed by incubation with Ponceau S (Sigma), for 2min. The dye was removed by incubation with washing buffer (PBS with 0.05% Tween 20) for 5min, on a rocking platform. Unoccupied protein binding sites on the membrane were blocked by incubation with blocking buffer (5% skimmed milk powder in washing buffer) for 1h, on a rocking platform. Incubation with primary antibody (table 7.1), diluted 1:500 to 1:1000, was carried out in blocking buffer for 1h and 30min, on a rocking platform. Membrane was then washed with washing buffer (three times, 5min each) on a rocking platform to remove unbound primary antibody. Next, membrane was incubated with HRP-conjugated secondary antibody (section 7.1.2.2), diluted 1:5000 in blocking buffer, for 45min, on a rocking platform. Membrane was then washed with washing buffer (three times, 5min each) on a rocking platform to remove unbound secondary antibody. Protein antibody complexes were detected by chemiluminescence after incubation with the Supersignal West Pico Chemiluminescent substrate (Thermo Scientific), according to manufacturer's instructions. All incubation steps were performed at RT.

7.2.5.3 Immunofluorescence

Immunofluorescence for conjugation experiments

The number of B-T_H cell conjugates showing pTyr or IFN-γ polarization to the contact zone was assessed by immunofluorescence. After centrifugation and incubation of B and T_H cells as described in section 7.2.6.3, cells were resuspended using a vortex, added to commercial poly-L-lysine coated coverslips and incubated for 20-30min in a humidified tissue culture incubator at 37ºC under 5% CO_2. Culture media was removed and cells were fixed in fixative solution (4% paraformaldehyde, 2% sucrose, PBS) for 20min at RT. At this point, in some experiments, 1mL of PBS was added to the coverslips with fixative solution and these were stored at 4ºC, covered with parafilm and protected from light. Next, excess fixative was removed by washing the coverslips three times with PBS. Cells

were then permeabilized by incubation with a solution of 0.2% Triton X-100 diluted in PBS for 10min at RT. The indicated primary antibodies (table 7.1) were diluted 1:50 in a solution of 0.2% Triton X-100 and 1% BSA in PBS. Incubation was performed in a dark humid chamber, for 1h at RT. Coverslips were washed three times in PBS to remove unbound primary antibody. When detecting IFN-γ, a secondary antibody (section 7.1.2.2) was diluted 1:250 in a solution of 0.2% Triton X-100 and 1% BSA in PBS. Incubation was performed in a dark humid chamber, for 1h at RT. When detecting actin, cells were incubated for 1h at RT with phalloidin-TRITC diluted 1:250 in a solution of 0.2% Triton X-100 and 1% BSA in PBS. To remove unbound secondary antibody or phalloidin-TRITC, coverslips were washed three times in PBS. Cells were fixed again by incubation with fixative solution for 5min. Finally, coverslips were washed three times with PBS to remove the fixative solution, rinsed in distilled water and mounted with Fluoromount-G (Southern Biotec). After drying for 1h at 37ºC, slides were stored at 4ºC until further use.
Slides were analyzed by confocal microscopy (LSM 510 META, Zeiss) using a Plan-Apochromat 63x (1.4 oil) objective, with electronic zoom 1 for counting purposes and electronic zoom 3 for representative images. Images were analyzed using the AimImageBrowser (Zeiss LSM data server, Zeiss) software.

Immunofluorescence of frozen spleen sections

Infection of splenic cellular populations by WT or M2Y mutant MuHV-4 was tracked by immunofluorescence of frozen spleen sections, prepared as described in section 7.2.9. Superfrost Plus slides (Thermo Scientific) containing 9µm thick spleen sections were air dried for 1h at RT. Slides were immersed in distilled water for 5min to remove the extra OCT compound. Slides were then dried and sections were encircled with a fat pen (Dako), to allow the use of different antibodies on the same slide, and dried for 1min. From this step forward incubations were made in a dark humid chamber. Hydration of the sections was performed by incubation with PBS for 10min at RT. Next, sections were permeabilized and blocked by incubation with a perm/block solution (0.3% Triton X-100, 5% normal goat serum, PBS) for 1h at RT. Primary antibodies (table 7.1) were diluted in a second perm/block solution (0.3% triton, 1% BSA, PBS) and added to the sections for 18h at 4ºC. Amount of each primary antibody used was optimized and dilution ranged from 1:100 to 1:200. To remove unbound primary antibody, sections were immersed three times in approximately 200mL of PBS for 10min at RT, in the dark. Secondary antibodies (section 7.1.2.2) were then diluted in the second perm/block solution and added to the sections for 1h at RT. Amount of each secondary antibody used was optimized and dilution ranged from 1:250 to 1:300. Next, sections were washed three times with PBS as mentioned above to remove unbound secondary antibody and mounted with Prolong Gold

with DAPI. After drying for 24h at RT, slides were sealed with nail polish to prevent dehydration and subsequent shrinking of the tissue and stored at 4ºC in the dark until further use.
Slides were analyzed by confocal microscopy (LSM 710, Zeiss) using either an EC Plan-Neofluar 40x (1.3 oil) or a Plan-Apochromat 63x (1.4 oil) objective. Images were analyzed using the FIJI software (Schindelin, Arganda-Carreras et al. 2012).

7.2.6 Conjugation assays

7.2.6.1 The cellular system: A20-T CD4⁺ Tg DO11.10

The cellular system A20-T $CD4^+$ Tg DO11.10 was used for the analysis of conjugate formation. A20 B cells were transduced as described in section 7.2.3.6, giving rise to A20 B cell lines stably expressing M2, M2Y, EGFP, EGFP-M2 or EGFP-M2Y. On the day prior to incubation with T cells, A20 B cell lines in exponential growth were pulsed with the indicated concentrations of OVAp. Briefly, cells were washed twice with conjugates media (section 7.2.3.1), resuspended at a cellular density of $2x10^6$/mL of conjugates media supplemented with the indicated concentrations of OVAp and incubated O/N in a humidified tissue culture incubator at 37ºC under 5% CO_2. TCR transgenic OVAp-specific T cells were obtained and prepared as described in section 7.2.3.2. A20 B cells and/or mouse $CD4^+$ T cells were washed and loaded, or not, with the indicated live dyes (section 7.1.2.3), as appropriate. B and T cells were again washed and then added in the indicated ratios to FACS tubes. These were centrifuged for 1min at 1500rpm to promote cell encounter, and incubated for a period of time, as is specified. Conjugates were then analyzed by flow cytometry or confocal microscopy.

7.2.6.2 Conjugate quantification by flow cytometry

For the quantification of conjugates by flow cytometry, non-fluorescent B cell lines were stained with 50nM of CMFDA live dye, diluted in RPMI 1640, for 30min at 37ºC, in the dark. In the case of EGFP-expressing B cell lines CMFDA was not used. Cells were then washed with conjugates media (section 7.2.3.1) and resuspended at a cellular density of $2x10^5$/150µL of media. T cells were prepared as described in section 7.2.3.2 and stained with 1µM of DDAO live dye, diluted in PBS, for 20min at 37ºC, in the dark. Next, cells were washed with conjugates media and resuspended at a cellular density of $1x10^5$/150µL. 150µL of both B and T cells were then added to a FACS tube, centrifuged at 1500rpm for 1min and incubated for the indicated times. This was done for each OVAp

concentration. Samples were then carefully resuspended on a vortex and analyzed on a LSR Fortessa flow cytometer (BD Biosciences) (section 7.2.4.3).

For the in vitro competition assay, M2-expressing B cells were stained with 50nM of CMFDA live dye, diluted in RPMI 1640, for 30min at 37ºC, in the dark. M2Y- or EGFP-M2Y-expressing B cells were stained with 2µM of CMTMR live dye, diluted in RPMI 1640, for 15min at 37ºC, in the dark. Next, cells were washed with conjugates media and resuspended at a cellular density of $1.5x10^5$/100µL of media. T cells were stained with DDAO live dye, as described above and resuspended at a cellular density of $1.5x10^5$/100µL of media. 100µL ($1.5x10^5$ cells) of each cellular population were added to the same FACS tube, centrifuged at 1500rpm for 1min and incubated for 30min. This was done for each OVAp concentration. Samples were then carefully resuspended on a vortex and analyzed on a LSR Fortessa flow cytometer (BD Biosciences) (section 7.2.4.3).

7.2.6.3 Conjugate analysis by confocal microscopy

For the quantification of conjugates by confocal microscopy, non-fluorescent B cell lines were stained with 1µM of CMFDA live dye, diluted in RPMI 1640, for 30min at 37ºC, in the dark. In the case of EGFP-expressing B cell lines CMFDA was not used. Cells were then washed with conjugates media (section 7.2.3.1) and resuspended at a cellular density of $5x10^5$/100µL of media. T cells were recovered after 5 days of resting and washed with T cell culture media (section 7.2.3.1). Cell suspension was then filtered and live resting T cells were sorted, based on their FSC-A/SSC-A profile (section 7.2.4.2). T cells were then washed and resuspended at a cellular density of $2.5x10^5$/100µL of T cell culture media. 100µL of each cellular population were added to the same FACS tube, centrifuged at 1500rpm for 1min and incubated for 30min in a water bath, in the dark. Cells were then resuspended using the vortex, added to commercial poly-L-lysine coated coverslips and processed for immunofluorescence as described on section 7.2.5.3.

For the quantification of conjugates showing IFN-γ polarization to the B-T_H contact zone, T cells were stained with 100µM of CMAC live dye, prior to incubation with B cells. B and T cells were incubated for 2.5h. The remaining steps were done as described above.

Image quantification was performed in a blinded fashion in randomly selected fields from at least three independent experiments. To evaluate the percentage of conjugates showing pTyr and/or IFN-γ polarization to the contact zone, only images with a minimum of three T cells were analyzed. Number of T cells conjugating was scored visually.

7.2.6.4 Analysis of calcium mobilization on T cells by flow cytometry

A20 B cell lines, loaded or not with OVAp, were processed as described in section 7.2.6.1. Mouse OVAp-specific $CD4^+$ T cells were obtained as described in section 7.2.3.2. T cells were recovered after 6.5-7 days of resting and washed with T cell culture media (section 7.2.3.1). Cell suspension was then filtered and live resting T cells were sorted, based on their FSC-A/SSC-A profile (section 7.2.4.2). Next, T cells were loaded with 5μM of Indo-1 AM (Invitrogen) (Valitutti, Dessing et al. 1993) for 35-45min in a humidified tissue culture incubator at 37ºC under 5% CO_2. From this point forward cells were protected from light and were used in the next 2h, before Indo-1 degradation. Cells were then incubated with A20 B cell lines for 5min at 37ºC. Before starting sample acquisition a baseline was set on the 405/525 emission ratio using Indo-1 loaded T cells. Ionomycin (Sigma) activated T cells were used as a positive control. Baseline was acquired for approximately 2min and samples were lightly vortexed and acquired for an additional 18min on a MoFlow cytometer.

7.2.7 Animal experiments

7.2.7.1 Ethics statement

The study accorded with the Portuguese official Veterinary Directorate (Portaria 1005/92), European Directive 2010/63/EU, and Federation of European Laboratory Animal Science Associations guidelines on laboratory animal welfare. It was approved by the Portuguese official veterinary department for welfare licensing (protocol AEC_2010_017_PS_Rdt_General) and by the IMM Animal Ethics Committee. Mice were sacrificed by CO2 inhalation or cervical dislocation.

7.2.7.2 Mice breeding for fetal liver dissection

72h before mating, females were housed with dirty bedding from male's cages, to stimulate estrus. Breeding trios (CD45.1xCD45.1, CD45.2xCD45.2, CD45.1xCD45.2) were then housed together overnight and the day of vaginal plug detection was set as day 0. Females were checked for pregnancy at day 13 and embryos were collected at day 15 and processed for fetal liver dissection (section 7.2.3.4).

7.2.7.3 Adoptive transfers

When testing the optimal conditions for the in vivo competition system, C57BL/6J mice were not irradiated or irradiated with 250rad or 500rad, using an Irradiator Gammacell ELAN 3000. 1-3.5x10^6 CD45.1 B cells, obtained as described in section 7.2.3.3, were washed with PBS, filtered (40µm) and adoptively transferred to the sex matched C57BL/6J mice via tail vein injection.

$Rag^{-/-}$ mice were irradiated at 600rad using an Irradiator Gammacell ELAN 3000. 2x10^6 transduced CD45.1, CD45.2 or CD45.1/2 fetal liver cells were washed with PBS, filtered (40µm) and adoptively transferred to sex matched irradiated $Rag^{-/-}$ mice via tail vein injection. These cells were obtained as described in section 7.2.3.4 and transduced as described in section 7.2.3.6.

Whenever mice were irradiated, antibiotics were added to drinking water 48h prior to transfer.

7.2.7.4 Immunization with NP-CGG

When testing the optimal conditions for the in vivo competition system, following adoptive transfer of CD45.1 B cells, C57BL/6J mice were intraperitoneally immunized with 100µg of NP-CGG (4-Hydroxy-3-nitrophenylacetyl hapten conjugated to Chicken Gamma Globulin) adsorbed to 3mg of Alum. Ten days post immunization, spleens were isolated for GC analysis by flow cytometry (section 7.2.4).

7.2.7.5 Mice infection

6- to 8-week old female C57BL/6 mice were inoculated intraperitoneally with 10^6 PFU of MuHV-4 viruses: vYFP or vM2Y-YFP (section 7.1.8). Virus inoculations were performed in 100µL of PBS. At different time points after infection, mice were sacrificed by CO_2 inhalation followed by cervical dislocation, and spleens were dissected and processed for subsequent analysis.

7.2.8 Virus assays

7.2.8.1 Virus infection of cells

BHK-21 cells were seeded in tissue culture flasks and grown to semi-confluence for virus stock production. Cell monolayers were adsorbed with virus suspension in 25% of the final appropriate culture medium for 1h at 37ºC, then covered with the remaining 75% of medium and incubated for the appropriate time.

7.2.8.2 Virus working stocks

Virus working stocks were grown by low multiplicity infection of BHK-21 cells (0.001 PFU/cell) in 175cm^2 culture flasks. When approximately 50% cytopathic effect (cpe) was visible (4-5 days), cells and supernatants were transferred to 50mL tubes. Cell-associated virus was centrifuged at 1500rpm for 10min at 4ºC. Next, it was resuspended in 2mL of fresh complete GMEM medium, subjected to freeze-thawing, and kept at -80ºC in 200µL aliquots. Supernatant-associated virus was centrifuged at 15000 rpm for 2h at 4ºC and pellet was resuspended in 2mL of fresh medium. 100µL aliquots were made and stored at -80ºC. Virus titers were determined in duplicates by suspension assay.

7.2.8.3 Infectious center assay

Spleens were dissected from mice individually into 5mL of complete GMEM (section 7.2.3.1). Single cell suspensions were obtained by mechanical disruption and cell debris was removed by filtering through a 100µm cell strainer. Next, cells were centrifuged at 1300rpm for 5 min at 4ºC. Red blood cells were lysed by incubation with 1mL of red blood cell lysis buffer (154mM ammonium chloride, 14mM sodium hydrogen carbonate, 1mM EDTA pH7.3) for 5 min on ice. Cells were then washed with 10mL of complete GMEM, pelleted by centrifugation at 1300rpm for 5min at 4ºC and resuspended in 5mL of complete GMEM. At this point, a small aliquot of cells was removed for cell count with trypan blue. 10-fold serial dilutions were prepared in duplicate. 1mL of this dilution was added to 5x10^5 BHK-21 cells in 6cm dishes, in a final volume of 5mL. The co-culture was incubated for 5 days at 37ºC in a humidified incubator with 5% CO2. Cell monolayers were then fixed with 4% formaldehyde in PBS for 10min, and stained with 0.05% toluidine blue solution for 5min. Viral plaques were counted using an Olympus SZ51 zoom stereo microscope and infectious centers were determined from the number of viral plaques in duplicate dishes.

7.2.8.4 Plaque assay (suspension assay)

Virus stocks (section 7.2.8.2) and infectious virus present in the spleen of infected mice were titrated by plaque assay (or suspension assay). Spleens were dissected from mice individually into 5mL of complete GMEM (section 7.2.3.1). Single cell suspensions were obtained by mechanical disruption and cell debris were removed by filtering through a 100µm cell strainer. Next, cells were centrifuged at 1300rpm for 5 min at 4ºC. Red blood cells were lysed by incubation with 1mL of red blood cell lysis buffer (154mM ammonium chloride, 14mM sodium hydrogen carbonate, 1mM EDTA pH7.3) for 5 min on ice. Cells were then washed with 10mL of complete GMEM, pelleted by centrifugation at 1300rpm for 5min at 4ºC and resuspended in 5mL of complete GMEM. Cell suspensions were subjected to freeze-thawing to disrupt cells and subjected to the vortex. Virus stocks or splenic cell suspensions were 10-fold serial diluted in 1mL of complete GMEM. Each dilution was incubated with $5x10^5$ BHK-21 cells for 1h at RT, on a rocking platform (15rpm). 3mL of media was added to each dilution, mixed by inversion and plated on 6cm dishes. The co-culture was incubated for 4 days at 37ºC in a humidified incubator with 5% CO2. Cell monolayers were then fixed with 4% formaldehyde in PBS for 10min, and stained with 0.05% toluidine blue solution for 5min. Viral plaques were counted using an Olympus SZ51 zoom stereo microscope and virus titers were determined from the number of viral plaques in duplicate dishes.

7.2.9 Frozen spleen sections

Four or eight days post infection, spleens from intraperitoneally infected mice (section 7.2.7.5) were dissected individually to 5mL of PBS. Fat tissue was carefully removed and the spleens were fixed by incubation in 10mL of fixative solution (1% fresh PFA, 10mM sodium metaperiodate, and 75mM L-lysine in PBS) for 24h at 4ºC. Spleens were then washed with 10mL of PBS and equilibrated by incubation in 5mL of a 30% sucrose solution for 18h at 4ºC. This solution was replaced a fresh solution of 30% sucrose and optimal cutting temperature compound (OCT), where spleens were incubated for 3-4h at 4ºC. Next, spleens were cut in half longitudinally and each half was transferred to appropriate tissue molds and embedded in OCT. Samples were then snap-frozen in isopentane cooled down to -70/-80ºC in liquid nitrogen. Samples were immediately stored at -20ºC and later on transferred to -80ºC for long-term storage.

9µm-thick longitudinal sections were obtained using the cryostat LEICA CM3050. Chamber and object temperature ranged from -18ºC to -20ºC. Two to three sections were

adhered to Superfrost Plus Slides (Thermo Scientific) and kept at RT for at least 5min. Finally, samples embedded in OCT were stored back at -80ºC while sections were stored at -20ºC until further use.

7.2.10 Statistical analysis

Statistical significance was evaluated with unpaired one-tailed t-test or non-parametric Mann-Whitney U test, as appropriate, using GraphPad Prism software. ns indicates $p>0.05$; * indicates $p<0.05$, ** indicates $p<0.01$, *** indicates $p<0.001$, **** indicates $p<0.0001$.

CHAPTER 8

REFERENCES

8 REFERENCES

Adler, H., M. Messerle, M. Wagner and U. H. Koszinowski (2000). "Cloning and mutagenesis of the murine gammaherpesvirus 68 genome as an infectious bacterial artificial chromosome." J Virol **74**(15): 6964-6974.

Alarcon, B., D. Mestre and N. Martinez-Martin (2011). "The immunological synapse: a cause or consequence of T-cell receptor triggering?" Immunology **133**(4): 420-425.

Allday, M. J., Q. Bazot and R. E. White (2015). "The EBNA3 Family: Two Oncoproteins and a Tumour Suppressor that Are Central to the Biology of EBV in B Cells." Curr Top Microbiol Immunol **391**: 61-117.

Allen, C. D., T. Okada and J. G. Cyster (2007). "Germinal-center organization and cellular dynamics." Immunity **27**(2): 190-202.

Ambroziak, J. A., D. J. Blackbourn, B. G. Herndier, R. G. Glogau, J. H. Gullett, A. R. McDonald, E. T. Lennette and J. A. Levy (1995). "Herpes-like sequences in HIV-infected and uninfected Kaposi's sarcoma patients." Science **268**(5210): 582-583.

Andjelkovic, M., D. R. Alessi, R. Meier, A. Fernandez, N. J. Lamb, M. Frech, P. Cron, P. Cohen, J. M. Lucocq and B. A. Hemmings (1997). "Role of translocation in the activation and function of protein kinase B." J Biol Chem **272**(50): 31515-31524.

Babcock, G. J., D. Hochberg and A. D. Thorley-Lawson (2000). "The expression pattern of Epstein-Barr virus latent genes in vivo is dependent upon the differentiation stage of the infected B cell." Immunity **13**(4): 497-506.

Bagni, R. and D. Whitby (2009). "Kaposi's sarcoma-associated herpesvirus transmission and primary infection." Curr Opin HIV AIDS **4**(1): 22-26.

Bannard, O., R. M. Horton, C. D. Allen, J. An, T. Nagasawa and J. G. Cyster (2013). "Germinal center centroblasts transition to a centrocyte phenotype according to a timed program and depend on the dark zone for effective selection." Immunity **39**(5): 912-924.

Barton, E., P. Mandal and S. H. Speck (2011). "Pathogenesis and host control of gammaherpesviruses: lessons from the mouse." Annu Rev Immunol **29**: 351-397.

Basu, S., A. Ray and B. N. Dittel (2013). "Differential representation of B cell subsets in mixed bone marrow chimera mice due to expression of allelic variants of CD45 (CD45.1/CD45.2)." J Immunol Methods **396**(1-2): 163-167.

Batista, F. D. and N. E. Harwood (2009). "The who, how and where of antigen presentation to B cells." Nat Rev Immunol **9**(1): 15-27.

Bennett, N. J., J. S. May and P. G. Stevenson (2005). "Gamma-herpesvirus latency requires T cell evasion during episome maintenance." PLoS Biol **3**(4): e120.

Bishop, G. A. and B. S. Hostager (2003). "The CD40-CD154 interaction in B cell-T cell liaisons." Cytokine Growth Factor Rev **14**(3-4): 297-309.

Blackman, M. A. and E. Flano (2002). "Persistent gamma-herpesvirus infections: what can we learn from an experimental mouse model?" J Exp Med **195**(7): F29-32.

Blackman, M. A., E. Flano, E. Usherwood and D. L. Woodland (2000). "Murine gamma-herpesvirus-68: a mouse model for infectious mononucleosis?" Mol Med Today **6**(12): 488-490.

Blasdell, K., C. McCracken, A. Morris, A. A. Nash, M. Begon, M. Bennett and J. P. Stewart (2003). "The wood mouse is a natural host for Murid herpesvirus 4." J Gen Virol **84**(Pt 1): 111-113.

Blaskovic, D., M. Stancekova, J. Svobodova and J. Mistrikova (1980). "Isolation of five strains of herpesviruses from two species of free living small rodents." Acta Virol **24**(6): 468.

Boname, J. M. and P. G. Stevenson (2001). "MHC class I ubiquitination by a viral PHD/LAP finger protein." Immunity **15**(4): 627-636.

Boos, H., R. Berger, C. Kuklik-Roos, T. Iftner and N. Mueller-Lantzsch (1987). "Enhancement of Epstein-Barr virus membrane protein (LMP) expression by serum, TPA, or n-butyrate in latently infected Raji cells." Virology **159**(1): 161-165.

Boulanger, E., L. Gerard, J. Gabarre, J. M. Molina, C. Rapp, J. F. Abino, J. Cadranel, S. Chevret and E. Oksenhendler (2005). "Prognostic factors and outcome of human herpesvirus 8-associated primary effusion lymphoma in patients with AIDS." J Clin Oncol **23**(19): 4372-4380.

Bowden, R. J., J. P. Simas, A. J. Davis and S. Efstathiou (1997). "Murine gammaherpesvirus 68 encodes tRNA-like sequences which are expressed during latency." J Gen Virol **78 (Pt 7)**: 1675-1687.

Bridgeman, A., P. G. Stevenson, J. P. Simas and S. Efstathiou (2001). "A secreted chemokine binding protein encoded by murine gammaherpesvirus-68 is necessary for the establishment of a normal latent load." J Exp Med **194**(3): 301-312.

Brinkmann, M. M., M. Glenn, L. Rainbow, A. Kieser, C. Henke-Gendo and T. F. Schulz (2003). "Activation of mitogen-activated protein kinase and NF-kappaB pathways by a Kaposi's sarcoma-associated herpesvirus K15 membrane protein." J Virol **77**(17): 9346-9358.

Brinkmann, M. M., M. Pietrek, O. Dittrich-Breiholz, M. Kracht and T. F. Schulz (2007). "Modulation of host gene expression by the K15 protein of Kaposi's sarcoma-associated herpesvirus." J Virol **81**(1): 42-58.

Brinkmann, M. M. and T. F. Schulz (2006). "Regulation of intracellular signalling by the terminal membrane proteins of members of the Gammaherpesvirinae." J Gen Virol **87**(Pt 5): 1047-1074.

Bustelo, X. R. (2000). "Regulatory and signaling properties of the Vav family." Mol Cell Biol **20**(5): 1461-1477.

Calame, K. L. (2001). "Plasma cells: finding new light at the end of B cell development." Nat Immunol **2**(12): 1103-1108.

Caldwell, R. G., J. B. Wilson, S. J. Anderson and R. Longnecker (1998). "Epstein-Barr virus LMP2A drives B cell development and survival in the absence of normal B cell receptor signals." Immunity **9**(3): 405-411.

Cannon, J. S., J. Nicholas, J. M. Orenstein, R. B. Mann, P. G. Murray, P. J. Browning, J. A. DiGiuseppe, E. Cesarman, G. S. Hayward and R. F. Ambinder (1999). "Heterogeneity of viral IL-6 expression in HHV-8-associated diseases." J Infect Dis **180**(3): 824-828.

Carbone, A., A. Gloghini, E. Vaccher, M. Cerri, G. Gaidano, R. Dalla-Favera and U. Tirelli (2005). "Kaposi's sarcoma-associated herpesvirus/human herpesvirus type 8-positive solid lymphomas: a tissue-based variant of primary effusion lymphoma." J Mol Diagn **7**(1): 17-27.

Cardin, R. D., J. W. Brooks, S. R. Sarawar and P. C. Doherty (1996). "Progressive loss of CD8+ T cell-mediated control of a gamma-herpesvirus in the absence of CD4+ T cells." J Exp Med **184**(3): 863-871.

Casola, S., K. L. Otipoby, M. Alimzhanov, S. Humme, N. Uyttersprot, J. L. Kutok, M. C. Carroll and K. Rajewsky (2004). "B cell receptor signal strength determines B cell fate." Nat Immunol **5**(3): 317-327.

Casper, C., W. G. Nichols, M. L. Huang, L. Corey and A. Wald (2004). "Remission of HHV-8 and HIV-associated multicentric Castleman disease with ganciclovir treatment." Blood **103**(5): 1632-1634.

Cen, O. and R. Longnecker (2015). "Latent Membrane Protein 2 (LMP2)." Curr Top Microbiol Immunol **391**: 151-180.

Cesarman, E. (2011). "Gammaherpesvirus and lymphoproliferative disorders in immunocompromised patients." Cancer Lett **305**(2): 163-174.

Cesarman, E. (2014). "Gammaherpesviruses and lymphoproliferative disorders." Annu Rev Pathol **9**: 349-372.

Cesarman, E. and D. M. Knowles (1999). "The role of Kaposi's sarcoma-associated herpesvirus (KSHV/HHV-8) in lymphoproliferative diseases." Semin Cancer Biol **9**(3): 165-174.

Chadburn, A., E. M. Hyjek, W. Tam, Y. Liu, T. Rengifo, E. Cesarman and D. M. Knowles (2008). "Immunophenotypic analysis of the Kaposi sarcoma herpesvirus (KSHV; HHV-8)-infected B cells in HIV+ multicentric Castleman disease (MCD)." Histopathology **53**(5): 513-524.

Chaki, S. P. and G. M. Rivera (2013). "Integration of signaling and cytoskeletal remodeling by Nck in directional cell migration." Bioarchitecture **3**(3): 57-63.

Chang, Y., E. Cesarman, M. S. Pessin, F. Lee, J. Culpepper, D. M. Knowles and P. S. Moore (1994). "Identification of herpesvirus-like DNA sequences in AIDS-associated Kaposi's sarcoma." Science **266**(5192): 1865-1869.

Cho, N. H., P. Feng, S. H. Lee, B. S. Lee, X. Liang, H. Chang and J. U. Jung (2004). "Inhibition of T cell receptor signal transduction by tyrosine kinase-interacting protein of Herpesvirus saimiri." J Exp Med **200**(5): 681-687.

Choi, J. K., B. S. Lee, S. N. Shim, M. Li and J. U. Jung (2000). "Identification of the novel K15 gene at the rightmost end of the Kaposi's sarcoma-associated herpesvirus genome." J Virol **74**(1): 436-446.

Choquet, S., V. Leblond, R. Herbrecht, G. Socie, A. M. Stoppa, P. Vandenberghe, A. Fischer, F. Morschhauser, G. Salles, W. Feremans, E. Vilmer, M. N. Peraldi, P. Lang, Y.

Lebranchu, E. Oksenhendler, J. L. Garnier, T. Lamy, A. Jaccard, A. Ferrant, F. Offner, O. Hermine, A. Moreau, S. Fafi-Kremer, P. Morand, L. Chatenoud, N. Berriot-Varoqueaux, L. Bergougnoux and N. Milpied (2006). "Efficacy and safety of rituximab in B-cell post-transplantation lymphoproliferative disorders: results of a prospective multicenter phase 2 study." Blood **107**(8): 3053-3057.

Christensen, J. P., R. D. Cardin, K. C. Branum and P. C. Doherty (1999). "CD4(+) T cell-mediated control of a gamma-herpesvirus in B cell-deficient mice is mediated by IFN-gamma." Proc Natl Acad Sci U S A **96**(9): 5135-5140.

Coen, N., S. Duraffour, R. Snoeck and G. Andrei (2014). "KSHV targeted therapy: an update on inhibitors of viral lytic replication." Viruses **6**(11): 4731-4759.

Collins, C. M., J. M. Boss and S. H. Speck (2009). "Identification of infected B-cell populations by using a recombinant murine gammaherpesvirus 68 expressing a fluorescent protein." J Virol **83**(13): 6484-6493.

Collins, C. M. and S. H. Speck (2014). "Expansion of murine gammaherpesvirus latently infected B cells requires T follicular help." PLoS Pathog **10**(5): e1004106.

Contreras-Salazar, B., B. Ehlin-Henriksson, G. Klein and M. G. Masucci (1990). "Up regulation of the Epstein-Barr virus (EBV)-encoded membrane protein LMP in the Burkitt's lymphoma line Daudi after exposure to n-butyrate and after EBV superinfection." J Virol **64**(11): 5441-5447.

Correia, B., S. A. Cerqueira, C. Beauchemin, M. Pires de Miranda, S. Li, R. Ponnusamy, L. Rodrigues, T. R. Schneider, M. A. Carrondo, K. M. Kaye, J. P. Simas and C. E. McVey (2013). "Crystal structure of the gamma-2 herpesvirus LANA DNA binding domain identifies charged surface residues which impact viral latency." PLoS Pathog **9**(10): e1003673.

Coscoy, L. (2007). "Immune evasion by Kaposi's sarcoma-associated herpesvirus." Nat Rev Immunol **7**(5): 391-401.

Coscoy, L. and D. Ganem (2000). "Kaposi's sarcoma-associated herpesvirus encodes two proteins that block cell surface display of MHC class I chains by enhancing their endocytosis." Proc Natl Acad Sci U S A **97**(14): 8051-8056.

Coscoy, L. and D. Ganem (2001). "A viral protein that selectively downregulates ICAM-1 and B7-2 and modulates T cell costimulation." J Clin Invest **107**(12): 1599-1606.

Cousins, E. and J. Nicholas (2014). "Molecular biology of human herpesvirus 8: novel functions and virus-host interactions implicated in viral pathogenesis and replication." Recent Results Cancer Res **193**: 227-268.

Dal Porto, J. M., S. B. Gauld, K. T. Merrell, D. Mills, A. E. Pugh-Bernard and J. Cambier (2004). "B cell antigen receptor signaling 101." Mol Immunol **41**(6-7): 599-613.

Damania, B. (2004). "Oncogenic gamma-herpesviruses: comparison of viral proteins involved in tumorigenesis." Nat Rev Microbiol **2**(8): 656-668.

Davison, A. J., R. Eberle, B. Ehlers, G. S. Hayward, D. J. McGeoch, A. C. Minson, P. E. Pellett, B. Roizman, M. J. Studdert and E. Thiry (2009). "The order Herpesvirales." Arch Virol **154**(1): 171-177.

Dawson, C. W., A. B. Rickinson and L. S. Young (1990). "Epstein-Barr virus latent membrane protein inhibits human epithelial cell differentiation." Nature **344**(6268): 777-780.

Dawson, C. W., G. Tramountanis, A. G. Eliopoulos and L. S. Young (2003). "Epstein-Barr virus latent membrane protein 1 (LMP1) activates the phosphatidylinositol 3-kinase/Akt pathway to promote cell survival and induce actin filament remodeling." J Biol Chem **278**(6): 3694-3704.

de Lima, B. D., J. S. May, S. Marques, J. P. Simas and P. G. Stevenson (2005). "Murine gammaherpesvirus 68 bcl-2 homologue contributes to latency establishment in vivo." J Gen Virol **86**(Pt 1): 31-40.

De Silva, N. S. and U. Klein (2015). "Dynamics of B cells in germinal centres." Nat Rev Immunol **15**(3): 137-148.

Decalf, J., C. Godinho-Silva, D. Fontinha, S. Marques and J. P. Simas (2014). "Establishment of murine gammaherpesvirus latency in B cells is not a stochastic event." PLoS Pathog **10**(7): e1004269.

Delgado-Eckert, E. and M. Shapiro (2011). "A model of host response to a multi-stage pathogen." J Math Biol **63**(2): 201-227.

Depoil, D., R. Zaru, M. Guiraud, A. Chauveau, J. Harriague, G. Bismuth, C. Utzny, S. Muller and S. Valitutti (2005). "Immunological synapses are versatile structures enabling selective T cell polarization." Immunity **22**(2): 185-194.

Devergne, O., E. Hatzivassiliou, K. M. Izumi, K. M. Kaye, M. F. Kleijnen, E. Kieff and G. Mosialos (1996). "Association of TRAF1, TRAF2, and TRAF3 with an Epstein-Barr virus LMP1 domain important for B-lymphocyte transformation: role in NF-kappaB activation." Mol Cell Biol **16**(12): 7098-7108.

Dittmer, D. P. and B. Damania (2013). "Kaposi sarcoma associated herpesvirus pathogenesis (KSHV)--an update." Curr Opin Virol **3**(3): 238-244.

Doherty, P. C., J. P. Christensen, G. T. Belz, P. G. Stevenson and M. Y. Sangster (2001). "Dissecting the host response to a gamma-herpesvirus." Philos Trans R Soc Lond B Biol Sci **356**(1408): 581-593.

Duchez, S., M. Rodrigues, F. Bertrand and S. Valitutti (2011). "Reciprocal polarization of T and B cells at the immunological synapse." J Immunol **187**(9): 4571-4580.

Dustin, M. L. (2014). "The immunological synapse." Cancer Immunol Res **2**(11): 1023-1033.

Efstathiou, S., Y. M. Ho and A. C. Minson (1990). "Cloning and molecular characterization of the murine herpesvirus 68 genome." J Gen Virol **71 (Pt 6)**: 1355-1364.

Ehtisham, S., N. P. Sunil-Chandra and A. A. Nash (1993). "Pathogenesis of murine gammaherpesvirus infection in mice deficient in CD4 and CD8 T cells." J Virol **67**(9): 5247-5252.

Eliopoulos, A. G. and L. S. Young (1998). "Activation of the cJun N-terminal kinase (JNK) pathway by the Epstein-Barr virus-encoded latent membrane protein 1 (LMP1)." Oncogene **16**(13): 1731-1742.

Epstein, M. A., B. G. Achong and Y. M. Barr (1964). "Virus Particles in Cultured Lymphoblasts from Burkitt's Lymphoma." Lancet **1**(7335): 702-703.

Etienne-Manneville, S. and A. Hall (2002). "Rho GTPases in cell biology." Nature **420**(6916): 629-635.

Evans, A. G., J. M. Moser, L. T. Krug, V. Pozharskaya, A. L. Mora and S. H. Speck (2008). "A gammaherpesvirus-secreted activator of Vbeta4+ CD8+ T cells regulates chronic infection and immunopathology." J Exp Med **205**(3): 669-684.

Feldman, E. R., M. Kara, C. B. Coleman, K. R. Grau, L. M. Oko, B. J. Krueger, R. Renne, L. F. van Dyk and S. A. Tibbetts (2014). "Virus-encoded microRNAs facilitate gammaherpesvirus latency and pathogenesis in vivo." MBio **5**(3): e00981-00914.

Feske, S., J. Giltnane, R. Dolmetsch, L. M. Staudt and A. Rao (2001). "Gene regulation mediated by calcium signals in T lymphocytes." Nat Immunol **2**(4): 316-324.

Flano, E., S. M. Husain, J. T. Sample, D. L. Woodland and M. A. Blackman (2000). "Latent murine gamma-herpesvirus infection is established in activated B cells, dendritic cells, and macrophages." J Immunol **165**(2): 1074-1081.

Flano, E., Q. Jia, J. Moore, D. L. Woodland, R. Sun and M. A. Blackman (2005). "Early establishment of gamma-herpesvirus latency: implications for immune control." J Immunol **174**(8): 4972-4978.

Flano, E., I. J. Kim, D. L. Woodland and M. A. Blackman (2002). "Gamma-herpesvirus latency is preferentially maintained in splenic germinal center and memory B cells." J Exp Med **196**(10): 1363-1372.

Fontinha, D., F. B. Lopes, S. Marques and J. P. Simas (2015). "Murid Gammaherpesvirus Latency-Associated Protein M2 Promotes the Formation of Conjugates between Transformed B Lymphoma Cells and T Helper Cells." PLoS One **10**(11): e0142540.

Francois, S., S. Vidick, M. Sarlet, D. Desmecht, P. Drion, P. G. Stevenson, A. Vanderplasschen and L. Gillet (2013). "Illumination of murine gammaherpesvirus-68 cycle reveals a sexual transmission route from females to males in laboratory mice." PLoS Pathog **9**(4): e1003292.

Frederico, B., B. Chao, C. Lawler, J. S. May and P. G. Stevenson (2015). "Subcapsular sinus macrophages limit acute gammaherpesvirus dissemination." J Gen Virol **96**(8): 2314-2327.

Frederico, B., B. Chao, J. S. May, G. T. Belz and P. G. Stevenson (2014). "A murid gamma-herpesviruses exploits normal splenic immune communication routes for systemic spread." Cell Host Microbe **15**(4): 457-470.

Frederico, B., R. Milho, J. S. May, L. Gillet and P. G. Stevenson (2012). "Myeloid infection links epithelial and B cell tropisms of Murid Herpesvirus-4." PLoS Pathog **8**(9): e1002935.

Friedl, P., A. T. den Boer and M. Gunzer (2005). "Tuning immune responses: diversity and adaptation of the immunological synapse." Nat Rev Immunol **5**(7): 532-545.

Fukuda, M. and Y. Kawaguchi (2014). "Role of the immunoreceptor tyrosine-based activation motif of latent membrane protein 2A (LMP2A) in Epstein-Barr virus LMP2A-induced cell transformation." J Virol **88**(9): 5189-5194.

Fukuda, M. and R. Longnecker (2004). "Latent membrane protein 2A inhibits transforming growth factor-beta 1-induced apoptosis through the phosphatidylinositol 3-kinase/Akt pathway." J Virol **78**(4): 1697-1705.

Fukuda, M. and R. Longnecker (2007). "Epstein-Barr virus latent membrane protein 2A mediates transformation through constitutive activation of the Ras/PI3-K/Akt Pathway." J Virol **81**(17): 9299-9306.

Ganem, D. (2007). Kaposi's Sarcoma-associated Herpesvirus. Fields' virology. B. N. Fields, D. M. Knipe and P. M. Howley. Philadelphia, Wolters Kluwer Health/Lippincott Williams & Wilkins.

Gaspar, M., J. S. May, S. Sukla, B. Frederico, M. B. Gill, C. M. Smith, G. T. Belz and P. G. Stevenson (2011). "Murid herpesvirus-4 exploits dendritic cells to infect B cells." PLoS Pathog **7**(11): e1002346.

Geere, H. M., Y. Ligertwood, K. M. Templeton, I. Bennet, B. Gangadharan, S. M. Rhind, A. A. Nash and B. M. Dutia (2006). "The M4 gene of murine gammaherpesvirus 68 modulates latent infection." J Gen Virol **87**(Pt 4): 803-807.

Geng, L. and X. Wang (2015). "Epstein-Barr Virus-associated lymphoproliferative disorders: experimental and clinical developments." Int J Clin Exp Med **8**(9): 14656-14671.

Giffin, L. and B. Damania (2014). "KSHV: pathways to tumorigenesis and persistent infection." Adv Virus Res **88**: 111-159.

Gillet, L., B. Frederico and P. G. Stevenson (2015). "Host entry by gamma-herpesviruses-lessons from animal viruses?" Curr Opin Virol **15**: 34-40.

Gires, O., U. Zimber-Strobl, R. Gonnella, M. Ueffing, G. Marschall, R. Zeidler, D. Pich and W. Hammerschmidt (1997). "Latent membrane protein 1 of Epstein-Barr virus mimics a constitutively active receptor molecule." EMBO J **16**(20): 6131-6140.

Glenn, M., L. Rainbow, F. Aurade, A. Davison and T. F. Schulz (1999). "Identification of a spliced gene from Kaposi's sarcoma-associated herpesvirus encoding a protein with similarities to latent membrane proteins 1 and 2A of Epstein-Barr virus." J Virol **73**(8): 6953-6963.

Godinho-Silva, C., S. Marques, D. Fontinha, H. Veiga-Fernandes, P. G. Stevenson and J. P. Simas (2014). "Defining immune engagement thresholds for in vivo control of virus-driven lymphoproliferation." PLoS Pathog **10**(6): e1004220.

Grakoui, A., S. K. Bromley, C. Sumen, M. M. Davis, A. S. Shaw, P. M. Allen and M. L. Dustin (1999). "The immunological synapse: a molecular machine controlling T cell activation." Science **285**(5425): 221-227.

Gray, L. S., J. R. Gnarra, J. A. Sullivan, G. L. Mandell and V. H. Engelhard (1988). "Spatial and temporal characteristics of the increase in intracellular Ca2+ induced in cytotoxic T lymphocytes by cellular antigen." J Immunol **141**(7): 2424-2430.

Guzman-Rojas, L., J. C. Sims-Mourtada, R. Rangel and H. Martinez-Valdez (2002). "Life and death within germinal centres: a double-edged sword." Immunology **107**(2): 167-175.

Hadinoto, V., M. Shapiro, C. C. Sun and D. A. Thorley-Lawson (2009). "The dynamics of EBV shedding implicate a central role for epithelial cells in amplifying viral output." PLoS Pathog **5**(7): e1000496.

Haller, C., S. Rauch and O. T. Fackler (2007). "HIV-1 Nef employs two distinct mechanisms to modulate Lck subcellular localization and TCR induced actin remodeling." PLoS One **2**(11): e1212.

Haller, C., S. Rauch, N. Michel, S. Hannemann, M. J. Lehmann, O. T. Keppler and O. T. Fackler (2006). "The HIV-1 pathogenicity factor Nef interferes with maturation of stimulatory T-lymphocyte contacts by modulation of N-Wasp activity." J Biol Chem **281**(28): 19618-19630.

Hardy, C. L., S. L. Silins, D. L. Woodland and M. A. Blackman (2000). "Murine gamma-herpesvirus infection causes V(beta)4-specific CDR3-restricted clonal expansions within CD8(+) peripheral blood T lymphocytes." Int Immunol **12**(8): 1193-1204.

Harwood, N. E. and F. D. Batista (2008). "New insights into the early molecular events underlying B cell activation." Immunity **28**(5): 609-619.

Hawkins, J. B., E. Delgado-Eckert, D. A. Thorley-Lawson and M. Shapiro (2013). "The cycle of EBV infection explains persistence, the sizes of the infected cell populations and which come under CTL regulation." PLoS Pathog **9**(10): e1003685.

He, B., N. Raab-Traub, P. Casali and A. Cerutti (2003). "EBV-encoded latent membrane protein 1 cooperates with BAFF/BLyS and APRIL to induce T cell-independent Ig heavy chain class switching." J Immunol **171**(10): 5215-5224.

Heath, E., N. Begue-Pastor, S. Chaganti, D. Croom-Carter, C. Shannon-Lowe, D. Kube, R. Feederle, H. J. Delecluse, A. B. Rickinson and A. I. Bell (2012). "Epstein-Barr virus infection of naive B cells in vitro frequently selects clones with mutated immunoglobulin genotypes: implications for virus biology." PLoS Pathog **8**(5): e1002697.

Herskowitz, J. H., M. A. Jacoby and S. H. Speck (2005). "The murine gammaherpesvirus 68 M2 gene is required for efficient reactivation from latently infected B cells." J Virol **79**(4): 2261-2273.

Hikida, M., S. Casola, N. Takahashi, T. Kaji, T. Takemori, K. Rajewsky and T. Kurosaki (2009). "PLC-gamma2 is essential for formation and maintenance of memory B cells." J Exp Med **206**(3): 681-689.

Hislop, A. D., G. S. Taylor, D. Sauce and A. B. Rickinson (2007). "Cellular responses to viral infection in humans: lessons from Epstein-Barr virus." Annu Rev Immunol **25**: 587-617.

Hladik, W., S. C. Dollard, J. Mermin, A. L. Fowlkes, R. Downing, M. M. Amin, F. Banage, E. Nzaro, P. Kataaha, T. J. Dondero, P. E. Pellett and E. M. Lackritz (2006). "Transmission of human herpesvirus 8 by blood transfusion." N Engl J Med **355**(13): 1331-1338.

Huppa, J. B. and M. M. Davis (2003). "T-cell-antigen recognition and the immunological synapse." Nat Rev Immunol **3**(12): 973-983.

Husain, S. M., E. J. Usherwood, H. Dyson, C. Coleclough, M. A. Coppola, D. L. Woodland, M. A. Blackman, J. P. Stewart and J. T. Sample (1999). "Murine gammaherpesvirus M2 gene is latency-associated and its protein a target for CD8(+) T lymphocytes." Proc Natl Acad Sci U S A **96**(13): 7508-7513.

Huse, M. (2012). "Microtubule-organizing center polarity and the immunological synapse: protein kinase C and beyond." Front Immunol **3**: 235.

Ide, L. M., E. Javazon and H. T. Spencer (2008). "Transduction of murine hematopoietic stem cells and in vivo selection of gene-modified cells." Methods Mol Biol **433**: 213-228.

Ikeda, M., A. Ikeda, L. C. Longan and R. Longnecker (2000). "The Epstein-Barr virus latent membrane protein 2A PY motif recruits WW domain-containing ubiquitin-protein ligases." Virology **268**(1): 178-191.

Incrocci, R., M. McCormack and M. Swanson-Mungerson (2013). "Epstein-Barr virus LMP2A increases IL-10 production in mitogen-stimulated primary B-cells and B-cell lymphomas." J Gen Virol **94**(Pt 5): 1127-1133.

Inoue, H., H. Nojima and H. Okayama (1990). "High efficiency transformation of Escherichia coli with plasmids." Gene **96**(1): 23-28.

Irving, B. A. and A. Weiss (1991). "The cytoplasmic domain of the T cell receptor zeta chain is sufficient to couple to receptor-associated signal transduction pathways." Cell **64**(5): 891-901.

Ishido, S., C. Wang, B. S. Lee, G. B. Cohen and J. U. Jung (2000). "Downregulation of major histocompatibility complex class I molecules by Kaposi's sarcoma-associated herpesvirus K3 and K5 proteins." J Virol **74**(11): 5300-5309.

Jacoby, M. A., H. W. t. Virgin and S. H. Speck (2002). "Disruption of the M2 gene of murine gammaherpesvirus 68 alters splenic latency following intranasal, but not intraperitoneal, inoculation." J Virol **76**(4): 1790-1801.

Kaplan, L. D. (2013). "Human herpesvirus-8: Kaposi sarcoma, multicentric Castleman disease, and primary effusion lymphoma." Hematology Am Soc Hematol Educ Program **2013**: 103-108.

Kaye, K. M., K. M. Izumi and E. Kieff (1993). "Epstein-Barr virus latent membrane protein 1 is essential for B-lymphocyte growth transformation." Proc Natl Acad Sci U S A **90**(19): 9150-9154.

Kedes, D. H., M. Lagunoff, R. Renne and D. Ganem (1997). "Identification of the gene encoding the major latency-associated nuclear antigen of the Kaposi's sarcoma-associated herpesvirus." J Clin Invest **100**(10): 2606-2610.

Kempkes, B. and E. S. Robertson (2015). "Epstein-Barr virus latency: current and future perspectives." Curr Opin Virol **14**: 138-144.

Kieff, E. and A. B. Rickinson (2007). Epstein-Barr virus and its replication. Fields' virology. B. N. Fields, D. M. Knipe and P. M. Howley. Philadelphia, Wolters Kluwer Health/Lippincott Williams & Wilkins.

Kilger, E., A. Kieser, M. Baumann and W. Hammerschmidt (1998). "Epstein-Barr virus-mediated B-cell proliferation is dependent upon latent membrane protein 1, which simulates an activated CD40 receptor." EMBO J **17**(6): 1700-1709.

Kim, I. J., E. Flano, D. L. Woodland, F. E. Lund, T. D. Randall and M. A. Blackman (2003). "Maintenance of long term gamma-herpesvirus B cell latency is dependent on CD40-mediated development of memory B cells." J Immunol **171**(2): 886-892.

Kim, O. J. and J. L. Yates (1993). "Mutants of Epstein-Barr virus with a selective marker disrupting the TP gene transform B cells and replicate normally in culture." J Virol **67**(12): 7634-7640.

Klein, U. and R. Dalla-Favera (2008). "Germinal centres: role in B-cell physiology and malignancy." Nat Rev Immunol **8**(1): 22-33.

Kong, K. F., T. Yokosuka, A. J. Canonigo-Balancio, N. Isakov, T. Saito and A. Altman (2011). "A motif in the V3 domain of the kinase PKC-theta determines its localization in the immunological synapse and functions in T cells via association with CD28." Nat Immunol **12**(11): 1105-1112.

Krummel, M. F. and M. D. Cahalan (2010). "The immunological synapse: a dynamic platform for local signaling." J Clin Immunol **30**(3): 364-372.

Kupfer, A., T. R. Mosmann and H. Kupfer (1991). "Polarized expression of cytokines in cell conjugates of helper T cells and splenic B cells." Proc Natl Acad Sci U S A **88**(3): 775-779.

Kupfer, H., C. R. Monks and A. Kupfer (1994). "Small splenic B cells that bind to antigen-specific T helper (Th) cells and face the site of cytokine production in the Th cells selectively proliferate: immunofluorescence microscopic studies of Th-B antigen-presenting cell interactions." J Exp Med **179**(5): 1507-1515.

Kurth, J., M. L. Hansmann, K. Rajewsky and R. Kuppers (2003). "Epstein-Barr virus-infected B cells expanding in germinal centers of infectious mononucleosis patients do not participate in the germinal center reaction." Proc Natl Acad Sci U S A **100**(8): 4730-4735.

Kurth, J., T. Spieker, J. Wustrow, G. J. Strickler, L. M. Hansmann, K. Rajewsky and R. Kuppers (2000). "EBV-infected B cells in infectious mononucleosis: viral strategies for spreading in the B cell compartment and establishing latency." Immunity **13**(4): 485-495.

Lacoste, V., A. Lavergne, B. de Thoisy, J. F. Pouliquen and A. Gessain (2010). "Genetic diversity and molecular evolution of human and non-human primate Gammaherpesvirinae." Infect Genet Evol **10**(1): 1-13.

Lagunoff, M. and D. Ganem (1997). "The structure and coding organization of the genomic termini of Kaposi's sarcoma-associated herpesvirus." Virology **236**(1): 147-154.

Lagunoff, M., R. Majeti, A. Weiss and D. Ganem (1999). "Deregulated signal transduction by the K1 gene product of Kaposi's sarcoma-associated herpesvirus." Proc Natl Acad Sci U S A **96**(10): 5704-5709.

Le Floc'h, A. and M. Huse (2015). "Molecular mechanisms and functional implications of polarized actin remodeling at the T cell immunological synapse." Cell Mol Life Sci **72**(3): 537-556.

LeBien, T. W. and T. F. Tedder (2008). "B lymphocytes: how they develop and function." Blood **112**(5): 1570-1580.

Lee, B. J., U. H. Koszinowski, S. R. Sarawar and H. Adler (2003). "A gammaherpesvirus G protein-coupled receptor homologue is required for increased viral replication in response to chemokines and efficient reactivation from latency." J Immunol **170**(1): 243-251.

Lee, B. S., X. Alvarez, S. Ishido, A. A. Lackner and J. U. Jung (2000). "Inhibition of intracellular transport of B cell antigen receptor complexes by Kaposi's sarcoma-associated herpesvirus K1." J Exp Med **192**(1): 11-21.

Lee, B. S., S. H. Lee, P. Feng, H. Chang, N. H. Cho and J. U. Jung (2005). "Characterization of the Kaposi's sarcoma-associated herpesvirus K1 signalosome." J Virol **79**(19): 12173-12184.

Lee, H., J. Guo, M. Li, J. K. Choi, M. DeMaria, M. Rosenzweig and J. U. Jung (1998). "Identification of an immunoreceptor tyrosine-based activation motif of K1 transforming protein of Kaposi's sarcoma-associated herpesvirus." Mol Cell Biol **18**(9): 5219-5228.

Lee, H., R. Veazey, K. Williams, M. Li, J. Guo, F. Neipel, B. Fleckenstein, A. Lackner, R. C. Desrosiers and J. U. Jung (1998). "Deregulation of cell growth by the K1 gene of Kaposi's sarcoma-associated herpesvirus." Nat Med **4**(4): 435-440.

Liang, X., C. M. Collins, J. B. Mendel, N. N. Iwakoshi and S. H. Speck (2009). "Gammaherpesvirus-driven plasma cell differentiation regulates virus reactivation from latently infected B lymphocytes." PLoS Pathog **5**(11): e1000677.

Liang, X., M. T. Pickering, N. H. Cho, H. Chang, M. R. Volkert, T. F. Kowalik and J. U. Jung (2006). "Deregulation of DNA damage signal transduction by herpesvirus latency-associated M2." J Virol **80**(12): 5862-5874.

Liang, X., Y. C. Shin, R. E. Means and J. U. Jung (2004). "Inhibition of interferon-mediated antiviral activity by murine gammaherpesvirus 68 latency-associated M2 protein." J Virol **78**(22): 12416-12427.

Lim, S. T., N. Rubin, J. Said and A. M. Levine (2005). "Primary effusion lymphoma: successful treatment with highly active antiretroviral therapy and rituximab." Ann Hematol **84**(8): 551-552.

Lu, M., H. Kawamoto, Y. Katsube, T. Ikawa and Y. Katsura (2002). "The common myelolymphoid progenitor: a key intermediate stage in hemopoiesis generating T and B cells." J Immunol **169**(7): 3519-3525.

Mackett, M., J. P. Stewart, V. P. S. de, M. Chee, S. Efstathiou, A. A. Nash and J. R. Arrand (1997). "Genetic content and preliminary transcriptional analysis of a representative region of murine gammaherpesvirus 68." J Gen Virol **78 (Pt 6)**: 1425-1433.

Macrae, A. I., E. J. Usherwood, S. M. Husain, E. Flano, I. J. Kim, D. L. Woodland, A. A. Nash, M. A. Blackman, J. T. Sample and J. P. Stewart (2003). "Murid herpesvirus 4 strain 68 M2 protein is a B-cell-associated antigen important for latency but not lymphocytosis." J Virol **77**(17): 9700-9709.

Madureira, P. A., P. Matos, I. Soeiro, L. K. Dixon, J. P. Simas and E. W. Lam (2005). "Murine gamma-herpesvirus 68 latency protein M2 binds to Vav signaling proteins and inhibits B-cell receptor-induced cell cycle arrest and apoptosis in WEHI-231 B cells." J Biol Chem **280**(45): 37310-37318.

Marques, S., M. Alenquer, P. G. Stevenson and J. P. Simas (2008). "A single CD8+ T cell epitope sets the long-term latent load of a murid herpesvirus." PLoS Pathog **4**(10): e1000177.

Marques, S., S. Efstathiou, K. G. Smith, M. Haury and J. P. Simas (2003). "Selective gene expression of latent murine gammaherpesvirus 68 in B lymphocytes." J Virol **77**(13): 7308-7318.

Martensson, I. L., N. Almqvist, O. Grimsholm and A. I. Bernardi (2010). "The pre-B cell receptor checkpoint." FEBS Lett **584**(12): 2572-2579.

Martinez-Guzman, D., T. Rickabaugh, T. T. Wu, H. Brown, S. Cole, M. J. Song, L. Tong and R. Sun (2003). "Transcription program of murine gammaherpesvirus 68." J Virol **77**(19): 10488-10503.

May, J. S., N. J. Bennett and P. G. Stevenson (2010). "An in vitro system for studying murid herpesvirus-4 latency and reactivation." PLoS One **5**(6): e11080.

Medvinsky, A., S. Rybtsov and S. Taoudi (2011). "Embryonic origin of the adult hematopoietic system: advances and questions." Development **138**(6): 1017-1031.

Mesri, E. A., M. A. Feitelson and K. Munger (2014). "Human viral oncogenesis: a cancer hallmarks analysis." Cell Host Microbe **15**(3): 266-282.

Metcalf, D. (2007). "On hematopoietic stem cell fate." Immunity **26**(6): 669-673.

Milho, R., B. Frederico, S. Efstathiou and P. G. Stevenson (2012). "A heparan-dependent herpesvirus targets the olfactory neuroepithelium for host entry." PLoS Pathog **8**(11): e1002986.

Milho, R., C. M. Smith, S. Marques, M. Alenquer, J. S. May, L. Gillet, M. Gaspar, S. Efstathiou, J. P. Simas and P. G. Stevenson (2009). "In vivo imaging of murid herpesvirus-4 infection." J Gen Virol **90**(Pt 1): 21-32.

Mills, D. M. and J. C. Cambier (2003). "B lymphocyte activation during cognate interactions with CD4+ T lymphocytes: molecular dynamics and immunologic consequences." Semin Immunol **15**(6): 325-329.

Minamitani, T., T. Yasui, Y. Ma, H. Zhou, D. Okuzaki, C. Y. Tsai, S. Sakakibara, B. E. Gewurz, E. Kieff and H. Kikutani (2015). "Evasion of affinity-based selection in germinal centers by Epstein-Barr virus LMP2A." Proc Natl Acad Sci U S A **112**(37): 11612-11617.

Minhas, V. and C. Wood (2014). "Epidemiology and transmission of Kaposi's sarcoma-associated herpesvirus." Viruses **6**(11): 4178-4194.

Monks, C. R., B. A. Freiberg, H. Kupfer, N. Sciaky and A. Kupfer (1998). "Three-dimensional segregation of supramolecular activation clusters in T cells." Nature **395**(6697): 82-86.

Morrison, S. J., H. D. Hemmati, A. M. Wandycz and I. L. Weissman (1995). "The purification and characterization of fetal liver hematopoietic stem cells." Proc Natl Acad Sci U S A **92**(22): 10302-10306.

Moser, J. M., M. L. Farrell, L. T. Krug, J. W. Upton and S. H. Speck (2006). "A gammaherpesvirus 68 gene 50 null mutant establishes long-term latency in the lung but fails to vaccinate against a wild-type virus challenge." J Virol **80**(3): 1592-1598.

Mullick, A., Y. Xu, R. Warren, M. Koutroumanis, C. Guilbault, S. Broussau, F. Malenfant, L. Bourget, L. Lamoureux, R. Lo, A. W. Caron, A. Pilotte and B. Massie (2006). "The cumate gene-switch: a system for regulated expression in mammalian cells." BMC Biotechnol **6**: 43.

Nador, R. G., E. Cesarman, A. Chadburn, D. B. Dawson, M. Q. Ansari, J. Sald and D. M. Knowles (1996). "Primary effusion lymphoma: a distinct clinicopathologic entity associated with the Kaposi's sarcoma-associated herpes virus." Blood **88**(2): 645-656.

Nash, A. A., B. M. Dutia, J. P. Stewart and A. J. Davison (2001). "Natural history of murine gamma-herpesvirus infection." Philos Trans R Soc Lond B Biol Sci **356**(1408): 569-579.

Niederman, J. C., G. Miller, H. A. Pearson, J. S. Pagano and J. M. Dowaliby (1976). "Infectious mononucleosis. Epstein-Barr-virus shedding in saliva and the oropharynx." N Engl J Med **294**(25): 1355-1359.

Niiro, H. and E. A. Clark (2002). "Regulation of B-cell fate by antigen-receptor signals." Nat Rev Immunol **2**(12): 945-956.

Ning, S., A. M. Hahn, L. E. Huye and J. S. Pagano (2003). "Interferon regulatory factor 7 regulates expression of Epstein-Barr virus latent membrane protein 1: a regulatory circuit." J Virol **77**(17): 9359-9368.

Nutt, S. L. and D. M. Tarlinton (2011). "Germinal center B and follicular helper T cells: siblings, cousins or just good friends?" Nat Immunol **12**(6): 472-477.

Ogawa, M., Y. Matsuzaki, S. Nishikawa, S. Hayashi, T. Kunisada, T. Sudo, T. Kina, H. Nakauchi and S. Nishikawa (1991). "Expression and function of c-kit in hemopoietic progenitor cells." J Exp Med **174**(1): 63-71.

Ogilvie, M. M. (2007). Herpesviruses. Medical microbiology : a guide to microbial infections : pathogenesis, immunity, laboratory diagnosis and control. D. Greenwood. Edinburgh, Churchill Livingstone**:** xvi, 778 p.

Ogura, M., K. Tobinai, K. Hatake, K. Ishizawa, N. Uike, T. Uchida, T. Suzuki, T. Aoki, T. Watanabe, D. Maruyama, M. Yokoyama, T. Takubo, H. Kagehara and T. Matsushima (2014). "Phase I / II study of brentuximab vedotin in Japanese patients with relapsed or refractory CD30-positive Hodgkin's lymphoma or systemic anaplastic large-cell lymphoma." Cancer Sci **105**(7): 840-846.

Ok, C. Y., L. Li and K. H. Young (2015). "EBV-driven B-cell lymphoproliferative disorders: from biology, classification and differential diagnosis to clinical management." Exp Mol Med **47**: e132.

Okada, T., M. J. Miller, I. Parker, M. F. Krummel, M. Neighbors, S. B. Hartley, A. O'Garra, M. D. Cahalan and J. G. Cyster (2005). "Antigen-engaged B cells undergo chemotaxis toward the T zone and form motile conjugates with helper T cells." PLoS Biol **3**(6): e150.

Okkenhaug, K. and B. Vanhaesebroeck (2003). "PI3K in lymphocyte development, differentiation and activation." Nat Rev Immunol **3**(4): 317-330.

Park, J., N. H. Cho, J. K. Choi, P. Feng, J. Choe and J. U. Jung (2003). "Distinct roles of cellular Lck and p80 proteins in herpesvirus saimiri Tip function on lipid rafts." J Virol **77**(16): 9041-9051.

Parry, C. M., J. P. Simas, V. P. Smith, C. A. Stewart, A. C. Minson, S. Efstathiou and A. Alcami (2000). "A broad spectrum secreted chemokine binding protein encoded by a herpesvirus." J Exp Med **191**(3): 573-578.

Persons, D. A., M. G. Mehaffey, M. Kaleko, A. W. Nienhuis and E. F. Vanin (1998). "An improved method for generating retroviral producer clones for vectors lacking a selectable marker gene." Blood Cells Mol Dis **24**(2): 167-182.

Pfeffer, S., A. Sewer, M. Lagos-Quintana, R. Sheridan, C. Sander, F. A. Grasser, L. F. van Dyk, C. K. Ho, S. Shuman, M. Chien, J. J. Russo, J. Ju, G. Randall, B. D.

Lindenbach, C. M. Rice, V. Simon, D. D. Ho, M. Zavolan and T. Tuschl (2005). "Identification of microRNAs of the herpesvirus family." Nat Methods **2**(4): 269-276.

Pierce, S. K. (2002). "Lipid rafts and B-cell activation." Nat Rev Immunol **2**(2): 96-105.

Pires de Miranda, M., M. Alenquer, S. Marques, L. Rodrigues, F. Lopes, X. R. Bustelo and J. P. Simas (2008). "The Gammaherpesvirus m2 protein manipulates the Fyn/Vav pathway through a multidocking mechanism of assembly." PLoS One **3**(2): e1654.

Pires de Miranda, M., F. B. Lopes, C. E. McVey, X. R. Bustelo and J. P. Simas (2013). "Role of Src homology domain binding in signaling complexes assembled by the murid gamma-herpesvirus M2 protein." J Biol Chem **288**(6): 3858-3870.

Polcicova, K., Z. Hrabovska, J. Mistrikova, J. Tomaskova, J. Pastorek, S. Pastorekova and J. Kopacek (2008). "Up-regulation of Murid herpesvirus 4 ORF50 by hypoxia: possible implication for virus reactivation from latency." Virus Res **132**(1-2): 257-262.

Polizzotto, M. N., T. S. Uldrick, D. Hu and R. Yarchoan (2012). "Clinical Manifestations of Kaposi Sarcoma Herpesvirus Lytic Activation: Multicentric Castleman Disease (KSHV-MCD) and the KSHV Inflammatory Cytokine Syndrome." Front Microbiol **3**: 73.

Prakash, O., O. R. Swamy, X. Peng, Z. Y. Tang, L. Li, J. E. Larson, J. C. Cohen, J. Gill, G. Farr, S. Wang and F. Samaniego (2005). "Activation of Src kinase Lyn by the Kaposi sarcoma-associated herpesvirus K1 protein: implications for lymphomagenesis." Blood **105**(10): 3987-3994.

Prakash, O., Z. Y. Tang, X. Peng, R. Coleman, J. Gill, G. Farr and F. Samaniego (2002). "Tumorigenesis and aberrant signaling in transgenic mice expressing the human herpesvirus-8 K1 gene." J Natl Cancer Inst **94**(12): 926-935.

Purushothaman, P., T. Uppal and S. C. Verma (2015). "Molecular biology of KSHV lytic reactivation." Viruses **7**(1): 116-153.

Qi, H., J. L. Cannons, F. Klauschen, P. L. Schwartzberg and R. N. Germain (2008). "SAP-controlled T-B cell interactions underlie germinal centre formation." Nature **455**(7214): 764-769.

Qiu, J., K. Cosmopoulos, M. Pegtel, E. Hopmans, P. Murray, J. Middeldorp, M. Shapiro and D. A. Thorley-Lawson (2011). "A novel persistence associated EBV miRNA expression profile is disrupted in neoplasia." PLoS Pathog **7**(8): e1002193.

Rangaswamy, U. S., B. M. O'Flaherty and S. H. Speck (2014). "Tyrosine 129 of the murine gammaherpesvirus M2 protein is critical for M2 function in vivo." PLoS One **9**(8): e105197.

Rangaswamy, U. S. and S. H. Speck (2014). "Murine gammaherpesvirus M2 protein induction of IRF4 via the NFAT pathway leads to IL-10 expression in B cells." PLoS Pathog **10**(1): e1003858.

Rebel, V. I., C. L. Miller, C. J. Eaves and P. M. Lansdorp (1996). "The repopulation potential of fetal liver hematopoietic stem cells in mice exceeds that of their liver adult bone marrow counterparts." Blood **87**(8): 3500-3507.

Rechsteiner, M. P., C. Berger, L. Zauner, J. A. Sigrist, M. Weber, R. Longnecker, M. Bernasconi and D. Nadal (2008). "Latent membrane protein 2B regulates susceptibility to induction of lytic Epstein-Barr virus infection." J Virol **82**(4): 1739-1747.

Renne, R., W. Zhong, B. Herndier, M. McGrath, N. Abbey, D. Kedes and D. Ganem (1996). "Lytic growth of Kaposi's sarcoma-associated herpesvirus (human herpesvirus 8) in culture." Nat Med **2**(3): 342-346.

Reth, M. (1989). "Antigen receptor tail clue." Nature **338**(6214): 383-384.

Rickinson, A. B. and E. Kieff (2007). Epstein-Barr Virus. Fields' virology. B. N. Fields, D. M. Knipe and P. M. Howley. Philadelphia, Wolters Kluwer Health/Lippincott Williams & Wilkins.

Rochford, R., M. L. Lutzke, R. S. Alfinito, A. Clavo and R. D. Cardin (2001). "Kinetics of murine gammaherpesvirus 68 gene expression following infection of murine cells in culture and in mice." J Virol **75**(11): 4955-4963.

Rodrigues, L., J. Filipe, M. P. Seldon, L. Fonseca, J. Anrather, M. P. Soares and J. P. Simas (2009). "Termination of NF-kappaB activity through a gammaherpesvirus protein that assembles an EC5S ubiquitin-ligase." EMBO J **28**(9): 1283-1295.

Rodrigues, L., M. Pires de Miranda, M. J. Caloca, X. R. Bustelo and J. P. Simas (2006). "Activation of Vav by the gammaherpesvirus M2 protein contributes to the establishment of viral latency in B lymphocytes." J Virol **80**(12): 6123-6135.

Rodrigues, L., N. Popov, K. M. Kaye and J. P. Simas (2013). "Stabilization of Myc through heterotypic poly-ubiquitination by mLANA is critical for gamma-herpesvirus lymphoproliferation." PLoS Pathog **9**(8): e1003554.

Roizman, B. and P. E. Pellett (2007). The Family Herpesviridae: A Brief Introduction. Fields' virology. B. N. Fields, D. M. Knipe and P. M. Howley. Philadelphia, Wolters Kluwer Health/Lippincott Williams & Wilkins.

Rooney, C. M., C. A. Smith, C. Y. Ng, S. K. Loftin, J. W. Sixbey, Y. Gan, D. K. Srivastava, L. C. Bowman, R. A. Krance, M. K. Brenner and H. E. Heslop (1998). "Infusion of cytotoxic T cells for the prevention and treatment of Epstein-Barr virus-induced lymphoma in allogeneic transplant recipients." Blood **92**(5): 1549-1555.

Roughan, J. E. and D. A. Thorley-Lawson (2009). "The intersection of Epstein-Barr virus with the germinal center." J Virol **83**(8): 3968-3976.

Rovedo, M. and R. Longnecker (2007). "Epstein-barr virus latent membrane protein 2B (LMP2B) modulates LMP2A activity." J Virol **81**(1): 84-94.

Rovedo, M. and R. Longnecker (2008). "Epstein-Barr virus latent membrane protein 2A preferentially signals through the Src family kinase Lyn." J Virol **82**(17): 8520-8528.

Sadler, R., L. Wu, B. Forghani, R. Renne, W. Zhong, B. Herndier and D. Ganem (1999). "A complex translational program generates multiple novel proteins from the latently expressed kaposin (K12) locus of Kaposi's sarcoma-associated herpesvirus." J Virol **73**(7): 5722-5730.

Sangster, M. Y., D. J. Topham, S. D'Costa, R. D. Cardin, T. N. Marion, L. K. Myers and P. C. Doherty (2000). "Analysis of the virus-specific and nonspecific B cell response to a persistent B-lymphotropic gammaherpesvirus." J Immunol **164**(4): 1820-1828.

Saxena, S. K., G. Shrivastava, S. Tiwari, M. A. Swamy and M. P. Nair (2012). "Modulation of HIV pathogenesis and T-cell signaling by HIV-1 Nef." Future Virol **7**(6): 609-620.

Sayos, J., C. Wu, M. Morra, N. Wang, X. Zhang, D. Allen, S. van Schaik, L. Notarangelo, R. Geha, M. G. Roncarolo, H. Oettgen, J. E. De Vries, G. Aversa and C. Terhorst (1998). "The X-linked lymphoproliferative-disease gene product SAP regulates signals induced through the co-receptor SLAM." Nature **395**(6701): 462-469.

Schindelin, J., I. Arganda-Carreras, E. Frise, V. Kaynig, M. Longair, T. Pietzsch, S. Preibisch, C. Rueden, S. Saalfeld, B. Schmid, J. Y. Tinevez, D. J. White, V. Hartenstein, K. Eliceiri, P. Tomancak and A. Cardona (2012). "Fiji: an open-source platform for biological-image analysis." Nat Methods **9**(7): 676-682.

Scholle, F., K. M. Bendt and N. Raab-Traub (2000). "Epstein-Barr virus LMP2A transforms epithelial cells, inhibits cell differentiation, and activates Akt." J Virol **74**(22): 10681-10689.

Schulz, T. F. and E. Cesarman (2015). "Kaposi Sarcoma-associated Herpesvirus: mechanisms of oncogenesis." Curr Opin Virol **14**: 116-128.

Schwickert, T. A., G. D. Victora, D. R. Fooksman, A. O. Kamphorst, M. R. Mugnier, A. D. Gitlin, M. L. Dustin and M. C. Nussenzweig (2011). "A dynamic T cell-limited checkpoint regulates affinity-dependent B cell entry into the germinal center." J Exp Med **208**(6): 1243-1252.

Seto, E., A. Moosmann, S. Gromminger, N. Walz, A. Grundhoff and W. Hammerschmidt (2010). "Micro RNAs of Epstein-Barr virus promote cell cycle progression and prevent apoptosis of primary human B cells." PLoS Pathog **6**(8): e1001063.

Shannon-Lowe, C. and M. Rowe (2014). "Epstein Barr virus entry; kissing and conjugation." Curr Opin Virol **4**: 78-84.

Sharp, T. V., H. W. Wang, A. Koumi, D. Hollyman, Y. Endo, H. Ye, M. Q. Du and C. Boshoff (2002). "K15 protein of Kaposi's sarcoma-associated herpesvirus is latently expressed and binds to HAX-1, a protein with antiapoptotic function." J Virol **76**(2): 802-816.

Siegel, A. M., J. H. Herskowitz and S. H. Speck (2008). "The MHV68 M2 protein drives IL-10 dependent B cell proliferation and differentiation." PLoS Pathog **4**(4): e1000039.

Simas, J. P. and S. Efstathiou (1998). "Murine gammaherpesvirus 68: a model for the study of gammaherpesvirus pathogenesis." Trends Microbiol **6**(7): 276-282.

Simas, J. P., S. Marques, A. Bridgeman, S. Efstathiou and H. Adler (2004). "The M2 gene product of murine gammaherpesvirus 68 is required for efficient colonization of splenic follicles but is not necessary for expansion of latently infected germinal centre B cells." J Gen Virol **85**(Pt 10): 2789-2797.

Simas, J. P., D. Swann, R. Bowden and S. Efstathiou (1999). "Analysis of murine gammaherpesvirus-68 transcription during lytic and latent infection." J Gen Virol **80 (Pt 1)**: 75-82.

Sousa-Squiavinato, A. C., R. N. Silvestre and D. Elgui De Oliveira (2015). "Biology and oncogenicity of the Kaposi sarcoma herpesvirus K1 protein." Rev Med Virol **25**(5): 273-285.

Souza, T. A., B. D. Stollar, J. L. Sullivan, K. Luzuriaga and D. A. Thorley-Lawson (2005). "Peripheral B cells latently infected with Epstein-Barr virus display molecular hallmarks of classical antigen-selected memory B cells." Proc Natl Acad Sci U S A **102**(50): 18093-18098.

Souza, T. A., B. D. Stollar, J. L. Sullivan, K. Luzuriaga and D. A. Thorley-Lawson (2007). "Influence of EBV on the peripheral blood memory B cell compartment." J Immunol **179**(5): 3153-3160.

Speck, S. H. and D. Ganem (2010). "Viral latency and its regulation: lessons from the gamma-herpesviruses." Cell Host Microbe **8**(1): 100-115.

Stevenson, P. G. and P. C. Doherty (1998). "Kinetic analysis of the specific host response to a murine gammaherpesvirus." J Virol **72**(2): 943-949.

Stevenson, P. G. and P. C. Doherty (1999). "Non-antigen-specific B-cell activation following murine gammaherpesvirus infection is CD4 independent in vitro but CD4 dependent in vivo." J Virol **73**(2): 1075-1079.

Stevenson, P. G. and S. Efstathiou (2005). "Immune mechanisms in murine gammaherpesvirus-68 infection." Viral Immunol **18**(3): 445-456.

Stevenson, P. G., S. Efstathiou, P. C. Doherty and P. J. Lehner (2000). "Inhibition of MHC class I-restricted antigen presentation by gamma 2-herpesviruses." Proc Natl Acad Sci U S A **97**(15): 8455-8460.

Sunil-Chandra, N. P., S. Efstathiou, J. Arno and A. A. Nash (1992). "Virological and pathological features of mice infected with murine gamma-herpesvirus 68." J Gen Virol **73 (Pt 9)**: 2347-2356.

Sunil-Chandra, N. P., S. Efstathiou and A. A. Nash (1993). "Interactions of murine gammaherpesvirus 68 with B and T cell lines." Virology **193**(2): 825-833.

Svobodova, J., D. Blaskovic and J. Mistrikova (1982). "Growth characteristics of herpesviruses isolated from free living small rodents." Acta Virol **26**(4): 256-263.

Swaminathan, S. (2008). "Noncoding RNAs produced by oncogenic human herpesviruses." J Cell Physiol **216**(2): 321-326.

Taylor, J. J., K. A. Pape and M. K. Jenkins (2012). "A germinal center-independent pathway generates unswitched memory B cells early in the primary response." J Exp Med **209**(3): 597-606.

Thompson, M. P. and R. Kurzrock (2004). "Epstein-Barr virus and cancer." Clin Cancer Res **10**(3): 803-821.

Thorley-Lawson, D. A. (2001). "Epstein-Barr virus: exploiting the immune system." Nat Rev Immunol **1**(1): 75-82.

Thorley-Lawson, D. A. (2005). "EBV the prototypical human tumor virus--just how bad is it?" J Allergy Clin Immunol **116**(2): 251-261; quiz 262.

Thorley-Lawson, D. A., K. A. Duca and M. Shapiro (2008). "Epstein-Barr virus: a paradigm for persistent infection - for real and in virtual reality." Trends Immunol **29**(4): 195-201.

Thorley-Lawson, D. A. and A. Gross (2004). "Persistence of the Epstein-Barr virus and the origins of associated lymphomas." N Engl J Med **350**(13): 1328-1337.

Thorley-Lawson, D. A., J. B. Hawkins, S. I. Tracy and M. Shapiro (2013). "The pathogenesis of Epstein-Barr virus persistent infection." Curr Opin Virol **3**(3): 227-232.

Thoulouze, M. I., N. Sol-Foulon, F. Blanchet, A. Dautry-Varsat, O. Schwartz and A. Alcover (2006). "Human immunodeficiency virus type-1 infection impairs the formation of the immunological synapse." Immunity **24**(5): 547-561.

Tomlinson, C. C. and B. Damania (2008). "Critical role for endocytosis in the regulation of signaling by the Kaposi's sarcoma-associated herpesvirus K1 protein." J Virol **82**(13): 6514-6523.

Tracy, S. I., K. Kakalacheva, J. D. Lunemann, K. Luzuriaga, J. Middeldorp and D. A. Thorley-Lawson (2012). "Persistence of Epstein-Barr virus in self-reactive memory B cells." J Virol **86**(22): 12330-12340.

Trautmann, A. and S. Valitutti (2003). "The diversity of immunological synapses." Curr Opin Immunol **15**(3): 249-254.

Tripp, R. A., A. M. Hamilton-Easton, R. D. Cardin, P. Nguyen, F. G. Behm, D. L. Woodland, P. C. Doherty and M. A. Blackman (1997). "Pathogenesis of an infectious mononucleosis-like disease induced by a murine gamma-herpesvirus: role for a viral superantigen?" J Exp Med **185**(9): 1641-1650.

Tsai, Y. H., M. F. Wu, Y. H. Wu, S. J. Chang, S. F. Lin, T. V. Sharp and H. W. Wang (2009). "The M type K15 protein of Kaposi's sarcoma-associated herpesvirus regulates microRNA expression via its SH2-binding motif to induce cell migration and invasion." J Virol **83**(2): 622-632.

Turner, M. and D. D. Billadeau (2002). "VAV proteins as signal integrators for multi-subunit immune-recognition receptors." Nat Rev Immunol **2**(7): 476-486.

Uchida, J., T. Yasui, Y. Takaoka-Shichijo, M. Muraoka, W. Kulwichit, N. Raab-Traub and H. Kikutani (1999). "Mimicry of CD40 signals by Epstein-Barr virus LMP1 in B lymphocyte responses." Science **286**(5438): 300-303.

Uppal, T., S. Banerjee, Z. Sun, S. C. Verma and E. S. Robertson (2014). "KSHV LANA--the master regulator of KSHV latency." Viruses **6**(12): 4961-4998.

Usherwood, E. J., A. J. Ross, D. J. Allen and A. A. Nash (1996). "Murine gammaherpesvirus-induced splenomegaly: a critical role for CD4 T cells." J Gen Virol **77 (Pt 4)**: 627-630.

Usherwood, E. J., J. P. Stewart and A. A. Nash (1996). "Characterization of tumor cell lines derived from murine gammaherpesvirus-68-infected mice." J Virol **70**(9): 6516-6518.

Valitutti, S. and M. Dessing (2000). "Measurement of calcium mobilization responses in killer cell/target conjugates by FACS analysis." Methods Mol Biol **121**: 305-311.

Valitutti, S., M. Dessing and A. Lanzavecchia (1993). "Role of cAMP in regulating cytotoxic T lymphocyte adhesion and motility." Eur J Immunol **23**(4): 790-795.

Van Dross, R., S. Yao, S. Asad, G. Westlake, D. J. Mays, L. Barquero, S. Duell, J. A. Pietenpol and P. J. Browning (2005). "Constitutively active K-cyclin/cdk6 kinase in Kaposi sarcoma-associated herpesvirus-infected cells." J Natl Cancer Inst **97**(9): 656-666.

Varma, R., G. Campi, T. Yokosuka, T. Saito and M. L. Dustin (2006). "T cell receptor-proximal signals are sustained in peripheral microclusters and terminated in the central supramolecular activation cluster." Immunity **25**(1): 117-127.

Vereide, D. T., E. Seto, Y. F. Chiu, M. Hayes, T. Tagawa, A. Grundhoff, W. Hammerschmidt and B. Sugden (2014). "Epstein-Barr virus maintains lymphomas via its miRNAs." Oncogene **33**(10): 1258-1264.

Victora, G. D. and L. Mesin (2014). "Clonal and cellular dynamics in germinal centers." Curr Opin Immunol **28**: 90-96.

Virgin, H. W. t., P. Latreille, P. Wamsley, K. Hallsworth, K. E. Weck, A. J. Dal Canto and S. H. Speck (1997). "Complete sequence and genomic analysis of murine gammaherpesvirus 68." J Virol **71**(8): 5894-5904.

Virgin, H. W. t., R. M. Presti, X. Y. Li, C. Liu and S. H. Speck (1999). "Three distinct regions of the murine gammaherpesvirus 68 genome are transcriptionally active in latently infected mice." J Virol **73**(3): 2321-2332.

Wakeling, M. N., D. J. Roy, A. A. Nash and J. P. Stewart (2001). "Characterization of the murine gammaherpesvirus 68 ORF74 product: a novel oncogenic G protein-coupled receptor." J Gen Virol **82**(Pt 5): 1187-1197.

Wang, D., D. Liebowitz and E. Kieff (1985). "An EBV membrane protein expressed in immortalized lymphocytes transforms established rodent cells." Cell **43**(3 Pt 2): 831-840.

Wang, G. H., T. L. Garvey and J. I. Cohen (1999). "The murine gammaherpesvirus-68 M11 protein inhibits Fas- and TNF-induced apoptosis." J Gen Virol **80 (Pt 10)**: 2737-2740.

Warncke, M., B. Vogt, J. Ulrich, M. D. von Laer, W. Beyer, H. Klump, B. Micheel and A. Sheriff (2004). "Efficient in vitro transduction of naive murine B cells with lentiviral vectors." Biochem Biophys Res Commun **318**(3): 673-679.

Waterstrat, A., Y. Liang, C. F. Swiderski, B. J. Shelton and G. Van Zant (2010). "Congenic interval of CD45/Ly-5 congenic mice contains multiple genes that may influence hematopoietic stem cell engraftment." Blood **115**(2): 408-417.

Weck, K. E., M. L. Barkon, L. I. Yoo, S. H. Speck and H. I. Virgin (1996). "Mature B cells are required for acute splenic infection, but not for establishment of latency, by murine gammaherpesvirus 68." J Virol **70**(10): 6775-6780.

Werner, M., E. Hobeika and H. Jumaa (2010). "Role of PI3K in the generation and survival of B cells." Immunol Rev **237**(1): 55-71.

Willer, D. O. and S. H. Speck (2003). "Long-term latent murine Gammaherpesvirus 68 infection is preferentially found within the surface immunoglobulin D-negative subset of splenic B cells in vivo." J Virol **77**(15): 8310-8321.

Yankee, T. M. and E. A. Clark (2000). "Signaling through the B cell antigen receptor in developing B cells." Rev Immunogenet **2**(2): 185-203.

Yasui, T., M. Luftig, V. Soni and E. Kieff (2004). "Latent infection membrane protein transmembrane FWLY is critical for intermolecular interaction, raft localization, and signaling." Proc Natl Acad Sci U S A **101**(1): 278-283.

Yates, J. L., N. Warren and B. Sugden (1985). "Stable replication of plasmids derived from Epstein-Barr virus in various mammalian cells." Nature **313**(6005): 812-815.

Ye, F. C., F. C. Zhou, J. P. Xie, T. Kang, W. Greene, K. Kuhne, X. F. Lei, Q. H. Li and S. J. Gao (2008). "Kaposi's sarcoma-associated herpesvirus latent gene vFLIP inhibits viral lytic replication through NF-kappaB-mediated suppression of the AP-1 pathway: a novel mechanism of virus control of latency." J Virol **82**(9): 4235-4249.

Yokosuka, T., W. Kobayashi, K. Sakata-Sogawa, M. Takamatsu, A. Hashimoto-Tane, M. L. Dustin, M. Tokunaga and T. Saito (2008). "Spatiotemporal regulation of T cell costimulation by TCR-CD28 microclusters and protein kinase C theta translocation." Immunity **29**(4): 589-601.

Young, L. S. and P. G. Murray (2003). "Epstein-Barr virus and oncogenesis: from latent genes to tumours." Oncogene **22**(33): 5108-5121.

Yuseff, M. I., P. Pierobon, A. Reversat and A. M. Lennon-Dumenil (2013). "How B cells capture, process and present antigens: a crucial role for cell polarity." Nat Rev Immunol **13**(7): 475-486.

Zhang, Y., M. Meyer-Hermann, L. A. George, M. T. Figge, M. Khan, M. Goodall, S. P. Young, A. Reynolds, F. Falciani, A. Waisman, C. A. Notley, M. R. Ehrenstein, M. Kosco-Vilbois and K. M. Toellner (2013). "Germinal center B cells govern their own fate via antibody feedback." J Exp Med **210**(3): 457-464.

Zhu, J. Y., M. Strehle, A. Frohn, E. Kremmer, K. P. Hofig, G. Meister and H. Adler (2010). "Identification and analysis of expression of novel microRNAs of murine gammaherpesvirus 68." J Virol **84**(19): 10266-10275.

Zou, P., J. Kawada, L. Pesnicak and J. I. Cohen (2007). "Bortezomib induces apoptosis of Epstein-Barr virus (EBV)-transformed B cells and prolongs survival of mice inoculated with EBV-transformed B cells." J Virol **81**(18): 10029-10036.

APPENDIX 1

PLOS | ONE

RESEARCH ARTICLE

Murid Gammaherpesvirus Latency-Associated Protein M2 Promotes the Formation of Conjugates between Transformed B Lymphoma Cells and T Helper Cells

Diana Fontinha[☯], **Filipa B. Lopes**[☯], **Sofia Marques, J. Pedro Simas***

Instituto de Medicina Molecular e Instituto de Microbiologia, Faculdade de Medicina, Universidade de Lisboa, Lisboa, Portugal

☯ These authors contributed equally to this work.
* psimas@medicina.ulisboa.pt

Citation: Fontinha D, Lopes FB, Marques S, Simas JP (2015) Murid Gammaherpesvirus Latency-Associated Protein M2 Promotes the Formation of Conjugates between Transformed B Lymphoma Cells and T Helper Cells. PLoS ONE 10(11): e0142540. doi:10.1371/journal.pone.0142540

Editor: Ari Waisman, University Medical Center of the Johannes Gutenberg University of Mainz, GERMANY

Received: October 1, 2015

Accepted: October 22, 2015

Published: November 6, 2015

Data Availability Statement: All relevant data are within the paper and its Supporting Information files.

Funding: The authors received funding for this work from Fundação para a Ciência e a Tecnologia (PTDC/SAU-MII/099314/2008).

Competing Interests: The authors have declared that no competing interests exist.

Abstract

Establishment of persistent infection in memory B cells by murid herpesvirus-4 (MuHV-4) depends on the proliferation of latently infected germinal center B cells, for which T cell help is essential. Whether the virus is capable of modulating B-T helper cell interaction for its own benefit is still unknown. Here, we investigate if the MuHV-4 latency associated M2 protein, which assembles multiprotein complexes with B cell signaling proteins, plays a role. We observed that M2 led to the upregulation of adhesion and co-stimulatory molecules in transduced B cell lines. In an MHC-II restricted OVA peptide-specific system, M2 polarized to the B-T helper contact zone. Furthermore, it promoted B cell polarization, as demonstrated by the increased proximity of the B cell microtubule organizing center to the interface. Consistent with these data, M2 promoted the formation of B-T helper cell conjugates. In an in vitro competition assay, this translated into a competitive advantage, as T cells preferentially conjugated with M2-expressing B cells. However, expression of M2 alone in B cells was not sufficient to lead to T cell activation, as it only occurred in the presence of specific peptide. Taken together, these findings support that M2 promotes the formation of B-T helper cell conjugates. In an in vivo context this may confer a competitive advantage to the infected B cell in acquisition of T cell help and initiation of a germinal center reaction, hence host colonization.

Introduction

Gammaherpesviruses establish life-long persistent infections and are highly prevalent in the human population. Latent infection of circulating memory B cells is crucial to persistence and hence disease ontogeny. To access the memory B cell compartment gammaherpesviruses, such as Epstein-Barr virus (EBV) and murid herpesvirus-4 (MuHV-4), take advantage of germinal

center (GC) reactions [1–7]. In the case of MuHV-4, at the latency peak (14dpi), it has been estimated that 70% of the infected B cells have a GC phenotype [8], which suggests some modulation of this route by the virus.

T cell help is critical for the initiation of a GC reaction in T cell-dependent immune responses. Before engaging in a cognate interaction with a B cell that will lead to its activation, proliferation and establishment of a GC [9], T helper (T_H) cells scan for the highest affinity with particular antigen-presenting cells (APC). Such transient interactions occur in the border area between follicles and T cell zones and are mediated by adhesion molecules, resulting in the formation of B-T_H cell conjugates. Upon peptide recognition, the formation of an organized signaling structure, the immunological synapse (IS), takes place [10]. This process has been shown to be highly dynamic as T cells can interact with several APCs simultaneously, selectively polarizing towards the strongest stimulus [11].

MuHV-4 course of infection in the spleen has been recently characterized [12]. The virus first infects macrophages that provide access to marginal zone B cells. These, in turn, relocate to the white pulp where the virus is transferred to follicular dendritic cells (DCs). MuHV-4 then reaches follicular B cells, which are able to participate in a GC reaction. At this pre-GC stage, the ability of the infected follicular B cells to attract T cell help would be a major advantage for these viruses. In fact, importance of T cell help is reflected in studies that show defects in in vivo B cell activation [13] or demonstrate lower latency levels in the absence of $CD4^+$ T cells [14, 15] or T follicular helper cells (T_{FH}) [16].

To investigate if MuHV-4 had the ability to modulate B-T_H cell interactions, the M2 protein was chosen as a potential candidate. It is one of the few viral proteins that is expressed during the latency phase [17]. It is a putative functional homologue of the transmembrane proteins LMP1 and LMP2A encoded by EBV, and K1 and K15 encoded by Kaposi sarcoma-associated herpesvirus (KSHV), which either mimic or interfere with BCR signaling [18–20]. Contrarily to these proteins, M2 is a soluble cytoplasmic protein. Its expression has been demonstrated in B cells [17] where it localizes to juxtamembranar areas of the cell, a process that relies on a C-terminal proline-rich SH3 binding region of M2 and its interaction with Src family kinases [21–23]. It contains two phosphosites (tyrosine residues Tyr^{120} and Tyr^{129}), that are constitutively phosphorylated by Src family kinases [18, 19], that form an unconventional immunoreceptor tyrosine activation motif (ITAM). This ITAM is implicated in M2 ability to work as a modulator protein, coordinating the assembly of multiprotein complexes with cell signaling proteins, namely NCK1, Vav1, PLCγ2, the tyrosine phosphatase SHP2 and the p85α subunit of PI3K [21]. Therefore, just like its putative functional homologues, M2 mediates the assembly of specific signalosomes. On the one hand, M2 interaction with the Fyn/Vav pathway leads to the activation of Vav1 [18, 19]. Furthermore, M2 drives tyrosine phosphorylation of PLCγ2. On the other hand, M2 expression leads to inhibition of AKT activation upon BCR stimulation. M2 is also known to drive IL-10 dependent B cell proliferation and differentiation [24]. IL-10 production increase upon expression of M2 in B cells is a consequence of the induction of IRF4 via the NFAT pathway [25]. In vivo, M2 is important for latency establishment and efficient proliferation of infected GC B cells [22, 26, 27]. Infection of mice with a virus encoding the M2Y mutant (designated vM2Y, with Tyr^{120} and Tyr^{129} residues mutated to phenylalanine) results in a delay in latency establishment [18]. More recently, it has been shown that in vivo only Tyr^{129} is critical for reactivation from latency and plasma cell differentiation [28].

Here, we investigated if the latency associated protein M2 encoded by MuHV-4 is able to modulate B-T_H cell interaction. We observed that B cells expressing M2 are more prone to recruit T cell help, promoting the formation of B-T_H cell conjugates. Furthermore, we showed that this function was dependent on the ITAM of M2, hence dependent on the ability to assemble multiprotein complexes with B cell signaling proteins. Overall, in vivo, this may confer a

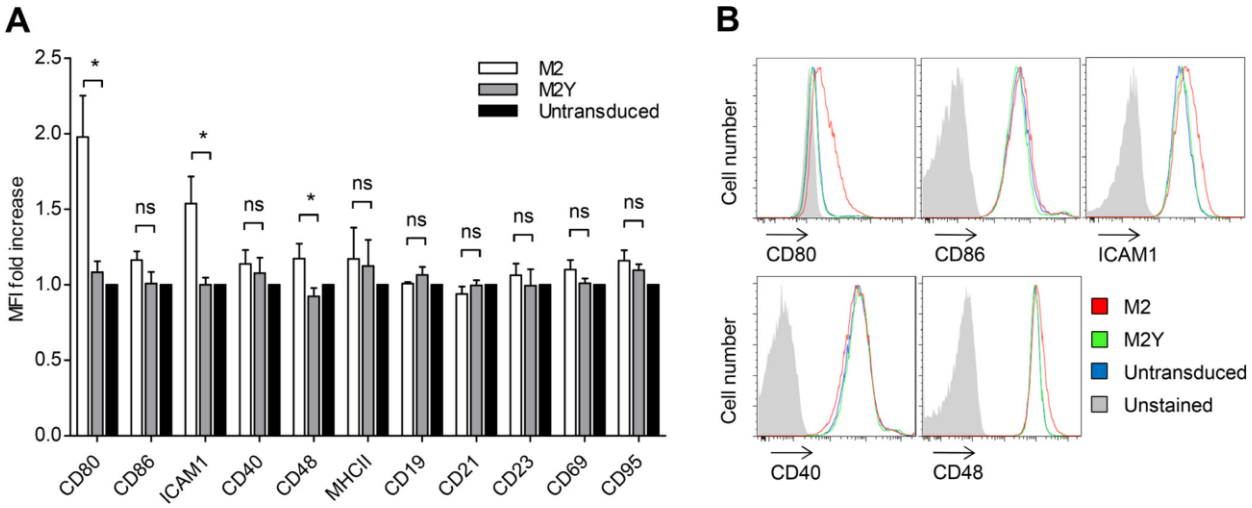

Fig 1. M2 expression leads to the upregulation of adhesion and co-stimulatory molecules in B cells. (A) Fold increase of the mean fluorescence intensities (MFI) of several surface molecules, relative to untransduced A20 B cells. A20 B cells (black bars) and A20 B cells stably expressing M2 (open bars) or M2Y (grey bars) were stained with fluorescently labelled antibodies and the surface expression of the indicated molecules was analyzed on a LSR Fortessa flow cytometer. Bars represent the mean of three independent experiments. Error bars represent standard error of the mean. Statistical significance was evaluated using a one-tailed Students t-test. (B) Representative FACS histogram plots for the indicated surface molecules.

doi:10.1371/journal.pone.0142540.g001

competitive advantage to the infected B cell in the recruitment of T cell help and initiation of a GC reaction, therefore host colonization.

Results

Expression of the Latently Associated Protein M2 Leads to the Upregulation of Adhesion and Co-Stimulatory Molecules in B Cells

In order to assess if M2 plays a role in B-T_H cell interactions we started by analyzing the influence of the viral protein on the levels of selected B cell surface molecules, some of which have been shown to be involved in IS formation [10, 29, 30]. In parallel, we used an M2 mutant protein (M2Y), which has the tyrosine residues 120 and 129 mutated to phenylalanines. These residues are not phosphorylated and the ability to assemble multiprotein complexes with B cell signaling proteins, and its downstream effects, are impaired [18, 19, 21]. A20 B cells stably expressing M2 or the M2Y mutant were stained for the indicated markers and analyzed by flow cytometry (Fig 1). Untransduced A20 B cells were used as a negative control. Fig 1A represents the mean fluorescence intensity (MFI) fold change of M2 or M2Y relative to that of the control. Levels of CD80, a co-stimulatory molecule [10, 29, 30], was two-fold higher in M2-expressing B cells than in the control. The cell adhesion molecules ICAM1 and CD48 [10, 29, 30] were 1.5- and 1.2-fold upregulated, respectively. These differences can be observed as a shift in fluorescence intensity in the representative FACS histograms (Fig 1B). This upregulation was specific as M2 did not significantly alter the levels of CD86, CD40, MHCII, CD19, CD21, CD23, CD69, and CD95. M2Y-expressing B cells did not show increased levels of any of these molecules, corroborating the use of M2Y as a negative control. Upregulation of CD80 and ICAM-1, as well as of CD86, was also observed in M2-expressing independent B cell lines (S1 Fig).

These results show that expression of M2 upregulates B cell co-stimulatory and adhesion molecules that participate in the formation of an IS. This function is dependent on tyrosine

phosphorylation at the ITAM, hence related to the ability of M2 to assemble multiprotein complexes with B cell signaling proteins.

M2 Polarizes to the B-T_H Contact Zone and Increases B Cell MTOC Polarization

During T cell scanning that takes place in the border area between follicles and T cell zones, B and T_H cells interact with each other forming conjugates. Upon cognate interaction and IS formation, cells undergo morphological and cytoskeletal changes, which result in the polarization of the microtubule organizing center (MTOC) [31–33], cellular organelles and signaling machinery to the contact zone [30, 34]. This polarization is reciprocal, as B cells also have the ability to polarize their MTOC and endocytic/exocytic compartments to the interface [35].

To address the effect of M2 expression in the formation of B-T_H cell conjugates, we used a MHC-II restricted cell system in which mouse A20 B cells, pulsed with ovalbumin peptide (OVAp), were conjugated with primary mouse OVAp-specific TCR-transgenic $CD4^+$ T cells purified from Balb/c DO11.10 mice [36]. We first assessed M2 cellular distribution in the context of B-T_H cell interaction by expressing M2 and M2Y eGFP-tagged proteins. Furthermore, to address B cell polarization, we measured the B cell MTOC distance to the contact zone (Fig 2). To that end, mouse A20 B cells transiently expressing M2-eGFP, M2Y-eGFP or eGFP (mock) were pulsed, or not, with 10μM of OVAp and incubated with T_H cells for 15min. Cells were then fixed and stained for pTyr (blue), and α-tubulin (red) (Fig 2A). Using this system we observed that M2 polarizes to the contact zone as visualized by the accumulation of GFP signal at the interface. This polarization is dependent on the integrity of the ITAM as M2Y remained localized in juxtamembrane areas of the cell (Fig 2A). Next, the distance of the B cell MTOC to the contact zone was quantified (Fig 2B). M2 expression decreased B cell MTOC distance to the contact zone in 3.3μm compared to the mock control, i.e. it increased its polarization toward the conjugating T_H cell. Nonetheless, this polarization was incomplete, as it has been previously described for B cells [35]. M2Y also caused a statistically significant difference compared to the mock control. However, this was approximately three times less than the difference promoted by the wild type protein.

We conclude that M2 polarizes to the B-T_H cellular interface in a MHC class II-restricted OVAp-specific manner, a process that is dependent on the protein phosphosites. Results also show that M2 promotes B cell polarization, as its expression increased MTOC proximity to the contact zone.

M2 Promotes the Formation of B-T_H Cell Conjugates

B and T_H cells interact with each other forming conjugates, a process that is mediated by adhesion molecules. Given that M2-expressing B cells showed increased levels of such molecules, we investigated if M2 had an impact in B-T_H cell conjugate formation (Fig 3). We used the MHC class II-restricted OVAp-specific system described above. Mouse A20 B cell lines, stably expressing M2 or M2Y, were loaded with CMFDA live dye and pulsed with increasing concentrations of OVAp. These were then incubated with T_H cells (loaded with DDAO live dye), in a 2:1 ratio, for 1, 3, 5 or 30 minutes. Conjugate formation was next assessed by flow cytometry, based on the percentage of $CMFDA^+DDAO^+$ events in the total $DDAO^+$ population. Fig 3A shows the fold increase of the percentage of T cells conjugating with M2-expressing B cells (black circles), relative to the percentage of T cells conjugating with M2Y-expressing B cells (grey squares), against increasing incubation times. In the absence of peptide or with low concentrations of peptide, such as 0.001μM, conjugate formation with M2-expressing B cells increased with incubation time reaching a three-fold plateau that was maintained after 30

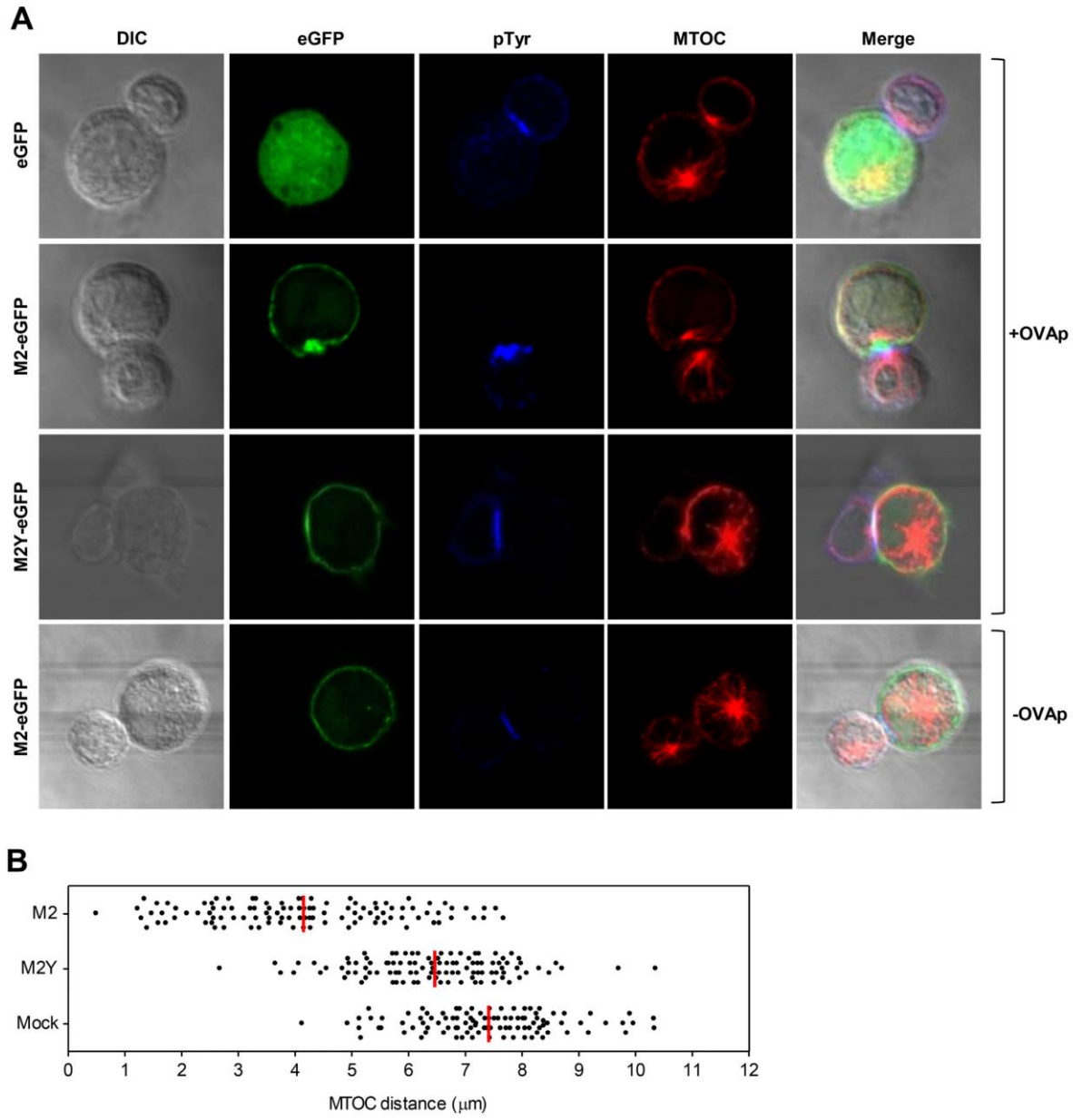

Fig 2. M2 polarizes to the B-T_H contact zone and increases B cell MTOC polarization. A20 B cells transiently expressing M2-eGFP, M2Y-eGFP or eGFP (green) were pulsed (three upper panels), or not (bottom panel), overnight with 10μM of OVA peptide (OVAp) and incubated with OVAp-specific $CD4^+$ T cells for 15 minutes. Cells were fixed and stained for pTyr (blue), and for MTOC with an anti-α-tubulin antibody (red). (A) Representative images of M2 and B cell MTOC polarization to the contact zone. (B) Quantification of MTOC distance. Distance of the B cell MTOC to the contact zone was measured from a total of 100 conjugates from three independent experiments. The mean distance is represented as a red line. Statistical significance between groups was analyzed by one way ANOVA, with $p<0.0001$.

doi:10.1371/journal.pone.0142540.g002

minutes of incubation. Fig 3B shows the percentage of M2 (black circles) or M2Y (grey squares) conjugates, after 30 minutes of incubation, upon variation of the OVAp concentration. Conjugate formation occurred in a peptide dose-dependent manner. In the absence of

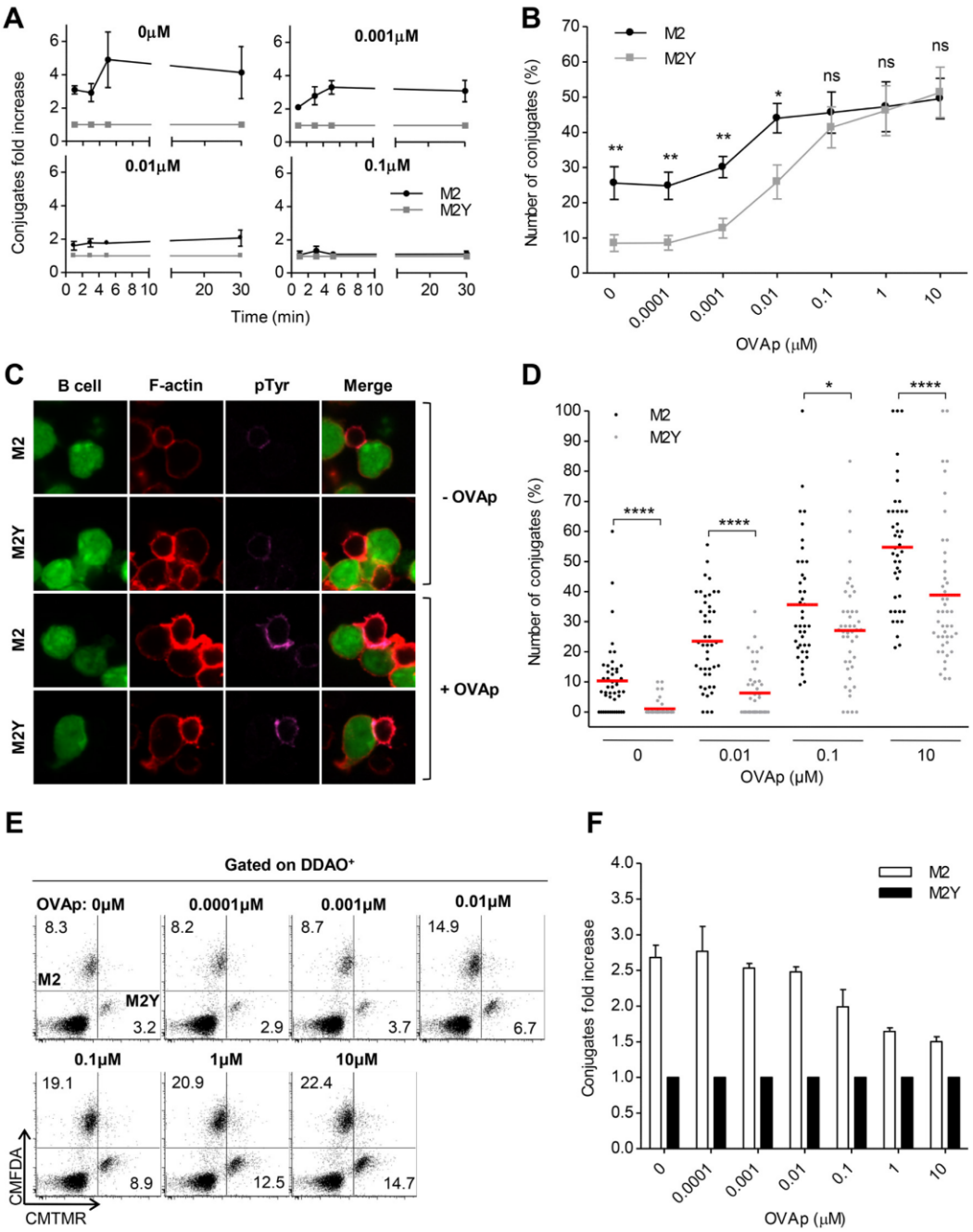

Fig 3. M2 promotes the formation of conjugates between B and T_H cells. A20 B cells stably expressing M2 or M2Y were pulsed overnight, or not, with different concentrations of OVA peptide (OVAp) and incubated with OVAp-specific $CD4^+$ T cells at a 2:1 ratio, for the indicated time periods. Prior to incubation B and T cell populations were incubated with the live dyes CMFDA, CMTMR, and DDAO, respectively, to allow their discrimination. (A) Fold increase of the number of conjugates formed with M2- (black circles) or M2Y- (grey squares) expressing B cells relative to M2Y condition, determined by flow cytometry. Conjugate formation was evaluated as the percentage of $CMFDA^+DDAO^+$ events in the total $DDAO^+$ population. (B) Percentage of conjugates after 30min of incubation upon variation of the OVAp concentration. (A) and (B) Symbols represent the mean of 4 independent experiments. (C) Representative images of pTyr polarization to the contact zone. After 30min of incubation, cells were fixed and stained for F-actin with TRITC-phalloidin (red), and for pTyr (purple). Images are from one representative experiment out of three. (D) Percentage of conjugates per field after 30min of incubation, as

determined by confocal microscopy, upon variation of the OVAp concentration. Conjugate count was blind and based on B-T_H cell contact and pTyr polarization to the contact zone. A total of 45 images were taken per sample from three independent experiments. Only images with a minimum of three T cells were considered for analysis. (E) Representative FACS plots of in vitro competition assay for each OVAp concentration. M2-expressing B cells, M2Y-expressing B cells and $CD4^+$ T cells were mixed at a 1:1:1 ratio and incubated for 30min. Conjugates were analyzed as the percentage of $CMFDA^+DDAO^+$ (M2 conjugates) or $CMTMR^+DDAO^+$ (M2Y conjugates) events in the total $DDAO^+$ population. Percentage of T cells conjugating with M2 or M2Y-expressing B cells is indicated in the respective quadrant. (F) Fold increase of the number of conjugates formed with M2- (open bars) or M2Y- (filled bars) expressing B cells relative to M2Y condition is represented in the graph. In flow cytometry experiments error bars represent standard error of the mean. Statistical significance between groups was evaluated by a one-tailed unpaired Student's t test. In confocal microscopy experiments statistical significance of the difference between groups was evaluated by a Mann-Whitney U test.

doi:10.1371/journal.pone.0142540.g003

peptide, less than 10% of the T_H cells conjugated with M2Y-expressing B cells. In contrast, the integrity of the phosphosites resulted in a three-fold increase in conjugate formation with M2-expressing B cells. Up to 0.01μM M2 was able to promote conjugate formation. However, in the presence of high concentrations of OVAp, M2 did not influence conjugate formation. We conclude that M2 promotes conjugate formation in the absence or with low concentrations of OVAp. Such ability is dependent on the phosphosites responsible for binding to B cell signaling proteins.

To further address conjugate formation, we analyzed B-T_H cell interaction by confocal microscopy, including a marker for phosphorylated tyrosines (pTyr). This is indicative of signaling and formation of a functional immunological synapse but, in this particular case, can be also associated with constitutive phosphorylation of the tyrosine residues of M2, and the consequent phosphorylation of Vav1 and PLCγ2 [18, 19, 21]. Using the MHC class II-restricted OVAp-specific system, M2- or M2Y-expressing B cell lines, loaded with different concentrations of peptide, and T_H cells were incubated in a 2:1 ratio, for 30 minutes. Prior to incubation, B cells were loaded with CMFDA live dye to allow their visualization. Cells were also stained for F-actin, to allow T cell, as well as B-T_H cell interaction, visualization. Conjugate count was blind and based on B-T_H cell contact and pTyr (purple) polarization to the contact zone (Fig 3C). Fig 3D shows the percentage of T cells conjugating with either M2- (black circles) or M2Y-expressing (grey circles) B cells. Corroborating the previous results, confocal microscopy revealed that M2 expression in B cells promoted conjugate formation with T_H cells, with pTyr polarization to the contact zone.

To understand whether the increase in conjugate formation translated into a competitive advantage, we performed an in vitro competition assay. T_H cells were simultaneously incubated with equal numbers of M2- and M2Y-expressing B cells in a 1:1:1 ratio. Both B cell populations were pulsed with the same OVAp concentration. Prior to incubation, the three populations were loaded with different live dyes to allow their discrimination (Fig 3E), as was performed above. Fig 3F shows the fold increase of the percentage of T cells conjugating with M2-expressing B cells (open bars) relative to the percentage of T cells conjugating with M2Y-expressing B cells (filled bars). On average, there were 2.5-fold more M2 conjugates when peptide concentration was low (up to 0.1 μM) or zero. This shows that T_H cells preferentially conjugated with B cells expressing the wild-type viral protein. To exclude the possibility of a cell line effect, all three experiments were repeated with independently generated B cell lines with similar results (S2 Fig).

Taken together, these data show that expression of M2 gives a competitive advantage to B cells by favoring the formation of conjugates with T_H cells, independently of specific antigen presentation.

M2-Expressing B Cells Do Not Promote T Cell Activation in the Absence of Specific Peptide

Cognate B-T_H cell interaction results in IS formation. This is a bidirectional communication system whereby signals transmitted at the contact interface can lead to activation of both target

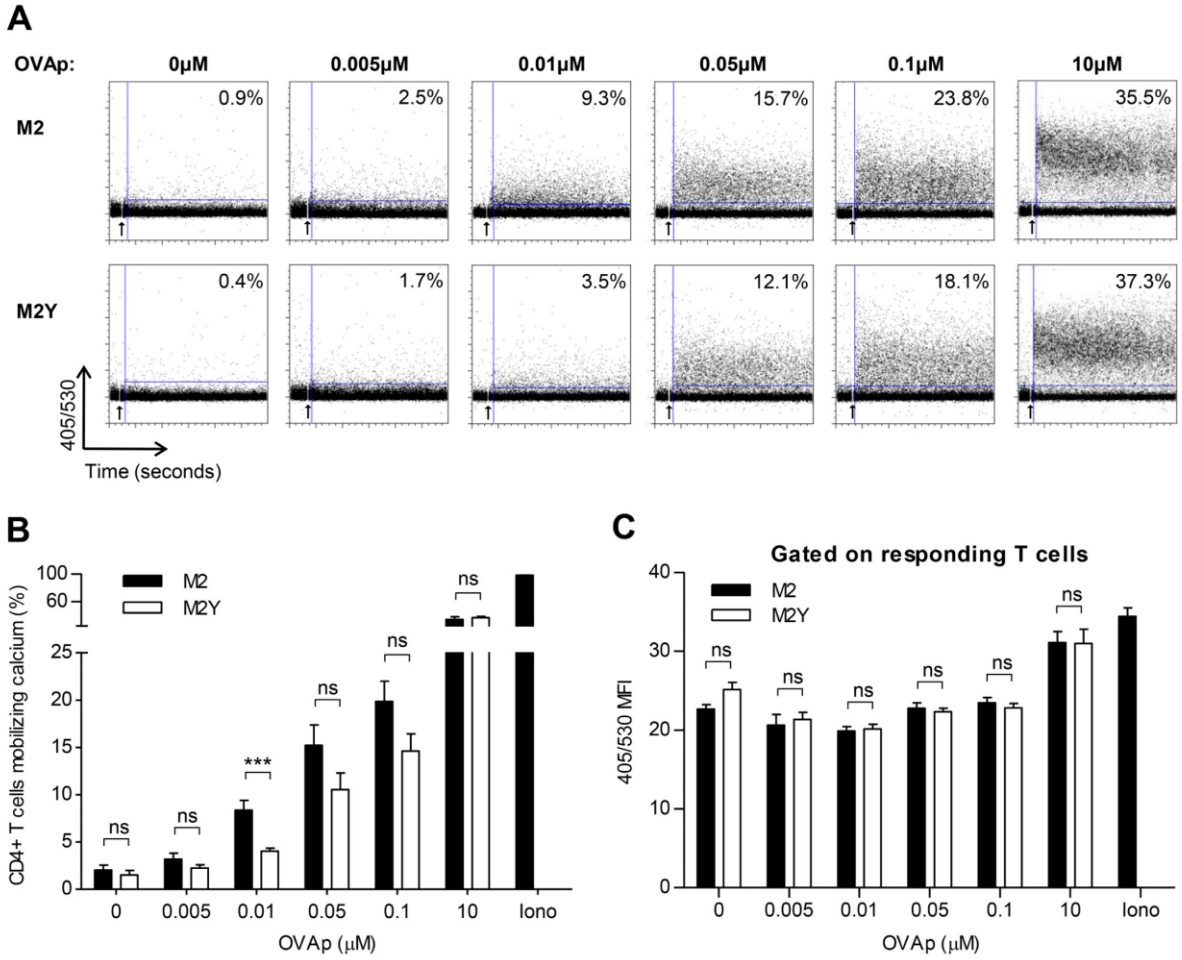

Fig 4. Calcium mobilization in T_H cells conjugated with M2-expressing B cells requires specific peptide presentation. A20 B cells stably expressing M2 or M2Y were pulsed overnight, or not, with different concentrations of OVAp and incubated with OVAp-specific $CD4^+$ T cells for 5 min. Prior to conjugation T cells were loaded with the calcium indicator Indo-I. Ionomycin was used as a positive control. (A) Representative FACS plots of calcium measurements. A baseline was established by acquiring unstimulated T_H cells alone, for approximately two minutes. Calcium fluxes were then measured on a MoFlow cytometer for 18 minutes (indicated by an arrow) and were based on the 405/530 emission ratio over time. 405/530 mean fluorescence intensity (MFI) is shown. (B) Average of the percentage of $CD4^+$ T cells mobilizing calcium when conjugated with M2-expressing (filled bars) or M2Y-expressing (open bars) B cells. (C) 405/530 MFI average within responding T cells. Graphs show results from three to seven experiments. Error bars represent standard error of the mean. Statistical significance of the difference between groups was evaluated by a one-tailed unpaired Student's T test.

doi:10.1371/journal.pone.0142540.g004

and effector cells. Thus, we next investigated if the competitive advantage in interaction with T helper cells, conferred by M2 expression in B cells, resulted in T cell activation. Using the MHC class II-restricted OVAp-specific system we assessed intracellular calcium concentration increase by flow cytometry (Fig 4), as a marker of T cell activation. Prior to incubation, T_H cells were loaded with the calcium indicator Indo-1, which changes its emission spectrum by chelating free calcium ions. As a result, the intensity of the emission at 405nm increases and, simultaneously, the intensity of the emission at 530nm decreases. Therefore, the 405/530 ratio provides a measure of intracellular calcium increase (Fig 4A). For each sample, a baseline was established by acquiring unstimulated T_H cells alone, for approximately two minutes [37]. Then, the effect of incubation with M2- or M2Y-expressing B cells on T_H cell intracellular

calcium increase was assessed (indicated by an arrow in Fig 4A). Values shown on Fig 4A refer to the percentage of responding T_H cells, i.e. T_H cells mobilizing calcium from one representative experiment. Ionomycin was used as a positive control, leading to activation of more than 97% of the T cell population. The percentage of responding T_H cells increased with the OVAp concentration (Fig 4B). In the absence of peptide M2 did not promote intracellular calcium increase. When pulsed with 0.01μM of OVAp, M2-expressing B cells led to an increase in the number of T_H cells mobilizing calcium, compared to M2Y-expressing B cells. To assess if M2-expressing B cells were also able to promote stronger individual responses, we quantified the 405/530 ratio MFI of responding T_H cells (Fig 4C). M2 and M2Y samples showed no statistically significant differences in MFI demonstrating that, even though there were more T_H cells mobilizing calcium, there was no difference in the magnitude of individual responses. This experiment was repeated with independent B cell lines, for some OVAp concentrations, with similar results (S3A Fig).

To further investigate if M2 expression in B cells could have an effect in promoting T_H cell activation we quantified T cell IFN-γ production and release by ELISA (Fig 5A). After 20h of incubation IFN-γ concentration was measured on culture supernatants by sandwich ELISA. In the absence of peptide we could not detect IFN-γ. For 0.1μM and 1μM of OVAp, M2 expression led to an increase in IFN-γ concentration, compared to the M2Y condition. The IFN-γ production increase observed by ELISA could be due to an increase in production per cell or due to an increase in the number of activated T_H cells. To discriminate between these two possibilities, we analyzed IFN-γ production by flow cytometry (Fig 5B and 5C). B and T_H cells were incubated in the presence of brefeldin A (BFA) to inhibit protein secretion. As shown in the upper panel of Fig 5B, M2-expressing B cells did not significantly promote IFN-γ production in the absence of peptide. From 0.01μM to 1μM of OVAp concentrations, M2 expression led to an increase in the percentage of T_H cells producing IFN-γ, compared to M2Y. Measurement of IFN-γ MFI of responding T_H cells showed no significant differences between M2 and M2Y conditions (Fig 5B, lower panel). This can be confirmed in the representative FACS plots (Fig 5C). Therefore, as observed in the calcium measurement experiment, we conclude that the increased IFN-γ production resulted from an increase in the number of activated T_H cells, and not from stronger individual responses.

We also assessed IFN-γ polarization to the contact zone by confocal microscopy (Fig 5D). Quantification of the percentage of T_H cells, conjugating with either M2- (black circles) or M2Y-expressing (grey circles) B cells, that polarize IFN-γ to the contact zone (Fig 5E), shows that there is a requirement for presentation of specific peptide. In the presence of peptide, conjugate formation with M2-expressing B cells resulted in more T_H cells activated compared to M2Y. This experiment was repeated with independent B cell lines, with similar results (S3B Fig).

Collectively, these experiments show that in the context of conjugate formation, expression of M2 in B cells does not promote T cell activation in the absence of specific peptide.

Discussion

With this work, we further characterized the role of the latency associated M2 protein, involved in the assembly of multiprotein complexes with cell signaling proteins [21], and linked it to the modulation of B-T_H cell interactions. Our data supports a model where expression of MuHV-4 M2 protein competitively promotes interaction with T_H cells in vitro, in the context of a MHC class II-restricted OVAp-specific cellular system. This process was independent of presentation of specific antigen and may be the outcome of the upregulation of adhesion molecules observed in M2-expressing B cells. However, in the absence of specific peptide, conjugate formation with M2-expressing B cells did not result in increased intracellular calcium levels or IFN-γ

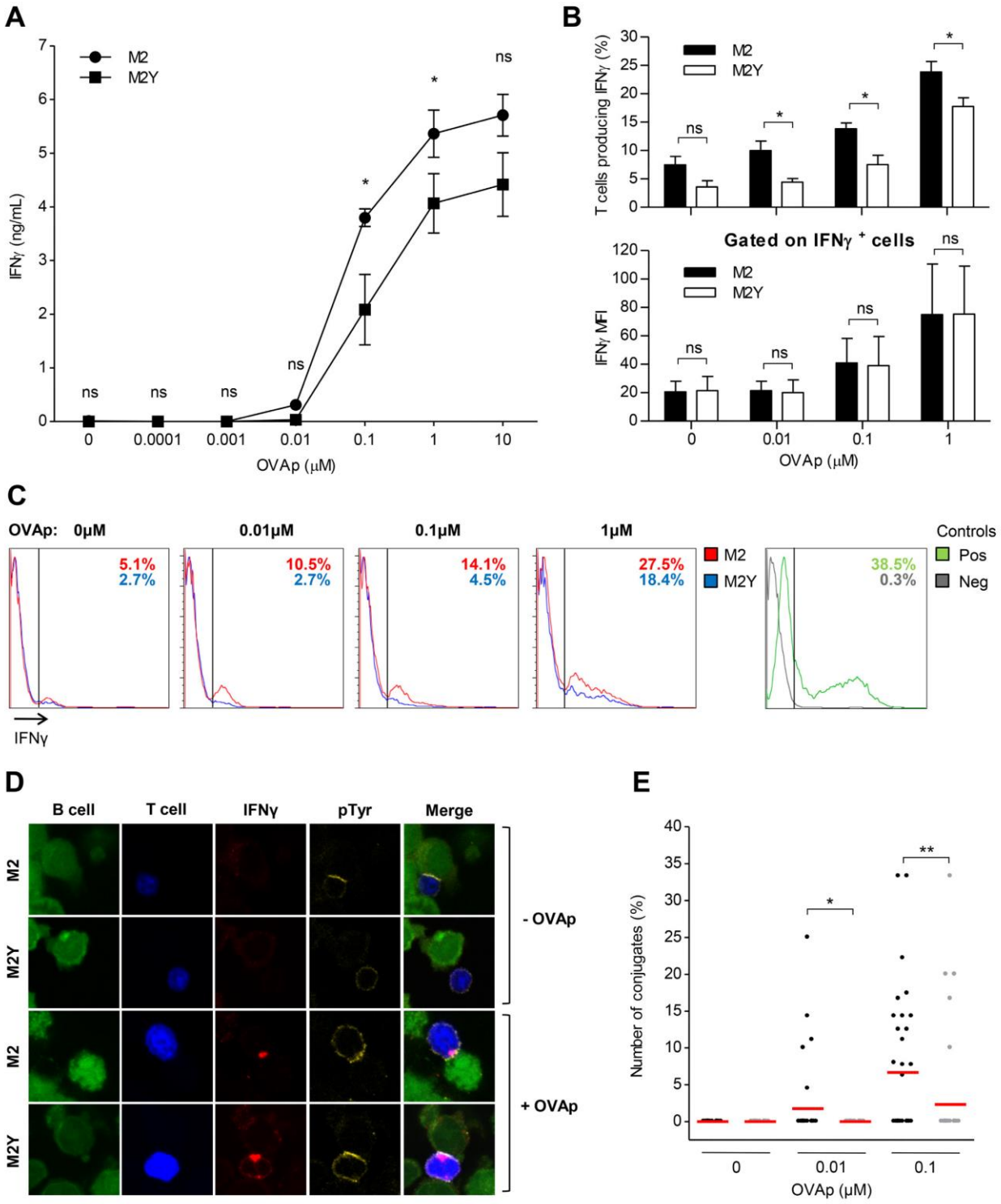

Fig 5. IFN-γ production in T_H cells conjugated with M2-expressing B cells requires specific peptide presentation. A20 B cells stably expressing M2 or M2Y were pulsed overnight, or not, with different concentrations of OVA peptide (OVAp) and incubated with OVAp-specific $CD4^+$ T cells. (A) Extracellular IFN-γ after 20h of incubation. After incubation the supernatant was recovered and analyzed by sandwich ELISA to determine IFN-γ concentration.

Supernatants of three independent experiments were tested in duplicate. (B) Upper panel: percentage of T cells producing IFN-γ after 5h of conjugation in the presence of brefeldin A (BFA). Cells were fixed and stained for CD4 with anti-CD4-APC, and for IFN-γ with anti-IFN-γ-PE, and analyzed on a FACS Calibur. Lower panel: IFN-γ mean fluorescence intensity (MFI) of responding T cells. Average of three independent experiments is shown. Statistical significance of the difference between groups was evaluated by a one-tailed unpaired Student's t test. (C) Representative FACS plots of intracellular IFN-γ production. (D) Representative confocal images of IFN-γ polarization to the contact zone. Prior to incubation B and T cells were labelled with CMFDA (green) and CMAC (blue) live dyes, respectively. Cells were incubated for 2.5h, fixed and stained for IFN-γ (red), and for pTyr (yellow). Images are from one representative experiment out of three and were obtained using a Zeiss LSM 510 META microscope. (E) Quantification of conjugates with IFN-γ polarization per image. Conjugates were evaluated by confocal microscopy based on B-T_H cell contact, and IFN-γ polarization (red). 45 to 55 images were acquired per sample from three independent experiments. Only images with a minimum of three T cells were considered for analysis. Statistical significance of the difference between groups was evaluated by a Mann-Whitney U test.

doi:10.1371/journal.pone.0142540.g005

production in T_H cells. Therefore, T cell activation upon conjugate formation was not driven by M2, but a product of cognate interaction. Nevertheless, concomitant with the increased number of conjugates, the number of activated T_H cells was higher in the presence of M2-expressing B cells.

B cell polarization has been rarely addressed in B-T_H cell interaction studies, although it has been described [35]. Here, we provided evidence of B cell polarization in B-T_H cell interaction. Collectively, B cell polarization and the upregulation of co-stimulatory molecules observed under M2 expression suggest a role for the viral protein in IS modulation.

Modulation of T-APC interaction, and more specifically IS, by a viral protein has been previously described. Protein Nef from Human Immunodeficiency Virus type 1 (HIV-1) has been shown to impair IS formation [38–41], as a means of optimizing the environment for HIV infection. In the *Gammaherpesvirinae* there are also two examples of impairment of B-T_H cell interactions and IS formation, namely K5 from Kaposi Sarcoma-associated Herpesvirus (KSHV) [42], and tyrosine kinase-interacting protein (Tip) from the T lymphotropic Herpesvirus Saimiri (HVS) [43]. In contrast, our results support a model where a viral protein promotes B-T_H cell interaction, instead of impairing it. This is concomitant with the high prevalence of infection in GC B cells. Such positive effect does not exclude the possibility that, at some point during infection, MuHV-4 impairs IS formation as a mechanism of immune evasion.

The inability of M2Y to promote B-T_H cell conjugate formation in vitro is in agreement with the delay in latency establishment observed in vivo with the recombinant M2Y virus [18]. However, this virus is still able to enter GC reactions, meaning that there are other players in this process. For example, the putative existence of a viral superantigen [44] may drive IS formation. Another possibility lies with the choice of B cells for latency establishment. This has been demonstrated not to be a stochastic event, in what concerns BCR specificity, and to be linked to the formation of GCs [45].

Despite the controversy regarding antigen dependence in the production of EBV-infected memory B cells, there is unequivocal evidence of the participation of EBV-infected B cells in the GC reaction [1, 2], as it is described for MuHV-4 [5–7]. However, the role that the virus plays in such process still lacks characterization. Although it is not clear yet, it is possible that KSHV also takes advantage of the GC reaction. Given that M2 is a putative functional homologue of LMP1 and LMP2A encoded by EBV, and K1 and K15 encoded by KSHV, our work sets the base for future studies with the mentioned proteins, in what regards T-APC interaction.

In this study we propose that the latency-associated M2 protein competitively promotes B-T_H cell interaction, a process that is dependent on the modulation of B cell signaling. In vivo, this ability to attract T cell help in a competitive manner during the T cell scanning process, carried out in secondary lymphoid organs, may account for the selection of infected B cells for GC initiation, a crucial step in latency establishment, hence host colonization.

Materials and Methods

Ethics Statement

The study accorded with the Portuguese official Veterinary Directorate (Portaria 1005/92), European Directive 2010/63/EU, and Federation of European Laboratory Animal Science Associations guidelines on laboratory animal welfare. It was approved by the Portuguese official veterinary department for welfare licensing (protocol AEC_2010_017_PS_Rdt_General) and by the IMM Animal Ethics Committee.

Mice

8-week to 4-month old Balb/c TCR transgenic DO11.10 mice (kindly provided by Prof. Luís Graça, Instituto de Medicina Molecular) were used for purification of $CD4^+$ T cells. Mice were bred and housed under specific pathogen-free conditions at Instituto de Medicina Molecular, Lisbon, Portugal. Mice were sacrificed by CO_2 inhalation or cervical dislocation.

Plasmids

pEGPF-M2, pEGFP-M2Y plasmids have been described [21]. To produce viral transduction particles for the creation of zeocin-resistant stable cell lines, M2 was cut from pMSCV-M2-IRES-GFP [19] with EcoRI and XhoI and subcloned to pMSV-K3-IRES-Zeo [20], replacing K3 and giving rise to pMSCV-M2-IRES-zeo. Similarly, pMSCV-M2Y-IRES-Zeo was constructed by excising M2Y from pMSCV-M2Y-IRES-GFP [19] and subcloning it as described for pMSCV-M2-IRES-Zeo. To produce viral transduction particles for the creation of zeocin-resistant, eGFP-expressing, stable cell lines, pMSCV-eGFP-M2-IRES-zeo and pMSCV-eGFP-M2Y-IRES-zeo plasmids were constructed, were eGFP is N-terminally fused to M2/M2Y. For that purpose, eGFP was amplified by PCR from pEGFP-N1 vector (Clontech). pEQPAM3 was the packaging vector used.

Antibodies

Primary antibodies used for confocal microscopy were: anti-F-actin (TRITC-phalloidin—Sigma), anti-alpha tubulin (clone DM1A, Sigma-aldrich), anti-pTyr-AF647 (clone PY99, Santa Cruz Biotechnology), anti-IFN-gamma (clone AN-18, BD Biosciences). Secondary antibodies used for confocal microscopy were: anti-rat AF568 (Molecular Probes) and anti-mouse AF594 (Molecular Probes). Antibodies used for flow cytometry were: anti-TCR DO11.10 PE (clone KJ1.26, MBL-medical and biological lab), anti-CD4 AF405 (clone RM4-5, Invitrogen), anti-CD80 PB (clone 16-10A1, BioLegend), anti-CD86 PE-Cy7 (clone PO3, BioLegend), anti-CD54 (ICAM1) APC (clone YN1/1.7.4, BioLegend), anti-CD40 PE-Cy7 (clone 3/23, BioLegend), anti-CD48 APC (clone HM48-1, BioLegend), anti-MHC-II PB (clone M5/114.15.2, BioLegend), anti-CD19 APC-H7 (clone 1D3, BD Biosciences), anti-CD21 APC (clone 7G6, BD Biosciences), anti-CD23 PE (clone B3B4, BD Biosciences), anti-CD69 FITC (clone H1.2F3, BioLegend), anti-CD95 PE (clone Jo2, BD Biosciences), anti-IFN-γ PE (clone XMG1.2, BD Biosciences). Primary antibodies used for western blot were: anti-EGFP (Clontech) and anti-actin (polyclonal, Sigma-Aldrich). Secondary antibodies used for western blot were anti-rabbit (GE Healthcare) and anti-mouse (Jackson Immunoresearch) antibodies, conjugated with horse radish peroxidase (HRP).

Cell Culture, Transfection and Transduction

HEK-293T cells were cultured in Dulbecco's modified Eagle's medium (DMEM) supplemented with 10% fetal bovine serum, 2mM glutamine, 100U/mL penicillin and streptomycin. A20 B

cells were grown in RPMI 1640 supplemented as described above. In the case of zeocin-resistant stable cell lines, 4μg/mL of zeocin was added to the culture. Conjugates were incubated in RPMI 1640 supplemented with 5% fetal bovine serum, 2mM glutamine, 100u/mL penicillin and streptomycin and 10mM HEPES. In the case of the analysis by flow cytometry of intracellular production of IFN-γ the media was supplemented with 5% fetal bovine serum, 10mM HEPES, 60U/mL rmIL-2 (Peprotech) and 10μg/mL of Brefeldin A (BFA, Sigma). Mouse $CD4^+$ T cells were isolated from the spleen of 8-week to 4-months old TCR transgenic DO11.10 mice using a mouse $CD4^+$ T cell isolation kit (Miltenyi Biotec), according to manufacturer's instructions. Purity was analyzed by flow cytometry and was above 90%. Cells were then stimulated with mouse T-activator CD3/CD28 Dynabeads® (Invitrogen), according to manufacturer's instructions. After Dynabeads® removal, cells were cultured for a resting period of 5–8 days in RPMI 1640 supplemented as described above in addition to 50μM 2-mercaptoethanol, 100μM sodium pyruvate, 10mM HEPES and 60U/mL rmIL-2. For confocal microscopy experiments, by the end of the resting period, live cells were sorted based on FSC-A/SSC-A parameters. For production of viral particles used for A20 B cell transduction, HEK-293T cells were transiently transfected by the Calcium Phosphate Method with 20μg of pEQPAM3 and 20μg of pMSCV-M2-IRES-Zeo, pMSCV-M2Y-IRES-Zeo, pMSCV-eGFP-M2-IRES-Zeo or pMSCV-eGFP-M2Y-IRES-Zeo. After transduction, B cells were cultured for two weeks in RPMI supplemented with 400μg/mL of zeocin. In the case of eGFP-M2/M2Y constructs, GFP+ cells were sorted after transduction and prior to culture with zeocin. All transductions were performed in the presence of 8μg/mL of polybrene.

Flow Cytometry

Live resting mouse $CD4^+$ T cells were sorted on a BD FACSaria flow cytometer at the end of the resting period, based on FSC-A/SSC-A parameters. After sorting, cells were immediately used for conjugation experiments. A20 B cells transiently expressing eGPF-M2 or eGFP-M2Y were sorted on a BD FACSaria flow cytometer for eGFP expressing cells, prior to their use. Splenocyte single cell suspensions were prepared from spleens recovered at 14dpi. Red blood cells were lysed in hypotonic NH_4Cl. Splenocyte suspensions or cell lines were incubated with Fc block prior to staining, washed with 1x PBS, and stained for 20min with primary antibodies. Cells were washed and incubated for 20min with streptavidin, when appropriate. All samples were resuspended in FACS buffer (1xPBS, 2% FBS) and analyzed on LSR Fortessa (BD Biosciences) using DIVA software (BD Biosciences) for acquisition. For conjugation experiments, cells were analyzed in supplemented culture media, instead of FACS buffer. For IFN-γ intracellular measurements a FACSCalibur was used along with CellQuest software (Becton-Dickinson Immunocytometry Systems, San José, CA). For this experiment cells were fixed with 4% paraformaldehyde (PFA) and permeabilized with 0.2% triton X-100 prior to incubation with detecting antibody. All steps until incubation with PFA were performed in FACS buffer supplemented with BFA. T cells incubated for 5h with 100 ng/ml phorbol-12-myristate-13-acetate (PMA, Sigma) and 2 μg/ml ionomycin (Sigma) were used as positive control. Data was analyzed using Flowjo (Tree Star).

Conjugation and Immunofluorescence

A20 B cells, stably expressing M2, M2Y, eGFP, eGPF-M2 or eGFP-M2Y, were pulsed overnight, or at least 2h, with the indicated concentrations of OVAp (OVA peptide 323–339; GenWay) in RPMI. Afterwards, A20 B cells and/or mouse $CD4^+$ T cells were loaded with one of the following live dyes, as indicated for each experiment: CellTracker™ Blue CMAC (7-amino-4-chloromethylcoumarin), CellTracker™ Green CMFDA

(5-chloromethylfluorescein diacetate), CellTrace™ Far-Red DDAO-SE, CellTracker™ Orange CMTMR ((5-(and-6)-(((4-chloromethyl)benzoyl)amino) tetramethylrhodamine) from Molecular Probes, Invitrogen. B and T cells were added in the indicated ratios, centrifuged for 1min to promote conjugate formation, and incubated for a period of time, as is specified. For confocal microscopy experiments, after conjugation, cells were gently resuspended, added to poly-L-lysine-coated coverslips (BD Biosciences) and incubated for the indicated time at 37°C. Cells were fixed with 4% paraformaldehyde and permeabilized with 0.2% Triton X-100. Samples were incubated with primary antibodies for 1h, followed by 1h of incubation with a species-specific secondary antibody, when necessary. DNA was detected with DAPI (Invitrogen). Coverslips were mounted in Mowiol (Fluka) or Fluoromount-G (Southern Biotec) and examined using a Carl Zeiss LSM 510 confocal microscope, with a Plan-Apochromat objective of 63x (1.4 oil). Analysis was performed using AimImageBrowser (Zeiss LSM data server). For flow cytometry experiments, after conjugation, cells were gently resuspended and analyzed on a LSR Fortessa flow cytometer (BD Biosciences).

Image Quantification

Image quantification was performed in a blinded fashion, in a minimum of 45 randomly selected fields, from a total of three independent experiments. Distances of the MTOC to the center of the B-T_H contact zone and signal quantifications were measured using AimImageBrowser (Zeiss LSM data server, Zeiss). To evaluate the percentage of conjugates showing pTyr and/or IFN-γ polarization to the contact zone, only images with a minimum of three T cells were analyzed. Number of T cells conjugating was scored visually.

Measurement of Calcium Fluxes

A20 B cells, loaded or not with OVAp, and mouse OVAp-specific $CD4^+$ T cells were processed as described above. T cells were loaded with 5μM Indo-1 AM (Invitrogen) [46] and conjugated for 5min with A20 B cell lines. Before starting sample acquisition a baseline was set on the 405/525 emission ratio using Indo-1 loaded T cells. Ionomycin (Sigma) activated T cells were used as a positive control. Baseline was acquired for approximately 2min and samples were acquired for an additional 18min on a MoFlow cytometer.

Enzyme Linked Immunosorbent Assay

A20 B cell lines were loaded, or not, with different concentrations of OVAp (aa 323–339) overnight. Cells were then conjugated with purified mouse $CD4^+$ T cells as described above and incubated for 20h. After the 20h incubation period, supernatant was recovered and stored at -20°C. IFN-γ production was quantified in the supernatants by sandwich ELISA using the commercial kit DuoSet® ELISA Development System (R&D systems), according to manufacturer's instructions. 96-well plates were analyzed on an Infinite® M200 (Tecan Group, Ltd). T cells cultured for two to four days in the presence of 3μg/mL of anti-CD3 antibody were used as positive control of T cell activation. B cells cultured for 48h in the presence of 2.5μg/mL of anti-CD40 antibody and 5μg/mL of the F(ab')2/F(ab) portion of an anti-mouse IgG antibody were used as positive control for B cell activation.

Statistical Analysis

Statistical significance was evaluated with unpaired one-tailed t-test, one-way ANOVA or non-parametric Mann-Whitney U test, as appropriate, using GraphPad Prism software. ns indicates

$p>0.05$; * indicates $p<0.05$, ** indicates $p<0.01$, *** indicates $p<0.001$, **** indicates $p<0.0001$.

Supporting Information

S1 Fig. M2-expressing independent B cell line shows upregulation of CD80, CD86 and ICAM-1. (A) M2/M2Y expression in total cellular lysates of the independent A20 B cell lines. eGFP or eGFP-M2/M2Y fusion proteins were detected on Western Blot with an anti-eGFP antibody. An anti-actin antibody was used to demonstrate that similar amounts of cellular lysates were used. An A20 B cell line expressing non-tagged M2 (lane 4) was used as a negative control. (B) Fold increase of the mean fluorescence intensities (MFI) of several surface molecules, normalized to eGFP A20 B cells. A20 B cell lines stably expressing eGFP, eGFP-M2 or eGFP-M2Y were stained with fluorescently labelled antibodies and the surface expression of the indicated molecules was analyzed on a LSR Fortessa flow cytometer. Bars represent the mean of eight independent experiments. Error bars represent standard error of the mean. Statistical significance was assessed with a one-tailed Students t-test.
(TIF)

S2 Fig. M2 expression in an independent B cell line promotes conjugation with T_H cells. eGFP independent B cell lines were pulsed overnight, or not, with different concentrations of OVAp and incubated with OVAp-specific $CD4^+$ T cells at a 2:1 ratio. (A) Percentage of conjugates after 30min of incubation upon variation of the OVAp concentration. T cell populations were loaded with DDAO, to allow their discrimination. Results shown correspond to mean of three independent experiments. Statistical significance refers to comparison between M2 and M2Y conditions. (B) Percentage of conjugates per image after 30min of incubation, determined by confocal microscopy, upon variation of the OVAp concentration. Conjugate count was blind and based on B-T_H contact and pTyr polarization to the contact zone. 15 to 35 images were taken per sample, for an equivalent number of analyzed T cells within each OVAp concentration. Only images with a minimum of three T cells were considered for analysis. Results are from one experiment. (C) Fold increase of the number of conjugates formed with eGFP-M2- (open bars) or eGFP-M2Y- (filled bars) expressing B cells relative to M2Y condition. eGFP-M2-expressing B cells, eGFP-M2Y-expressing B cells and $CD4^+$ T cells were mixed at a 1:1:1 ratio and incubated for 30min. Prior to conjugation M2Y-expressing B and T cell populations were labeled with the live dyes CMTMR and DDAO, respectively, to allow their discrimination. Conjugate formation was analyzed on a LSR Fortessa flow cytometer as the percentage of $eGFP^+DDAO^+$ (M2) or $eGFP^+CMTMR^+DDAO^+$ (M2Y) events in the total $DDAO^+$ population. (D) Representative FACS plots for each OVAp concentration. Percentage of T cells conjugating with M2- or M2Y-expressing B cells is indicated in the respective quadrant. In flow cytometry experiments, error bars represent standard error of the mean. Statistical significance between groups was evaluated by a one-tailed unpaired Student's t test. In confocal microscopy experiments, statistical significance of the difference between groups was evaluated by a Mann-Whitney U test.
(TIF)

S3 Fig. An independent M2-expressing B cell line requires specific peptide to promote T_H cell activation. (A) Average of the percentage of $CD4^+$ T cells mobilizing calcium when conjugated with eGFP-M2-expressing (black bars), eGFP-M2Y-expressing (white bars) or eGFP-expressing (grey bars) B cells. eGFP independent B cell lines were pulsed overnight, or not, with different concentrations of OVAp and incubated with OVAp-specific $CD4^+$ T cells for 5 min. Prior to conjugation T cells were loaded with Indo-I, a calcium indicator. Ionomycin was

used as a positive control. Calcium fluxes were measured on a MoFlow cytometer for 21 minutes and were based on the 405/530 emission ratio over time. Graph shows results from one experiment. (B) Quantification of conjugates showing IFN-γ polarization to the contact zone per field. Prior to incubation B and T cells were labelled with CMFDA and CMAC live dyes, respectively. Cells were incubated for 2.5h, fixed and stained for IFN-γ and pTyr. Conjugates were evaluated by confocal microscopy based on B-T_H contact and IFN-γ polarization. Only images with a minimum of three T cells were considered for analysis. Statistical significance of the difference between groups was evaluated by a Mann-Whitney U test.
(TIF)

Acknowledgments

We would like to thank Dr. Salvatore Valitutti for the MTOC experiments conducted in his lab. We also thank the Flow Cytometry Unit at the Instituto Gulbenkian de Ciência for their assistance in setting up the measurement of intracellular calcium levels by flow cytometry. Finally, we thank Dr. Marta Alenquer for initial observations regarding this study and for the development of the cloning strategy for the independent cell lines.

Author Contributions

Conceived and designed the experiments: DF FBL SM JPS. Performed the experiments: DF FBL SM. Analyzed the data: DF FBL SM JPS. Contributed reagents/materials/analysis tools: DF FBL SM JPS. Wrote the paper: DF JPS.

References

1. Thorley-Lawson DA, Hawkins JB, Tracy SI, Shapiro M. The pathogenesis of Epstein-Barr virus persistent infection. Current opinion in virology. 2013; 3(3):227–32. doi: 10.1016/j.coviro.2013.04.005 PMID: 23683686; PubMed Central PMCID: PMC3789532.
2. Roughan JE, Thorley-Lawson DA. The intersection of Epstein-Barr virus with the germinal center. Journal of virology. 2009; 83(8):3968–76. doi: 10.1128/JVI.02609-08 PMID: 19193789; PubMed Central PMCID: PMC2663245.
3. Simas JP, Efstathiou S. Murine gammaherpesvirus 68: a model for the study of gammaherpesvirus pathogenesis. Trends in microbiology. 1998; 6(7):276–82. PMID: 9717216.
4. Barton E, Mandal P, Speck SH. Pathogenesis and host control of gammaherpesviruses: lessons from the mouse. Annual review of immunology. 2011; 29:351–97. doi: 10.1146/annurev-immunol-072710-081639 PMID: 21219186.
5. Flano E, Kim IJ, Woodland DL, Blackman MA. Gamma-herpesvirus latency is preferentially maintained in splenic germinal center and memory B cells. The Journal of experimental medicine. 2002; 196 (10):1363–72. PMID: 12438427; PubMed Central PMCID: PMC2193987.
6. Willer DO, Speck SH. Long-term latent murine Gammaherpesvirus 68 infection is preferentially found within the surface immunoglobulin D-negative subset of splenic B cells in vivo. Journal of virology. 2003; 77(15):8310–21. PMID: 12857900; PubMed Central PMCID: PMC165249.
7. Kim IJ, Flano E, Woodland DL, Lund FE, Randall TD, Blackman MA. Maintenance of long term gammaherpesvirus B cell latency is dependent on CD40-mediated development of memory B cells. Journal of immunology. 2003; 171(2):886–92. PMID: 12847258.
8. Collins CM, Boss JM, Speck SH. Identification of infected B-cell populations by using a recombinant murine gammaherpesvirus 68 expressing a fluorescent protein. Journal of virology. 2009; 83 (13):6484–93. doi: 10.1128/JVI.00297-09 PMID: 19386718; PubMed Central PMCID: PMC2698576.
9. Allen CD, Okada T, Cyster JG. Germinal-center organization and cellular dynamics. Immunity. 2007; 27(2):190–202. doi: 10.1016/j.immuni.2007.07.009 PMID: 17723214; PubMed Central PMCID: PMC2242846.
10. Grakoui A, Bromley SK, Sumen C, Davis MM, Shaw AS, Allen PM, et al. The immunological synapse: a molecular machine controlling T cell activation. Science. 1999; 285(5425):221–7. PMID: 10398592.

11. Depoil D, Zaru R, Guiraud M, Chauveau A, Harriague J, Bismuth G, et al. Immunological synapses are versatile structures enabling selective T cell polarization. Immunity. 2005; 22(2):185–94. doi: 10.1016/j.immuni.2004.12.010 PMID: 15723807.

12. Frederico B, Chao B, May JS, Belz GT, Stevenson PG. A murid gamma-herpesviruses exploits normal splenic immune communication routes for systemic spread. Cell host & microbe. 2014; 15(4):457–70. doi: 10.1016/j.chom.2014.03.010 PMID: 24721574.

13. Stevenson PG, Doherty PC. Non-antigen-specific B-cell activation following murine gammaherpesvirus infection is CD4 independent in vitro but CD4 dependent in vivo. Journal of virology. 1999; 73(2):1075–9. PMID: 9882308; PubMed Central PMCID: PMC103927.

14. Ehtisham S, Sunil-Chandra NP, Nash AA. Pathogenesis of murine gammaherpesvirus infection in mice deficient in CD4 and CD8 T cells. Journal of virology. 1993; 67(9):5247–52. PMID: 8394447; PubMed Central PMCID: PMC237922.

15. Usherwood EJ, Ross AJ, Allen DJ, Nash AA. Murine gammaherpesvirus-induced splenomegaly: a critical role for CD4 T cells. The Journal of general virology. 1996; 77 (Pt 4):627–30. PMID: 8627250.

16. Collins CM, Speck SH. Expansion of murine gammaherpesvirus latently infected B cells requires T follicular help. PLoS pathogens. 2014; 10(5):e1004106. doi: 10.1371/journal.ppat.1004106 PMID: 24789087; PubMed Central PMCID: PMC4006913.

17. Marques S, Efstathiou S, Smith KG, Haury M, Simas JP. Selective gene expression of latent murine gammaherpesvirus 68 in B lymphocytes. Journal of virology. 2003; 77(13):7308–18. PMID: 12805429; PubMed Central PMCID: PMC164786.

18. Pires de Miranda M, Alenquer M, Marques S, Rodrigues L, Lopes F, Bustelo XR, et al. The Gammaherpesvirus m2 protein manipulates the Fyn/Vav pathway through a multidocking mechanism of assembly. PloS one. 2008; 3(2):e1654. doi: 10.1371/journal.pone.0001654 PMID: 18301737; PubMed Central PMCID: PMC2244710.

19. Rodrigues L, Pires de Miranda M, Caloca MJ, Bustelo XR, Simas JP. Activation of Vav by the gammaherpesvirus M2 protein contributes to the establishment of viral latency in B lymphocytes. Journal of virology. 2006; 80(12):6123–35. doi: 10.1128/JVI.02700-05 PMID: 16731951; PubMed Central PMCID: PMC1472561.

20. Madureira PA, Matos P, Soeiro I, Dixon LK, Simas JP, Lam EW. Murine gamma-herpesvirus 68 latency protein M2 binds to Vav signaling proteins and inhibits B-cell receptor-induced cell cycle arrest and apoptosis in WEHI-231 B cells. The Journal of biological chemistry. 2005; 280(45):37310–8. doi: 10.1074/jbc.M507478200 PMID: 16150693.

21. Pires de Miranda M, Lopes FB, McVey CE, Bustelo XR, Simas JP. Role of Src homology domain binding in signaling complexes assembled by the murid gamma-herpesvirus M2 protein. The Journal of biological chemistry. 2013; 288(6):3858–70. doi: 10.1074/jbc.M112.439810 PMID: 23258536; PubMed Central PMCID: PMC3567640.

22. Macrae AI, Usherwood EJ, Husain SM, Flano E, Kim IJ, Woodland DL, et al. Murid herpesvirus 4 strain 68 M2 protein is a B-cell-associated antigen important for latency but not lymphocytosis. Journal of virology. 2003; 77(17):9700–9. PMID: 12915582; PubMed Central PMCID: PMC187398.

23. Liang X, Shin YC, Means RE, Jung JU. Inhibition of interferon-mediated antiviral activity by murine gammaherpesvirus 68 latency-associated M2 protein. Journal of virology. 2004; 78(22):12416–27. doi: 10.1128/JVI.78.22.12416–12427.2004 PMID: 15507628; PubMed Central PMCID: PMC525078.

24. Siegel AM, Herskowitz JH, Speck SH. The MHV68 M2 protein drives IL-10 dependent B cell proliferation and differentiation. PLoS pathogens. 2008; 4(4):e1000039. doi: 10.1371/journal.ppat.1000039 PMID: 18389062; PubMed Central PMCID: PMC2270344.

25. Rangaswamy US, Speck SH. Murine gammaherpesvirus M2 protein induction of IRF4 via the NFAT pathway leads to IL-10 expression in B cells. PLoS pathogens. 2014; 10(1):e1003858. doi: 10.1371/journal.ppat.1003858 PMID: 24391506; PubMed Central PMCID: PMC3879372.

26. Simas JP, Marques S, Bridgeman A, Efstathiou S, Adler H. The M2 gene product of murine gammaherpesvirus 68 is required for efficient colonization of splenic follicles but is not necessary for expansion of latently infected germinal centre B cells. The Journal of general virology. 2004; 85(Pt 10):2789–97. doi: 10.1099/vir.0.80138–0 PMID: 15448339.

27. Jacoby MA, Virgin HWt, Speck SH. Disruption of the M2 gene of murine gammaherpesvirus 68 alters splenic latency following intranasal, but not intraperitoneal, inoculation. Journal of virology. 2002; 76 (4):1790–801. PMID: 11799175; PubMed Central PMCID: PMC135904.

28. Rangaswamy US, O'Flaherty BM, Speck SH. Tyrosine 129 of the murine gammaherpesvirus M2 protein is critical for M2 function in vivo. PloS one. 2014; 9(8):e105197. doi: 10.1371/journal.pone.0105197 PMID: 25122496; PubMed Central PMCID: PMC4133380.

29. Monks CR, Freiberg BA, Kupfer H, Sciaky N, Kupfer A. Three-dimensional segregation of supramolecular activation clusters in T cells. Nature. 1998; 395(6697):82–6. doi: 10.1038/25764 PMID: 9738502.

30. Huppa JB, Davis MM. T-cell-antigen recognition and the immunological synapse. Nature reviews Immunology. 2003; 3(12):973–83. doi: 10.1038/nri1245 PMID: 14647479.

31. Geiger B, Rosen D, Berke G. Spatial relationships of microtubule-organizing centers and the contact area of cytotoxic T lymphocytes and target cells. The Journal of cell biology. 1982; 95(1):137–43. PMID: 6982900; PubMed Central PMCID: PMC2112358.

32. Kupfer A, Dennert G. Reorientation of the microtubule-organizing center and the Golgi apparatus in cloned cytotoxic lymphocytes triggered by binding to lysable target cells. Journal of immunology. 1984; 133(5):2762–6. PMID: 6384372.

33. Kupfer A, Swain SL, Janeway CA Jr., Singer SJ. The specific direct interaction of helper T cells and antigen-presenting B cells. Proceedings of the National Academy of Sciences of the United States of America. 1986; 83(16):6080–3. PMID: 3526350; PubMed Central PMCID: PMC386442.

34. Friedl P, den Boer AT, Gunzer M. Tuning immune responses: diversity and adaptation of the immunological synapse. Nature reviews Immunology. 2005; 5(7):532–45. doi: 10.1038/nri1647 PMID: 15999094.

35. Duchez S, Rodrigues M, Bertrand F, Valitutti S. Reciprocal polarization of T and B cells at the immunological synapse. Journal of immunology. 2011; 187(9):4571–80. doi: 10.4049/jimmunol.1100600 PMID: 21930964.

36. Robertson JM, Jensen PE, Evavold BD. DO11.10 and OT-II T cells recognize a C-terminal ovalbumin 323–339 epitope. Journal of immunology. 2000; 164(9):4706–12. PMID: 10779776.

37. Valitutti S, Dessing M. Measurement of calcium mobilization responses in killer cell/target conjugates by FACS analysis. Methods in molecular biology. 2000; 121:305–11. doi: 10.1385/1-59259-044-6:305 PMID: 10818736.

38. Haller C, Rauch S, Fackler OT. HIV-1 Nef employs two distinct mechanisms to modulate Lck subcellular localization and TCR induced actin remodeling. PloS one. 2007; 2(11):e1212. doi: 10.1371/journal.pone.0001212 PMID: 18030346; PubMed Central PMCID: PMC2075162.

39. Haller C, Rauch S, Michel N, Hannemann S, Lehmann MJ, Keppler OT, et al. The HIV-1 pathogenicity factor Nef interferes with maturation of stimulatory T-lymphocyte contacts by modulation of N-Wasp activity. The Journal of biological chemistry. 2006; 281(28):19618–30. doi: 10.1074/jbc.M513802200 PMID: 16687395.

40. Saxena SK, Shrivastava G, Tiwari S, Swamy MA, Nair MP. Modulation of HIV pathogenesis and T-cell signaling by HIV-1 Nef. Future virology. 2012; 7(6):609–20. doi: 10.2217/FVL.12.42 PMID: 22844345; PubMed Central PMCID: PMC3404840.

41. Thoulouze MI, Sol-Foulon N, Blanchet F, Dautry-Varsat A, Schwartz O, Alcover A. Human immunodeficiency virus type-1 infection impairs the formation of the immunological synapse. Immunity. 2006; 24(5):547–61. doi: 10.1016/j.immuni.2006.02.016 PMID: 16713973.

42. Coscoy L, Ganem D. A viral protein that selectively downregulates ICAM-1 and B7-2 and modulates T cell costimulation. The Journal of clinical investigation. 2001; 107(12):1599–606. doi: 10.1172/JCI12432 PMID: 11413168; PubMed Central PMCID: PMC200195.

43. Cho NH, Feng P, Lee SH, Lee BS, Liang X, Chang H, et al. Inhibition of T cell receptor signal transduction by tyrosine kinase-interacting protein of Herpesvirus saimiri. The Journal of experimental medicine. 2004; 200(5):681–7. doi: 10.1084/jem.20040924 PMID: 15337788; PubMed Central PMCID: PMC2212737.

44. Evans AG, Moser JM, Krug LT, Pozharskaya V, Mora AL, Speck SH. A gammaherpesvirus-secreted activator of Vbeta4+ CD8+ T cells regulates chronic infection and immunopathology. The Journal of experimental medicine. 2008; 205(3):669–84. doi: 10.1084/jem.20071135 PMID: 18332178; PubMed Central PMCID: PMC2275388.

45. Decalf J, Godinho-Silva C, Fontinha D, Marques S, Simas JP. Establishment of murine gammaherpesvirus latency in B cells is not a stochastic event. PLoS pathogens. 2014; 10(7):e1004269. doi: 10.1371/journal.ppat.1004269 PMID: 25079788; PubMed Central PMCID: PMC4117635.

46. Valitutti S, Dessing M, Lanzavecchia A. Role of cAMP in regulating cytotoxic T lymphocyte adhesion and motility. European journal of immunology. 1993; 23(4):790–5. doi: 10.1002/eji.1830230403 PMID: 8384558.

APPENDIX 2

OPEN ACCESS Freely available online

PLOS | PATHOGENS

Establishment of Murine Gammaherpesvirus Latency in B Cells Is Not a Stochastic Event

Jérémie Decalf[•], **Cristina Godinho-Silva**[•], **Diana Fontinha, Sofia Marques, J. Pedro Simas***

Instituto de Medicina Molecular, Faculdade de Medicina, Universidade de Lisboa, Lisboa, Portugal

Abstract

Murid γ-herpesvirus-4 (MuHV-4) promotes polyclonal B cell activation and establishes latency in memory B cells via unclear mechanisms. We aimed at exploring whether B cell receptor specificity plays a role in B cell susceptibility to viral latency and how this is related to B cell activation. We first observed that MuHV-4-specific B cells represent a minority of the latent population, and to better understand the influence of the virus on non-MuHV-4 specific B cells we used the SW_{HEL} mouse model, which produce hen egg lysozyme (HEL)-specific B cells. By tracking HEL^+ and HEL^- B cells, we showed that in vivo latency was restricted to HEL^- B cells while the two populations were equally sensitive to the virus in vitro. Moreover, MuHV-4 induced two waves of B cell activation. While the first wave was characterized by a general B cell activation, as shown by HEL^+ and HEL^- B cells expansion and upregulation of CD69 expression, the second wave was restricted to the HEL^- population, which acquired germinal center (GC) and plasma cell phenotypes. Antigenic stimulation of HEL^+ B cells led to the development of HEL^+ GC B cells where latent infection remained undetectable, indicating that MuHV-4 does not benefit from acute B cell responses to establish latency in non-virus specific B cells but relies on other mechanisms of the humoral response. These data support a model in which the establishment of latency in B cells by γ-herpesviruses is not stochastic in terms of BCR specificity and is tightly linked to the formation of GCs.

Citation: Decalf J, Godinho-Silva C, Fontinha D, Marques S, Simas JP (2014) Establishment of Murine Gammaherpesvirus Latency in B Cells Is Not a Stochastic Event. PLoS Pathog 10(7): e1004269. doi:10.1371/journal.ppat.1004269

Editor: Pinghui Feng, University of Southern California, United States of America

Received March 11, 2013; **Accepted** June 10, 2014; **Published** July 31, 2014

Funding: Research in JPS's lab was supported by a grant from the Portuguese Fundação para a Ciência e Tecnologia (FCT) (PTDC/SAU-MII/099314/2008). JD was recipient of a FCT fellowship. The funders had no role in study design, data collection and analysis, decision to publish, or preparation of the manuscript.

Competing Interests: The authors have declared that no competing interests exist.

* Email: psimas@fm.ul.pt

• These authors contributed equally to this work.

Introduction

The murid γ-herpesvirus-4 (MuHV-4, also known as MHV-68 or γHV-68) has led to valuable insights in understanding human γ-herpesvirus related diseases caused by Epstein-Barr virus (EBV) and Kaposi's sarcoma associated herpesvirus (KSHV) [1]. Whereas primo infection by γ-herpesviruses can be responsible for lymphoproliferative disorders in immune competent hosts, they are usually well controlled [2]. As with EBV, MuHV-4 is mainly lymphotropic and establishes latency in class-switched and germinal center (GC) B cells [3,4]. The course of the infection in mice is now well described (see [5] and [1]). Upon intranasal inoculation, infection starts with an acute lung infection controlled by the $CD8^+$ T cell response. The virus then disseminates to secondary lymph organs via serial events of lymphoid/myeloid cellular exchanges [6] where it promotes a CD4-dependent polyclonal B cell response and finally establishes latency in long-lived memory B cells [1,5,7,8]. This polyclonal B cell activation can lead to the emergence of auto-antibodies but MuHV-4 infection is usually not associated with the development of auto-immune diseases or lymphomas in immune competent mice [9]. $CD4^+$ T cells, and in particular follicular helper T cells [10], have been shown to be essential for the establishment of MuHV-4 latency. Antibody-mediated depletion experiments [11,12] as well as work performed on MHC class II deficient mice [13] (which are $CD4^+$ T cells deficient) have led to similar observations, that the absence of $CD4^+$ T cells leads to lower latency levels.

On the virus side, few proteins have been shown to be involved in the establishment of latency [1]. Among them, M2 has received particular interest for its ability to interfere with B cell activation. Studies performed with M2-deficient MuHV-4 have shown its essential role in the establishment of latency, although it is not required for acute lung infection [14,15]. Biochemical analysis have established that M2 is able to interact with the Fyn/Vav, Plcγ2 and PI3K pathways, involved in BCR signaling [16–18]. In vivo, B cells infected by M2-deficient MuHV-4 have been shown to acquire a GC phenotype comparable with the WT virus, but were unable to class-switch and differentiate into plasma cells [19]. MuHV-4 LANA has recently been shown to stabilize cellular Myc and promotes its activity, leading to B cell proliferation, a process required for GC formation and viral latency [20].

The lower level of viral latency observed in mice deprived of $CD4^+$ T cells as well as with M2-deficient MuHV-4 are good examples showing that the establishment of MuHV-4 latency relies on mechanisms that mix the physiologic B cell response and the intervention of viral modulators. Several questions remain to be explored to better understand this complex interaction: How does MuHV-4 trigger a polyclonal B cell activation? Are latently infected B cells also polyclonal, or is latency restricted to MuHV-4 specific B cells? Finally, what are the respective roles for the virus and the B cells in the establishment of latency?

Until recently, those were difficult questions to address experimentally because of two major hurdles on the virus and the B cell sides. At peak of latency (~14 days post-infection in

Author Summary

Murid γ-herpesvirus-4 (MuHV-4) is a good model to study infectious mononucleosis in mice, in which the virus ultimately establishes life-long latency in B cells. Whereas several viral proteins have been shown to modulate B cell behavior, in the present study we aimed at clarifying the parameters that dictate the establishment of viral latency from the B cell perspective. Indeed, the B cell repertoire is highly diverse and it remains unknown whether latency takes place randomly in B cells. To study this question, we isolated latently infected B cells in which we observed a low frequency of virus-specific B cells, suggesting that viral latency is not restricted to this population. To better understand MuHV-4 influence on non-virus specific B cells, we then followed the fate of B cells specific for a foreign antigen, hen egg lysozyme (HEL). While in vitro experiments showed that HEL-specific B cells could be acutely infected by MuHV-4, these cells were resistant to MuHV-4 latent infection in vivo. These results suggest that while establishment of γ-herpesvirus latency is not restricted to virus-specific B cells, it does not take place randomly in B cells and relies on mechanisms that remain to be identified.

C57BL/6 mice), latently infected B cells represent a low percentage of total B cells [3,4] and tracking these cells was impossible until the development of a YFP expressing MuHV-4 [4]. On the B cell side, questions concerning BCR specificity are delicate to address due to the enormous diversity of the B cell repertoire and to the difficulty to trace one clonal population, but major improvement was made with the development of the switch hen egg lysozyme mice (SW_{HEL}) [21–24]. Based on the MD4 model [25], SW_{HEL} mice have been engineered to contain up to ~10% of HEL-specific B cells. But contrary to MD4 mice, SW_{HEL} HEL^+ B cells can perform GC reactions in a competitive environment, class-switch and differentiate in long-lived memory B cells. Moreover, HEL-specific (HEL^+) and non-specific (HEL^-) populations can easily be distinguished by direct staining of the BCR with fluorescently labeled HEL.

In the present study, we aimed at clarifying the role of BCR specificity in the establishment of MuHV-4 latency in B cells. Taking advantage of the SW_{HEL} mice and the YFP-MuHV-4 we designed experiments to study in parallel how MuHV-4 influences a normal B cell repertoire (HEL^-) and a clonal population of non-virus specific B cells (HEL^+) in order to determine in which population latency is established and how this relates with B cell activation.

Results

MuHV-4 latency is not restricted to virus-specific B cells

To evaluate the frequency of MuHV-4 specific B cells in infected and non-infected populations, we challenged C57BL/6 mice with YFP-MuHV-4. Infected and non-infected $CD19^+$ B cells were sorted at 14 dpi based on their YFP expression and used in an ELISPOT assay to evaluate the number of total IgGs and anti-MuHV-4 IgGs secreting cells (Figure 1A). Both YFP^- and YFP^+ B cells showed a low frequency of virus-specific antibody-secreting cells (ASC) cells when compared to the total ASC. That is, ~10% of total ASC for the YFP^-, and ~1% for the YFP^+ populations, showing that in both populations the majority of ASC are not MuHV-4 specific. As the frequency of GC B cells ($GL\text{-}7^+$, $CD95^+$) is significantly different between YFP^+ and YFP^- B cells (Figure 1B), we tried to refine our analysis by sorting infected and non-infected GC cells based on GL-7 and CD95 expression. Yet, purified cells died quickly and could not be used for ELISPOT assays, probably due to anti-CD95 induced apoptosis [26]. Our ELISPOT assay did not include the monitoring of IgGs specific for non-structural proteins. However, it would be unlikely if they accounted for the 90 to 99% of the ASC not detected in our anti-MuHV-4 IgGs assay. These data indicate that latent infection is not restricted to MuHV-4 specific B cells and that the virus is able to promote the activation of non-virus-specific B cells independently of their infection status. In order to explore these two points, we next used the SW_{HEL} mice [21], which allowed us to monitor MuHV-4 influence on non-virus-specific HEL^+ B cells.

HEL^+ B cells are not latently infected by MuHV-4

SW_{HEL} mice were infected with YFP-MuHV-4 and we monitored YFP expression in HEL^+ and HEL^- B cells 14 dpi (Figure 2A). While we did not detect YFP expression in the HEL^+ population, HEL^- B cells harbored a frequency of YFP^+ cells comparable with what has been previously reported in WT B cells [4]. We confirmed that HEL^- B cells are solely latently infected by sorting HEL^+ and HEL^- B cells on which we monitored reactivation of latent virus by ex vivo explant co-culture assay (Figure 2B) and the presence of viral DNA by limiting dilution PCR (Figure 2C). It is important to note that HEL^- B cells emerge from a spontaneous replacement of the Vh10 exon encoding for the HEL-specific heavy chain leading to the reconstitution of a polyclonal repertoire [21], minimizing the impact of genetic differences between these two populations. However, HEL^+ B cells only belong to the B-2 lineage, while HEL^- differentiate into both B-1 and B-2 B cells [21]. It is unknown in which population of B cells MuHV-4 latency is established. To evaluate if the B-2 bias of the HEL^+ B cells would account for their resistance to latent infection, we phenotyped latently infected cells in C57BL/6 mice (Figure S1). B-2 B cells represented the vast majority of YFP^+ B cells, but a small fraction of latently infected cells was also detected in B-1a and B-1b B cells. The proportion of B-2, B-1a and B-1b in YFP^+ and YFP^- B cells corresponded to what has been described for naïve animals, with the B-2 lineage being dominant in splenic B cells [27]. Overall, these data make it unlikely that the B-2 commitment of HEL^+ B cells would explain their resistance to MuHV-4 latency.

Finally, to monitor that MuHV-4 latency in SW_{HEL} HEL^- B cells reproduces what has been described in a normal repertoire, we determined the phenotype of YFP^+ HEL^- B cells (Figure 3). As for WT B cells (Figure 1B), ~75% of YFP^+ HEL^- B cells harbored a $GL\text{-}7^+$ $CD95^+$ phenotype, with a minor fraction harboring a plasma cell phenotype and ongoing class-switch ($CD138^+$ IgM^-). Together these data show that HEL^+ B cells are not latently infected by MuHV-4 while latency takes place normally in HEL^- B cells.

HEL^+ and HEL^- B cells are both sensitive to MuHV-4 infection in vitro

MuHV-4 poorly infects B cells in vitro [28], but work by Frederico et al overcame this hurdle by developing an in vitro co-culture assay, and showed that MuHV-4 transits by myeloid cells in order to get access to B cells [29]. Taking advantage of this experimental setting we investigated whether the absence of latently infected HEL^+ B cells in vivo was due to an intrinsic resistance of these cells to the virus. As the YFP-MuHV-4 used for in vivo experiments allows the detection of latently infected cells we used in this experiment an EF1α-eGFP$^+$ MuHV-4, in which GFP expression can be detected 48 h post infection. We used in

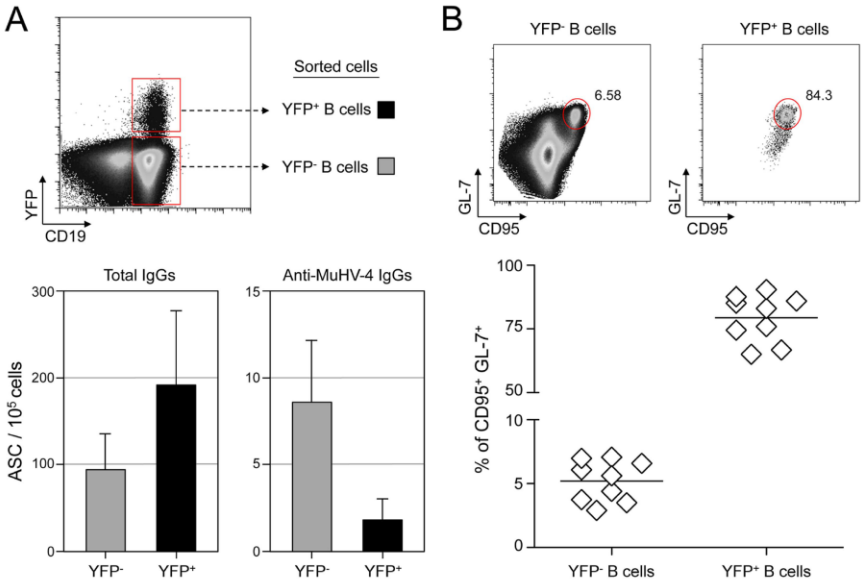

Figure 1. MuHV-4 specific B cells represent a minor part of infected and non-infected cells. (A) As presented in the FACS plot, infected ($CD19^+$ YFP^+, black bars) and non-infected ($CD19^+$ YFP^-, grey bars) B cells were sorted from C57BL/6 mice 14 dpi. Cells were used to assess the frequency of total (left) and MuHV-4 specific (right) antibody-secreting cells (ASC) by ELISPOT. These data are from 3 independent experiments, in each experiment spleens from 3 to 4 mice where pooled before performing the sorts. Post-sorts purities were systematically >95% for YFP^+ B cells and >98% for YFP^- B cells. (B) To monitor the frequency of GC cells in YFP^- and YFP^+ B cells, spleens from YFP-MuHV-4 infected C57BL/6 mice (n = 9) were isolated at 14 dpi for FACS analysis. All the mice harbored a frequency of infected B cells >0,05%, with at least 500 events in the YFP^+ gate. A representative FACS plot showing the frequency of $CD95^+$ $GL\text{-}7^+$ cells is shown on top and compiled data obtained from 4 independent experiments is shown below. Bars represent the average percentage.
doi:10.1371/journal.ppat.1004269.g001

parallel $gp150^+$ and a $gp150^-$ viruses, the later leading to a better B cell infection in co-culture assay [29].

We co-cultured freshly isolated SW_{HEL} splenocytes with infected RAW-264 or BHK-21 cells, or exposed the splenocytes to free viruses (Figure 4). 48 h post co-culture, cells were harvested and GFP expression was monitored in both HEL^+ and HEL^- B cells. Contrasting with our in vivo observations, we observed that both populations were equally sensitive to MuHV-4 infection when co-cultured with infected RAW-264, while they remained not infected with exposed to free virions or co-cultured with infected BHK-21 (Figure 4). Fitting with previous observations, percentages of infection were greater with a gp150-deficient virus. Overall, these in vitro data show that the absence of latently infected HEL^+ B cells in vivo is not due to an intrinsic resistance of these cells to the virus.

MuHV-4 induces transient B cell activation, but HEL^+ B cells are excluded from late phases of the humoral response

MuHV-4 is known to induce proliferation of both T cells and B cells [30]. To evaluate the influence of MuHV-4 on early B cell activation, we performed a kinetic analysis monitoring the number and CD69 expression of HEL^+ and HEL^- B cells isolated from spleen and cervical lymph nodes (CLN) (Figure 5). We observed an increased number of both HEL^+ and HEL^- B cells in the spleen and CLN, which peaked at 14 dpi (Figure 5A), suggesting that MuHV-4-driven B cell proliferation does not rely on the infection status. We monitored CD69 expression by two complementary methods: measuring the intensity of CD69 expression (Figure 5B) and by evaluating the percentage of $CD69^{high}$ cells (Figure 5C). In the spleen, beside a small population of $CD69^{high}$ cells observed on HEL^- B cells at 7 and 14 dpi (Figure 5C), we did not detect a significant increase of CD69 expression on HEL^+ and HEL^- B cells. On the opposite, in the CLN we observed a peak of CD69 expression on both HEL^+ and HEL^- B cells at 7 dpi, which disappeared at 14 dpi. In both organs, YFP^+ B cells were restricted to the HEL^- B cells indicating that this transient activation of HEL^+ B cells is not sufficient to allow viral latency (Figure S2).

As MuHV-4 is known to establish latency in GC B cells, we next monitored the late phase of the B cell response by following the frequency of GC and plasma cells in HEL^+ and HEL^- B cells (Figure 6A & 6B). Although our ELISPOT (Figure 1), proliferation (Figure 5A) and early activation (Figure 5B & 5C) data suggested a polyclonal B cell activation upon MuHV-4 infection, HEL^+ B cells did not acquire a GC or plasma cells phenotype at 14 dpi (Figure 6A). In contrast, HEL^- B cells entered GC reactions and differentiated into plasma cells (Figure 6B). The frequency of YFP^+ cells in HEL^- GC was ~8%, in accordance to what we observed in C57BL/6 mice (Figure 6C).

Spatial organization of the GC is an essential component of the B cell response as it dictates the interaction between B cells and the other cellular players such as follicular helper T cells and dendritic cells [31]. To have an insight into the organization of the HEL^+ and HEL^- B cells in infected mice, we performed immunofluorescent staining on spleen sections from naïve and 14 dpi SW_{HEL} mice (Figure 7). As natural YFP signal was lost during fixation, infected cells were revealed with an Alexa-488 anti-GFP antibody. In naïve mice (Figure 7A), HEL^+ B cells were homogeneously spread in the B cell area of the follicle, and no GFP^+ or GC cells were observed. At 14 dpi, clusters of $GL\text{-}7^+$ cells were present in the B cell area (Figure 7B), in which latently infected cells were found but HEL^+ B cells were excluded. The number of GFP^+ cells

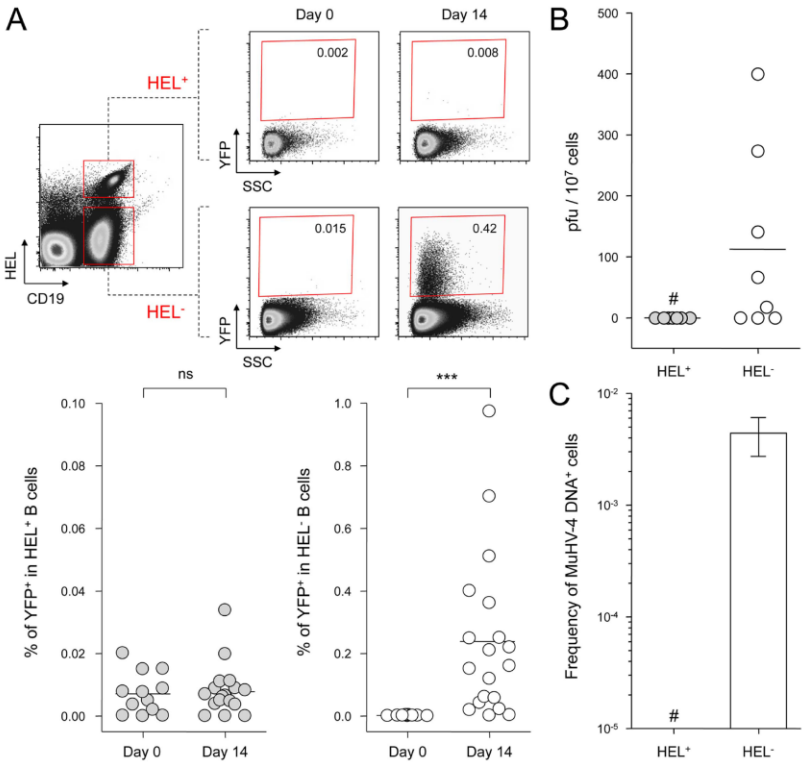

Figure 2. MuHV-4 latent infection is restricted to polyclonal HEL$^-$ B cells. SW_{HEL} mice were left untreated or infected for 14 days with YFP-MuHV-4 virus at 10^4 PFU. Splenocytes were isolated and analyzed by FACS or sorted for plaque assay and limiting dilution PCR analysis. HEL$^+$ and HEL$^-$ B cells were identified based on HEL-A647 binding and CD19 expression. (A) On top are representative FACS plots showing the percentage of YFP$^+$ cells in both populations at 0 and 14 dpi. Data are compiled in the graphics below showing percentage of YFP$^+$ cells in HEL$^+$ (grey circles) and HEL$^-$ (white circles) B cells at day 0 (n = 12) and 14 (n = 16) dpi. The bar represents the average percentage. (B) To detect presence of latent MuHV-4, a plaque assay was performed on sorted HEL$^+$ and HEL$^-$ B cells 14 dpi (n = 8). # indicates that no plaques were detected in HEL$^+$ B cells and based on the average number of HEL+ B cells plated, we estimate the level of latent infection to be <1 PFU/382000 in this population. The analysis of lysed cells showed an absence of preformed viral particles in both populations. (C) Limiting dilution PCR was performed to detect viral genome in sorted HEL$^+$ and HEL$^-$ B cells from day 14 infected SW_{HEL} mice. Data are representative of two independent experiments in which splenocytes were pooled before sorting (n = 3 & n = 2). The frequency of cells harboring MuHV-4 DNA is shown, # indicates signal below the assay's limit of detection. We evaluated the frequency of MuHV-4 DNA$^+$ cells in HEL$^+$ B cells to be ≤1/36770 and ≤1/102891 for the two experiments we performed. Error bars indicate the 95% confidence interval. Purity of sorted cells was systematically above 90%.
doi:10.1371/journal.ppat.1004269.g002

varied greatly between GCs; a heterogeneity also seen in C57BL/6 mice [32]. However, no matter the number of GFP$^+$ cells present, we systematically observed an exclusion of the HEL$^+$ B cells from the GC (Figure 7B).

These histological data confirm our phenotypical analysis (Figure 6) and overall these data show that while HEL$^+$ B cells are sensitive to MuHV-4 infection in vitro (Figure 4) and get activated in vivo (Figure 5), they do not support latent infection and do not participate to the GC reaction induced by MuHV-4.

SW_{HEL} mice develop an anti-MuHV-4 IgG response but fail to secrete long-lasting anti-HEL IgGs

To support our phenotypic and histologic observations, PBS or MuHV-4 challenged SW_{HEL} mice were bled to measure plasmatic levels of anti-MuHV4 and anti-HEL IgG_1, IgG_{2a} and IgG_{2b} (Figure 8). We were not able to quantify the amount of circulating antibodies as no standards were available, but the magnitude of these responses was assessed by systematically analyzing the time points from identical mice together, limiting the impact of technical variations. MuHV-4 has been previously shown to trigger an anti-viral response dominated by the production IgG_{2a} and IgG_{2b} [8] and our kinetic analysis followed the same pattern (Figure 8, left graphic). This response appeared between 7 and 14 dpi and gradually increased. For the anti-HEL response, although we did not detect a HEL$^+$ GC response, we observed a peak of anti-HEL IgG_{2a} and IgG_{2b} antibodies 14 dpi, which declined quickly thereafter (Figure 8, right graphic). Naïve SW_{HEL} mice have a basal level anti-HEL IgGs [21] and the expansion and transient activation of HEL$^+$ B cells observed in the CLN after MuHV-4 infection (Figure 5) could account for this burst of anti-HEL IgGs. However, the fact that this anti-HEL response is transient indicates the absence of a long-term anti-HEL response, fitting with our previous observations.

MuHV-4 does not benefit from acute B cell responses to establish latency in non-virus-specific B cells

Our data show that HEL$^+$ B cells are not latently infected and do not participate in the GC response induced by MuHV-4 while they are equally sensitive to infection in vitro. Moreover, our ELISPOT data show that viral latency is not restricted to virus-specific B cells, indicating that latency is established in B cells of other specificities. This set of observations leads us to propose that

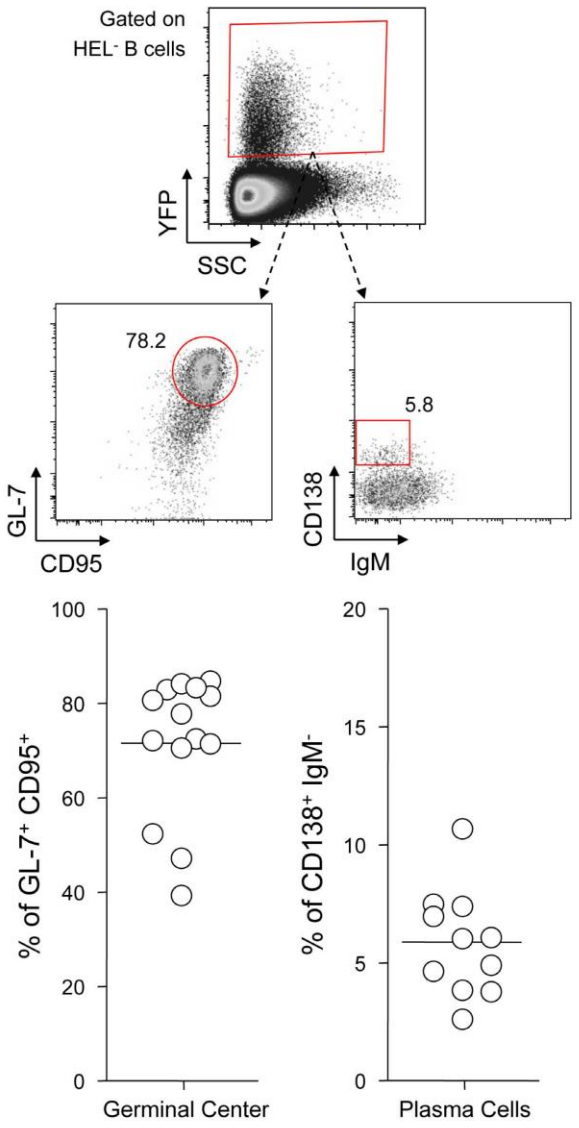

Figure 3. YFP$^+$ HEL$^-$ B cells differentiate into GC and plasma cells. Splenocytes were isolated from SW_{HEL} mice 14 dpi and analyzed by FACS. Cells were gated on the HEL$^-$ CD19$^+$ population. On top is shown a typical phenotype of YFP$^+$ HEL$^-$ B cells, monitoring GC (CD95$^+$ GL-7$^+$) and plasma cells (IgM$^-$ CD138$^+$). Data were compiled in the graphics below; showing the percentage of GC cells (n = 14) and plasma cells (n = 11) in YFP$^+$ HEL$^-$ B cells.
doi:10.1371/journal.ppat.1004269.g003

the establishment of latency is not a stochastic event and takes place in a restricted population of polyclonal B cells. This model implies that MuHV-4 does not overcome the stimulatory signals provided by the BCR stimulation and the cognate CD4 help, but manages to benefit from it in order to settle in long-lived memory B cells.

To test if MuHV-4 could benefit from acute CD4-dependent B cell responses, we stimulated a physiological number of adoptively transferred HEL$^+$ B cells in C57BL/6 mice with sheep red blood cells (SRBC) conjugated to recombinant HEL [23]. We used an adoptive transfer assay in order to avoid competition between HEL$^+$ B cells in SW_{HEL} mice, in particular from being in too great an excess over the available SRBC-specific CD4 help. Indeed, SW_{HEL} immunized with SRBC-HEL showed a poor GC response (~1% of GC HEL$^+$ B cells, Figure S3A) when compared to C57BL/6 adoptively transferred with HEL$^+$ B cells (~70% of GC HEL$^+$ B cells, Figure S3B). We controlled that SRBC-HEL could not induce an endogenous HEL-specific B cell response in C57BL/6 mice by co-transferring SRBC-HEL with or without HEL$^+$ B cells and showed that transferred HEL$^+$ B cells were required for the emergence of HEL$^+$ GC B cells (Figure S3B).

As schematized in Figure 9A, we transferred HEL$^+$ B cells 24 h before infection and immunized the infected mice with SRBC+/− HEL at 0, 4, 7 or 10 dpi. We decided to test different time of immunization, as it is currently unknown when the virus/B cell encounter happens and whether it infects naïve or activated B cells in vivo. At 14 dpi, we monitored the GC differentiation and percentage of infection in HEL$^+$ and HEL$^-$ B cells (Figure 9B). Immunization with SRBC-HEL at either of the time point tested triggered the GC differentiation of HEL$^+$ B cells when compared to mice immunized with SRBC alone (Figure 9B, top left) while it did not affect the GC phenotype of HEL$^-$ B cells (Figure 9B, bottom left). The magnitude of the GC response observed in HEL$^+$ B cells was different between the time of immunization, certainly due to a mixed influence of the GC dynamic and survival of the transferred cells. While we could detect for the first time a HEL$^+$ GC response in the context of MuHV-4 infection, these cells remained YFP$^-$ (Figure 9B, top right), YFP$^+$ cells being restricted to the HEL$^-$ population (Figure 9B, bottom right), in which frequency of infection was not affected by SRBC-HEL immunization. We verified that adoptively transferred B cells could get latently infected by transferring WT CD45.1$^+$ splenocytes into WT CD45.2$^+$ recipient mice and showed that frequency of infection and GC differentiation was equivalent between donor and recipient cells (Figure S4).

These data support the fact that HEL$^+$ GC B cells are resistant to MuHV-4 latency and that MuHV-4 does not benefit from acute B cell responses to establish latency in non-virus-specific B cells, likely relying on other mechanisms yet to be identified.

Discussion

In this study, we attempted at better understanding how γ-herpesviruses establish latency in B cells with a particular focus on the role of the BCR specificity. By following HEL$^+$ B cells in MuHV-4 infected SW_{HEL} mice, we were able to monitor the behavior of non-virus specific B cells during the establishment of MuHV-4 latency and showed that those cells were excluded from the latently infected population.

Previous studies have established that MuHV-4 latency depends on B cell activation and proliferation [33], but it is still not clear whether MuHV-4 can drive such activation independently of BCR specificity. When we compared the proliferation and CD69 expression of HEL$^+$ and HEL$^-$ B cells, we observed that both populations behave in a similar manner, with proliferation in both spleen and CLN and a transient CD69 upregulation in the CLN. This confirms previous work that showed CD69 upregulation on B cells exposed to MuHV-4 in vitro and a temporary B cell proliferation in MHC-II-deficient I-A^b−/− mice [7]. However, HEL$^+$ B cells did not participate to the long-term humoral response, as they did not differentiate into GC or plasma cells. We think we observed here two distinct waves of activatory signals. The first wave triggering a non-specific activation of the global B cell population, followed by a second wave that promotes the differentiation into GC of a restricted pool of B cells. The respective role of these two waves in the establishment of latency is

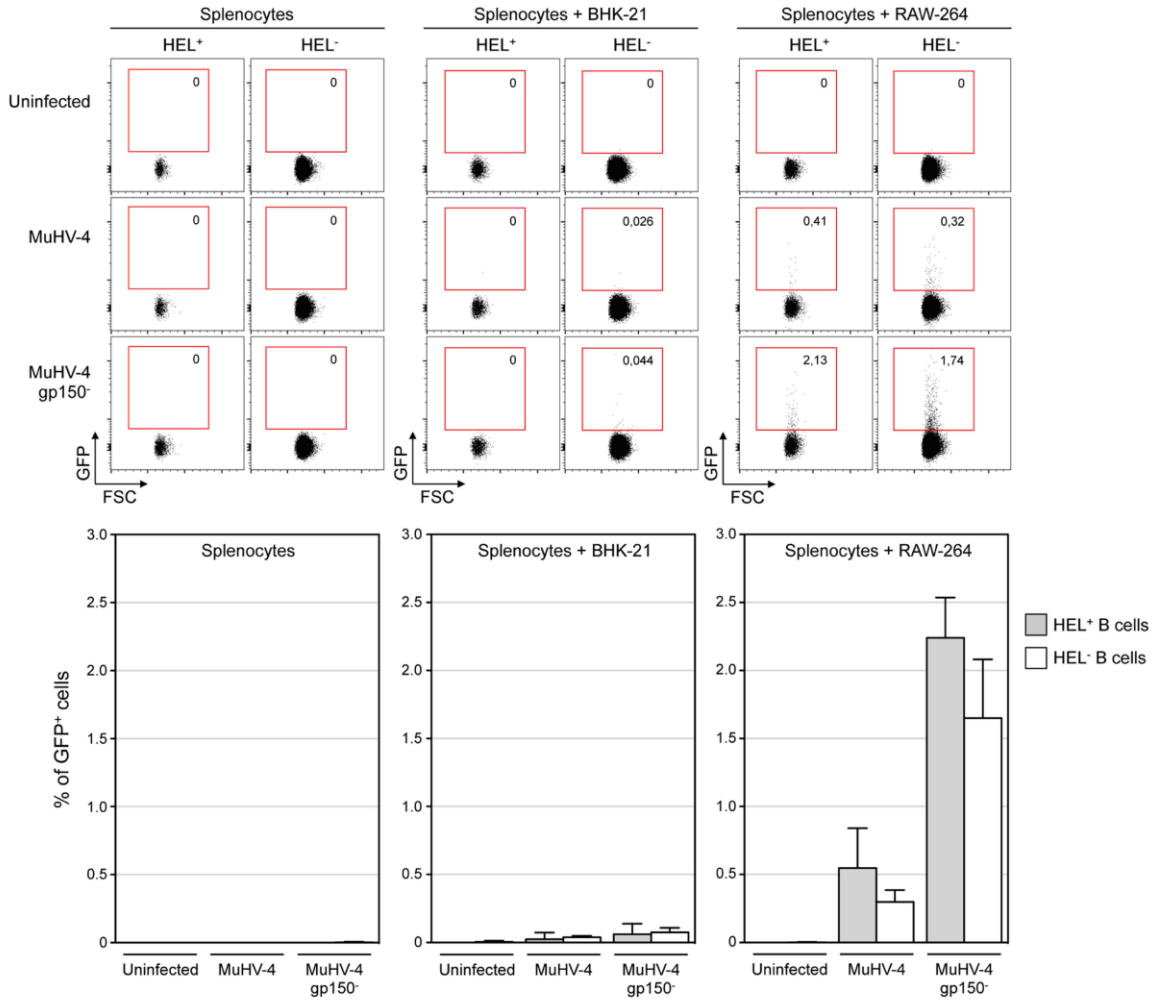

Figure 4. HEL$^+$ and HEL$^-$ B cells are both infected by MuHV-4 in vitro. In vitro infection by co-culture assay was performed as described in the material and methods. Briefly, freshly isolated SW_{HEL} splenocytes were exposed to free viruses or co-culture with BHK-21 or RAW-264 cells previously infected with EF1α-eGFP$^+$ or EF1α-eGFP$^+$-gp150$^-$ MuHV-4. GFP expression in HEL$^+$ and HEL$^-$ B cells was monitored by FACS after 48 h of co-culture. Representative FACS plots are shown on top, compiled data representing average percentage and standard deviation are shown below. Splenocytes were identified based on FSC SSC parameters, excluding BHK-21 and RAW-264. Cells were then gated on CD19$^+$ CD11b$^-$ and GFP expression was monitored in HEL$^+$ and HEL$^-$ B cell. Data were obtained from two independent experiments with two splenocytes suspensions in each.

doi:10.1371/journal.ppat.1004269.g004

not completely clear, but the first wave of activation is not sufficient to allow the establishment of latency in B cells, as supported by the fact that HEL$^+$ B cells do not get latently infected. While we do not identify the mechanism driving the first wave of activation, it has been shown that both T cells and B cells are responsible for the MuHV-4 driven splenomegaly [30], suggesting that the first wave of activation is not due to factors specific of the B cell response, and is probably cytokine mediated.

Concerning the second wave of activation, correlation analysis performed on our dataset showed that frequency of YFP$^+$ cells in HEL$^-$ B cells correlates positively with the magnitude of the GC response (Figure 10). This is in accordance with recent observations by Collins et al who observed a positive correlation between the frequency of YFP$^+$ cells and the frequency of follicular helper T cells, an essential player of the GC response [10]. That said, the fact that HEL$^+$ B cells are sensitive to the virus in vitro but do not get latently infected and are excluded from the GC reaction go against a model where MuHV-4 could drive a stochastic manipulation of the B cells and would instead rely on BCR specificity.

One previous study looked at the influence of MuHV-4 on non-virus specific B cells by reconstituting μMT B cell −/− mice with B cells from MD4 mice (designated HELMET mice [34]). In MuHV-4 infected HELMET, HEL$^+$ B cells expressed CD69 and proliferated but contrary to our results, MuHV-4 latency was detected in HEL$^+$ B cells by PCR. The absence of competition in HELMET mice, where B cells are all HEL-specific could account for these discrepancies. Indeed, in SW_{HEL} mice, HEL$^+$ B cells coexist with a majority of polyclonal B cells. Our in vitro infection by co-culture assay supports the fact that HEL$^+$ B cells are sensitive to MuHV-4, suggesting that a selection mechanism might occur in vivo, leading to the disappearance of these infected cells. In HELMET mice, the absence of competition could allow for the survival of latently infected HEL$^+$ B cells. This role for competition

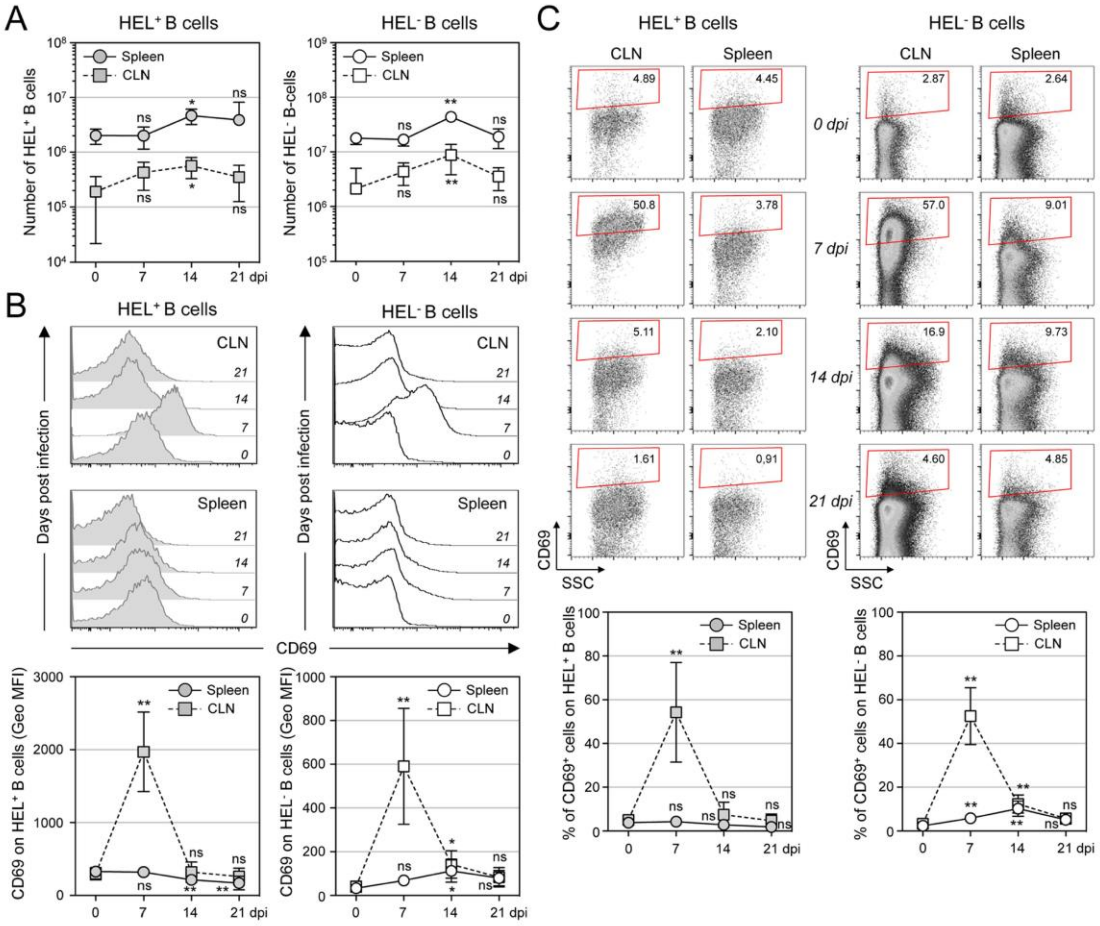

Figure 5. Proliferation and transient activation of total B cells. Spleens and CLN from YFP-MuHV-4 infected SW_{HEL} mice were harvested at 0, 7, 14 and 21 dpi and cells were stained with CD69 PE, CD19 APC-Cy7 and HEL-A647. (A) Live cells were enumerated, and the number of HEL^+ and HEL^- B cells was established based on their frequency obtained from the FACS data. (B) Representative FACS histograms showing CD69 expression on HEL^+ (grey curves) and HEL^- (white curves) B cells isolated from CLN and spleen at the different time points are shown. CD69 was monitored by measuring the Geo MFI and compiled values are shown in the graphic below. (C) On the same samples, the frequency of $CD69^{high}$ cells was evaluated. Representative FACS plots are shown and compiled percentages are presented in the graphic below. These data were obtained from two independent experiments, with a total 5 to 6 mice per time point. In the graphics, mean values are reported and error bars represent the standard deviation.

doi:10.1371/journal.ppat.1004269.g005

is supported by the work of Kim et al [35] who studied how latency evolved in mice containing $CD40^+$ and $CD40^-$ B cells. Although the two populations got latently infected, latency was ultimately lost in $CD40^-$ B cells and GC differentiation was restricted to $CD40^+$ B cells.

To explore whether the presence of CD4 T cell dependent antigens could be involved in the selection of latently infected cells, we triggered an endogenous anti-HEL response concomitantly with MuHV-4 infection. Although we were able to induce the emergence of HEL^+ GC B cells, these cells remained refractory to latent infection. These data support that, at least in our experimental setting, MuHV-4 cannot hitchhike an acute humoral response to gain access to GC B cells and might instead benefit from other antigen/BCR interactions. In humans, it is estimated that up to 20% of a normal B cell repertoire is made of self-reactive B cells that need to be constantly kept under control [36,37]. One of the tolerance mechanism is the induction of a functional unresponsive state known as anergy, which requires endogenous BCR signaling [38,39]. The high prevalence of self-reactive B cells offers a good opportunity for γ-herpesviruses to manipulate these processes in order to retrieve B cells from their anergic state and promote polyclonal B cells activation in an antigen-dependent manner. Supporting this point, recent studies performed in humans [40] and mice [41,42] have shown that γ-herpesviruses are found in self-reactive B cells. Two studies have explored MuHV-4 impact on anergic B cells [42,43], but it is still not clear how MuHV-4 can modulate this processes. SW_{HEL}×ML5 mice [21], in which HEL^+ B cells are anergic due to the presence of soluble HEL, could be an alternative model to study the influence of the virus on competent anergic B cells.

Further work will be required to elucidate how MuHV-4 promotes GC B cells differentiation independently of their infection status, and how this event is linked to the establishment of latently infected B cells in memory B cells. γ-herpesviruses are known to be

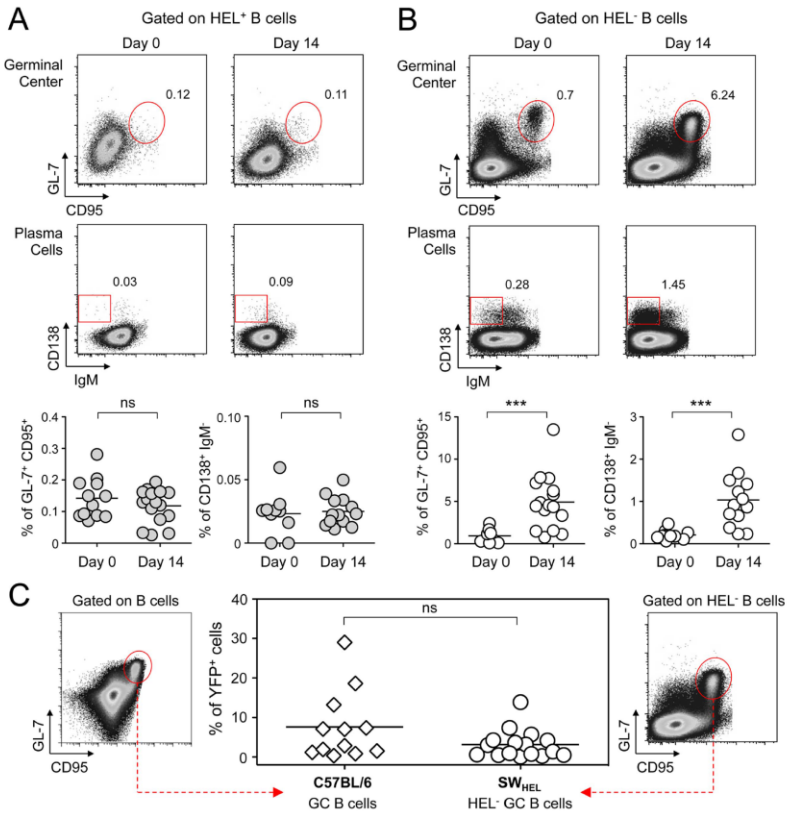

Figure 6. GC and plasma cell differentiation are restricted to the HEL$^-$ B cells. Splenocytes were purified from SW_{HEL} mice at 0 and 14 dpi and analyzed by FACS. Cells were gated on (A) HEL$^+$ or (B) HEL$^-$ B cells for phenotype analysis, monitoring the frequency of GC (CD95$^+$ GL-7$^+$) and plasma cells (IgM$^-$ CD138$^+$). Top parts of the figures show representative FACS plots, bottom parts are the compilation of data obtained from different SW_{HEL} mice (GC: day 0 n = 12; day 14 n = 16/Plasma cells: day 0 n = 10; day 14 n = 13). (C) Germinal center cells in C57BL/6 B cells and HEL$^-$ B cells harbor an equivalent frequency of YFP$^+$ cells. Frequency of YFP$^+$ cells in GC cells was evaluated 14 dpi by gating on the CD95$^+$ GL-7$^+$ population from total B cells of C57BL/6 mice (left dot plot and diamonds, n = 12) or from HEL$^-$ B cells of SW_{HEL} mice (right dot plot and circles, n = 16). The bar represents the average percentage.
doi:10.1371/journal.ppat.1004269.g006

mildly pathogenic in immune-competent hosts and it has been shown that MuHV-4 latent infection does not induce autoimmune disorders and actually confers protection in lupus-prone animals [41]. This highlights the fact that the interrelationship between MuHV-4 and B cells is complex and that co-evolution between γ-herpesviruses and their host as allowed for the emergence of subtle mechanisms that promote B cell activation but limits associated immune disorders in order to establish life-long latency.

Materials and Methods

Ethics statement

This study was carried out in strict accordance with the recommendations of the Portuguese official Veterinary Directorate, which complies with the Portuguese Law (Portaria 1005/92). The Portuguese Experiments on Animal Act strictly comply with the European Guideline 86/609/EEC and follow the FELASA (Federation of European Laboratory Animal Science Associations) guidelines and recommendations concerning laboratory animal welfare. All animal experiments were approved by the Portuguese official veterinary department for welfare licensing under the protocol number AEC_2010_017_PS_Rdt_General and the IMM Animal Ethics Committee.

Mice

SW_{HEL} mice [21] were obtained from Dr Antonio Freitas, Institut Pasteur, Paris, in accordance with Dr Robert Brink, Garvan Institute, Melbourne. To screen for expression of the V_H10_{tar} heavy chain and the $V_κ10$-κ light chain genotyping was performed on DNA isolated from mouse-tails using DirectPCR solution (Viagen). Mice heterozygous for both genes were used for experiments. HEL$^+$ B cells were identified by FACS and confocal microscopy (see details below) by direct labeling with recombinant HEL (Sigma-Aldrich) conjugated with Alexa 647 (noted HEL-A647). This conjugation was made with the Alexa Fluor Antibody Labeling Kit (Invitrogen) following manufacturer instructions. A Bio-Gel P-6 (Biorad) loaded column was used to separate HEL-A647 conjugates from free dye. C57BL/6, CD45.1 and CD45.2 mice and were purchased from Charles Rivers Laboratories. Mice were between 7 and 15 weeks old at time of infection and were sacrificed by CO_2 inhalation or cervical dislocation.

Viruses

The YFP expressing MuHV-4 [4] was obtained from Dr Samuel Speck, Emory Vaccine Center, Atlanta. EF1α-eGFP$^+$ MuHV-4 and EF1α-eGFP$^+$-gp150$^-$ MuHV-4 [29] were obtained

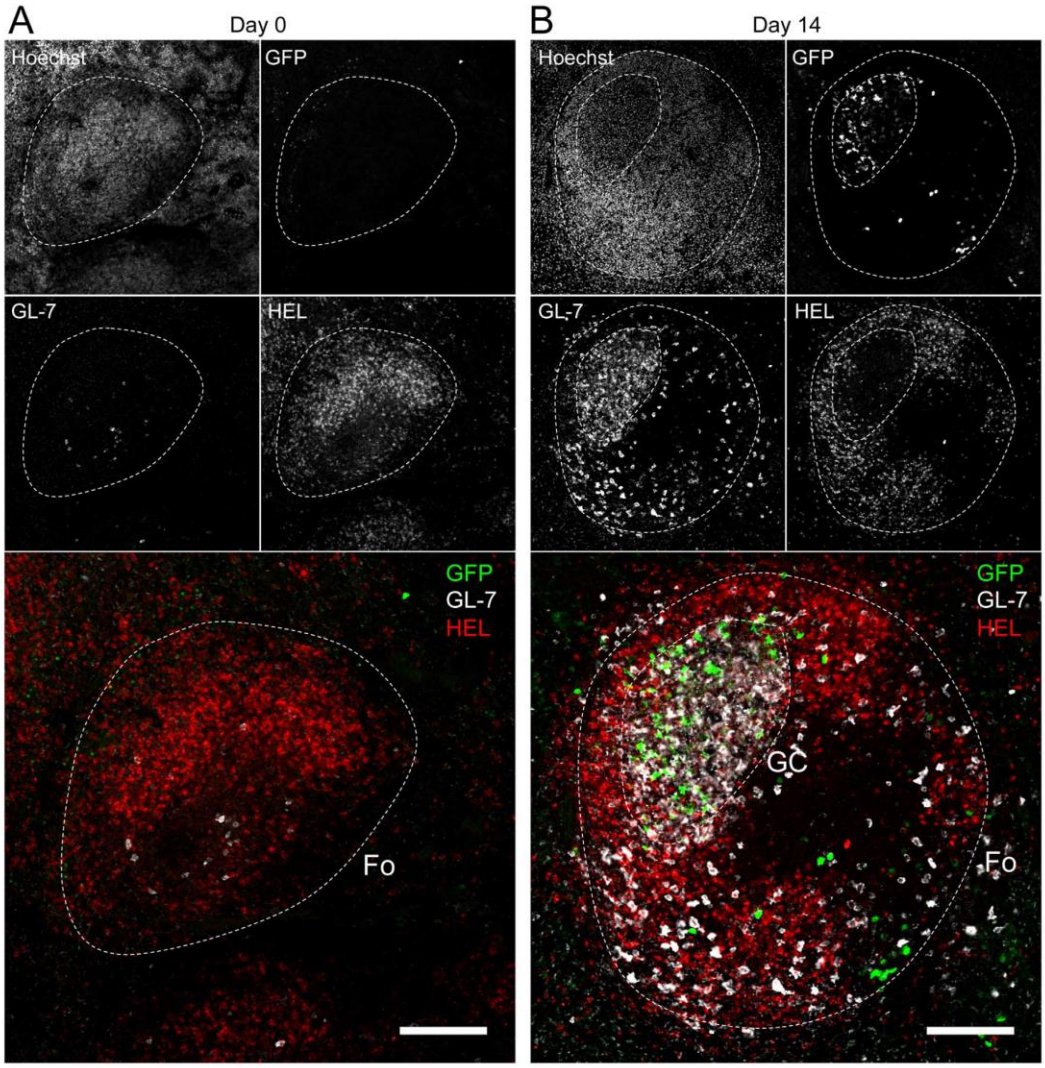

Figure 7. HEL$^+$ B cells are excluded from the GC. Spleens were isolated from (A) day 0 (n = 2) and (B) day 14 (n = 4) infected SW_{HEL} mice for microscopy analysis. Spleens were treated as indicated in the material and methods, and stained with an anti-GFP, anti-GL-7, HEL and nuclei dye Hoechst. Separate channels are shown as thumbnails, in the merge image below nuclei were excluded for clarity. Follicles (Fo) were localized based on Hoechst signal, showing delimited clusters of nuclei. GCs were identified as clusters of GL-7$^+$ cells. Spleen sections were thoroughly analyzed and images shown are typical organization of splenic follicles of SW_{HEL} mice at 0 and 14 dpi. At 14 dpi, infected cells were mainly localized within the GC, from which HEL$^+$ B cells were systematically excluded. Scale bars represent 100 μm.
doi:10.1371/journal.ppat.1004269.g007

from Philip Stevenson, University of Cambridge, Cambridge. Viral stocks were prepared by infecting BHK-21 cells and titrated by plaque assay using previously published procedures [44,45]. For infections, mice were anaesthetized with isoflurane and inoculated intranasally with 10^4 pfu of YFP-MuHV-4 under 20 μl of PBS.

IgGs secreting cells ELISPOT assay

ELISPOT assay to enumerate MuHV-4 specific B cells was adapted from [8]. Briefly, purified MuHV-4 were disrupted for 10 min in PBS+0.05% Triton X-100 and plated at 5×10^6 PFU/well in 96-well MultiScreen HA mixed cellulose filter plates (Millipore, Billerica, MA). Plates were incubated overnight at 4°C, washed with PBS and blocked for 1 h at 37°C with complete medium (RPMI-1640+10% heat inactivated FBS, 2 mM glutamine, 100 U/ml penicillin and streptomycin and 1 mM sodium pyruvate). Latently infected (CD19$^+$ YFP$^+$) and non-infected (CD19$^+$ YFP$^-$) B cells were sorted from spleens on a FACS Aria (BD Biosciences). Serial four-fold dilutions of sorted cells were prepared in complete medium and added under 100 ul/well in four replicate wells per cell amount. Cells were incubated overnight at 37°C in a humid 5% CO_2 incubator. Plates were washed with PBS and incubated for 2 h at room-temperature with Alkaline phosphatase (AP)-conjugated rabbit anti-mouse IgG (H+L) antibodies (Southern Biotech) diluted 1/500 in PBS+0.5% FBS. After thorough washes spots were revealed at room temperature with 1 mg/ml of 5-bromo-4-chloro-3-indolyl phosphate (Sigma) in diethanolamine buffer. Upon optimal spot development plates were washed and dried. Blue spots representing single antibody-secreting cells (ASC) were counted under an Olympus SZ51

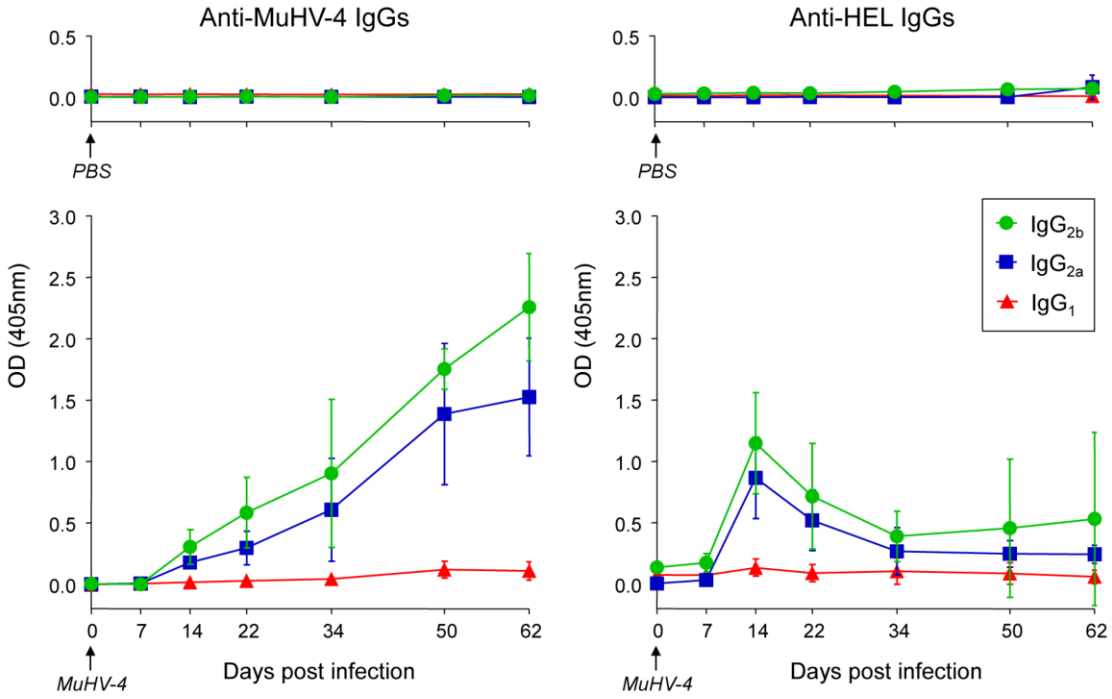

Figure 8. SW_{HEL} mice mount a long-lasting anti-MuHV-4 antibody response. SW_{HEL} mice were inoculated intranasally with PBS (n = 2) or MuHV-4 (n = 6). At indicated time points, mice were bled and sera were analyzed by ELISA to monitor levels of circulating anti-MuHV-4 and anti-HEL IgG_1 (red triangles), IgG_{2a} (blue squares) and IgG_{2b} (green circles). For MuHV-4 infected mice, 3 independent experiments with 2 mice in each were analyzed. As no standard were available to quantify these antibodies, samples of different time points from identical mice were run together to be able to compare the absorbance at 405 nm.
doi:10.1371/journal.ppat.1004269.g008

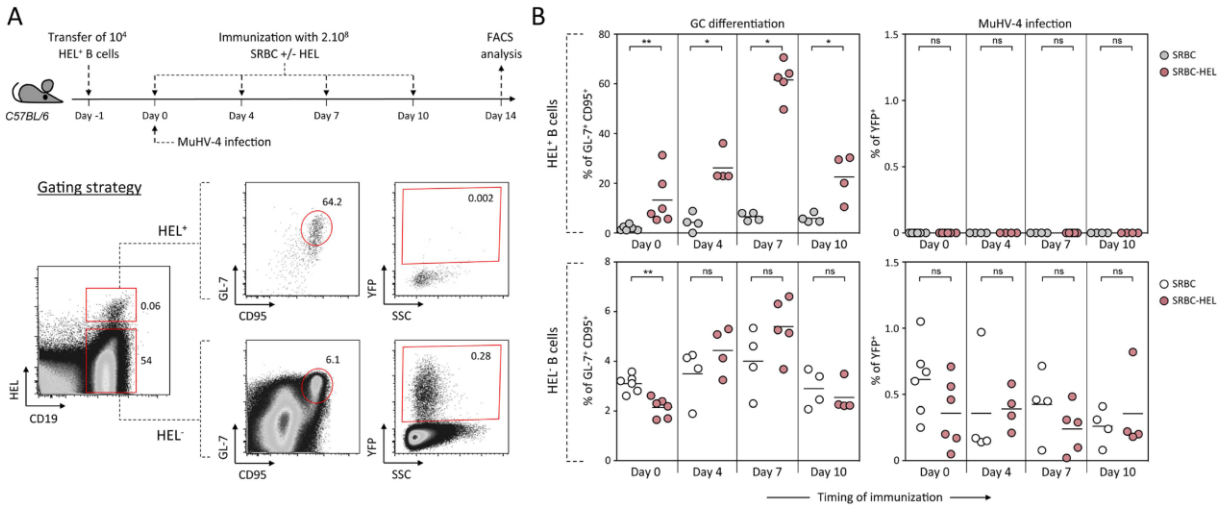

Figure 9. Activated HEL^+ B cells remain refractory to MuHV-4 infection. (A) Experimental design: Bulk SW_{HEL} splenocytes containing 10^4 HEL^+ B cells were transferred in C57BL/6 mice 24 h prior YFP-MuHV-4 infection. Recipient mice were challenged intravenously by a single immunization with 2.10^8 SRBC or SRBC-HEL performed at 0, 4, 7 or 10 dpi. At 14 dpi, spleens were collected and analyzed by FACS. As shown in the representative FACS plots, transferred HEL^+ were identified with HEL-A647 staining while transferred HEL^- B cells could not be discriminated from endogenous B cells. On both HEL^+ and HEL^- (transferred+endogenous) B cells, GC differentiation and percentage of infection was determined using GL-7/CD95 and YFP expression respectively. (B) For each time of immunization, frequency of GC B cells and YFP^+ B cells were compared between SRBC and SRBC-HEL immunized mice in both HEL^+ (top panel) and HEL^- B cells (bottom panel). Each dot represents an individual mouse and bars represent the average percentages. The data were obtained from 4 to 6 mice per experimental group.
doi:10.1371/journal.ppat.1004269.g009

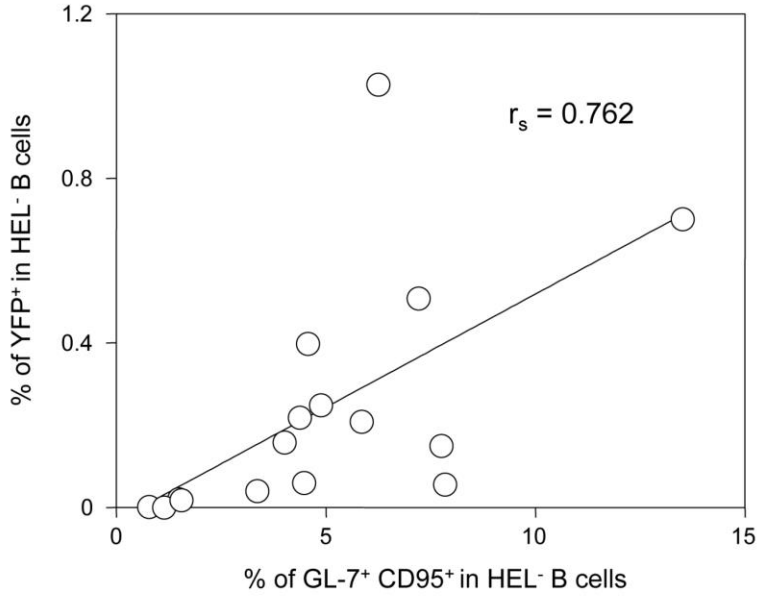

Figure 10. The frequency of infection correlates with the magnitude of the germinal center response in HEL$^-$ B cells. To study the interrelationship between the GC response and the frequency of YFP$^+$ cells, matched data obtained from SW_{HEL} mice 14 dpi (n = 16) were plotted against each other. For each SW_{HEL} mouse, the Y-axis shows the frequency of YFP$^+$ cells in HEL$^-$ B cells (data from Figure 2A) and the X-axis shows the frequency of GC (data from Figure 6B). R_s was calculated using Spearman's rank correlation coefficient.
doi:10.1371/journal.ppat.1004269.g010

microscope. Total number of ASC were determined as described above except that plates were coated with 0.5 µg/well of a goat anti-mouse κ antibodies (Southern Biotech) diluted in PBS.

In vitro infection by co-culture assay

In vitro infection by co-culture assay was adapted from [29]. 24 h prior co-culture, 3.10^5 RAW-264 and BHK-21 cells were seeded in 24-well plate. After cell adhesion (4–6 h), media was removed and cell infected overnight with indicated MuHV-4 at 9.10^5 pfu per condition. The next day, spleens were harvested and single cell suspensions were prepared by spleen disruption, filtration on 100 µm cell strainer and red blood cells removal by centrifugation on ficoll gradient (Biowest). Splenocytes were washed and added to cells at 10^6/well. As a negative control, splenocytes were exposed to free viruses. In order to have enough cells to work with, spleens from two SW_{HEL} mice were pooled. For each experiments, two suspensions were analysed in parallel. After 48 h of co-culture, cells were harvested and stained with CD11b (to exclude RAW-264 cells), CD19 and HEL. Infection of RAW-264 was systematically evaluated 24 h post infection by monitoring GFP expression in cells not co-cultured with splenocytes (data not shown).

Flow cytometry

Single cell suspensions were prepared from spleens. Red blood cells were lysed in hypotonic NH_4Cl and stainings were performed at 4°C in PBS+4% FCS and 1 mM EDTA. Briefly, cells were blocked by 10 min incubation with FcBlock (anti-CD16/32, 2.4G2, BD bioscience), washed, and stained for 20 min. For biotinilated antibodies, extra 20 min incubation with streptavidin was performed. MuHV-4 infected cells were monitored based on their endogenous YFP expression. The following antibodies were used: anti-CD69 PE (H1.2F3), anti-CD95 PE (Jo2), anti-CD19 APC-Cy7 or APC-H7 (1D3), anti-IgM PE (R6-60.2), anti-IgD Biotin (11-26c.2a), CD11b PE or v450 (M1/70) (BD Biosciences); CD45.2 Brilliant Violet 510 (104) (BioLegend); anti-CD45.1 PeCy7 (A20), and anti-GL-7 Biotin (Ebioscience). Streptavidin-Cy5 (BD Biosciences) was used to reveal biotinilated antibodies. HEL specific B cells were identified with the HEL-A647 conjugate described above. Samples were acquired on a FACS Canto or on a LSR Fortessa (BD Biosciences), using DIVA software (BD Biosciences) for acquisition and Flowjo v.6.4.7 (Tree Star) for analysis. Cells were gated on live cells based on FSC/SSC parameters and cell doublets were excluded based on FSC-W signal.

Immunofluorescence histology

Spleens were fixed overnight at 4°C in periodate-lysin-paraformaldehyde (PLP) [46,47] and dehydrated by successive 2 h incubation in 10%, 20% and 30% sucrose solutions at 4°C. Spleens were then embedded in OCT (Tissue Tek), frozen and sectioned (40 µm). For immunofluorescence staining, sections were encircled with a Fatpen and rehydrated 10 min in phosphate buffer. All incubations were made in humid chamber, protected from light. Sections were permeabilized for 1 h at room temperature in 1% triton and blocked 1 h in 1% BSA+FcBlock (anti-CD16/32, 2.4G2, BD bioscience). Stainings were performed using the following reagents: anti-GFP Alexa 488 (Invitrogen), anti-GL-7 Biotin (GL-7, Ebioscience), HEL-A647 (described above) and Hoechst 33343 (Invitrogen). Streptavidin Alexa568 (Invitrogen) was used for biotinilated antibodies, incubated 1 h at room temperature. Slides were washed, mounted in Fluoromount-G (SouthernBiotech) and kept at 4°C. Images were acquired on a LSM 510 META point scanning confocal microscopes (Zeiss) and analyzed using LSM Image Browser (Zeiss) and Photoshop CS2 (Adobe).

Cell sorting and in vitro reactivation assay

HEL^+ B cells ($CD19^+$, HEL^+) and HEL^- B cells ($CD19^+$, HEL^-) were sorted using a FACS Aria (BD Biosciences) and used for in vitro reactivation assay to quantify latent infection. Serial dilutions of freshly isolated cells were co-cultured with BHK-21 in complete media supplemented with 50 µg/ml of Gentamycin (Invitrogen). Lysing half of the sorted cells by a quick freeze/thaw cycle before coculture allowed us to assess the presence of preformed viral particles, indicative of lytic infection. After 5 days, BHK-21 were fixed with 4% paraformaldehyde and stained with toluidine blue for plaque counting. The number of plaques in each sample was expressed as plaques forming unit (pfu)/10^7 cells.

Limiting dilution PCR analysis

The frequency of virus-genome-positive cells was determined from pools of 2 to 3 spleens by limiting dilution combined with real-time PCR as previously described [48]. Sorted HEL^+ and HEL^- B cells were serially two-fold diluted and eight replicates of each dilution were analysed by real time PCR (Rotor Gene 6000, Corbett Life Science). The primer/probe sets were specific for the MuHV-4 M9 gene (5′ primer: GCCACGGTGGCCCTCTA; 3′ primer: CAGGCCTCCCTCCCTTTG; probe: 6-*FAM*-CTTCTGTTGATCTTCC–*MGB*). Samples were subjected to a melting step of 95°C for 10 min followed by 40 cycles of 15 s at 95°C and 1 min at 60°C. Positive *vs.* negative reactions were scored using the Rotor Gene 6000 software. Our data were compatible with the single-hit Poisson model (SHPM) as tested by modeling the limiting dilution data according to a generalized linear log-log model fitting the SHPM and checking this model by an appropriate slope test as described [3,49]. A regression plot of input cell number against log fraction-negative samples was used to estimate the frequency of cells with viral genomes. Estimation of the cell subset frequency of MuHV-4 infection consisted of computation by maximal-likelihood estimation as follows: let f be the estimate of the cell frequency; the maximum likelihood of f is the value of f that maximizes

$$\log(L)=\sum_{i=1}^{k}\left[\log\left(\frac{n!}{ri!(ni!-ri!)}\right)+ri\log(Pi)+(ni-ri)\log(1-Pi)\right]$$

where $\log(L)$ is the natural logarithm of the likelihood function L and Pi is given by $Pi=exp(-f\ xi)$ according to the SHPM. The variance of f was calculated as the negative reciprocal of the second derivative of $\log(L)$, $\mathrm{var}(f)=1/[d^2\ \log(L)/df^2]$. The 95% confidence interval (CI) for f was calculated as 95% CI $(f)=f\pm1.96\mathrm{SE}\ (f)$. Abbreviations are as follows: $k=$ the number of groups of replicate PCRs, numbered $i=1,\ 2,\ \ldots\ k$; $ni=$ the number of replicate reactions; $ri=$ the number of observed negative PCRs; and $mi=$ the observed fraction of negatives $(mi=ri/ni)$.

Adoptive transfers and SRBC+/−HEL immunization

Freshly isolated bulk splenocytes from SW_{HEL} mice containing 10^4 HEL^+ B cells were transferred into C57BL/6 mice by intravenous injection, as previously described [50]. Sheep red blood cells (SRBC) were obtained from Miguel Fevereiro, Laboratório Nacional de Investigação Veterinária, Lisbon. Recombinant HEL was covalently conjugated to SRBC with 1-ethyl-3-(3-dimethylaminopropyl)-carbodiimide hydrochloride (Sigma-Aldrich) as described [25]. Conjugation was confirmed by FACS by staining mock or HEL-conjugated SRBC with the HyHEL10 (an anti-HEL IgG_1 [21]) followed by an anti-IgG_1 APC (BD Biosciences). HEL-A647 was used to identify transferred HEL^+ B cells.

Anti-HEL and anti-MuHV-4 IgGs ELISA

To measure anti-HEL and anti-MuHV-4 antibody production, sera were regularly collected by facial-vein bleeding. To measure HEL-specific antibodies, maxisorp plates (Nunc) were coated with 60 µl of recombinant HEL (10 µg/ml) diluted in NPP buffer (adapted from [21]). For MuHV-4 antibodies, plates were coated with viral particles disrupted with 0,1% triton and diluted in NPP buffer (adapted from [7]). Coated plates were incubated overnight at 4°C and blocked for 1 h with 100 µl PBS+1% BSA. Sera were diluted to 1/200 in PBS+0,1% BSA and 50 µl were incubated 2 h at room temperature. IgG_1, IgG_{2a} and IgG_{2b} subclasses were measured using 50 µl of anti-mouse IgG_1, IgG_{2a} and IgG_{2b} conjugated to alkalyne-phosphatase (SouthernBiotech) diluted to 1/500 and incubated 1 h at room temperature. Bound antibodies were revealed using 100 µl of 1 mg/ml P-Nitrophenyl Phosphate (MP Biomedical) prepared in NPP buffer and incubated 40 min at 37°C. Absorbance was measured at 405 nm.

Statistics

p values were calculated using non-parametric Mann-Whitney U test; ns indicates $p>0.05$, * indicates $p\leq0,05$, ** indicates $p\leq0,005$, and *** indicates $p\leq0,001$.

Supporting Information

Figure S1 B-2 lineage represents the majority of latently infected B cells. C57BL/6 (n = 5) were infected with YFP-MuHV-4 and spleens were analyzed 14 dpi. Cells were stained with CD19, CD5 and CD43 to identify B-2 ($CD5^-$ $CD43^-$), B-1a ($CD5^+$ $CD43^+$) and B-1b ($CD5^-$ $CD43^+$) B cells. (A) Representative FACS plots from YFP^- (left) and YFP^+ (right) B cells are shown. (B) Average population percentages obtained from the 5 mice are shown for the YFP^- (grey bars) and YFP^+ (black bars) B cells.
(TIF)

Figure S2 MuHV-4 is restricted to HEL^- B cells in both LNs and spleen (complement to Figure 5). Spleens and CLN from YFP-MuHV-4 infected SW_{HEL} mice were harvested at 0, 7, 14 and 21 dpi and cells were stained with CD69 PE, CD19 APC-Cy7 and HEL-A647. Frequency of infected cells was monitored in HEL^+ (Left panel) and HEL^- B cells (right panel) based on YFP expression. Representative FACS plots are shown and compiled percentages are presented in the graphic below. These data were obtained from two independent experiments, with a total of 5 to 6 mice per time point. In the graphics, mean values are reported and error bars represent the standard deviation.
(TIF)

Figure S3 Poor GC response in SW_{HEL} mice and absence of endogenous HEL^+ B cell activation in C57BL/6 challenged with SRBC-HEL. (A) SW_{HEL} mice were immunized intravenously with 2.10^8 SRBC (n = 3) or 2.10^8 SRBC-HEL (n = 3). 7 days post-challenge splenocytes were harvested and analyzed by FACS. Representative FACS plots shows frequency of GC cells ($CD95^+$ $GL\text{-}7^+$) in HEL^+ B cell from mice challenged with SRBC or SRBC-HEL. (B) C57BL/6 were immunized intravenously with 2.10^8 SRBC-HEL in presence (n = 3) or absence (n = 3) of co-transferred 10^4 HEL^+ B-cells. 7 days post-challenge splenocytes were harvested and analyzed by FACS. Representative FACS plots shows the frequency of HEL^+

B-cells and their GC phenotype ($CD95^+$ $GL\text{-}7^+$) in each condition. A HEL^+ B cell population with a GC phenotype was only detected when HEL^+ B cells were co-transferred with SRBC-HEL, indicating that SRBC-HEL alone induced an undetectable HEL-specific response in C57BL/6.
(TIF)

Figure S4 Adoptively transferred B cells get latently infected. 24 h prior MuHV-4 YFP infection, CD45.2 C57BL/6 recipient mice (n = 6) received intravenously 10^7 bulk splenocytes freshly isolated from CD45.1 C57BL/6 donor mice. At 14 dpi, spleens were isolated and cells stained with anti-CD19, CD95 and GL-7 as well as with anti-CD45.1 and CD45.2 in order to discriminate between donor ($CD45.1^+$) and endogenous ($CD45.2^+$) B cells. MuHV-4 infection in $CD45.1^+$ and $CD45.2^+$ B cells was evaluated by monitoring the frequency of YFP^+ cells in each population (top panel). GC phenotype was assessed by monitoring CD95 and GL-7 expression on $CD45.1^+$ and $CD45.2^+$ B cells (central panel) as well as on YFP^+ B cells in each population (bottom panel). For each panel, representative FACS plots and compiled data are shown. Bars represent average percentages.
(TIF)

Acknowledgments

We would like to thanks the Histology, Flow Cytometry and Bio-Imaging units of the Instituto de Medicina Molecular for their assistance in performing these experiments. We also thank Bruno Frederico (University of Cambridge) for his help with the in vitro co-culture assay. We finally acknowledge Tri Giang Phan (Garvan Institute, Sydney) and Philip Stevenson (University of Cambridge) for the thoughtful discussions and feedback.

Author Contributions

Conceived and designed the experiments: JD CGS SM JPS. Performed the experiments: JD CGS DF SM. Analyzed the data: JD CGS DF SM JPS. Wrote the paper: JD JPS.

References

1. Barton E, Mandal P, Speck SH (2011) Pathogenesis and host control of gammaherpesviruses: lessons from the mouse. Annu Rev Immunol 29: 351–397. doi:10.1146/annurev-immunol-072710-081639.
2. Thorley-Lawson DA, Gross A (2004) Persistence of the Epstein-Barr virus and the origins of associated lymphomas. N Engl J Med 350: 1328–1337. doi:10.1056/NEJMra032015.
3. Marques S, Efstathiou S, Smith KG, Haury M, Simas JP (2003) Selective gene expression of latent murine gammaherpesvirus 68 in B lymphocytes. J Virol 77: 7308–7318. doi:10.1128/JVI.77.13.7308-7318.2003.
4. Collins CM, Boss JM, Speck SH (2009) Identification of Infected B-Cell Populations by Using a Recombinant Murine Gammaherpesvirus 68 Expressing a Fluorescent Protein. J Virol 83: 6484–6493. doi:10.1128/JVI.00297-09.
5. Stevenson PG, Simas JP, Efstathiou S (2009) Immune control of mammalian gamma-herpesviruses: lessons from murid herpesvirus-4. J Gen Virol 90: 2317–2330. doi:10.1099/vir.0.013300-0.
6. Frederico B, Chao B, May JS, Belz GT, Stevenson PG (2014) A Murid Gamma-Herpesviruses Exploits Normal Splenic Immune Communication Routes for Systemic Spread. Cell Host Microbe 15: 457–470. doi:10.1016/j.chom.2014.03.010.
7. Stevenson PG, Doherty PC (1999) Non-antigen-specific B-cell activation following murine gammaherpesvirus infection is CD4 independent in vitro but CD4 dependent in vivo. J Virol 73: 1075–1079.
8. Sangster MY, Topham DJ, DCosta S, Cardin RD, Marion TN, et al. (2000) Analysis of the virus-specific and nonspecific B cell response to a persistent B-lymphotropic gammaherpesvirus. J Immunol 164: 1820–1828.
9. Sunil-Chandra NP, Arno J, Fazakerley J, Nash AA (1994) Lymphoproliferative disease in mice infected with murine gammaherpesvirus 68. Am J Pathol 145: 818–826.
10. Collins CM, Speck SH (2014) Expansion of Murine Gammaherpesvirus Latently Infected B Cells Requires T Follicular Help. PLoS Pathog 10: e1004106. doi:10.1371/journal.ppat.1004106.
11. Ehtisham S, Sunil-Chandra NP, Nash AA (1993) Pathogenesis of murine gammaherpesvirus infection in mice deficient in CD4 and CD8 T cells. J Virol 67: 5247–5252.
12. Dutia BM, Clarke CJ, Allen DJ, Nash AA (1997) Pathological changes in the spleens of gamma interferon receptor-deficient mice infected with murine gammaherpesvirus: a role for CD8 T cells. J Virol 71: 4278–4283.
13. Cardin RD, Brooks JW, Sarawar SR, Doherty PC (1996) Progressive loss of CD8+ T cell-mediated control of a gamma-herpesvirus in the absence of CD4+ T cells. J Exp Med 184: 863–871.
14. Simas JP, Marques S, Bridgeman A, Efstathiou S, Adler H (2004) The M2 gene product of murine gammaherpesvirus 68 is required for efficient colonization of splenic follicles but is not necessary for expansion of latently infected germinal centre B cells. J Gen Virol 85: 2789–2797. doi:10.1099/vir.0.80138-0.
15. Jacoby MA, Virgin HW, Speck SH (2002) Disruption of the M2 gene of murine gammaherpesvirus 68 alters splenic latency following intranasal, but not intraperitoneal, inoculation. J Virol 76: 1790–1801. doi:10.1128/JVI.76.4.1790-1801.2002.
16. Pires de Miranda M, Alenquer M, Marques S, Rodrigues L, Lopes F, et al. (2008) The Gammaherpesvirus m2 protein manipulates the Fyn/Vav pathway through a multidocking mechanism of assembly. PLoS ONE 3: e1654. doi:10.1371/journal.pone.0001654.
17. Rodrigues L, Pires de Miranda M, Caloca MJ, Bustelo XR, Simas JP (2006) Activation of Vav by the gammaherpesvirus M2 protein contributes to the establishment of viral latency in B lymphocytes. J Virol 80: 6123–6135. doi:10.1128/JVI.02700-05.
18. Pires de Miranda M, Lopes FB, McVey CE, Bustelo XR, Simas JP (2013) Role of Src Homology Domain Binding in Signaling Complexes Assembled by the Murid γ-Herpesvirus M2 Protein. J Biol Chem 288: 3858–3870. doi:10.1074/jbc.M112.439810.
19. Liang X, Collins CM, Mendel JB, Iwakoshi NN, Speck SH (2009) Gammaherpesvirus-driven plasma cell differentiation regulates virus reactivation from latently infected B lymphocytes. PLoS Pathog 5: e1000677. doi:10.1371/journal.ppat.1000677.
20. Rodrigues L, Popov N, Kaye KM, Simas JP (2013) Stabilization of Myc through heterotypic poly-ubiquitination by mLANA is critical for γ-herpesvirus lymphoproliferation. PLoS Pathog 9: e1003554. doi:10.1371/journal.ppat.1003554.
21. Phan TG, Amesbury M, Gardam S, Crosbie J, Hasbold J, et al. (2003) B Cell Receptor-independent Stimuli Trigger Immunoglobulin (Ig) Class Switch Recombination and Production of IgG Autoantibodies by Anergic Self-Reactive B Cells. J Exp Med 197: 845–860. doi:10.1084/jem.20022144.
22. Brink R, Phan TG, Paus D, Chan TD (2008) Visualizing the effects of antigen affinity on T-dependent B-cell differentiation. Immunol Cell Biol 86: 31–39. doi:10.1038/sj.icb.7100143.
23. Paus D, Phan TG, Chan TD, Gardam S, Basten A, et al. (2006) Antigen recognition strength regulates the choice between extrafollicular plasma cell and germinal center B cell differentiation. J Exp Med 203: 1081–1091. doi:10.1084/jem.20060087.
24. Chan TD, Gardam S, Gatto D, Turner VM, Silke J, et al. (2010) In vivo control of B-cell survival and antigen-specific B-cell responses. Immunol Rev 237: 90–103. doi:10.1111/j.1600-065X.2010.00942.x.
25. Goodnow CC, Crosbie J, Adelstein S, Lavoie TB, Smith-Gill SJ, et al. (1988) Altered immunoglobulin expression and functional silencing of self-reactive B lymphocytes in transgenic mice. Nature 334: 676–682. doi:10.1038/334676a0.
26. Wang J, Taniuchi I, Maekawa Y, Maureen H, Cooper MD, et al. (1996) Expression and function of Fas antigen on activated murine B cells. Eur J Immunol 26: 92–96.
27. Baumgarth N (2010) The double life of a B-1 cell: self-reactivity selects for protective effector functions. Nat Rev Immunol 11: 34–46. doi:10.1038/nri2901.
28. Dutia BM, Stewart JP, Clayton RA, Dyson H, Nash AA (1999) Kinetic and phenotypic changes in murine lymphocytes infected with murine gammaherpesvirus-68 in vitro. J Gen Virol 80 (Pt 10): 2729–2736.
29. Frederico B, Milho R, May JS, Gillet L, Stevenson PG (2012) Myeloid Infection Links Epithelial and B Cell Tropisms of Murid Herpesvirus-4. PLoS Pathog 8. doi:10.1371/journal.ppat.1002935.
30. Usherwood EJ, Ross AJ, Allen DJ, Nash AA (1996) Murine gammaherpesvirus-induced splenomegaly: a critical role for CD4 T cells. J Gen Virol 77: 627–630.
31. Phan TG, Gray EE, Cyster JG (2009) The microanatomy of B cell activation. Curr Opin Immunol 21: 258–265. doi:10.1016/j.coi.2009.05.006.
32. Collins CM, Speck SH (2012) Tracking murine gammaherpesvirus 68 infection of germinal center B cells in vivo. PLoS ONE 7: e33230. doi:10.1371/journal.pone.0033230.
33. Moser JM, Upton JW, Allen RD, Wilson CB, Speck SH (2005) Role of B-cell proliferation in the establishment of gammaherpesvirus latency. J Virol 79: 9480–9491. doi:10.1128/JVI.79.15.9480-9491.2005.
34. McClellan KB, Gangappa S, Speck SH, Virgin HW (2006) Antibody-independent control of gamma-herpesvirus latency via B cell induction of anti-viral T cell responses. PLoS Pathog 2: e58. doi:10.1371/journal.ppat.0020058.

35. Kim I-J, Flaño E, Woodland DL, Lund FE, Randall TD, et al. (2003) Maintenance of Long Term γ-Herpesvirus B Cell Latency Is Dependent on CD40-Mediated Development of Memory B Cells. J Immunol 171: 886–892.
36. Wardemann H, Yurasov S, Schaefer A, Young JW, Meffre E, et al. (2003) Predominant autoantibody production by early human B cell precursors. Science 301: 1374–1377. doi:10.1126/science.1086907.
37. Koelsch K, Zheng N-Y, Zhang Q, Duty A, Helms C, et al. (2007) Mature B cells class switched to IgD are autoreactive in healthy individuals. J Clin Invest 117: 1558–1565. doi:10.1172/JCI27628.
38. Cambier JC, Gauld SB, Merrell KT, Vilen BJ (2007) B-cell anergy: from transgenic models to naturally occurring anergic B cells? Nat Rev Immunol 7: 633–643. doi:10.1038/nri2133.
39. Zikherman J, Parameswaran R, Weiss A (2012) Endogenous antigen tunes the responsiveness of naive B cells but not T cells. Nature: 1–6. doi:10.1038/nature11311.
40. Tracy SI, Kakalacheva K, Lunemann JD, Luzuriaga K, Middeldorp J, et al. (2012) Persistence of Epstein-Barr Virus in Self-Reactive Memory B Cells. J Virol 86: 12330–12340. doi:10.1128/JVI.01699-12.
41. Larson JD, Thurman JM, Rubtsov AV, Claypool D, Marrack P, et al. (2012) Murine gammaherpesvirus 68 infection protects lupus-prone mice from the development of autoimmunity. Proc Natl Acad Sci U S A 109: E1092–E1110. doi:10.1073/pnas.1203019109.
42. Getahun A, Smith MJ, Kogut I, van Dyk LF, Cambier JC (2012) Retention of Anergy and Inhibition of Antibody Responses during Acute Gammaherpesvirus 68 Infection. J Immunol. doi:10.4049/jimmunol.1201407.
43. Gauld SB, De Santis JL, Kulinski JM, McGraw JA, Leonardo SM, et al. (2013) Modulation of B-cell tolerance by Murine Gammaherpesvirus 68 infection: requirement for Orf73 viral gene expression and follicular helper T cells. Immunology 139: 197–204. doi:10.1111/imm.12069.
44. de Lima BD, May JS, Marques S, Simas JP, Stevenson PG (2005) Murine gammaherpesvirus 68 bcl-2 homologue contributes to latency establishment in vivo. J Gen Virol 86: 31–40. doi:10.1099/vir.0.80480-0.
45. Simas JP, Bowden RJ, Paige V, Efstathiou S (1998) Four tRNA-like sequences and a serpin homologue encoded by murine gammaherpesvirus 68 are dispensable for lytic replication in vitro and latency in vivo. J Gen Virol 79: 149–153.
46. McLean IW, Nakane PK (1974) Periodate-lysine-paraformaldehyde fixative. A new fixation for immunoelectron microscopy. J Histochem Cytochem 22: 1077–1083. doi:10.1177/22.12.1077.
47. Beuneu H, Deguine J, Breart B, Mandelboim O, Di Santo JP, et al. (2009) Dynamic behavior of NK cells during activation in lymph nodes. Blood 114: 3227–3234. doi:10.1182/blood-2009-06-228759.
48. Marques S, Alenquer M, Stevenson PG, Simas JP (2008) A single CD8+ T cell epitope sets the long-term latent load of a murid herpesvirus. PLoS Pathog 4: e1000177. doi:10.1371/journal.ppat.1000177.
49. Bonnefoix T, Bonnefoix P, Callanan M, Verdiel P, Sotto J-J (2001) Graphical Representation of a Generalized Linear Model-Based Statistical Test Estimating the Fit of the Single-Hit Poisson Model to Limiting Dilution Assays. J Immunol 167: 5725–5730.
50. Phan TG, Gardam S, Basten A, Brink R (2005) Altered migration, recruitment, and somatic hypermutation in the early response of marginal zone B cells to T cell-dependent antigen. J Immunol 174: 4567–4578.

APPENDIX 3

OPEN ACCESS Freely available online

PLOS | PATHOGENS

Defining Immune Engagement Thresholds for *In Vivo* Control of Virus-Driven Lymphoproliferation

Cristina Godinho-Silva[1☯], Sofia Marques[1☯], Diana Fontinha[1], Henrique Veiga-Fernandes[1], Philip G. Stevenson[2], J. Pedro Simas[1]*

1 Instituto de Medicina Molecular, Faculdade de Medicina, Universidade de Lisboa, Lisboa, Portugal, **2** Sir Albert Sakzewski Virus Research Center and Queensland and Children's Medical Research Institute, University of Queensland, Brisbane, Queensland, Australia

Abstract

Persistent infections are subject to constant surveillance by $CD8^+$ cytotoxic T cells (CTL). Their control should therefore depend on MHC class I-restricted epitope presentation. Many epitopes are described for γ-herpesviruses and form a basis for prospective immunotherapies and vaccines. However the quantitative requirements of *in vivo* immune control for epitope presentation and recognition remain poorly defined. We used Murid Herpesvirus-4 (MuHV-4) to determine for a latently expressed viral epitope how MHC class-I binding and CTL functional avidity impact on host colonization. Tracking MuHV-4 recombinants that differed only in epitope presentation, we found little latitude for sub-optimal MHC class I binding before immune control failed. By contrast, control remained effective across a wide range of T cell functional avidities. Thus, we could define critical engagement thresholds for the *in vivo* immune control of virus-driven B cell proliferation.

Citation: Godinho-Silva C, Marques S, Fontinha D, Veiga-Fernandes H, Stevenson PG, et al. (2014) Defining Immune Engagement Thresholds for *In Vivo* Control of Virus-Driven Lymphoproliferation. PLOS Pathog 10(6): e1004220. doi:10.1371/journal.ppat.1004220

Editor: Edward Usherwood, Dartmouth Medical School, United States of America

Received March 26, 2014; **Accepted** May 13, 2014; **Published** June 26, 2014

Data Availability: The authors confirm that all data underlying the findings are fully available without restriction. All data included in manuscript and supporting file.

Funding: JPS was funded by Fundação para a Ciência e Tecnologia (PTDC/SAU-MII/099314/2008); HMSP-ICT/0021/2010) Portugal. CGS, SM, and DF were supported by scholarships from Fundação para a Ciência e Tecnologia, Portugal. PGS is an ARC Future Fellow. The funders had no role in study design, data collection and analysis, decision to publish, or preparation of the manuscript.

Competing Interests: The authors have declared that no competing interests exist.

* Email: psimas@fm.ul.pt

☯ These authors contributed equally to this study.

Introduction

The gamma-herpesviruses (γHVs) infect >90% of humans and cause diseases including nasopharyngeal carcinoma, African Burkitt's lymphoma and Kaposi's Sarcoma. Their colonization of circulating memory B cells is crucial to persistence and hence to disease ontogeny. Viral latency gene expression in B cells provides an immune target [1] that has been exploited to prevent lymphoproliferative disease in acutely immunodeficient patients by T cell transfer [2]. However, extending this approach to established cancers and developing related vaccines have proved difficult. A significant problem is that the narrow species tropisms of human γHVs severely restrict *in vivo* analysis, and hence an understanding of how empirical therapies such as adoptive T cell transfer work.

Immune recognition can be assayed *in vitro*; but while Epstein-Barr virus (EBV) latency gene products drive autonomous B cell proliferation *in vitro*, most *in vivo* infected cells are resting memory B cells that have passed though lymphoid germinal centers (GCs) [3]. This makes difficult *in vitro* analysis of *in vivo* immune control. One way to make progress is to study related viruses that are experimentally more accessible. Probably the best characterized is Murid Herpesvirus-4 (MuHV-4, archetypal strain MHV-68) [4–6]. MuHV-4 is more closely related to the Kaposi's Sarcoma-associated Herpesvirus (KSHV) than to EBV [7]. However it shares many features of host colonization with EBV, for example it exploits lymphoid GCs to establish persistence in circulating memory B cells [8–10]. Therefore it can be used to reveal fundamental mechanisms of γHV/host interaction.

MuHV-4 studies have shown that γHV-driven lymphoproliferation occurs in complex lesions incorporating T cell evasion and infected cells with distinct patterns of viral gene expression [10]. In addition to cis-acting T cell evasion during episome maintenance [11,12], EBV inhibits the transporter associated with antigen processing (TAP) via BNLF2a [13–15] and MHC class I export to the cell surface via BILF1 [16,17]; KSHV degrades MHC class I and other immune receptors via K3 and K5 [18]; and MuHV-4 degrades MHC class I and TAP via MK3 [19–21]. Disrupting MK3 impairs virus-driven lymphoproliferation [22].

The γHVs also evade immune recognition during latency by expressing few CTL targets. However a gene that modulates signaling through the B cell receptor - M2 in MuHV-4 [23–26], LMP-2A in EBV [27] and K1 in KSHV [28] - is expressed more widely than growth program genes [3], and shows protein sequence diversity [29–33] consistent with immune selection. More directly, the presence of an $H2K^d$ binding epitope in M2 [34,35] significantly reduces long-term MuHV-4 latent loads in BALB/c mice [29]. Therefore despite viral evasion, CTL help to regulate long-term infection [36,37], and CTL recognition of M2/K1/LMP-2A, which in EBV may extend also to EBNA3A/B/C

Author Summary

Chronic viral infections cause huge morbidity and mortality worldwide. γ-herpesviruses provide an example relevant to all human demographics, causing, *inter alia*, Hodgkin's disease, Burkitt's lymphoma, Kaposi's Sarcoma, and nasopharyngeal carcinoma. The proliferation of latently infected B cells and their control by $CD8^+$ T cells are central to pathogenesis. Although many viral T cell targets have been identified *in vitro*, the functional impact of their engagement *in vivo* remains ill-defined. With the well-established Murid Herpesvirus-4 infection model, we used a range of recombinant viruses to define functional thresholds for the engagement of a latently expressed viral epitope. These data advance significantly our understanding of how the immune system must function to control γ-herpesvirus infection, with implications for vaccination and anti-cancer immunotherapy.

[38,39], provides a potential point of attack. LMP-2A is also a candidate vaccine target for nasopharyngeal carcinoma [40]. Thus, how M2/K1/LMP-2A recognition works *in vivo* is important to understand.

CTL effector capacity broadly correlates with functional avidity, as determined by the capacity of T cell receptor (TcR) engagement to trigger CTL proliferation, cytokine production and target cell lysis at limiting antigen dose [41]. Therefore with limited γHV protein expression during latency, peptide affinity for MHC class I and TcR functional avidity are likely to be crucial for immune control. The diversity of LMP-2A, K1 and M2 prompted us to analyze *in vivo* the consequences of varying MHC class I binding and TcR functional avidity for a single epitope derived from M2. These parameters affected dramatically the control of virus-driven lymphoproliferation, even in the context of immune evasion. The capacity of MuHV-4 to correlate biochemical interactions with *in vivo* immune function allowed us to establish quantitative guidelines for infection control.

Results

Characterization of altered peptide ligands (APLs) by MHC class I binding and TcR functional avidity

To understand the CTL recognition requirements for γHV infection control, we expressed from MuHV-4 a well-characterized, $H2K^b$-restricted epitope comprising amino acid residues 257–264 of ovalbumin (OVA), or APL derivatives (Figure 1A). OVA binds to $H2K^b$ with high affinity ($K_D = 4.1$ nM) [42]. We compared OVA and APL binding by $H2K^b$ stabilization on TAP-deficient RMA/S cells (Figure 1B) [43]. The OVA concentration giving 50% maximal stabilization (EC_{50}) was 40 nM, in close agreement with published data [44]. APLs Q4, V4, G4 and R4 were similar to OVA (EC_{50} within 2-fold), consistent with residue 4 being solvent-exposed in the $H2K^b$-peptide complex [45]. E1 required 6-fold more peptide for equivalent $H2K^b$ stabilization, consistent with this residue being only partly exposed; A8, which has a mutated anchor residue, required 10-fold more peptide again; and the control peptide A5A8, with 2 mutated anchor residues, gave no significant stabilization. The $H2K^b$/OVA/β_2M complex has an estimated half-life of 8 h [44]. Its stability is determined primarily by the peptide off-rate, so the E1 complex is likely to have a half-life of approximately 1.3 h.

We assessed the functional avidity of the $H2K^b$-OVA-specific TcR of OT-I [46] for each APL by *ex vivo* stimulation of $CD8^+$ T cells from OT-I mice with graded peptide doses (Figure 1C). There was a clear hierarchy in dose-response, with OVA>Q4 (14-fold)>V4 (a further 279-fold)>G4 (53-fold further still), consistent with published data [47]. The R4 antagonist peptide [48,49] gave no stimulation. As predicted E1 and A8, which have lower MHC class I binding, generated the lowest dose-responses.

Generation of MuHV-4 recombinants expressing OVA or APLs linked to M2

We next introduced each epitope at the MuHV-4 M2 C-terminus to ensure expression in latency without compromising M2 function [29]. CTL recognition of an endogenous M2 epitope reduces long-term MuHV-4 latent loads in $H2^d$ mice [29]. The lack of an endogenous $H2^b$-restricted M2 epitope therefore allowed us to introduce new targets in a context where this is known to be important. Each recombinant virus was also made with a yellow fluorescent protein (YFP) reporter construct [50] to aid infection tracking (Figure S1). Correct epitope insertion and assembly of the surrounding genome were demonstrated by PCR of plaque-purified viral DNA (Figure 1D). Each recombinant virus showed equivalent *in vitro* growth (Figure 1E), equivalent lytic replication in the lungs of intranasally (i.n.) infected C57BL/6 mice (Figure 1F) - with peak titers at 4–7 days post-inoculation and clearance by day 11 - and normal latency establishment in $H2^d$ BALB/c mice - with equivalent splenic infectious center assay titers 14 days after i.n. inoculation (Figure 1G). Therefore none showed a replication defect independent of $H2^b$-restricted latent epitope expression.

MHC class I binding by a latency-associated epitope impairs host colonization

We then tested latency establishment in $H2^b$ mice. Infectious center assays (Figure 2A) showed attenuation of any virus with an $H2K^b$ binding epitope attached to M2 (vOVA, vQ4, vV4, vG4, vR4): splenic infection was established at day 11, but then cleared rather than amplified by days 14–21. In contrast, the virus expressing a poorly binding epitope (vA8) was indistinguishable from the epitope-negative wild-type (vWT). Interestingly vE1, which expresses an epitope with 6-fold lower EC_{50} for $H2K^b$ stabilization (Figure 1B), showed an intermediate phenotype with normal titers at day 11 followed by a gradual reduction.

Not every latently infected cell necessarily reactivates its virus *ex vivo*. We therefore used PCR of viral DNA at limiting dilution (Figure 2B; Table 1) as a second measure of infected cell frequency. We looked at the peak of latent infection (14 days post-inoculation) and at the steady state (50 days). These results supported the infectious centre assays: vOVA, vQ4, vV4, vG4 and vR4 were all markedly attenuated (>100-fold reduction); vA8 was equivalent to vWT; and vE1 showed an intermediate phenotype, with strongly decreased acute titers but long-term titers close to vA8 and vWT. MuHV-4-specific CTL responses peak at 14–21 days post-infection [51]. Thus a weakly binding latent epitope (E1) allowed some control when CTL responses were at their peak, but not in the long-term when CTL responses decrease in size.

MuHV-4 colonizes multiple cell types in acutely infected spleens. Many are B cells, which change in phenotype as they pass through germinal centers; others are myeloid cells. The main proliferating population is GC B cells, and these also connect most directly to the long-term latency reservoir of resting memory B cells [9,10]. Therefore to understand better the relationship between acute and long-term viral loads, we measured viral genome prevalence in flow cytometrically sorted GC B cells (Figure 2C; Table 2). They showed marked reductions for vOVA, vQ4, vV4, vG4 and vR4, equivalent frequencies for vA8 and

A

MuHV-4 recombinants	Epitope Sequence
vOVA	M2 - SIINFEKL
vQ4	M2 - SIIQFEKL
vV4	M2 - SIIVFEKL
vG4	M2 - SIIGFEKL
vR4	M2 - SIIRFEKL
vE1	M2 - EIINFEKL
vA8	M2 - SIINFEKA

B

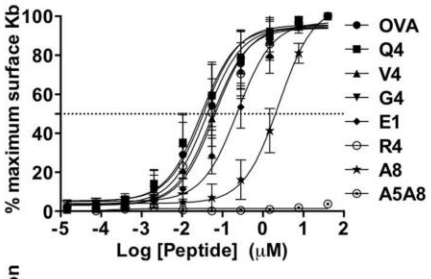

Peptide	EC_{50} (μM)	EC_{50} APL/OVA
OVA	0.040	1.0
Q4	0.030	0.8
G4	0.034	0.9
R4	0.056	1.4
V4	0.063	1.6
E1	0.235	5.9
A8	2.466	61.7
A5A8	-----	-----

C

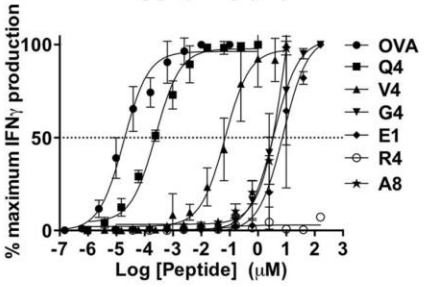

OT-I sensitivity

Peptide	EC_{50} (μM)	EC_{50} APL/OVA
OVA	1.82E-05	1.00E+00
Q4	2.43E-04	1.35E+01
V4	6.85E-02	3.76E+03
G4	3.61E+00	1.98E+05
E1	7.78E+00	4.27E+05
R4	-------	-------
A8	1.03E+01	5.64E+06

D

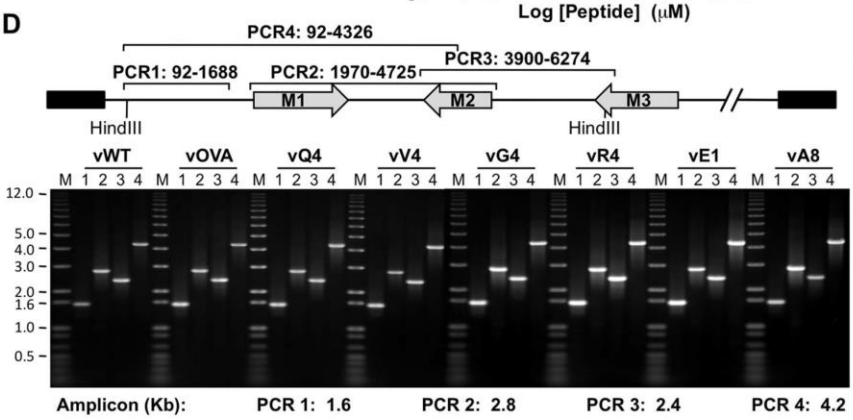

E

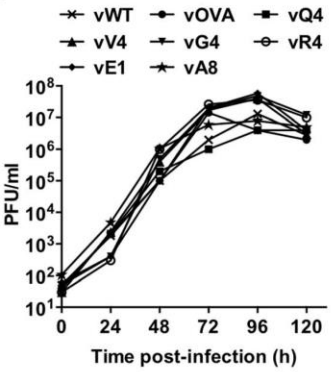

F

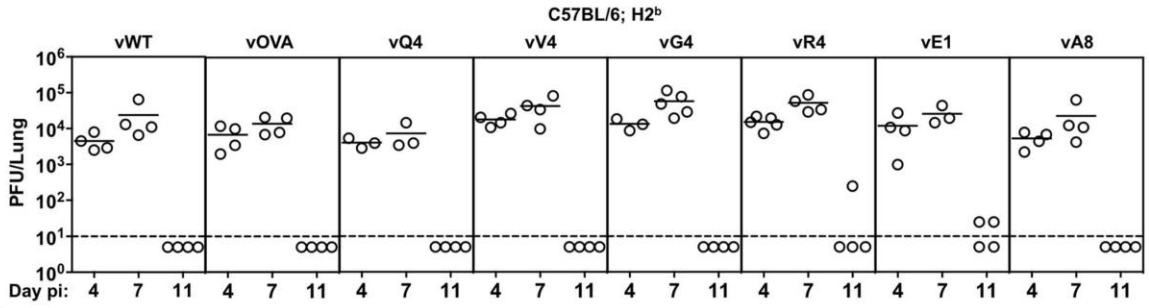

G

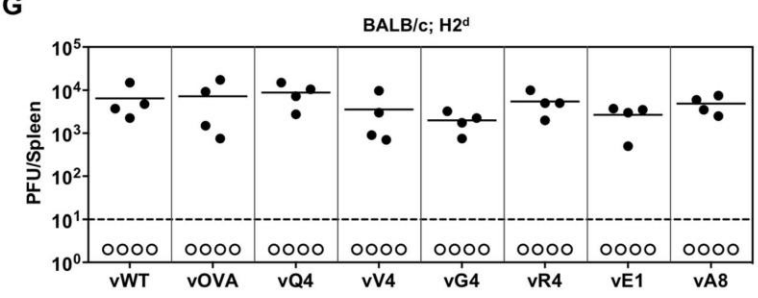

Figure 1. Characterization of APLs by MHC class I binding and TcR functional avidity, and generation of MuHV-4 recombinants expressing OVA or APLs linked to M2. (A) Amino acid sequences used to generate MuHV-4 recombinants. Blue residues denote amino acid alterations introduced into native OVA. (B) Capacity of OVA and APL peptides to stabilize $H2K^b$ on TAP deficient RMA/S cells. Half-maximum effective concentration (EC_{50}) values were calculated from dose-response curves. The experiment was repeated 3 times. (C) Functional avidities of OT-I CTL for OVA and APL peptides were determined by IFNγ production. EC_{50} and APL/OVA EC_{50} ratios are shown. This experiment was repeated in duplicates 4 times (D) PCR analysis of recombinant viral DNA to confirm genome integrity in the *Hin*DIII-E region, with schematic representation of the MuHV-4 genome, amplicon genomic co-ordinates and predicted PCR product sizes. (E) Multi-step growth curves of viruses in BHK-21 (0.01 PFU/cell). Virus titres were determined by plaque assay. *In vitro* lytic replication kinetics of the recombinant viruses were not significant different from vWT ($p>0.05$, by ordinary one-way ANOVA followed by Dunnett's multiple comparisons test). (F) Virus replication in lungs of i.n. infected C57BL/6 ($H2^b$) mice was quantified by plaque assay. No MuHV-4 recombinant showed a deficit relative to vWT ($p>0.05$, using ordinary one-way ANOVA followed by Tukey's multiple comparisons test). (G) Latent infection in spleens of BALB/c ($H2^d$) mice was determined by explant co-culture assay (closed symbols) at 14 days post-infection. Pre-formed infectious virus were measured by plaque assay (open symbols). Latent loads of MuHV-4 recombinants expressing OVA or APLs were not significantly different to vWT ($p>0.05$, by ordinary one-way ANOVA followed by Dunnett's multiple comparisons test). In panels F and G each point shows the titre of 1 mouse, horizontal lines show arithmetic means and dashed horizontal lines indicate the detection limit of the assay.
doi:10.1371/journal.ppat.1004220.g001

vWT, and intermediate frequencies for vE1. These data were further supported by *in situ* hybridization for latently expressed viral tRNA/miRNA homologs [29] (Figure 2D), which showed abundant GC infection by vWT and vA8, severely impaired infection by vOVA, vQ4, vV4, vG4 and vR4, and intermediate infection by vE1. Therefore susceptibility to CTL attack during acute lymphoproliferation varied with cell type, and the relative sparing of $vE1^+$ GC B cells appeared to allow high long-term viral loads.

CTL responses to epitopes expressed in latent infection

We measured epitope-specific CTL responses with $H2K^b$-peptide tetramers (Figure 2E) and by staining for intracellular IFN-γ after *ex vivo* stimulation (Figure 2F). Responses to vA8 were uniformly low despite high viral loads, presumably because this epitope was not produced in sufficient amounts to compensate for its poor $H2K^b$ binding. Responses to vOVA, vQ4, vV4, vG4 and vR4 were detectable, although small compared to those reported for lytic antigens [51]. Surprisingly, the largest CTL response was elicited by the intermediate phenotype virus, vE1. This could not be explained by lytic infection, since this was high in lungs for all viruses (Figure 1F).

We confirmed the functionality of vE1-specific CTL by *in vivo* killing of CFSE-labelled, peptide-exposed targets (Figure 2G,H): vE1-induced CTL showed target cell elimination comparable to vOVA, whereas mice infected with vWT or vA8 showed none. Therefore the relatively weak $H2K^b$ binding of E1 was sufficient to stimulate large, functional CTL responses, but not for those CTL to curtail efficiently virus-driven lymphoproliferation. This result suggested that at least for vE1, most CTL stimulation comes from a population distinct from that engaged in lymphoproliferation.

CTL functional avidity also determines infection control by latency epitope recognition

The capacity of C57BL/6 mice to control MuHV-4-driven lymphoproliferation through the recognition of latently expressed OVA, Q4, V4, G4 or R4 indicated that the key requirement in a polyclonal TcR setting is the availability of an epitope capable of strong MHC class I binding: T cells from the naive repertoire could recognize either OVA or an APL. However responses to EBV can involve oligoclonal or even monoclonal CTL expansions [52–54]. Therefore to understand better the quantitative requirements of TcR functional avidity for *in vivo* γHV control, we focussed on the well-characterized OT-I TcR (Figure 3).

We first infected OT-I mice with MuHV-4 expressing OVA or APLs with comparable $H2K^b$ binding (Q4, V4, G4, R4), and measured host colonization by infectious center assay of spleens 9 and 11 days later (Figure 3A). vE1 and vA8 were not utilized since they bind MHC class I less efficiently precluding analysis of T cell functional avidity because target concentrations are different. There was a clear correlation between CTL functional avidity (Figure 1C) and *in vivo* virus control. The antagonist epitope (R4) allowed no control - titers were equivalent to those of the epitope-negative vWT; the others showed a hierarchy of control (OVA> Q4>V4>G4) that matched exactly their hierarchy of functional avidity (and not their minor differences in $H2K^b$ binding). Low titers of pre-formed infectious virus were found in some mice, but generally in proportion to their latent titers, consistent with reactivation of a fixed fraction of the latent viral load; we saw no evidence that M2-associated epitope presentation created a significant new lytic CTL target.

To confirm that the immune control was by CTL, we treated mice with a depleting, CD8-specific mAb from the time of infection (Figure 3B–D). Each virus then reached equivalent titers to the wild-type. While the depletions were highly effective (Figure 3C), they had little effect on the day 11 spleen titers of vWT (Figure 3D). This result was consistent with previous publications [36,55] and with the lack of known $H2^b$-restricted MuHV-4 latency epitopes. Thus, introducing latent epitope recognition caused new, CD8-dependent virus attenuation in proportion to the functional avidity of that epitope for the dominant TcR.

CTL functional avidity in the context of normalized T cell repertoire

OT-I mice provided a useful starting point for *in vivo* analysis of single TcR function. However their limited $CD4^+$ T cell repertoire impairs GC formation and so the ability of MuHV-4 to drive B cell proliferation. Hence, to define the impact of TcR functional avidity in an environment more conducive to lymphoproliferation, we adoptively transferred lymphocytes from Rag-$1^{-/-}$OT-I mice and purified $CD4^+$ T cells from C57BL/6 mice into $TcR\alpha^{-/-}$ recipients (Figure 4A). Thus the reconstituted mice had polyclonal $CD4^+$ T cells and a $TcR\alpha\beta^+CD8^+$ T cell compartment of modest size that was restricted to OT-I cells. (Most $CD8^+$ T cells of $TcR\alpha^{-/-}$ mice are $TcR\gamma\delta^+TcR\alpha\beta^-$.) Infecting these with vWT led to a robust proliferation of infected GC B cells (Figure S2 and S3). Infecting them with vOVA elicited a strong OT-I response (Figure 4B) and suppression of splenic colonization (Figure 4C); by contrast vR4, which expressed an antagonist epitope, elicited no OT-I response and reached high titers (Figure 4C). Therefore these mice provided a new and informative window onto how TcR engagement by a latency epitope affects virus-driven lymphoproliferation.

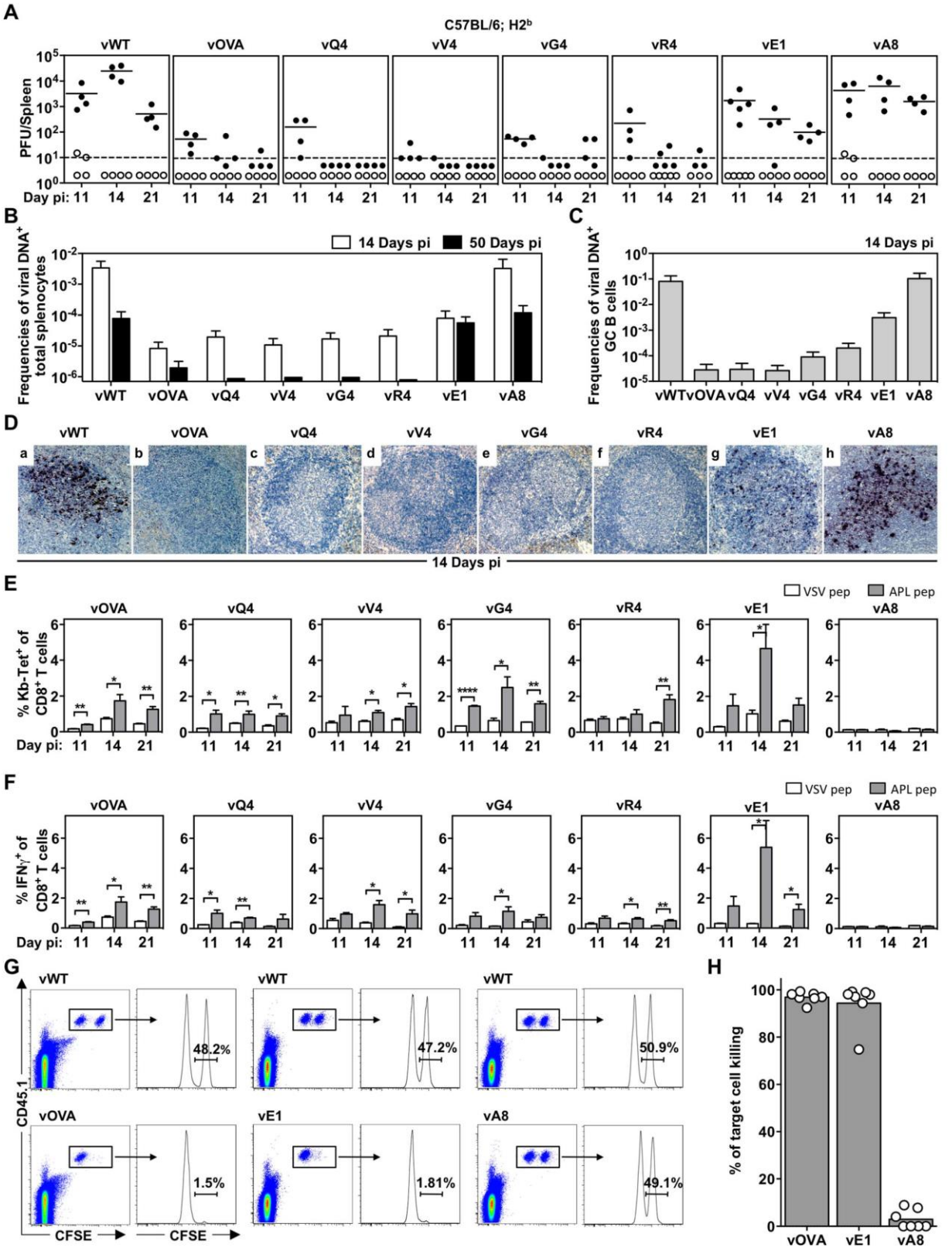
A
C57BL/6; H2b
vWT
vOVA
vQ4
vV4
vG4
vR4
vE1
vA8
PFU/Spleen
Day pi: 11 14 21
B
14 Days pi
50 Days pi
Frequencies of viral DNA+ total splenocytes
C
14 Days pi
Frequencies of viral DNA+ GC B cells
D
14 Days pi
E
VSV pep
APL pep
% Kb-Tet+ of CD8+ T cells
F
% IFNγ+ of CD8+ T cells
G
CD45.1
CFSE
48.2%
47.2%
50.9%
1.5%
1.81%
49.1%
H
% of target cell killing

Figure 2. MHC class I binding by a latency-associated epitope impairs host colonization. C57BL/6 mice were infected i.n. with 10^4 PFU of the indicated viruses. (A) The latent load in spleens was determined by explant co-culture assay (closed symbols) and pre-formed infectious virus was quantified by plaque assay (open symbols). Each point shows the titre of 1 mouse, horizontal lines arithmetic means and dashed horizontal line limit of detection of assay. At day 14, vOVA, vQ4, vV4, vG4, vR4 and vE1 latent loads were significantly below vWT ($p<0.05$, by two-tailed unpaired t-test). vA8 latency loads were not significantly different from vWT ($p = 0.07$). (B–C) Reciprocal frequencies of viral DNA^+ cells in (B) total splenocytes or (C) GC B cells. Bars represent the frequency of viral DNA^+ cells with 95% confidence intervals. (D) Representative spleen sections showing dark stained latently infected cells by *in situ* hybridization. (E) % tetramer positive $CD8^+$ T cells at each time point from spleens (arithmetic mean +/− SEM of 3 independent assays). * $p<0.05$, ** $p<0.01$, **** $p<0.0001$; using a two-tailed unpaired t-test. (F) Functional capacity of splenic CTL determined by intracellular interferon-gamma staining after *ex vivo* stimulation. Data show % $CD8^+$ T cells responding to each peptide (arithmetic mean +/− SEM of 3 independent assays). * $p<0.05$, ** $p<0.01$; using a two-tailed unpaired t-test. (G–H) *In vivo* CTL activity at 11 days post-infection. (G) At day 10 post-infection 50:50 mixes consisting of 2×10^6 unpulsed $CD45.1^+$ $CFSE^{lo}$ splenocytes and 2×10^6 OVA-, E1- or A8-pulsed $CD45.1^+$ $CFSE^{hi}$ splenocytes were transferred intravenously into vOVA, vE1 or vA8 infected C57BL/6 mice. The same mix of cells was transferred into vWT infected mice C57BL/6 as internal control. In the next day, the proportion of $CFSE^{hi}$ and $CFSE^{lo}$ cells among $CD45.1^+$ cells recovered from the spleen was analysed by FACS. Representative FACS plots showing % of unpulsed $CD45.1^+$ $CFSE^{lo}$ and OVA-, E1, or A8-pulsed $CD45.1^+$ $CFSE^{hi}$ splenocytes. (H) % target cell killing. Three to four mice were analyzed per group, and experiments repeated three times.
doi:10.1371/journal.ppat.1004220.g002

Sub-optimal CTL functional avidity still allows control of virus-driven lymphoproliferation

We then infected reconstituted mice with MuHV-4 expressing OVA or APLs (Figure 5). At day 16 post-infection OT-I T cell expansion was greatest for vOVA, reduced for vQ4, reduced further for vV4, and close to background for vG4 and vR4 (Figure 5A). Thus it correlated well with the epitope functional avidity measured in Figure 1C (OVA>Q4>V4>G4>R4). Specifically, the 14-fold avidity reduction of Q4 only modestly reduced CTL cell expansion, and the 4000-fold reduction of V4 caused further reduction but still did not ablate it entirely. The CTL response declined to background only when the avidity was reduced 200,000-fold (G4). Therefore the immune response showed a surprisingly large tolerance for sub-optimal TcR engagement.

Similar results were obtained for OT-I T cell activation (loss of CD62L, Figure 5B). We analyzed CTL function further by intracellular staining for IFN-γ (Figure 5C) and Granzyme B (Figure 5D) after *ex vivo* stimulation with the corresponding peptide epitope. The responses to vG4 and vR4 were hard to assess due to low CTL numbers; but those to vQ4 and vV4 showed comparable functionality to vOVA. (Note that the peptide concentration used was only just sufficient for maximal stimulation by V4 in Figure 1C) Therefore there was no sign of vQ4 and vV4 eliciting CTL responses that were functionally impaired (or functionally enhanced); they simply elicited responses that were smaller.

Virus titers (Figure 5E) were reduced markedly by OVA expression, only marginally less by Q4, and not significantly by G4 or R4. V4 expression gave an intermediate phenotype, with titers significantly below those of the vWT control and significantly above those of vOVA. The frequencies of viral DNA^+ cells in spleens (Figure 5F and Table S1) showed a similar hierarchy (vWT = vG4 = vR4>vV4>vQ4>vOVA). The viral DNA^+ frequencies of flow cytometrically sorted GC B cells (Figure 5G and Table 3) showed less discrimination. Nonetheless the trends were similar, and these results were further corroborated by analysis of YFP expression in GC B cells (Figure S4). Therefore high functional avidity (vOVA) gave marked CTL expansion and low virus titers; a 14-fold avidity reduction (vQ4) have remarkably similar results; a 200,000-fold avidity reduction abolished virus control (vG4); and a 4000-fold reduction gave an intermediate phenotype (vV4). OT-I TcR engagement by M2-derived OVA was therefore considerably above the threshold required for *in vivo* viral control, and low functional avidity compromised viral control via reduced CTL expansion, rather than by differentially affecting CTL effector function.

Table 1. Reciprocal frequency of MuHV-4 infection in total splenocytes[a] of C57BL/6 mice.

Virus	Day p.i.	Reciprocal frequency[b] of viral DNA^+ cells (95% CI)	
vWT	14	296	(179–856)
	50	12,770	(7,900–33,288)
vOVA	14	121,005	(75,230–309,065)
	50	517,114	(316,845–1,405,472)
vQ4	14	51,426	(32,333–125,586)
	50	id	≥1,149,446[c]
vV4	14	92,857	(57,599–239,405)
	50	id	≥1,053,659[c]
vG4	14	59,253	(37,537–140,588)
	50	id	≥1,053,659[c]
vR4	14	47,755	(29,622–123,123)
	50	id	≥1,264,391[c]
vE1	14	12,576	(7,445–40,375)
	50	17,810	(11,400–40,677)
vA8	14	307	(212–962)
	50	8462	(4970–28,436)

[a]Data were obtained from pools of 4 to 5 spleens.
[b]Frequencies were calculated by limiting-dilution analysis with 95% confidence intervals (CI).
[c]Estimated based upon less than 3 different dilution sets.
id; indeterminable.
doi:10.1371/journal.ppat.1004220.t001

Discussion

Gamma-herpesvirus epitope recognition by CTL has been studied extensively [1,54], but ours is the first quantitative assessment of how epitope/MHC class I/TcR complex formation affects host colonization. Where no latency epitope expression existed, introducing one led to a profound, CTL-dependent suppression of virus-driven lymphoproliferation. This was consistent with the impact of endogenous epitope presentation in $H2^d$ mice [29]. The latter affected only long-term viral loads; OVA expression in $H2^b$ mice also conferred susceptibility to CTL during acute lymphoproliferation, when trans-acting immune evasion operates [1]. This greater effect of epitope presentation possibly reflected differences in host susceptibility to immune evasion: the MuHV-4 K3 degrades $H2K^b$ relatively poorly [19] and degrades TAP better in $H2^d$ than $H2^b$ cells [20].

The precise cellular targets for $CD8^+$ T cell recognition of M2-linked epitopes remain unknown. One possibility is proliferating germinal centre B cells, as B cells are a major site of M2 expression

Table 2. Reciprocal frequency of MuHV-4 infection in GC B cells[a] of C57BL/6 mice at 14 days post-infection.

Virus	Reciprocal frequency[b] of viral DNA$^+$ cells (95% CI)		% Cells[c]	% Purity[d]
vWT	12	(8–34)	4.63	96.1
vOVA	35,463	(21,819–94,657)	4.06	96.3
vQ4	33,847	(19,882–113,738)	3.63	97.6
vV4	44,687	(23,952–92,597)	4.03	97.4
vG4	11,092	(7,184–24,318)	5.76	96.0
vR4	5,016	(3,268–10,785)	5.66	97.5
vE1	323	(211–687)	4.13	96.5
vA8	10	(6–25)	4.18	96.6

[a]Data were obtained from pools of 5 spleens.
[b]Frequencies were calculated by limiting-dilution analysis with 95% confidence intervals (CI).
[c]The percentage of GC B cells from total spleen was estimated by FACS analysis.
[d]The purity of sorted cells was determined by FACS analysis.
doi:10.1371/journal.ppat.1004220.t002

[10,34]. Infected B cells could also be recognized before the onset of proliferation; and as myeloid cells transfer infection to B cells [56], CD8$^+$ T cells could also suppress lymphoproliferation indirectly, by targeting infected myeloid cells [1].

A key point for physiologically relevant epitope presentation is that it conforms to normal latent gene expression. Exogenous promoters such as HCMV IE1 show activity independent of endogenous viral gene expression [57] and this can lead to attenuation [58]. Previous analysis of endogenous M2 epitope [29] established its importance for determining the different long-term latent loads of H2^d and H2^b mice. Here, to identify presentation thresholds, we made use of the well-characterized SIINFEKL epitope, attaching it to a neutral region of M2 (its C-terminus). This allowed the generation of a very well-defined model epitope with the kinetics and copy number of a known endogenous epitope. Epitope presentation varies with MHC class I genotype. C57BL/6 mice have only 2 MHC class I molecules and appear not to recognize an endogenous M2 epitope. In this context, M2-SIINFEKL illustrated the impact of strong epitope presentation, and wild-type M2 (or M2-vA8) that of poor epitope presentation. The SIINFEKL variants covered the range between, and so allowed us to identify functional recognition thresholds.

Small differences (<1.6-fold) in H2K^b epitope binding had no obvious impact on *in vivo* CTL efficacy, but a 60-fold reduction abolished protection and a 6-fold reduction showed a partial phenotype. Thus, M2-linked epitope presentation left little room for sub-optimal MHC class I binding. By contrast when H2K^b binding was maintained, reducing TcR functional avidity 14-fold had little effect, reducing it 200,000-fold abolished control, and reducing it 4,000-fold gave an intermediate phenotype. Therefore this aspect of recognition was more flexible even for monoclonal, Rag-1$^{-/-}$ CTL, and a polyclonal population could attack any epitope so long as its MHC class I binding was strong.

In complex viral infections, larger CTL responses are not necessarily more effective responses. These parameters can correlate: MuHV-4 lacking its K3 evasion gene elicits more CTL and achieves lower titers [22]; and our reconstituted mice showed a correlation between more CTL and less virus. But as with latent epitope presentation downstream of ORF73 [11], OVA-specific CTL responses that completely suppressed lymphoproliferation were small compared to lytic epitope responses [51]; and mice infected with vE1 made large epitope-specific responses yet showed poor virus control. We hypothesize that CTL can be stimulated by the key, self-renewing population of infected B cells, when infection is suppressed, but also by infected cells less important to host colonization, when large responses may achieve little. Crucially, viral evasion may make the self-renewing population harder to target. Thus, vE1 showed a strong acute reduction in total viral DNA$^+$ cell frequencies, but relative sparing of GC B cells and consequently high long-term virus loads. A position 1 mutation also impairs the control by Rag-1$^{-/-}$OT-I mice of MuHV-4 expressing OVA from an HCMV IE1 promoter [59]. However such mice lack B cells or CD4$^+$ T cells, and without CD4$^+$ T cells MuHV-4 causes a lethal, chronic lytic infection even with a strong, polyclonal CTL response [60,61]. Our reconstituted mice maintained both virus-driven lymphoproliferation and infection control without outgrowth of CTL escape mutants. Thus we could relate directly quantitative changes in epitope recognition to the control of lymphoproliferation.

An important task with EBV is to predict *in vivo* CTL efficacy. Extrapolating from CTL numbers and *in vitro* assays alone is clearly problematic. For example, large responses to lytic epitopes in infectious mononucleosis [54] could be interpreted as important, or simply as poor latency epitope recognition when better recognition might preclude large lytic responses and avoid symptoms. The precise relatedness of EBV memory B cell colonization via GCs to MuHV-4 memory B cell colonization via GCs is unknown. But all γHVs have evolved to colonize lymphocytes with maximal efficiency, within limits set ultimately by the immune system, so similar quantitative thresholds would not be surprising. Our data therefore have important general implications for γHV-specific CTL function, and for predicting *in vivo* CTL efficacy from biochemical measures.

Materials and Methods

Ethics statement

The study accorded with the Portuguese official Veterinary Directorate (Portaria 1005/92), European Guideline 86/609/EEC, and Federation of European Laboratory Animal Science Associations guidelines on laboratory animal welfare. It was approved by the Portuguese official veterinary department for welfare licensing (protocol AEC_2010_017_PS_Rdt_General) and by the IMM Animal Ethics Committee.

Mice

CD45.1 C57BL/6, OT-I, Rag-1$^{-/-}$ and TcRα$^{-/-}$ mice were obtained from Jackson Laboratories. CD45.1 Rag-1$^{-/-}$ OT-I

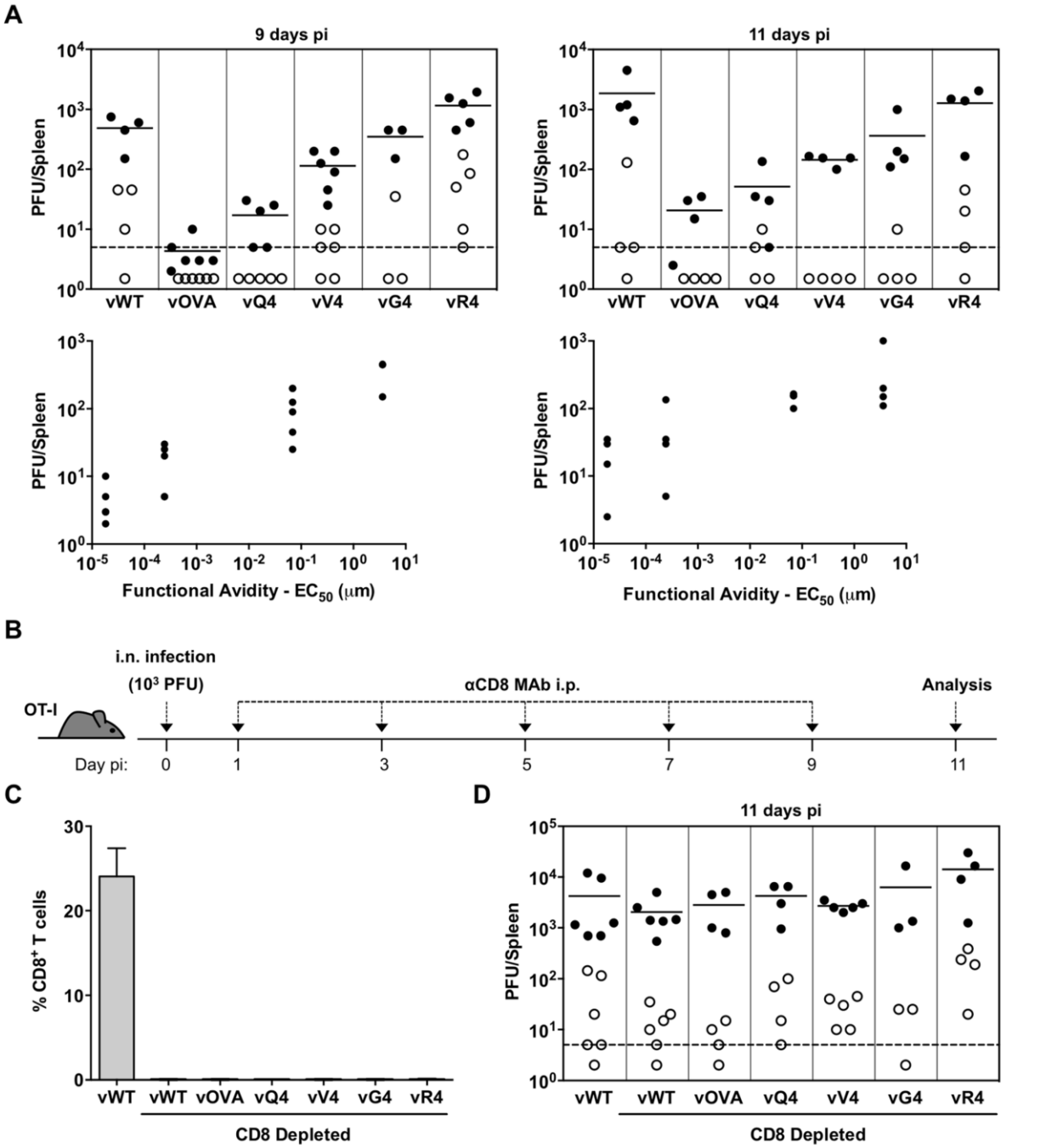

Figure 3. CTL functional avidity also determines infection control by latently expressed epitope recognition. (A) OT-I mice were infected i.n. (10^3 PFU). Splenocytes were titrated for latent virus by explant co-culture (closed circles) and for pre-formed infectious virus by plaque assay (open circles). At 9 days vOVA, vQ4 and vV4 showed significantly less latent infection compared to vWT (vOVA $p = 0.0014$, vQ4 $p = 0.004$, vV4 $p = 0.009$; by Student's 2-tailed unpaired t-test). vG4 and vR4 latent infections were not significantly different to vWT (vG4 $p = 0.46$, vR4 $p = 0.09$). Graphs show the correlation between TcR functional avidity (determined in Figure 1C) and splenic latent load (day 9: $p = 0.04$, $r_s = 0.91$; day 11 $p = 0.05$, $r_s = 0.90$; according to Pearson's correlation). (B) CD8 T^+ cells were depleted from i.n. infected OT-I mice by intraperitoneal injection of anti-CD8 monoclonal antibody (MAb). (B) Schematic diagram of the experimental setting. (C) Data show the percentage of $CD8^+$ T cells of total splenocytes (arithmetic mean +/− SEM) in control (non-depleted) and depleted mice. (D) Spleens were titrated for latent (closed circles) and lytic (open circles) infection. Latent loads of the epitope recombinants were not significantly different to vWT latent loads in CD8-depleted mice ($p > 0.05$; ordinary one-way ANOVA followed by Dunnett's multiple comparisons test). Data were reproduced in two independent experiments. Each point shows the titre of 1 mouse, horizontal lines arithmetic means and dashed lines the limit of detection of the assay.
doi:10.1371/journal.ppat.1004220.g003

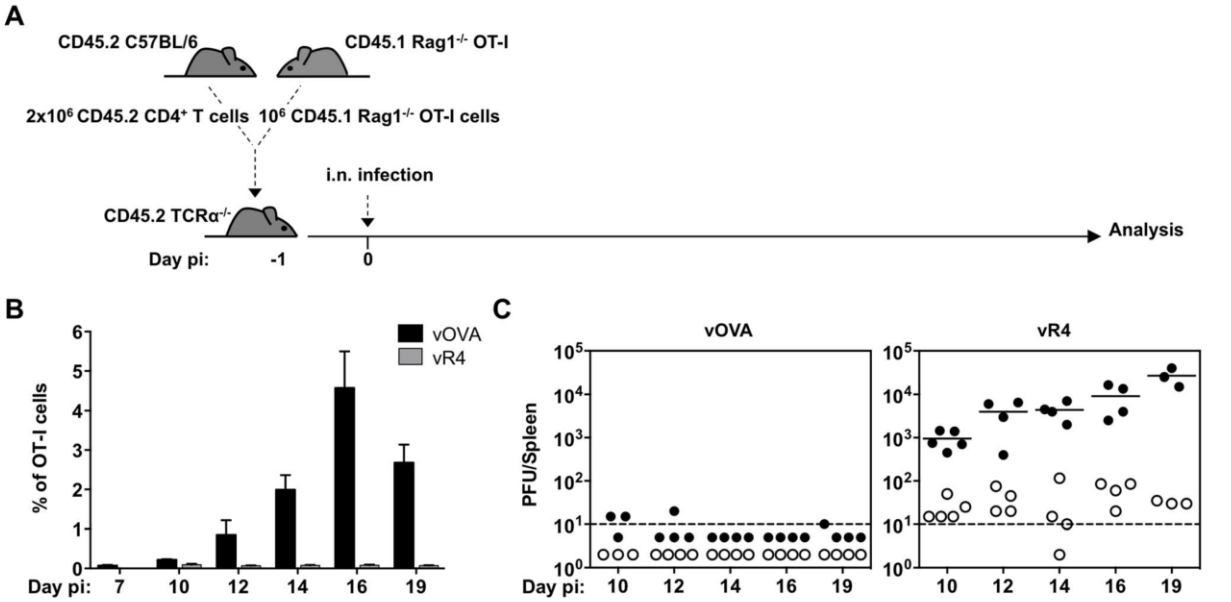

Figure 4. vOVA infection of TCR$\alpha^{-/-}$ mice reconstituted with CD4$^+$/OT-I T cells elicits a strong OT-I response and suppression of splenic colonization. CD4$^+$ T cells from C57BL/6 lymph nodes and OT-I T cells from CD45.1 Rag-1$^{-/-}$ OT-I lymph nodes were intravenously transferred to TcR$\alpha^{-/-}$ mice one day prior to infection with vOVA or vR4 (10^3 PFU). (A) Schematic diagram of the experimental setting. (B) Kinetics of *in vivo* OT-I CTL expansion in spleens of mice infected with vOVA (black bars) or vR4 (grey bars) determined by FACS staining of CD45.1$^+$CD8α^+ cells (arithmetic mean +/− SEM). (C) Latent infection in spleens was quantified by explant co-culture assay (closed circles) and pre-formed infectious virus by plaque assay (open circles). Each circle shows the titre of 1 mouse. Horizontal bars show arithmetic means. The dashed line shows the limit of detection of the assay.
doi:10.1371/journal.ppat.1004220.g004

mice were obtained by breeding OT-I onto a CD45.1 Rag-1$^{-/-}$ background. C57BL/6 and BALB/c mice were purchased from Charles River Laboratories. All mice were housed under specific pathogen-free conditions at the Instituto de Medicina Molecular and used when 6–12 weeks old. For adoptive transfers to TcR$\alpha^{-/-}$ mice, CD4$^+$ T cells were purified by negative selection from pooled lymph nodes of naïve C57BL/6 mice using the CD4$^+$ T cell isolation kit (Miltenyi Biotech). OT-I T cells were obtained from pooled lymph nodes of naïve CD45.1 Rag-1$^{-/-}$ OT-I mice. 2×10^6 CD4$^+$ T cells and 10^6 CD45.1 Rag-1$^{-/-}$ OT-I T cells were adoptively transferred to TcR$\alpha^{-/-}$ recipients via tail vein injection one day prior to infection.

Generation of recombinant viruses

MuHV-4 recombinants were generated from BAC-cloned viral genomes [29]. OVA and APL epitopes were introduced by PCR at the M2 C-terminus. Briefly, the M2 downstream region (genomic co-ordinates 3846-4029) containing a *Hind*III restriction site followed by the epitope coding region and a stop codon were PCR amplified (Table S2) to attach each epitope to the M2 C-terminus. The PCR products were inserted downstream of a *Hin*DIII/*Xho*I MuHV-4 genomic fragment (nt 4029–5362) in pSP72 (Promega), using a genomic *Bgl*II site (nt 3846) and the engineered *Hin*DIII (nt 4029) restriction site. The constructs were then subcloned into a *Hin*DIII-E MuHV-4 genomic fragment in the pST76K-SR shuttle plasmid, using genomic *Bln*I (nt 3908) and *Xho*I (nt 5362) restriction sites. All PCR-derived regions were sequenced to confirm the integrity of the introduced epitopes and the M2 flanking region. Each recombinant *Hin*DIII-E shuttle plasmid was transformed into *E.coli* carrying the wild type MuHV-4 BAC (pHA3) or a YFP$^+$ BAC [50] obtained from Dr Samuel Speck (Emory Vaccine Center, Atlanta). Following multi-step selection, recombinant BAC clones were identified by restriction digestion with *Hin*DIII. The integrity of each BAC was confirmed by digestion with *Bam*HI and *Eco*RI. All viruses were reconstituted by transfecting BAC DNA into BHK-21 cells using FuGENE 6 or X-tremeGENE HP (Roche Applied Science). The *lox*P-flanked BAC cassette was then removed by viral passage through NIH-3T3-CRE cells and limiting dilution cloning. The integrity of each reconstituted virus was checked by PCR of viral DNA across the *Hin*DIII-E region and DNA sequencing across M2.

Cell culture and viruses

Murine RMA/S cells were cultured in RPMI 1640 with 10% fetal calf serum, 2 mM glutamine and 100 U/ml penicillin and 100 µg/ml streptomycin. NIH-3T3 (ATCC)-CRE cells [22] were grown in Dulbecco's modified Eagle's medium (DMEM) with 10% fetal calf serum, 2 mM glutamine, 100 U/ml penicillin and 100 µg/ml streptomycin. Baby hamster kidney fibroblast cells (BHK-21, ATCC) were cultured in Glasgow's modified Eagle's medium (GMEM) supplemented as above plus 10% tryptose phosphate broth. To prepare viral stocks, low multiplicity infections (0.001 PFU per cell) of NIH-3T3-CRE or BHK-21 cells were harvested after 4 days and titrated by plaque assay [29].

H2K^b stabilization assay and OVA/APLs stimulatory potency

H2K^b stabilization was determined with TAP-deficient RMA/S cells. These were incubated overnight at 26°C to promote the export of empty H2K^b complexes, then loaded with graded concentrations of OVA or APL peptides (Thermo Scientific) for 2 h at 26°C and subsequently transferred to 37°C for 2 h to

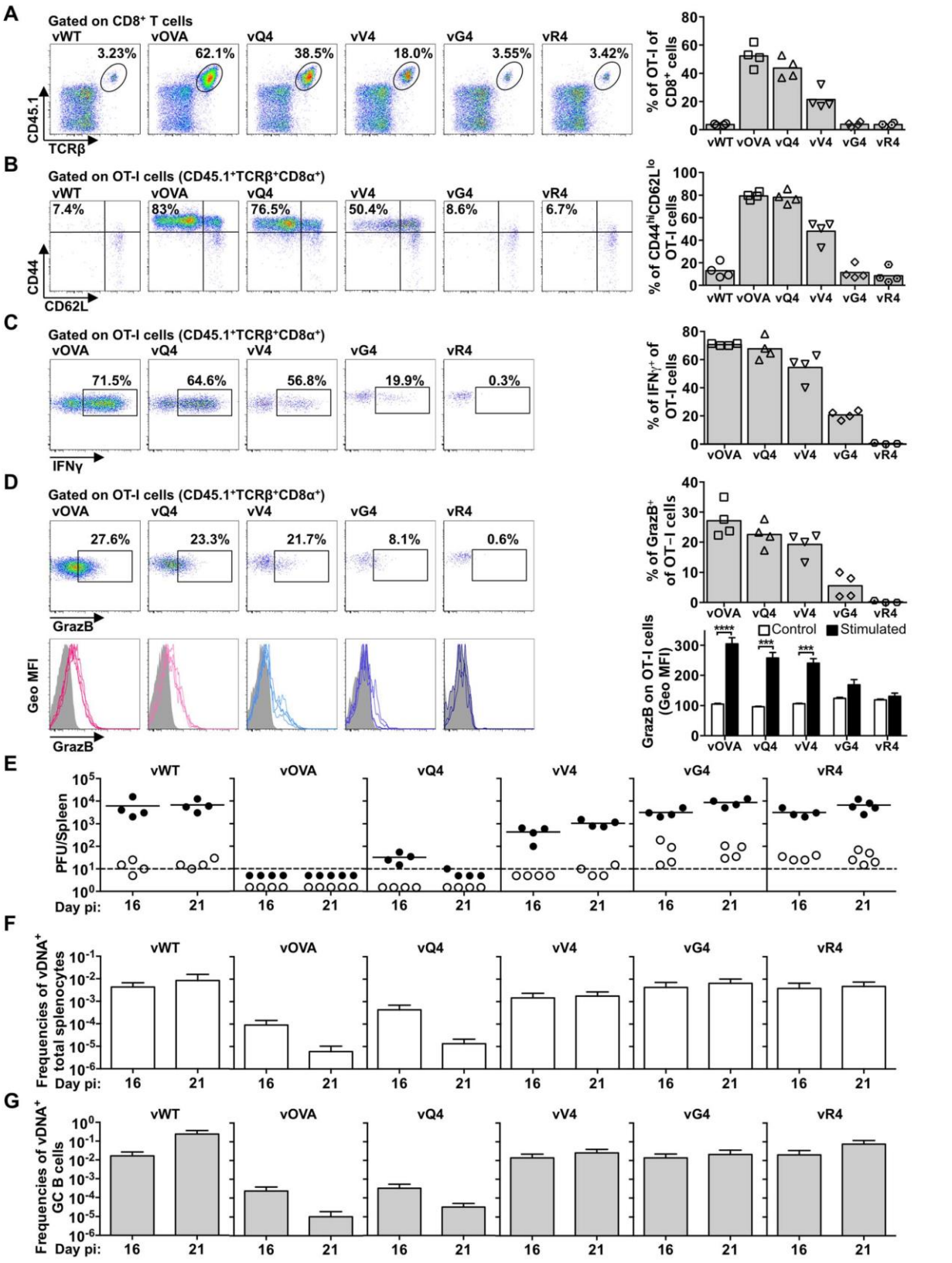
A
Gated on CD8+ T cells
vWT
vOVA
vQ4
vV4
vG4
vR4
3.23%
62.1%
38.5%
18.0%
3.55%
3.42%
CD45.1
TCRβ
% of OT-I of CD8+ cells
B
Gated on OT-I cells (CD45.1+TCRβ+CD8α+)
7.4%
83%
76.5%
50.4%
8.6%
6.7%
CD44
CD62L
% of CD44hiCD62Llo OT-I cells
C
Gated on OT-I cells (CD45.1+TCRβ+CD8α+)
71.5%
64.6%
56.8%
19.9%
0.3%
IFNγ
% of IFNγ+ of OT-I cells
D
Gated on OT-I cells (CD45.1+TCRβ+CD8α+)
27.6%
23.3%
21.7%
8.1%
0.6%
GrazB
Geo MFI
% of GrazB+ of OT-I cells
Control
Stimulated
GrazB on OT-I cells (Geo MFI)
E
PFU/Spleen
Day pi:
16
21
F
Frequencies of vDNA+ total splenocytes
G
Frequencies of vDNA+ GC B cells

Figure 5. Suboptimal CTL functional avidity still allows control of virus-driven lymphoproliferation. Reconstituted TcR$\alpha^{-/-}$ mice (described in Figure 4A). were i.n. infected. (A–D) At 16 days the frequency, phenotype and effector function of transferred OT-I T cells was analyzed by flow cytometry. (A) Representative FACS plots from individual animals show the frequency of OT-I (CD45.1$^+$TcRβ^+CD8α^+) cells within total CD8$^+$ T cells. vOVA, vQ4 and vV4 induced significant expansion of OT-I cells in comparison with vWT ($p<0.0001$, $p<0.0001$, $p=0.002$, respectively; by ordinary one-way ANOVA followed by Tukey's multiple comparisons test). vWT, vG4 and vR4 did not significantly increase OT-I cell numbers ($p>0.9$). (B) The activation phenotype of OT-I cells was determined by staining he CD45.1$^+$TcRβ^+CD8α^+ population for CD44 and CD62L. vOVA, vQ4 and vV4 induced significantly more OT-I cell activation than vWT ($p<0.0001$); vG4 and vR4 were not significantly different from vWT ($p>0.9$). (C–D) The effector function of OT-I cells was determined as % CD45.1$^+$TcRβ^+CD8α^+ cells producing (C) IFN-γ and (D) granzyme B by intracellular cytokine staining following *ex vivo* stimulation with OVA or the corresponding APL peptide. Histograms show geometric mean fluorescence intensities of granzyme B staining relative to an antibody isotype control (shaded area). Representative FACS plots from individual animals (left panels) and compiled percentages (right panels) are shown. Each point shows 1 mouse; 4 mice were analyzed per group; the bars shows means. *** $p<0.001$, **** $p<0.0001$; using Student's 2-tailed unpaired t-test. (E) At 16 and 21 days, spleens were titrated for latent virus (closed circles) and infectious virus (open circles). Each circle shows the titre of 1 mouse and the horizontal bars show means. The dashed line shows the limit of detection of the assay. At 16 and 21 days vOVA, vQ4 and vV4 showed significantly lower latent loads than vWT (d16: vOVA $p=0.02$, vQ4 $p=0.02$, vV4 $p=0.03$; d21: vOVA $p=0.004$, vQ4 $p=0.006$, vV4 $p=0.02$; by ordinary one-way ANOVA and Dunnett's multiple comparisons test). Latent loads of vG4 and vR4 were not significantly different from vWT (d16: vG4 $p=0.4$, vR4 $p=0.4$; d21: vG4 $p=0.8$, vR4 $p=1.0$). (F–G) Reciprocal frequencies of viral DNA$^+$ cells in (F) total splenocytes and (G) purified GC B cells. Bars show frequencies of viral DNA-positive cells with 95% confidence intervals.
doi:10.1371/journal.ppat.1004220.g005

destabilize empty MHC molecules [43]. The cells were then washed twice, stained with anti-H2K^b (AF6-88.5.5.3, eBioscience), and analysed on a LSR Fortessa (BD Biosciences). Mean fluorescence intensities were determined with FlowJo (Tree Star). To measure the *ex vivo* stimulation of naïve OT-I T cells by OVA and APLs, CD8$^+$ T cells from the spleens of naïve OT-I mice were purified by negative selection (CD8$^+$ T cell isolation kit, Miltenyi Biotech); for equivalent peptide/MHC class I numbers, irradiated (7500 rads) RMA/S cells were loaded with different peptides at 26°C, then incubated at 37°C; and 5×10^4 OT-I T cells were cultured with 2.5×10^4 RMA/S cells for 72 h at 37°C. IFNγ levels in culture supernatants were measured by ELISA (DuoSet ELISA development kit, R&D Systems). The data were fitted to sigmoidal dose-response curves and EC_{50} values calculated using GraphPad Prism.

In vivo infections and virus assays

Groups of 6- to 8-week old BALB/c and C57BL/6 mice were inoculated i.n. with 10^4 PFU of MuHV-4. 8- to 12-week old OT-I and TCR$\alpha^{-/-}$ mice were inoculated i.n. with 10^3 PFU of MuHV-4. All virus inoculations were in 20 µl of PBS under isofluorane anaesthesia. At different days post-infection lungs or spleens were removed and processed for subsequent analysis. Titres of infectious virus were determined by plaque assay of freeze-thawed lung or spleen homogenates using BHK-21 cells. Latent virus loads were quantified by explant co-culture of splenocytes with BHK-21 cells. Plates were incubated for 4 (plaque assay) or 5 (explant co-culture assay) days, then fixed with 4% formaldehyde and stained with 0.1% toluidine blue. Viral plaques were counted with a plate microscope. The frequency of MuHV-4 genome-positive cells was determined by limiting dilution combined with real time PCR [10]. Splenocytes were pooled from 4–5 mice. GC B cells (CD19$^+$CD95^{hi}GL7^{hi}) were purified from pools of 4 or 5 spleens using a BD FACSAria Flow Cytometer (BD Biosciences). Cells were serially two-fold diluted and eight replicates of each dilution were analysed by real time PCR (Rotor Gene 6000, Corbett Life Science). The primer/probe sets were specific for the MuHV-4 M9 gene (5′ primer: GCCA-CGGTGGCCCTCTA; 3′ primer: CAGGCCTCCCTCCCTT-TG; probe: 6-FAM-CTTCTGTTGATCTTCC-MGB). Samples

Table 3. Reciprocal frequency of MuHV-4 infection in GC B cells[a] of reconstituted TCR$\alpha^{-/-}$ mice.

Virus	Day p.i.	Reciprocal frequency[b] of viral DNA$^+$ cells (95% CI)		% Cells[c]	% Purity[d]
vWT	16	61	(38–158)	3.13	97.3
	21	4	(3–9)	6.36	97.4
vOVA	16	41,748	(25,873–108,104)	1.95	97.0
	21	id	>96,432[e]	4.88	98.4
vQ4	16	3,042	(1,874–8,064)	3.50	97.0
	21	29,920	(19,237–67,294)	4.87	97.0
vV4	16	72	(45–176)	3.00	98.2
	21	39	(25–84)	8.83	99.0
vG4	16	72	(45–176)	3.08	97.0
	21	32	(18–108)	6.68	98.0
vR4	16	50	(29–167)	2.46	97.4
	21	16	(9–53)	7.99	97.0

[a]Data were obtained from pools of 4 to 5 spleens.
[b]Frequencies were calculated by limiting-dilution analysis with 95% confidence intervals (CI).
[c]The percentage of GC B cells from total spleen was estimated by FACS analysis.
[d]The purity of sorted cells was determined by FACS analysis.
[e]Estimated based upon less than 3 different dilution sets.
id; indeterminable.
doi:10.1371/journal.ppat.1004220.t003

were subjected to a melting step of 95°C for 10 min followed by 40 cycles of 15 s at 95°C and 1 min at 60°C. Real-time PCR data was analysed on the Rotor Gene 6000 software. The purity of sorted populations was always >96%. *In situ* hybridization with a digoxigenin-labelled riboprobe encompassing MuHV-4 vtRNAs 1–4 and microRNAs 1–6 was performed on formalin-fixed, paraffin-embedded spleen sections [29], using probes generated by T7 transcription of pEH1.4.

In vivo cytotoxicity assay

Splenocytes from naïve CD45.1 C57BL/6 mice were used as targets and controls. Targets were pulsed with 1 μM OVA, E1 or A8 peptides for 1 h at 37°C, then labeled with 1 μM carboxyfluorescein succinimidyl ester (CFSE) (Molecular Probes). Controls were left unpulsed and labeled with 0.1 μM CFSE. Cells were washed three times then injected intravenously as a 50:50 mix of $CFSE^{hi}$ and $CFSE^{lo}$ cells (4×10^6) into mice infected with vWT, vOVA, vE1 or vA8. The same mixes were injected intravenously into vWT infected C57BL/6 controls to ensure equal transfer. On the next day splenocytes were harvested and the proportion of $CFSE^{hi}$ and $CFSE^{lo}$ cells among CD45.1 splenocytes was analysed by FACS. Target cell killing was calculated as (% $CFSE^{lo}$/% $CFSE^{hi}$), with % = 100−(ratio in vWT infected/ratio in vOVA, vE1 or vA8 infected)×100.

$CD8^+$ T cell depletions

MuHV-4 infected OT-I mice were depleted of $CD8^+$ T cells by 5 intraperitoneal injections of 200 μg monoclonal antibody YTS 169.4. Splenocytes from control or depleted mice were stained with anti-CD8α (53-6.7) (BD Pharmingen) and analysed on a LSR Fortessa (BD Biosciences).

Ex vivo stimulation and intracellular cytokine staining

Splenocytes (2×10^6) from infected mice were stimulated for 5 h at 37°C with 10 μg/ml peptide (OVA, APLs or VSV $NP_{52\text{-}59}$) in RPMI 1640/10% fetal calf serum/2 mM glutamine/100 U/ml penicillin/100 μg/ml streptomycin/50 μM 2-mercaptoethanol/10 U/ml recombinant murine IL-2 (PeproTech)/10 μg/ml Brefeldin A. Cells were then washed, blocked with anti-CD16/32 (2.4G2) (BD Pharmingen), surface stained with anti-CD8α ± anti-CD45.1 (for OT-I T cells), fixed and permeabilized with Foxp3 staining buffer (eBioscience) and stained with anti-IFNγ (XMG1.2) (BD Pharmingen), anti-Granzyme B (NGZB) or anti-IgG2ak Isotype control (eBioscience). Samples were analysed on a LSR Fortessa (BD Biosciences).

Flow cytometry

Splenocytes were treated with red blood cell lysis buffer, blocked with anti-CD16/32 (2.4G2, BD Pharmingen, 10 min), and stained at 4°C in PBS/2% FCS 30 minutes: anti-CD95 (Jo2), anti-CD19 (1D3), anti-CD8α (53-6.7), anti-IFNγ (XMG1.2) (BD Pharmingen); anti-CD45.1 (A20), anti-CD45.2 (104), anti-CD44 (IM7), anti-CD62L (MEL-14) (Biolegend); anti-GL7 (GL7), anti-$H2K^b$ (AF6-88.5.5.3), anti-TCRβ (H57-597), anti-GranzymeB (NGZB), anti-IgG2ak Iso control (eBR2a) (eBioscience). For biotinylated antibodies, an additional 20 minutes incubation with streptavidin was performed. MuHV-4 infected cells were identified by YFP expression. $H2K^b$ tetramers conjugated to PE were a kind gift from Dr Hidde L. Ploegh (Whitehead Institute for Biomedical Research, Massachusetts Institute of Technology, Cambridge). Conditional ligand was exchanged for SIINFEKL (OVA), SIIQFEKL (Q4), SIIVFEKL (V4), SIIGFEKL (G4), SIIRFEKL (R4), EIINFEKL (E1) or RGYVYQGL (VSV $NP_{52\text{-}59}$) peptides (Thermo Scientific). Streptavidin-APC or -PerCP (BD Pharmingen) was used to reveal biotinylated antibodies. Samples were acquired on a LSR Fortessa using DIVA (BD Biosciences) and analysed with FlowJo (Tree Star, Inc.).

Statistical analysis

Data comparisons between groups were performed by an unpaired two-tailed t-test or ordinary one-way ANOVA as appropriate. Mean +/− SEM and statistics were calculated with GraphPad Prism Software. For limiting dilution analysis 95% confidence intervals were determined as described [10].

PCR primers

Primers used for attaching each epitope to MuHV-4 M2 C-terminus are detailed in supplemental Table S2.

Supporting Information

Figure S1 Characterization of MuHV-4 YFP recombinants expressing OVA or APLs linked to M2. (A) PCR analysis of recombinant viral DNA to confirm genome integrity in the HinDIII-E region. High molecular weight DNA was purified from lytically infected BHK-21 cells. A schematic representation of the MuHV-4 genome, amplicon genomic coordinates and expected size for each PCR product are shown. (B) Latent infection in spleens of intranasally infected (10^4 PFU) BALB/c ($H2^d$) mice was quantified by explant co-culture assay (closed symbols) at day 14 post-infection. Pre-formed infectious virus was measured by plaque assay (open symbols). Latent loads of MuHV-4 YFP recombinants expressing OVA or APLs were not significantly different from MuHV-4 YFP (vWT) ($p>0.05$, by ordinary one-way ANOVA followed by Dunnett's multiple comparisons test). Each point shows the titre of 1 mouse, horizontal lines indicate arithmetic means and the dashed horizontal line the limit of detection of the assay. Data were reproduced in two independent experiments. (C) Phenotype of infected cells (YFP expressing cells) was analysed by FACS, by overlapping GC ($CD19^+CD95^{hi}GL7^{hi}$) B cells and YFP^+ B cells FACS plots. Representative FACS plots from individual animals are shown. Five animals were analysed per group and data were reproduced in two independent experiments.
(TIF)

Figure S2 Reconstitution of $TCR\alpha^{-/-}$ mice with $CD4^+$ T cells leads to robust GC reactions upon MuHV-4 infection. 2×10^6 $CD4^+$ T cells purified from pooled lymph nodes of naïve C57BL/6 mice were intravenously transferred into age and sex matched $TCR\alpha^{-/-}$ mice one day prior to infection with 10^3 PFU of MuHV-4 YFP (vWT). At 14 days post-infection mice were sacrificed, spleens were dissected and single splenocyte suspensions were stained for GC B cells and analysed by FACS. (A) Schematic diagram of the experimental setting. (B) Representative FACS plots show the frequency of GC ($CD19^+CD95^{hi}GL7^{hi}$) B cells in spleens of the following experimental controls: non-transferred naïve $TCR\alpha^{-/-}$ mice, CD4-transferred naïve $TCR\alpha^{-/-}$ mice, non-transferred $TCR\alpha^{-/-}$ mice infected with vWT, CD4-transferred $TCR\alpha^{-/-}$ mice infected with vWT, and CD4 and OT-I T cells co-transferred $TCR\alpha^{-/-}$ mice infected with vWT. Four mice were analysed per group and data were reproduced in two independent experiments.
(TIF)

Figure S3 $TCR\alpha^{-/-}$ mice reconstituted with $CD4^+$ and OT-I T cells show robust proliferation of MuHV-4 infected GC B cells. $CD4^+$ T cells from C57BL/6 lymph

nodes and OT-I T cells from CD45.1 Rag-1$^{-/-}$ OT-I mice lymph nodes were intravenously transferred to TCRα$^{-/-}$ mice 1 day prior to infection with MuHV-4 YFP (10^3 PFU). (A) Schematic diagram of the experimental setting. (B) Frequencies of GC (CD19^{+}CD95^{hi}GL7^{hi}) B cells. (C) Frequency of YFP^{+} cells in GC B cells. (D) Phenotype of infected cells analyzed by overlapping GC B cells and YFP^{+} B cells FACS plots. Representative FACS plots from individual animals are shown (top panels) and compiled percentages are presented in the graphics below. Each point represents an individual mouse; grey bars indicate the average percentage.
(TIF)

Figure S4 YFP expression in GC B cells of reconstituted TCRα$^{-/-}$ mice infected with MuHV-4 recombinants expressing OVA or APLs. TCRα$^{-/-}$ mice were adoptively transferred with polyclonal CD4^{+} T cells and CD45.1 Rag1$^{-/-}$ OT-I cells one day prior to infection (10^3 PFU) with MuHV-4 YFP (vWT) or MuHV-4 YFP expressing the indicated epitopes. At 16 (A and B) and 21 (C and D) days post-infection spleens were removed and analysed by FACS. (A and C) Frequencies of GC (CD19^{+}CD95^{hi}GL7^{hi}) B cells. (B and D) Frequency of YFP^{+} cells in GC B cells. FACS plots show data obtained from pools of 4 or 5 spleens per group of animals.
(TIF)

Table S1 Reciprocal frequency of MuHV-4 infection in total splenocytes[a] of reconstituted TCRα$^{-/-}$ mice.
(DOC)

Table S2 Primers used for attaching each epitope to MuHV-4 M2 C-terminus.
(DOC)

Acknowledgments

The authors thank Bruno Frederico for initial help making some recombinant viruses.

Author Contributions

Conceived and designed the experiments: CGS SM HVF PGS JPS. Performed the experiments: CGS SM DF. Analyzed the data: CGS SM DF HVF PGS JPS. Contributed reagents/materials/analysis tools: CGS SM. Contributed to the writing of the manuscript: CGS PGS JPS.

References

1. Stevenson PG, Simas JP, Efstathiou S (2009) Immune control of mammalian gamma-herpesviruses: lessons from murid herpesvirus-4. J Gen Virol 90: 2317–2330.
2. Bollard CM, Rooney CM, Heslop HE (2012) T-cell therapy in the treatment of post-transplant lymphoproliferative disease. Nat Rev Clin Oncol 9: 510–519.
3. Thorley-Lawson DA (2001) Epstein-Barr virus: exploiting the immune system. Nat Rev Immunol 1: 75–82.
4. Simas JP, Efstathiou S (1998) Murine gammaherpesvirus 68: a model for the study of gammaherpesvirus pathogenesis. Trends Microbiol 6: 276–282.
5. Speck SH, Ganem D (2010) Viral latency and its regulation: lessons from the gamma-herpesviruses. Cell Host Microbe 8: 100–115.
6. Nash AA, Dutia BM, Stewart JP, Davison AJ (2001) Natural history of murine gamma-herpesvirus infection. Philos Trans R Soc Lond B Biol Sci 356: 569–579.
7. Virgin HWt, Latreille P, Wamsley P, Hallsworth K, Weck KE, et al. (1997) Complete sequence and genomic analysis of murine gammaherpesvirus 68. J Virol 71: 5894–5904.
8. Simas JP, Marques S, Bridgeman A, Efstathiou S, Adler H (2004) The M2 gene product of murine gammaherpesvirus 68 is required for efficient colonization of splenic follicles but is not necessary for expansion of latently infected germinal centre B cells. J Gen Virol 85: 2789–2797.
9. Flano E, Kim IJ, Woodland DL, Blackman MA (2002) Gamma-herpesvirus latency is preferentially maintained in splenic germinal center and memory B cells. J Exp Med 196: 1363–1372.
10. Marques S, Efstathiou S, Smith KG, Haury M, Simas JP (2003) Selective gene expression of latent murine gammaherpesvirus 68 in B lymphocytes. J Virol 77: 7308–7318.
11. Bennett NJ, May JS, Stevenson PG (2005) Gamma-herpesvirus latency requires T cell evasion during episome maintenance. PLoS Biol 3: e120.
12. Levitskaya J, Coram M, Levitsky V, Imreh S, Steigerwald-Mullen PM, et al. (1995) Inhibition of antigen processing by the internal repeat region of the Epstein-Barr virus nuclear antigen-1. Nature 375: 685–688.
13. Hislop AD, Ressing ME, van Leeuwen D, Pudney VA, Horst D, et al. (2007) A CD8+ T cell immune evasion protein specific to Epstein-Barr virus and its close relatives in Old World primates. J Exp Med 204: 1863–1873.
14. Horst D, van Leeuwen D, Croft NP, Garstka MA, Hislop AD, et al. (2009) Specific targeting of the EBV lytic phase protein BNLF2a to the transporter associated with antigen processing results in impairment of HLA class I-restricted antigen presentation. J Immunol 182: 2313–2324.
15. Croft NP, Shannon-Lowe C, Bell AI, Horst D, Kremmer E, et al. (2009) Stage-specific inhibition of MHC class I presentation by the Epstein-Barr virus BNLF2a protein during virus lytic cycle. PLoS Pathog 5: e1000490.
16. Zuo J, Currin A, Griffin BD, Shannon-Lowe C, Thomas WA, et al. (2009) The Epstein-Barr virus G-protein-coupled receptor contributes to immune evasion by targeting MHC class I molecules for degradation. PLoS Pathog 5: e1000255.
17. Zuo J, Quinn LL, Tamblyn J, Thomas WA, Feederle R, et al. (2011) The Epstein-Barr virus-encoded BILF1 protein modulates immune recognition of endogenously processed antigen by targeting major histocompatibility complex class I molecules trafficking on both the exocytic and endocytic pathways. J Virol 85: 1604–1614.
18. Fruh K, Bartee E, Gouveia K, Mansouri M (2002) Immune evasion by a novel family of viral PHD/LAP-finger proteins of gamma-2 herpesviruses and poxviruses. Virus Res 88: 55–69.
19. Boname JM, Stevenson PG (2001) MHC class I ubiquitination by a viral PHD/LAP finger protein. Immunity 15: 627–636.
20. Boname JM, de Lima BD, Lehner PJ, Stevenson PG (2004) Viral degradation of the MHC class I peptide loading complex. Immunity 20: 305–317.
21. Boname JM, May JS, Stevenson PG (2005) The murine gamma-herpesvirus-68 MK3 protein causes TAP degradation independent of MHC class I heavy chain degradation. Eur J Immunol 35: 171–179.
22. Stevenson PG, May JS, Smith XG, Marques S, Adler H, et al. (2002) K3-mediated evasion of CD8(+) T cells aids amplification of a latent gamma-herpesvirus. Nat Immunol 3: 733–740.
23. Rodrigues L, Pires de Miranda M, Caloca MJ, Bustelo XR, Simas JP (2006) Activation of Vav by the gammaherpesvirus M2 protein contributes to the establishment of viral latency in B lymphocytes. J Virol 80: 6123–6135.
24. Pires de Miranda M, Lopes FB, McVey CE, Bustelo XR, Simas JP (2013) Role of Src homology domain binding in signaling complexes assembled by the murid gamma-herpesvirus M2 protein. J Biol Chem 288: 3858–3870.
25. Siegel AM, Herskowitz JH, Speck SH (2008) The MHV68 M2 protein drives IL-10 dependent B cell proliferation and differentiation. PLoS Pathog 4: e1000039.
26. Rangaswamy US, Speck SH (2014) Murine gammaherpesvirus M2 protein induction of IRF4 via the NFAT pathway leads to IL-10 expression in B cells. PLoS Pathog 10: e1003858.
27. Burkhardt AL, Bolen JB, Kieff E, Longnecker R (1992) An Epstein-Barr virus transformation-associated membrane protein interacts with src family tyrosine kinases. J Virol 66: 5161–5167.
28. Lee H, Guo J, Li M, Choi JK, DeMaria M, et al. (1998) Identification of an immunoreceptor tyrosine-based activation motif of K1 transforming protein of Kaposi's sarcoma-associated herpesvirus. Mol Cell Biol 18: 5219–5228.
29. Marques S, Alenquer M, Stevenson PG, Simas JP (2008) A single CD8+ T cell epitope sets the long-term latent load of a murid herpesvirus. PLoS Pathog 4: e1000177.
30. Wang X, Liu X, Jia Y, Chao Y, Xing X, et al. (2010) Widespread sequence variation in the Epstein-Barr virus latent membrane protein 2A gene among northern Chinese isolates. J Gen Virol 91: 2564–2573.
31. Stebbing J, Bourboulia D, Johnson M, Henderson S, Williams I, et al. (2003) Kaposi's sarcoma-associated herpesvirus cytotoxic T lymphocytes recognize and target Darwinian positively selected autologous K1 epitopes. J Virol 77: 4306–4314.
32. Guihot A, Dupin N, Marcelin AG, Gorin I, Bedin AS, et al. (2006) Low T cell responses to human herpesvirus 8 in patients with AIDS-related and classic Kaposi sarcoma. J Infect Dis 194: 1078–1088.
33. Brander C, O'Connor P, Suscovich T, Jones NG, Lee Y, et al. (2001) Definition of an optimal cytotoxic T lymphocyte epitope in the latently expressed Kaposi's sarcoma-associated herpesvirus kaposin protein. J Infect Dis 184: 119–126.
34. Husain SM, Usherwood EJ, Dyson H, Coleclough C, Coppola MA, et al. (1999) Murine gammaherpesvirus M2 gene is latency-associated and its protein a target for CD8(+) T lymphocytes. Proc Natl Acad Sci U S A 96: 7508–7513.
35. Usherwood EJ, Roy DJ, Ward K, Surman SL, Dutia BM, et al. (2000) Control of gammaherpesvirus latency by latent antigen-specific CD8(+) T cells. J Exp Med 192: 943–952.

36. Stevenson PG, Cardin RD, Christensen JP, Doherty PC (1999) Immunological control of a murine gammaherpesvirus independent of CD8+ T cells. J Gen Virol 80 (Pt 2): 477–483.
37. Tibbetts SA, van Dyk LF, Speck SH, Virgin HWt (2002) Immune control of the number and reactivation phenotype of cells latently infected with a gammaherpesvirus. J Virol 76: 7125–7132.
38. Midgley RS, Bell AI, McGeoch DJ, Rickinson AB (2003) Latent gene sequencing reveals familial relationships among Chinese Epstein-Barr virus strains and evidence for positive selection of A11 epitope changes. J Virol 77: 11517–11530.
39. Midgley RS, Bell AI, Yao QY, Croom-Carter D, Hislop AD, et al. (2003) HLA-A11-restricted epitope polymorphism among Epstein-Barr virus strains in the highly HLA-A11-positive Chinese population: incidence and immunogenicity of variant epitope sequences. J Virol 77: 11507–11516.
40. Chen Y, Yao K, Wang B, Qing J, Liu G (2008) Potent dendritic cell vaccine loaded with latent membrane protein 2A (LMP2A). Cell Mol Immunol 5: 365–372.
41. Vigano S, Utzschneider DT, Perreau M, Pantaleo G, Zehn D, et al. (2012) Functional avidity: a measure to predict the efficacy of effector T cells? Clin Dev Immunol 2012: 153863.
42. Matsumura M, Saito Y, Jackson MR, Song ES, Peterson PA (1992) In vitro peptide binding to soluble empty class I major histocompatibility complex molecules isolated from transfected Drosophila melanogaster cells. J Biol Chem 267: 23589–23595.
43. Schumacher TN, Heemels MT, Neefjes JJ, Kast WM, Melief CJ, et al. (1990) Direct binding of peptide to empty MHC class I molecules on intact cells and in vitro. Cell 62: 563–567.
44. Chen W, Khilko S, Fecondo J, Margulies DH, McCluskey J (1994) Determinant selection of major histocompatibility complex class I-restricted antigenic peptides is explained by class I-peptide affinity and is strongly influenced by nondominant anchor residues. J Exp Med 180: 1471–1483.
45. Fremont DH, Stura EA, Matsumura M, Peterson PA, Wilson IA (1995) Crystal structure of an H-2Kb-ovalbumin peptide complex reveals the interplay of primary and secondary anchor positions in the major histocompatibility complex binding groove. Proc Natl Acad Sci U S A 92: 2479–2483.
46. Alam SM, Travers PJ, Wung JL, Nasholds W, Redpath S, et al. (1996) T-cell-receptor affinity and thymocyte positive selection. Nature 381: 616–620.
47. Zehn D, Lee SY, Bevan MJ (2009) Complete but curtailed T-cell response to very low-affinity antigen. Nature 458: 211–214.
48. Jameson SC, Carbone FR, Bevan MJ (1993) Clone-specific T cell receptor antagonists of major histocompatibility complex class I-restricted cytotoxic T cells. J Exp Med 177: 1541–1550.
49. Hogquist KA, Jameson SC, Heath WR, Howard JL, Bevan MJ, et al. (1994) T cell receptor antagonist peptides induce positive selection. Cell 76: 17–27.
50. Collins CM, Boss JM, Speck SH (2009) Identification of infected B-cell populations by using a recombinant murine gammaherpesvirus 68 expressing a fluorescent protein. J Virol 83: 6484–6493.
51. Stevenson PG, Belz GT, Altman JD, Doherty PC (1999) Changing patterns of dominance in the CD8+ T cell response during acute and persistent murine gamma-herpesvirus infection. Eur J Immunol 29: 1059–1067.
52. Price DA, Brenchley JM, Ruff LE, Betts MR, Hill BJ, et al. (2005) Avidity for antigen shapes clonal dominance in CD8+ T cell populations specific for persistent DNA viruses. J Exp Med 202: 1349–1361.
53. Callan MF, Steven N, Krausa P, Wilson JD, Moss PA, et al. (1996) Large clonal expansions of CD8+ T cells in acute infectious mononucleosis. Nat Med 2: 906–911.
54. Hislop AD, Taylor GS, Sauce D, Rickinson AB (2007) Cellular responses to viral infection in humans: lessons from Epstein-Barr virus. Annu Rev Immunol 25: 587–617.
55. Ehtisham S, Sunil-Chandra NP, Nash AA (1993) Pathogenesis of murine gammaherpesvirus infection in mice deficient in CD4 and CD8 T cells. J Virol 67: 5247–5252.
56. Frederico B, Chao B, May JS, Belz GT, Stevenson PG (2014) A murid gammaherpesviruses exploits normal splenic immune communication routes for systemic spread. Cell Host Microbe 15: 457–470.
57. Smith CM, Gill MB, May JS, Stevenson PG (2007) Murine gammaherpesvirus-68 inhibits antigen presentation by dendritic cells. PLoS ONE 2: e1048.
58. El-Gogo S, Flach B, Staib C, Sutter G, Adler H (2008) In vivo attenuation of recombinant murine gammaherpesvirus 68 (MHV-68) is due to the expression and immunogenicity but not to the insertion of foreign sequences. Virology 380: 322–327.
59. Loh J, Popkin DL, Droit L, Braaten DC, Zhao G, et al. (2012) Specific mutation of a gammaherpesvirus-expressed antigen in response to CD8 T cell selection in vivo. J Virol 86: 2887–2893.
60. Cardin RD, Brooks JW, Sarawar SR, Doherty PC (1996) Progressive loss of CD8+ T cell-mediated control of a gamma-herpesvirus in the absence of CD4+ T cells. J Exp Med 184: 863–871.
61. Belz GT, Stevenson PG, Castrucci MR, Altman JD, Doherty PC (2000) Postexposure vaccination massively increases the prevalence of gamma-herpesvirus-specific CD8+ T cells but confers minimal survival advantage on CD4-deficient mice. Proc Natl Acad Sci U S A 97: 2725–2730.